DEVELOPMENT OF UNIFORM AND INDUSTRY WIDE TEST PROTOCOLS FOR HIGH TEMPERATURE SOLIDE OXIDE CELL/STACK ASSEMBLY

by

Marco Graziadio

DEVELOPMENT OF UNIFORM AND INDUSTRY WIDE TEST PROTOCOLS FOR HIGH TEMPERATURE SOLIDE OXIDE CELL/STACK ASSEMBLY

Marco Graziadio

Thesis submitted for the Degree of

Doctor of Philosophy

Supervisors: **Prof. Maurizio Carlini**

Dr. Stephen J. McPhail

Università degli Studi della Tuscia di Viterbo

A.A 2018/2019

Sommario

LIST OF FIGURES

LIST OF TABLES

TERMS AND DEFINITIONS

To better understand the functionality of the Re-SOC and avoid any confusion, for the purposes of this document, the following terms and definitions shall apply.

Table 1. *Terms and Definition.*

Active electrode area (A)= effective electrode area	Geometric area of the electrode where the electrochemical reaction takes place. Area perpendicular to the direction of the current flow, usually expressed in m^2 or cm^2. NOTE: Usually this corresponds to the smaller area of the **negative electrode** and **positive electrode**.
Area Specific Resistance (ASR)	Internal resistance of any component of a cell or a stack. It is normalized by the area and has a unit of $\Omega\ cm^2$.
Bipolar plate (Interconnect)	Conductive plate separating individual cells in a stack, acting as current collector and gas distributor for the electrodes of the **SOC**. The **bipolar plate** usually incorporates flow field on both sides for the distribution of reactants and removal of products. The bipolar plate provides a physical barrier to avoid mixing of oxidant and fuel. The bipolar plate is also known as **interconnect**.
Cell	A **cell** consists of two electrodes – a **positive electrode** and a **negative electrode** – with an electrolyte between them.
Current collector	Electronically conductive material in a cell that collects/conducts electrons from/to the electrodes.
Current density	Current per unit **active electrode area** (usually expressed in A m^{-2} or A cm^{-2})
Degradation rate	Rate at which a **cell**/**stack**'s performance deteriorates over time. Performance in this instance refers to the intended operation mode of the SOC (fuel production or electrical power generation). The degradation rate can be used to measure both recoverable and permanent losses in cell/stack performance. Depending on the operating mode, degradation rate can be expressed by the rate of evolution of any quantity of interest, which serves as an indicator of a **cell**/**stack**'s performance, for instance electrical current, fuel production rate, voltage, electrical power or area specific resistance. It is recommended to use always a sign before the number to indicate univocally the variation direction of the quantity. A positive sign means that the quantity is increasing with time and a negative sign means that the quantity is decreasing with time. Usually the degradation rate of a cell/stack is a function of time. Therefore, the time frame under which the degradation rate is evaluated should always be indicated.
Derived quantities	Values that can be derived or calculated from **test input parameters** and/or **test output parameters** (e.g. current density, reactant utilization, electrical efficiency). In comparison to **test output parameters**, **derived quantities** are not directly measurable

Electric efficiency	Ratio of net electric power produced by a fuel cell power system to the total enthalpy flow supplied to the fuel cell power system (based on LHV).
Lower heating value (LHV)	The lower heating value of a fuel is defined as the amount of heat released by combusting a specified quantity (initially at 25°C) and returning the temperature of the combustion products to 150°C, which assumes the latent heat of vaporization of water in the reaction products is not recovered. The lower heating value is obtained by subtracting the latent heat of vaporization of the water vapour from the higher heating value.
Negative electrode	Electrode at which fuel gas is consumed or produced. It may also be called fuel electrode. In the fuel cell mode, it is actually called anode where the fuel is oxidized. In the steam electrolysis mode, it is called cathode where steam is reduced producing H_2.
Positive electrode	Electrode at which O_2 is consumed or produced. It may also be called oxidant electrode. In the fuel cell mode, it is actually called cathode where O_2 is reduced producing oxide ions going through the electrolyte. In the steam electrolysis mode, it is called anode where two oxide ions are recombined to form one molecule of O_2.
Reactant utilization (U_{gas})	Gas utilization at the negative electrode (**fuel utilization in SOFC mode**, **steam conversion rate in SOEC mode**) or gas utilization at the positive electrode (air utilization or oxygen utilization in SOFC mode)
Repeating Unit (RU)	An elementary unit which periodically repeats itself to form a **stack**. It is composed of one single cell and two half-interconnects on both sides of the single cell and usually also sealant to assure gas-tightness and contact layers to minimize contact resistances between cells and interconnects.
Solid Oxide Cell (SOC)	**Cell** composed of three functional elements (negative electrode, electrolyte and positive electrode) based on ceramic oxide materials. Two electrodes made of ionic and/or electronic conducting ceramics are attached to one purely ionic conducting solid oxide ceramic electrolyte. Furthermore, the cell may contain a support layer which may be a ceramic layer or a non-ceramic layer as is the case for metal-supported cells. **SOC**s can be used as an **SOFC** or an **SOEC**.
Solid Oxide Electrolysis Cell (SOEC)	An **SOEC** is an **SOC** operated in the electrolysis mode, i.e., reversed fuel cell mode. It can be used to produce hydrogen from steam or to produce CO from CO2. Electricity and also eventual heat are used as energy input.
Solid Oxide Fuel Cell (SOFC)	An **SOFC** is an **SOC** operated in the fuel cell mode. It is used for cogeneration of electricity and heat using fuels such as natural gas. In some applications only the electricity part is used and the co-generated heat is just dissipated.

Stack	A fuel cell stack or an electrolyser stack is composed of a number of **repeating units**. Normally two endplates (top plate and bottom plate) are used to facilitate applying a compression force to all **repeating units**.
Test Input Parameter (TIP)	Parameters whose values can be set in order to define the test conditions of the test system including the operating conditions of the test object. TIPs have to be controllable and measurable. Values of TIPs are known before conducting the test. TIPs can be either static or variable. Static TIPs stay constant and variable TIPs are varied during the test
Test Output Parameter (TOP)	Parameters that indicate the response of the test system/test object as a result of variation of TIPs. Values of TOPs are unknown before conducting the test and will be measured during the test. TOPs must be measurable.
Thermoneutral voltage (V_{tn})	Thermoneutral voltage relates to the enthalpy of a reaction. An electrolysis cell operates adiabatically at *Vtn*, i.e, no heat exchange is needed between the electrolyzer and its environment. In other words, heat produced in the cell due to the internal resistance (Joule heat) compensates exactly the heat needed by the endothermic electrolysis reaction. The electricity input to the electrolyzer matches exactly the enthalpy of the electrolysis reaction.
Open Circuit Voltage (OCV)	The measured voltage of an electrochemical system without external electrical current.
Voltage of a cell (V_{cell})	Voltage measured between the positive and negative electrode of a cell.
Voltage of a RU (V_{RU})	Voltage measured between the two bipolar plates of a RU.
Voltage of the stack (V_{stack})	The voltage measured between the two current connection terminals (for instance two endplates) of the stack. It should be noted that the stack voltage can be different from the sum of all RU voltages in the stack due to non-negligible voltage drops caused by contact resistances between endplates and their adjacent RUs.

SYMBOLS

Table 2 shows the symbols and units that are used in this PhD's thesis:

Table 2. *Symbols.*

Symbol	Definition	Unit
A_{active}	Active (surface) area of the cell/stack electrode(s)	m^2
c_i	Molar concentration of component *i*	mol/m^3
F	Faraday constant (96485,3)	A·s/mol
$q_{v,neg,in}$	Total volumetric flow rate at negative electrode inlet (at SPT)	m^3/s, l/min
$q_{v,pos,in}$	Total volumetric flow rate of positive electrode inlet (at SPT)	m^3/s, l/min
$q_{v,neg,out}$	Total volumetric flow rate at negative electrode outlet (at SPT)	m^3/s, l/min
$q_{v,pos,out}$	Total volumetric flow rate of positive electrode outlet (at SPT)	m^3/s, l/min
$q_{v,i,neg,in}$	Volumetric flow rate of gas component i at negative electrode inlet	m^3/s, l/min
$q_{v,i,pos,in}$	Volumetric flow rate of gas component i at positive electrode inlet	m^3/s, l/min
$q_{v,i,neg,out}$	Volumetric flow rate of gas component i at negative electrode outlet	m^3/s, l/min
$q_{v,i,pos,out}$	Volumetric flow rate of gas component i at positive electrode outlet	m^3/s, l/min
$q_{m,neg,in}$	Total mass flow rate at negative electrode inlet (at SPT)	kg/s, g/min
$q_{m,pos,in}$	Total mass flow rate of positive electrode inlet (at SPT)	kg/s, g/min
$q_{m,neg,out}$	Total mass flow rate at negative electrode outlet (at SPT)	kg/s, g/min
$q_{m,pos,out}$	Total mass flow rate of positive electrode outlet (at SPT)	kg/s, g/min
$q_{m,i,neg,in}$	Mass flow rate of gas component i at negative electrode inlet	kg/s, g/min
$q_{m,i,pos,in}$	Mass low rate of gas component i at positive electrode inlet	kg/s, g/min
$q_{m,i,neg,out}$	Mass flow rate of gas component i at negative electrode outlet	kg/s, g/min
$q_{m,i,pos,out}$	Mass flow rate of gas component i at positive electrode outlet	kg/s, g/min

$q_{v,i}$	Volumetric flow rate of reactant component i at SPT	m^3/s, l/min
I	Current	A
J	Current density	A/cm^2
n	Number of transferred electrons	-
N_{points}	Number of measuring points	-
$N_{periods}$	Number of measuring periods	-
N_{cycles}	Number of cycles	-
N	Number of cells in a series connection	-
p_0	Standard pressure (101,325)	kPa
p_{vessel}	Pressure inside containment vessel	kPa
$p_{neg,in}$	Pressure of negative electrode gas at cell/stack inlet	kPa
$p_{neg,out}$	Pressure of negative electrode gas at cell/stack outlet	kPa
$p_{pos,in}$	Pressure of positive electrode gas at cell/stack inlet	kPa
$p_{pos,out}$	Pressure of positive electrode gas at cell/stack outlet	kPa
P_{el}	Electric power	W
P_d	Electric power density	W/cm^2
R_g	Universal gas constant (8,3145)	J/(mol·K)
t	Time	s,min,h
t_{acq}	Data acquisition time	s,min,h
t_{op}	Duration time of operation at given conditions	s,min,h
T_0	Standard temperature (273,15)	K
T_{min}	Minimum temperature during cycling	K
$T_{neg,in}$	Temperature of negative electrode gas stream at cell/stack inlet	°C, K
$T_{pos,in}$	Temperature of positive electrode gas stream at cell/stack inlet	°C, K
$T_{neg,out}$	Temperature of negative electrode gas stream at cell/stack outlet	°C, K
$T_{pos,out}$	Temperature of positive electrode gas stream at cell/stack outlet	°C, K
$T_{PH,neg}$	Temperature of the pre-heater for preheating the negative electrode gas stream	°C, K
$T_{PH,pos}$	Temperature of the pre-heater for preheating the positive electrode gas stream	°C, K
T_{TP}	Temperature of Top Plate	°C, K
T_{BP}	Temperature of Bottom Plate	°C, K
$T_{cell/stack}$	Temperature of the cell or stack	°C, K
$T_{furnace}$	Temperature of the furnace	°C, K
T_{av}	Average temperature of the stack	°C, K

ΔT_{max}	Maximum temperature difference between reactants and the stack temperature during start-up	°C, K
$U_{gas,neg}$	Reactant utilization at the negative electrode (fuel utilization in fuel cell mode, steam conversion in electrolysis mode)	-
$U_{gas,\ pos}$	Reactant utilization at the positive electrode (air utilization or oxygen utilization, valid only in fuel cell mode)	-
V_{stack}	Voltage of the stack	V
V_{cell}	Voltage of the cell	V
$V_{RU,i}$	Voltage of repeating unit (RU) *i* in the stack	V
$V_{RU,av}$	Average RU voltage of all RU in the stack	V
F_{compr}	Compression force applied onto the cell/stack	N
Q	Electrical Charge	C
$x_{i,neg}$	Molar fraction of component *i* in the negative electrode gas stream at cell/stack	-
$x_{i,pos}$	Molar fraction of component *i* in the positive electrode gas stream at cell/stack	-
$\eta_{H2,produced}$	Hydrogen production electric efficiency	-
$\eta_{,el}$	Electric efficiency	-
Cp	Heat capacity	J/(mol·K)
H	Enthalpy	J/mol
R	Resistance	Ω
R_{LF}	Low frequency resistance	Ω·cm^2 Ω·m^2
R_{HF}	High frequency resistance	Ω·cm^2 Ω·m^2
ΔY	Degradation rate	V*s
ASR	Area specific resistance	Ω ·m^2
f	Perturbation frequency	Hz
Ω	Angular perturbation frequency	rad/s
$\bar{I}$	Amplitude of alternating current	A
$\bar{V}$	Amplitude of alternating voltage	V
Φ	Phase angle	rad
I	Imaginary unit	-
Z	Impedance	Ω
	Specific impedance	Ω·cm^2 Ω·m^2

|Z|	Modulus of impedance	Ω
	Modulus of Specific impedance	$\Omega \cdot cm^2$ $\Omega \cdot m^2$
Z'	Real part of impedance	Ω
	Real part of specific impedance	$\Omega \cdot cm^2$ $\Omega \cdot m^2$
Z''	Imaginary part of impedance	Ω
	Imaginary part of specific impedance	$\Omega \cdot cm^2$ $\Omega \cdot m^2$

ABSTRACT

One of the most interesting features of Reversible Solid Oxide Cells (Re-SOC) is the capability to operate efficiently in both fuel cell and electrolysis modes.

The possibility to work in both ways guarantees multiple benefits: fuel flexibility, insignificant emissions, silent operation and affordability. These characteristics are the pillars on which this technology stands for over current power and substance generation systems.

To introduce innovative technologies into industrial and consumer environments it is necessary that essential requirements in Regulations and the associated technical specifications in Codes and Standards (RCS) be established. In the case of Solid Oxide Cell and Hydrogen Technologies, these have centered around two main themes:

- Safety standards, that are essential safety requirements imposed by normative bodies to reduce the risk of hazards during operation;
- Technical specifications, that define specifications and procurement of testing samples, the overall test matrix and test procedures, and which can also include validation of the cell/stack assembly unit and systems in terms of flexibility, environmental sustainability and efficiency.

The main objective of my thesis was to develop uniform and industry wide test procedures for high temperature solid oxide cells/stacks in order to beef up the extent of knowledge with the aim to accelerate the development and the market penetration of hydrogen and fuel cell (H2&FC) energy systems in Europe and the world. The work addresses safety aspects closely related with industrial practices and the International Electrotechnical Commission (IEC) looks into the practice of activities and outcomes with IEC guidelines and expectations.

Founded in 1906, the IEC is the world's leading organization for the preparation and publication of International Standards for all electrical, electronic and related technologies, known collectively as "electro technology". IEC provides a platform to companies, industries and governments for meeting, discussing and developing the International Standards they require.

The "IEC 62282-8" series specifically, aims to develop performance test methods for power storage and buffering systems based on electrochemical modules (combining electrolysis and fuel cells, in particular regenerative fuel cells), taking into consideration both options of re-electrification and substance (and heat) production for sustainable integration of Renewable Energy Sources.

This international standard is to be used for data exchanges in commercial transactions between cell/stack manufacturers and system developers or for acquiring data on a cell or stack in order to estimate the performance of a system based on it. Users of this international standard may selectively execute test items suitable for their purposes from those described in this international standard.

Based on the SOCTESQA project structure and strong collaboration between several European research centres, several test procedures have been developed, each of which aims to cover a wide range of fields of application, e.g. stationary and mobile applications and both fuel cell and electrolysis modes. In turn, each of these test programs can contain several test modules, e.g. current-voltage curves, impedance spectra, dynamic cycles or long-term stationary operation. Based on a large amount of data collected during the experimental campaigns, a critical evaluation of all the results obtained will allow:

1. To identify the most important key operating parameters that may in some way influence the degradation, performance and / or cycling ability of the cell / stack;
2. To investigate the presence of a possible dishomogeneity in results among stacks tested in different laboratories in order to find solutions that can improve the test bench system;
3. To determine the strengths and weaknesses of each test module with the aim of improving them and understanding which procedures can be considered essential and which are not;
4. To extrapolate new performance indicators and methodologies useful for immediately understanding the quality of a generic stack;
5. To develop a complete guide for the management of the Re-SOC stack that must to be respected by anyone who intends to use this device;
6. To develop a complete guideline for collecting and reporting data on research and experimental development;
7. To improve the already existing analysis techniques to make them more accurate and reliable;
8. To provide characterization tools to monitor the health status of the device and extrapolate information useful for the manufacturers to create robust, durable and affordable cells / stacks;

1. INTRODUCTION

Most of the global warming problems in recent decades are the result of human activities such as burning fossil fuels, farming and other industrial processes. In particular, the rapid acceleration of CO_2 and other GreenHouse Gases (GHG) emitted to the atmosphere caused by the combustion of fossil fuels have altered the natural thermal and chemical balances of the planet, causing instabilities with potentially grave consequences for civilization and the ecosystem [1][2][3][4].

Thus, in view of a no-regret policy, it is necessary to decrease the concentration of GHG, through for example the use of standalone or hybrid renewable energy systems. However, these produce a varying supply of energy, especially in large scale and require solutions in terms of grid balancing and power buffering [5][6][7].

One of the most promising devices for the required energy storage and the consequent matching of supply and demand, are Reversible Solid Oxide Cells also known with the acronym of Re-SOC. This technology which can operate efficiently in both fuel cell and electrolysis operating modes has the following attractive features (demonstrated or potential):

- High efficiency in SOFC mode thanks to the direct conversion of chemical energy into electricity;
- Fuel Flexibility, possibility to integrate a large variety of energy sources. Other than pure hydrogen, the Re-SOC can operate on reformates (via external reformation) or on hydrocarbons and other fuels (via internal reforming or direct utilization);
- Insignificant emissions, the electrochemical reactions that take place into the device do not produce CO_2 when the supply is fed only wit Hydrogen
- Adaptability and capability, possibility to cover a wide range of applications in function of local energy needs. Applications include power system ranging from watt-sized devices to multimegawatt power plants and potential markets cover portable, transportation, and stationary sectors;
- Affordability, competitive in costs;
- And others.

Thus, the Re-SOC possesses all the desired characteristics to serve as a technology base for green, flexible, and efficient energy systems in the future [8][9][10][11][12][13].

To introduce innovative technologies into industrial and consumer environments it is necessary that essential requirements in regulations and the associated technical specifications in codes and standards (RCS) be established. In the case of Solid Oxide Cell and Hydrogen Technologies, these have centered around two main themes:

- Safety standards, that are essential safety requirements imposed by normative bodies to reduce the risk of hazards during operation;
- Technical specifications, that define specifications and procurement of testing samples, the overall test matrix and test procedures, and which can also include validation of the cell/stack assembly unit and systems in terms of flexibility, environmental sustainability and efficiency [14][15].

In order to beef up the extent of knowledge with the aim to accelerate the development and the market penetration of hydrogen and fuel cell (H2&FC) energy system in Europe and in the world, many research institutions (ENEA, CEA, DTU, DLR, etc) and industrial companies worldwide (SUNFIRE, SOLIDPOWER, ELRINGKLINGER, etc) are involved in the development and improvements of Re-

SOC, addressing not only the study of the micro-structure of the SOC system (regarding anode/cathode structure, materials for electrolyte, etc) but also the test procedure activities.

In addition, it is important to develop uniform and robust test procedures with the purpose of covering the wide range of power generation modalities that solid oxide cell technology is suited for: stationary micro-CHP, mobile Auxiliary Power Unit (APU) and power-to-gas systems [16][17].

Only few documents can be found in the literature, which address the description and specification of test procedures for SOFCs: these address only single cell tests or system level tests under steady state conditions. The most relevant were developed in the frame of the "FCTESQA" project, which generated test modules for SOFC single cells and stacks in steady state durability tests. In other European projects ("RELHY" or "ADEL"), concerning electrolysis operation, a first protocol of transient operation in SOEC mode was defined and tested for a single cell. None of the existing protocols are focused on the development of test procedures of solid oxide cell/stack systems under dynamic operation conditions or in the reversible mode [18][19].

However, different stacks cannot be easily compared due to non-standardized test programs and discordant results due to different test set-ups. Thus, it is important to mobilise and coordinate several cell and stack testing research institutes and cell and stack manufacturers with the aim of creating a collaborative scientific network to identify the most relevant parameters addressing performance and endurance followed by investigation, adaptation and alignment of data in terms of repeatability, reliability and accuracy among the partners.

Within the SOCTESQA Project, a full set of application specific testing procedures addressing function, performance, durability and degradation have been developed. Besides the technical targets of the testing procedures, health and safety aspects and environmental issues have been addressed in accordance with common practice for similar laboratory activity.

The test procedures aim to cover a wide range of application fields, e.g. stationary and mobile applications and both fuel cell and electrolysis modes. In this context the focus of the test procedures lies on three different operating modes:

- Solid oxide fuel cell (SOFC) operation under electrical current profiles and thermal cycling conditions;
- Solid oxide electrolysis (SOEC) operation under dynamic current profiles;
- Combined SOFC/SOEC operation.

The final test protocols aim to provide guidelines in the characterization of real-time performance and durability of the Re-SOC cell/stack.

Besides the generation of the test protocols, the collaboration among the project partners has provided for the first time access to a large amount of reliable, accurate scientific data regarding stacks tested in different labs, which could be used for a deeper comprehension of all the mechanisms occurring within the Re-SOC device and the evaluation of degradation.

The number and the complexity of the intertwined chemical, electrochemical and thermo-fluid dynamic mechanisms driving the energy conversion of hydrogen into electrical power and heat or vice-versa call for more accurate analysis tools and techniques so as to correctly address the role of these mechanisms in immediate performance and endurance, since jV and EIS methods (Chapter 4) do not provide in-depth data. Additionally, the lack of comparable data among Re-SOC stacks tested in different labs is always a barrier to overcome.

That is why a thorough analysis of all the data collected during the experimental campaigns is essential in order to extrapolate the largest amount of useful information, highlight the pros and cons of the test modules and at the same time identify the critical issues emerged in the project and draft a

list of recurring errors in order to generate more robust test protocols or reinforce those created during the project.

In order to reach the stated objectives, together with the different test modules, a part of the results will be evaluated by application of two specific diagnostic tools: Distributed Relaxation Times (DRT) analysis and Differential Resistance Analysis (DRA).

Distributed Relaxation Times (DRT) analysis is a recently developed method employed in order to deconvolute the electrochemical impedance spectroscopy (EIS) measurements. This enables to shed light on the diverse physicochemical processes occurring within the cells by individuating the characteristic relation time of these.

Differential Resistance Analysis (DRA) is a new approach based on the analysis of the volt-ampere characteristics with increased information capability with respect to Degradation Rate (DR) evaluation. It operates with the differential resistance, i.e. with the derivative of the voltage with respect to the current (dV/dI = Rd) which is more sensitive to small deviations and thus increases the sensitivity of the analysis. Being a new diagnostic tool, literature based on Re-SOC stack investigation is currently totally non-existent.

These approaches will not only help to better understand the electrochemical dynamics that occur within the cell / stack, but will allow to exploit the different results obtained in the best way in order to extract crucial information to study the complex behaviour of the cell / stack in terms of performance and resistance.

In particular, we will see how these diagnostic tools could be optimally integrated into the Re-SOC study pushing the overall study beyond the state-of-art.

1.1. Overall strategy of the work plan

To achieve the research goals, the scientific activity has been divided into four parts each of them concerning the specific research questions above mentioned.

Figure 1 shows the workflow diagram of the entire work also expressed in months. Each dotted set represents specific objectives to be achieved. For the realization of the work, three workflow paths must be taken into consideration. First of all, the development of the test protocols following the technical guidelines of the SOCTESQA project, followed by a long experimental campaign split into 4 validation tests in which the stacks were tested under different operating conditions.

The generation of elaborate processing procedures for the cell/ stack assembly applicable not only in research but also in industrial practice will be the basis to form of an easy-to-understand guideline to cell/stack characterization.

After collecting and reporting all the data obtained, the second part refers to the study of the results in order to confirm a first reproducibility among the partners. Then the critical analysis started with the aim of finding solutions, performance indicators and all relevant information to understand possible connections between the variables. During this part, the two diagnostic techniques were used: the differential resistance analysis (DRA) and the distributed relaxation times (DRT) analysis for understanding the process degradation occurring in the stack.

The third part concerns the study of all critical issues related to the test modules. Recommendations were given to optimize and improve the tests together with a new data processing that facilitates the interpretation of the results ensuring a greater understanding of the quality of the stack.

The fourth and final part regards the insertion process of all the results achieved during the entire PhD period in the document "IEC 62282-8" with the aim of updating the old version and adapting it at the new detailed specifications of SOC cell/stack assembly unit.

The details of the work steps are described as follows:

- The first step concerns the specifications and the definition of the overall test matrix for the SOFC, the SOEC and the combined SOFC/SOEC operation modes. It is important that the test matrix reveals and confirms industry needs. This test matrix and the available test facility characteristics will be the basis for the drafting and definition of the generic test modules and programs. In parallel the test specimens will be defined and procured from solid oxide cell/stack manufacturers. The specific test programs will be defined by integration of the application specific conditions into the generic test modules;
- After the initial definition stage, a test bench validation among the testing project partners has been figured out with the aim of finding solutions to possible test station differences and align the performance of the stack monitored through electrochemical characterization test, e.g. Electrochemical Impedance Spectroscopy (EIS) analysis and current-voltage curves. The efforts for in-depth characterization of the test bench are finalized at obtaining sufficient accuracy, reliability and repeatability of measurements in order for the test procedures to be able to act as benchmark for the definition of international standardization for Re-SOC stack testing;
- Specific test programs have been applied to the SOC cell/stack assembly. The results of the specific test programs are the basis for the validation of the generic test modules. The test modules are then reviewed and modified based on experimental results. Establishment and validation of the generic test modules take places in compliance with the applied specific test programs and consider any relevant feedback from these activities. After a second series of validation and review a final round robin test has been performed and reviewed to ensure comparability of the results obtained in different test laboratories;
- The results of EIS analysis and jV curves of the stacks have been analysed by DRT and DRA. The two diagnostic tools represent together with the EIS analysis and the jV curves, good indicators for better understanding the results among the different partners, giving solidity to the work and useful parameters to characterize and improve the performance of the stack;
- In the final part, after the revision of all test modules in order to optimize and improve them, the work has been concluded with the upgrading of the IEC 62282 in order to create a new standard that describes all the test programs and test modules for a single cell or stack that can be employed in energy storage systems using reversible solid oxide cells (Re-SOC).

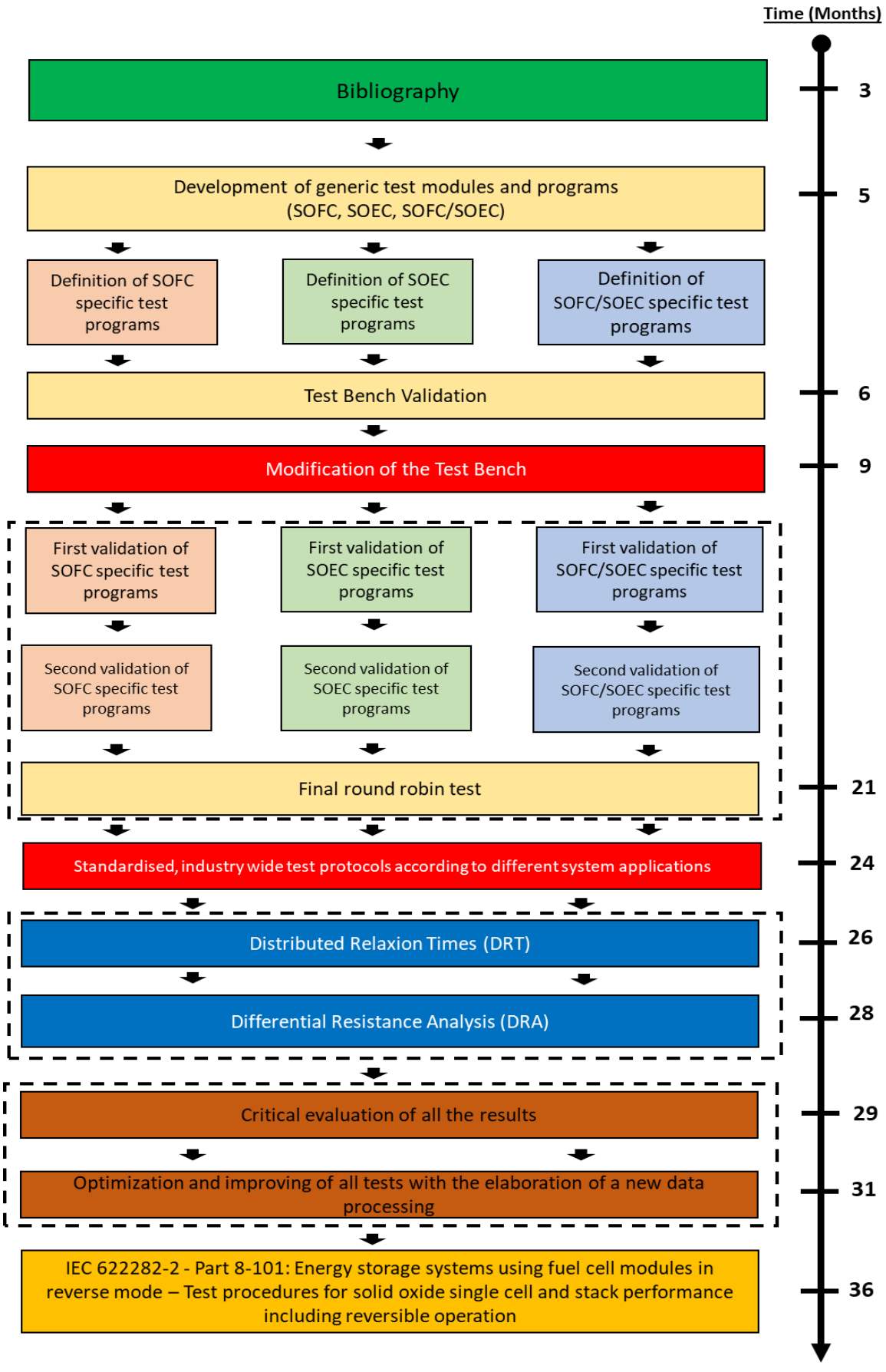

Figure 1. *PhD workflow diagram.*

1.2. Outline

In this work, the operating principles of Re-SOCs and general aspects about the materials and design related to this technology are briefly described in Chapter 3.

In Chapter 4 a description of the principal characterization techniques employed in this work is provided, with particular attention dedicated to the DRT and the novel DRA methodologies and all their useful implications in the analysis of the EIS and jV measurements.

The experimental campaigns, the testing procedures and the experimental apparatus employed are reported in Chapter 5.

In Chapter 6, the experimental results and the discussions related to them are widely reported. In particular, in the first part, after showing the test bench improvements, the contribution of the SOCTESQA Project on the research is presented. Within the SOCTESQA project, test procedures for SOC cell/stack assembly have been developed. Based on those initial results and using them as starting points, the second part regards the application of DRT and DRA methodologies both of which have demonstrated to be advanced characterization techniques for better understanding the process degradation behind the stack. In addition, a critical analysis of all the test results achieved during the experimental campaigns together with those related to the derived quantities and those extrapolated from the different analysis is presented.

Finally, in Chapter 7, the results obtained from the experimental investigations are resumed and conclusions are provided.

2. FUNDAMENTALS

The fundamental aspects of the entire work are summarized in this chapter.

For this reason, after a brief description of the general operating principles and benefits of Re-SOC, all those relevant concepts that will be instrumental for the explanation of the experimental results within this work will be taken into account with particular attention. These also include all the methodology behind the DRT and DRA analysis.

2.1. Operating principles of Reversible Solid Oxide Cells

A reversible solid oxide cell (**Re-SOC**) is a single high-temperature device that can perform efficiently in both fuel cell (**SOFC**) and electrolysis (**SOEC**) operating modes. This implies the following:

- *Electrochemical Conversion (SOFC)* by combination of a fuel (hydrogen, hydrocarbons, alcohols, etc.), with air, used for cogeneration of electricity and heat, avoiding the intermediate steps of combustion - thermal energy - mechanical energy - electrical energy, that are present typically in conventional power generating systems based on internal combustion engines [20].
- *Electrolysis Conversion (SOEC)* producing hydrogen from water or chemicals such as syngas from mixture of water and carbon dioxide, when coupled with an electric power sources. In this case, electricity and also possibly heat are used as energy input [21].

State-of-the-art solid oxide cells (**SOC**) consist of three functional elements (negative electrode, electrolyte and positive electrode) based on ceramic oxide materials of which two electrodes made of ionic and/or electronic conducting ceramics are attached to one purely ionic conducting solid oxide ceramic electrolyte.

Given the capability of Re-SOC to use different reactant supplies, the electrode reactions depend on the stream feedstock. In the simplest case that is using just hydrogen and water, the overall reaction (Eq. 1) can be described as the combination of single reactions that occur respectively at the positive (Eq. 2) and negative electrode (Eq. 3).

$$H_2 + O^{2-} \underset{SOEC}{\overset{SOFC}{\rightleftharpoons}} H_2O + 2e^- \qquad \text{Fuel/Negative electrode} \qquad \text{(Eq.1)}$$

$$\frac{1}{2}O_2 + 2e^- \underset{SOEC}{\overset{SOFC}{\rightleftharpoons}} O^{2-} \qquad \text{Oxygen/Positive electrode} \qquad \text{(Eq.2)}$$

$$H_2 + \frac{1}{2}O_2 \underset{SOEC}{\overset{SOFC}{\rightleftharpoons}} H_2O \qquad \text{Overall reaction} \qquad \text{(Eq.3)}$$

Therefore, SOFC mode corresponds to the reaction carried out from left to right, and SOEC mode to the opposite way. Thus, it is possible to compare physically and operationally electrolysis cells to a normal fuel cells operating with opposite electrode polarity. Figure 3 illustrates the operating principles of the Re-SOC.

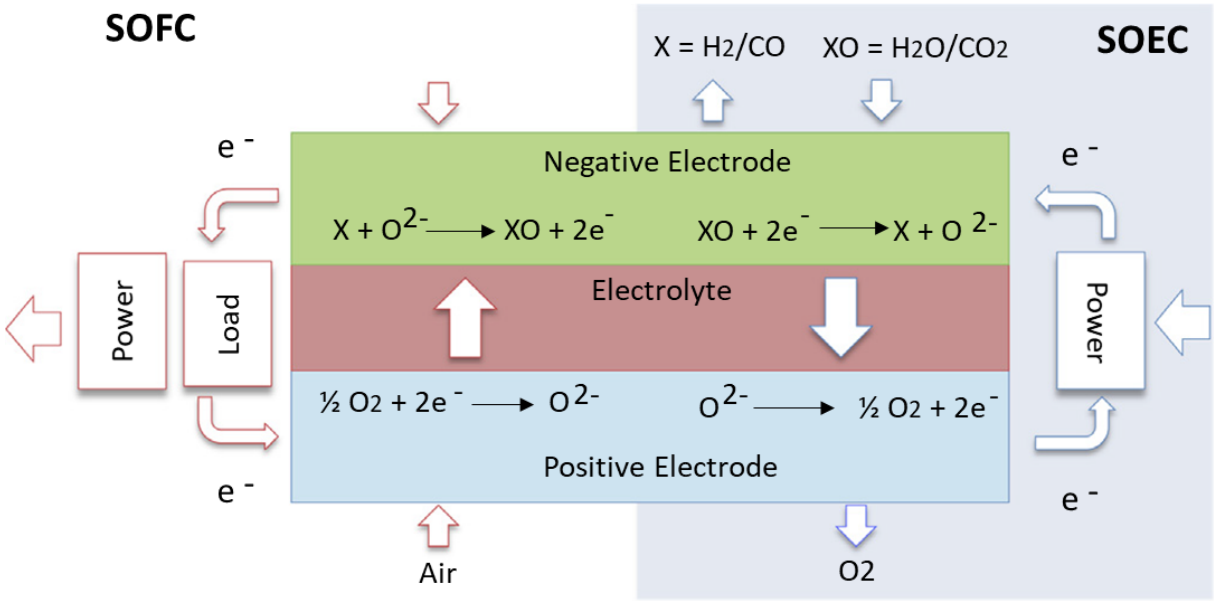

Figure 2. *The Re-SOC device generates high efficiency electricity or chemical storage depending on the functionality of the operation [10].*

2.1.1. The benefits of choosing Re-SOC

In the last decade, the Re-SOC system has drawn the attention of different markets since it possesses the desired characteristics to serve as a technology base for green, flexible and efficient energy systems. The present paragraph has the intent to show all the Re-SOC attractive features (demonstrated or potential), depending on the working configuration, as follows below:

- ***High efficiency, including at small scale:*** differently to conventional technologies such as combustion engines and gas turbines, the device is able to convert directly the chemical energy of fuel into electrical power, avoiding the inefficient steps of combustion and transformation of heat to mechanical work in order to drive the electrical generator. Compared to combustion-based technologies that can only reach 55% electrical efficiency in very large-scale power plants, ideally the Re-SOC device can reach up to 70% of the inlet fuel energy independent of scale, that makes it unique in its kind;
- ***Fuel flexibility:*** thanks to the high operating temperature (650 - 800 °C), low molecular weight hydrocarbons can be internally reformed, without the need for an external reformer. With appropriate conditioning, in order to remove harmful contaminants and to ensure a proper balance of the specific carbon compounds, such diverse fuels can be utilized as natural gas, biogas, ethanol, methanol, propane, LPG (liquefied petroleum gas) and even diesel and jet fuel. In addition, the simultaneous reduction of H_2O and CO_2 to produce syngas in SOEC, increases the utility of these devices within the present energy infrastructure and has the additional benefit of increasing the energy density of an energy storage application by storing a synthetic hydrocarbon mixture rather than hydrogen;
- ***Insignificant emissions:*** thanks to the high efficiency, for a given amount of power produced less primary fuel is required, which means less CO2 is emitted to the atmosphere. If the fuel is obtained from renewable sources, such as biogas, the operation is effectively carbon-neutral, and ultra-clean. Same situation for nitrous oxides (NOx) or fine particulate matter due to the avoidance of combustion processes that usually produce them. Sulphur compounds must to be removed before feeding the cell to avoid poisoning, which means inherently insignificant (SOx) emissions;

- ***Silent operation:*** although initially it does not seem to be important, one of the most remarkable advantages of using the Re-SOC device is the absence of moving parts for power generation thus giving the opportunity to use it both in open spaces and closed areas since the system runs essentially vibration and noise-free;
- ***Adaptability:*** based on the number of cells present in the stack, the device is suitable for a variety of application and adaptable for local energy needs maintaining their properties of fuel flexibility and high electrical and thermal efficiency. Since the systems can be built to any scale between several watts up to several hundreds of kilowatts, the most promising areas for their immediate utilization are:
    1. Mobile, military and strategic (<1kW);
    2. Auxiliary Power Units (APU) and back-up power (1-250 kW);
    3. Stationary small-scale combined heat and power (m-CHP) (1-5 kW);
    4. Stationary medium-large scale (0.1-10MW);
- ***Decarbonisation:*** efficiently producing hydrogen from renewable sources is an important step toward decarbonizing the world energy system;
- ***Electrical Energy Storage (EES) application:*** working as combination between fuel cell system and hydrogen production and storage gives Re-SOC other important features such as the possibility to work as a EES system since it can offer capacity and power independence in the production, storage and use of energy. This additional feature enables to increase penetration of renewable and distributed generation.

On the other hand, problems in durability over extended operating periods, due to the high temperature, costly balance of plant (BOP) required for fuel processing and thermal management have to be solved. However, these problems seem not be insurmountable thanks to the continuous efforts that these devices are receiving from academic and commercial focus.

In order for Re-SOCs to be commercialized, two other important features must be considered:

1. Efficient and stable cyclic operation: Re-SOC stack can operate in SOFC mode without any problem during cyclic (electrochemical-electrolytic) operation, with a performance degradation that respects the normal value that takes place in SOFC devices, while the electrolysis mode typically shows higher degradation rates [9]. However, a complete literature for fuel/electrolysis cells addressing the load cycling issue is still missing.
2. Acceptable electrode performance reversibility and stability: performance stability of both electrodes strongly depends on the microstructure. The oxygen electrode shows performance reversibility at low currents, but displays irreversibility in electrolysis mode at higher current with consequent decay of the performance [9] [11] [12]. To improve this issue, studies should investigate mainly the electrode microstructure to circumvent oxygen pressure build-up at electrode/electrolyte interface. Instead, the hydrogen electrode shows a good performance reversibility in both modes even though improvement could be done to find a solution to facilitate both water (steam) and hydrogen transport to and from reaction sites [9].

2.2. Technology of Re-SOC

The Re-SOC is fundamentally and technologically based on SOFC technology characterized by the use of a solid state construction (ceramic and metal) and high operating temperature (600 – 1000°C). The combination of these features leads to a number of distinctive and attractive attributes including cell and stack design flexibility, multiple fabrication options, multi-fuel capability, and operating temperature choices.

As shown in Figure 3, a typical Re-SOC cell (for explanatory purposes, planar geometry is shown, but the principle applies to tubular geometries as well) is an assembly of two electrodes (with contact layers) and the electrolyte which is integrated in a cell housing. For testing a single cell, ideally, the cell housing design and materials are optimized in such a way so as not to have an influence on cell performance measurement. Therefore, usually the electrical contact resistances of the electrodes in the cell housing are negligible and the supply of the electrodes with fuel and oxidant gases in the cell housing is presumed ideally mixed.

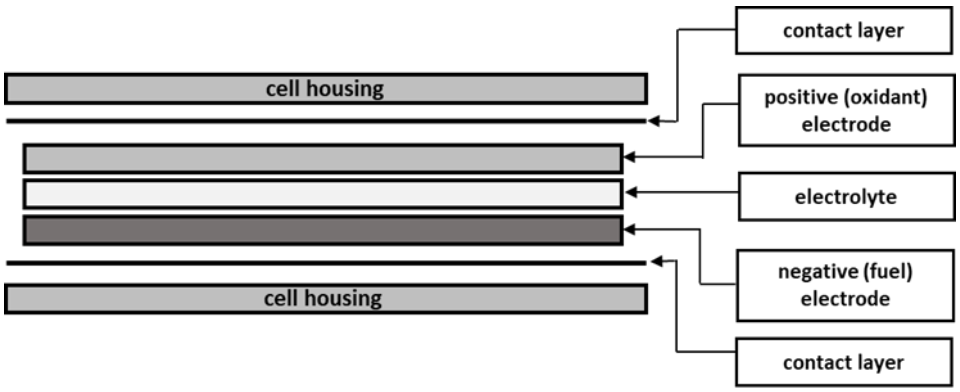

Figure 3. *Scheme of a planar type single cell test object consisting of an SOC in cell housing.*

Attending to the fact that this work deals with Re-SOC devices the electrodes, thanks to their capability of working both as cathodes and as anodes depending on the SOFC/SOEC operating modes, in order to avoid confusion and uncertainty among users and operators will be named as follows:

- Negative electrode (anode SOFC or cathode SOEC);
- Positive electrode (cathode SOFC or anode SOEC);

More specifically it is possible to recognize inside the cell:

- ***Electrolyte.*** The general requirements are **high ionic conductivity**, **null electronic conductivity**, **chemical stability** in both oxidizing and reducing environments, good mechanical proprieties and **long term stability**. Moreover, the electrolyte layer must be gas tight in order to avoid cross leakage of the fuel and the oxidant gas. The most conventional material for SOC electrolyte is 8YSZ ((YSZ: 8% Yttria-Stabilized-Zirconia), which possesses a good conductivity, a good thermal expansion coefficient (TEC), and good chemical/mechanical stability over a wide range of oxygen partial pressures and temperatures [22] [23].
- ***Negative electrode.*** The most commonly applied negative electrode material is a Ni/YSZ cermet, which is a mixture of nickel oxide and YSZ powders that, after the sintering of the material and a reduction procedure during the start-up phase of the cell or stack, results in a final structure in which the skeleton of YSZ stabilizes the porosity of the electrode and provides the separation of finely dispersed metallic Ni particles, that act as a catalyst for the oxidation reaction of the hydrogen. The structure results in stable, well performing and low cost anodes. Nevertheless, even though Ni is a good catalyst for H_2 oxidation, it suffers from carbon deposition when the cells are fed with carbon based, non-conventional fuels and it is extremely sensitive to the poisoning effects of contaminants such as sulphur and tar compounds [24].

- ***Positive electrode.*** Positive electrode materials should possess high electrical conductivity and high electrocatalytic activity for the oxygen reduction reaction. Substances based on perovskyte materials of ABO_3 type are generally used as cathode material. Among them, $La_{0.6}Sr_{0.4}Fe_{0.8}Co_{0.2}O_3$ (LSCF) seems to be a good compromise between thermal expansion mismatch and electrochemical performance. The advantage of such **mixed ionic-electronic conducting** cathodes is their increased reactive catalytic surface area over the whole perovskite grain [26] [27].

Figure 4 shows the scheme of an SOC-stack, consisting of multiple repeating units (RUs) which are assembled in series. The waved line in the middle shows that the number of repeating units is not specified. Electrical contacts and the gas distribution are provided by interconnects and the top/bottom plates. The stack results are generated by the repeating units, which might be influenced by electrical contact and gas flow conditions.

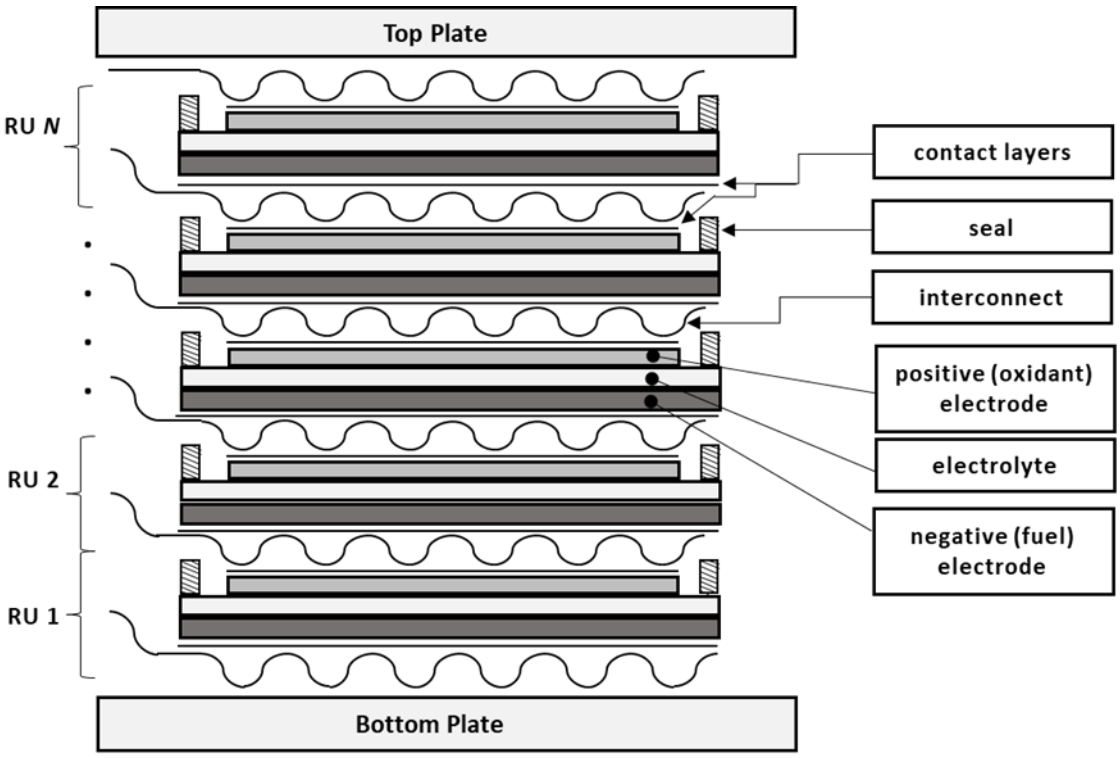

Figure 4. *Scheme of a planar geometry SOC stack with N RU including supporting structure (top and bottom plates).*

In that case, other two fundamental components are needed to be specified:

- ***Bipolar plate.*** Also known as interconnect (layers), it is a conductive plate separating individual cells in a stack, acting as current collector and gas distributor for the electrodes of the SOC. The bipolar plate usually incorporates flow field on both sides for the distribution of reactants and removal of products. The bipolar plate provides a physical barrier to avoid mixing of oxidant and fuel. Thus, it requires a number of different properties to be achieved, such as good electrical conductivity, gas tightness, chemical compatibility with the adjacent electrodes, high corrosion resistance to the gases, good thermal expansion coefficient (TEC) matching and low costs. Principally, interconnects can be divided into two classes of constituent materials: ceramic and metallic materials.

All ceramic interconnects are based on $LaCrO_3$. It is stable but possesses a good electrical conductivity only at temperatures above 800 °C. Moreover, their cost is significantly high, and since the general trend in SOFC systems is to reduce the operating temperatures, in order to reduce costs and ensure longer operations, this type of materials have lost their appeal in favour of metallic interconnects. Metallic alloys have replaced ceramic interconnects due to their ease of manufacture, lower material cost and most importantly, higher electronic and thermal conductivities. However, these metallic alloys present a critical issue during long-term operation of the fuel cell stack: volatilization of Cr-containing species (e.g. CrO_3 and $Cr(OH)_2O_2$) that end up depositing on the surface of the cathode leading to a rapid deterioration of the O_2 reduction rate [28] [29].

- ***Sealant (in planar stacks).*** In a planar configuration, gaskets are required to avoid leakages of gas between the bipolar plates and the electrodes. Seal should be electrically insulating, chemically compatible with different oxide and metallic cell components and stable under thermal cycling between room temperature and operating temperature.
  Also in this case, there are two classes of seals: rigid and compressive. Glass or glass ceramics have demonstrated to be chemically stable in both oxidizing and reducing environments. However, due to the addition of barium or calcium silicates to fulfil the requirements of thermal expansion coefficient, diffusion and segregation of species may occur during long term operation at the interface with the cell. Besides glass-ceramics, compressive seals have also been investigated. They are generally metallic gaskets or mica-based materials. To achieve low leakage rates they generally require high mechanical loads, but possess however a good matching of TEC and chemical stability [30] [31] [32].

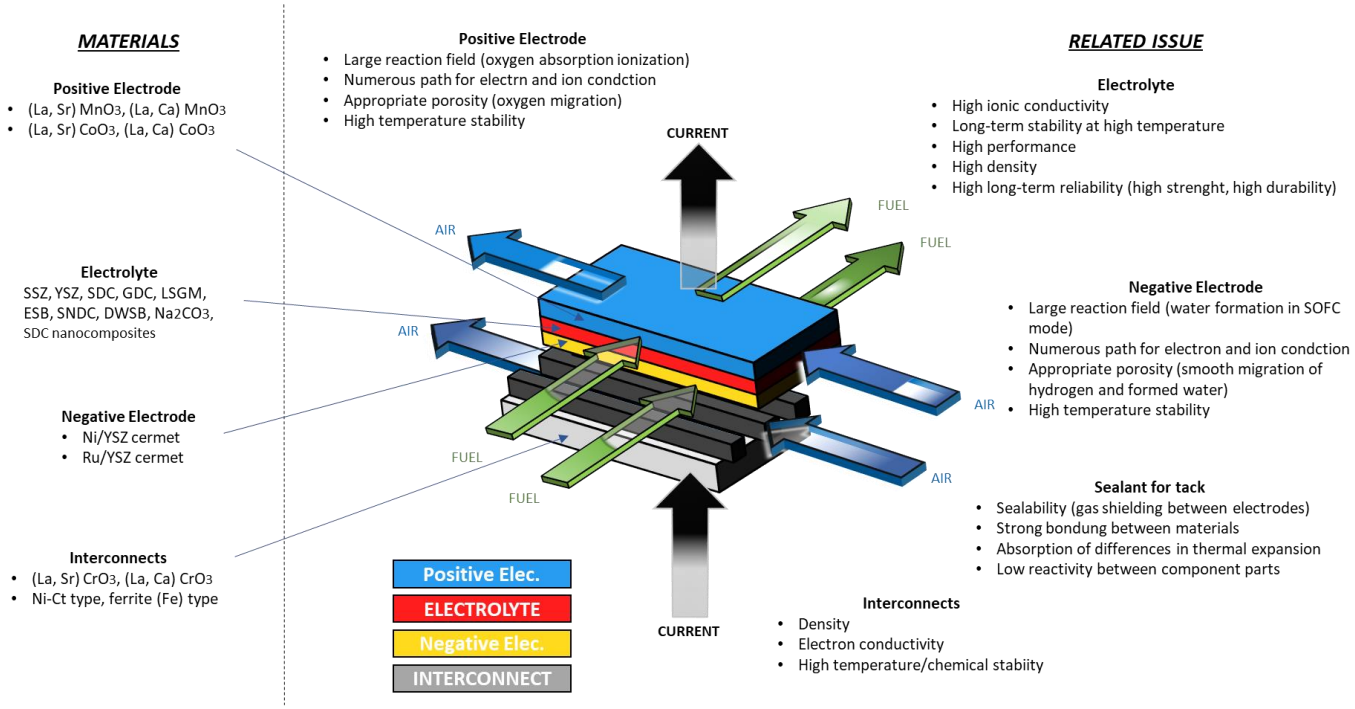

Figure 5. *Materials and related issues for Re-SOC [21].*

When single cells are connected in series to form a stack of the desired power output, other fundamental components are needed: the interconnect layer or bipolar plate and in the case of planar cells, the sealant layers.

2.2.1. Other information related to Re-SOC

The electrochemical reactions occur in the presence of a triple phase boundary (TPB), Figure 6, which can be conceived as a region of contact between three different phases which are electrolyte, electrode and a gaseous fuel. The electrochemical reactions that fuel cells use to produce electricity occur in the presence of these three phases, so the triple phase boundaries can be thought of as the active areas of the cell.

Different mechanisms bring these reactants to a TPB to carry out this reaction. The kinetics of this reaction is one of the limiting factors in cell performance, so increasing the TPB density will increase the reaction rate, and thus increase cell performance. Analogously, TPB density will also influence the kinetics of the oxidation reaction that occurs between oxygen ions and fuel on the anode side of the cell. Transport to and from each TPB will also affect kinetics, so optimization of the pathways to get reactants and products to the active area is also an important consideration.

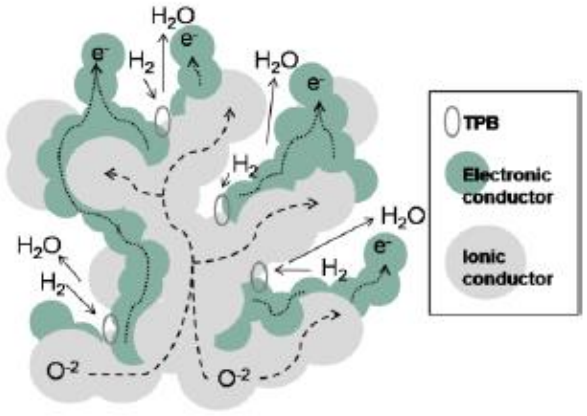

Figure 6. *Diagram of a state of-the-art cermet negative electrode illustrating the paths of electrons and O^{2-} ions in the structure* [25].

However, as regards internal configuration, a Re-SOC cells can be configured to be self-supporting (electrolyte-supported, anode-supported, cathode-supported) or external supporting (interconnect-supported, substrate-supported). Several fabrication processes have been investigated for making SOC cells including conventional ceramic processing methods (e.g. tape casting, tape calendaring, screen printing, and extrusion) and deposition techniques (e.g. plasma spraying, spin coating, dig coating, electrochemical vapour deposition, electrophoretic deposition) depending on the configuration of the cells in the stack.

In addition, stack designs being developed include tubular design, the segmented-cells-in-series design, the monolithic design, and the planar design currently being the most common. These design options permit flexibility to shape the Re-SOC into a structure having the desired electrical and electrochemical performance along with required thermal management, mechanical integrity, and dimensional constraint (if any) to meet operating requirements of specified power generation applications [33].

2.3. Theory of operation

An overview of the general operational features and performance characteristics of a Re-SOC in both fuel cell and electrolyser modes is provided here to facilitate ensuing discussions related to thermo-

neutral voltage and desirable cell operating conditions. Additional background on characteristics of Re-SOC systems can be found in this paragraph.

2.3.1. Reversible cell potential

The theoretical maximum potential difference in a Re-SOC is given by the reversible cell potential, which is obtained under thermodynamically reversible conditions. The following passages develop some thermodynamic relations leading to the analytical expression of the abovementioned potential.

Fuel cells, as any other chemical or electrochemical device, are driven by reactions involving consumption of reactants and generation of products. Equation (4) represents a general reaction involving two reactants and two products.

$$aA + bB \leftrightarrow cC + dD \quad \text{(Eq. 4)}$$

where a, b, c and d are the stoichiometric coefficients of species A, B, C and D respectively.

In the chemistry field, the Gibbs free energy (ΔG) – which is a function of thermodynamic state – expresses the tendency of a reaction to occur under constant temperature and pressure conditions. When $\Delta G<0$ the reaction is said to be spontaneous hence it is shifted towards the product formation, when $\Delta G=0$ the reaction is in equilibrium and when $\Delta G>0$ the reaction is shifted towards the formation of reactants. The Gibbs free energy can be expressed in terms of the activities of the reactants and products, namely:

$$\Delta G = \Delta G° + RT \ln\left(\frac{\gamma_C^c [C]^c * \gamma_D^d [D]^d}{\gamma_A^a [A]^a * \gamma_B^b [B]^b}\right) \quad \text{(Eq. 5)}$$

where ΔG^o is the Gibbs free energy under standard ambient temperature and pressure conditions (SATP[1]), R is the ideal gas constant, T the operating temperature, $[K]$ is the concentration of species K, k its stoichiometric coefficient and γ_K its activity coefficient.

From a thermodynamic point of view, the theoretical maximum work output generated by the stack (fuel cell mode) or the minimum electric input required (electrolysis mode) is determined by the free energy of the electrochemical reaction, which is related to the cell's reversible potential (E_N) via the following relationship:

$$\Delta G = -n_e F E_N \quad \text{(Eq. 6)}$$

where n_e is the number of electrons transferred during the reaction and F is Faraday's constant.

E_N is typically the voltage measured at open circuit (OCV) and it is defined by the Nernst equation.

$$E_N = -\frac{\Delta G°}{n_e F} + \frac{RT}{n_e F} \ln\left(\frac{[A]^a * [B]^b}{[C]^c * [D]^d}\right) - \frac{RT}{n_e F} \ln\left(\frac{\gamma_C^c * \gamma_D^d}{\gamma_A^a * \gamma_B^b}\right) \quad \text{(Eq. 7)}$$

The high operating temperatures of Re-SOCs (600-900ºC) and the relatively low operating pressures (1-3 bar) enable to consider the fluids as ideal gases, hence the activity coefficients take a value of one and the species concentrations can be replaced by their partial pressures. Attending to the aforementioned properties, the Nernst potential (i.e. reversible potential) of a Re-SOC for the particular case when it operates under hydrogen as the only fuel and in open circuit voltage takes the following expression:

$$E_N = -\frac{\Delta G_{rxn}(T_{op})}{2F} + \frac{RT_{op}}{2F} \ln\left(\frac{p_{H2,bulk} * p_{O2,bulk}^{0.5}}{p_{H2O,bulk}}\right) \quad \text{(Eq. 8)}$$

where $\Delta G_{rxn}(T_{op})$ is the Gibbs free energy of the H_2 oxidation reaction at the operating temperature of the cell, while $p_{H2,bulk}$, $p_{H2O,bulk}$, $p_{O2,bulk}$ denote the partial pressure of species *K* in the bulk composition, that is to say the composition under open circuit voltage (OCV).

Considering that the partial pressure exerted by a gas in a mixture is directly proportional to its mole fraction (Eq. (9)), the Equation (8) can also be described as written below in Equation (10):

$$P_i = y_i * P \quad \text{(Eq. 9)}$$

$$E_N^{OCV} = -\frac{\Delta G_{rxn}(T_{op})}{2F} - \frac{RT_{op}}{2F}\ln\left(\frac{y_{eq}^{H2O}}{y_{eq}^{H2} * (y_{eq}^{O2}\frac{P}{P^\circ})^{0.5}}\right) \quad \text{(Eq. 10)}$$

where $y_{H_2}, y_{H_2O}, y_{O_2}$ are the equilibrium mole fractions of H_2, H_2O and O_2 at the electrode/electrolyte interfaces (prior to the electrochemical reaction, *P* is the operating pressure of the cell and *P°* is the reference pressure [34].

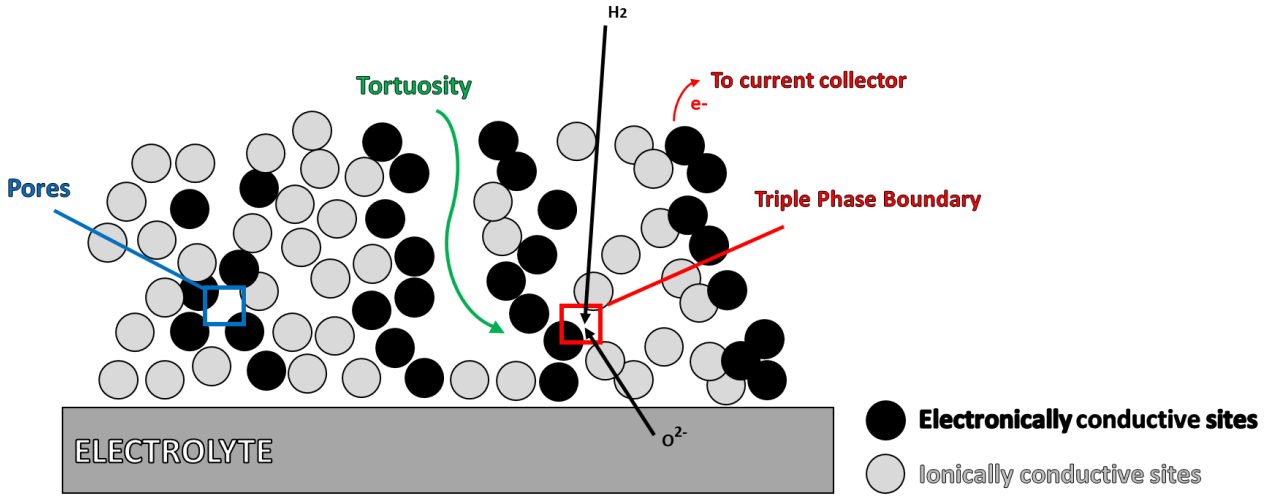

Figure 7. *Composite negative electrode microstructure* [35].

2.3.2. Electrochemical losses (irreversibilities)

The OCV is the voltage measured when no current is being drawn from the system. However, when the system is operating and a current is being drawn or supplied, the operating voltage varies from the OCV due to three main irreversible losses: **Ohmic** losses, **Activation** and **Concentration** overpotentials. Thus, the operating voltage is simply the difference between the OCV and the cell's overpotentials [36]:

$$V_{cell} = E_N^{OCV} - \left(U_{act,pos} + U_{act,neg}\right) - U_{ohm} - \left(U_{conc,pos} + U_{conc,neg}\right) - U_{leak} \quad (6)$$

where E_N^{OCV} is the Nernst potential under OCV, $U_{act,pos}$ and $U_{act,neg}$ the activation overpotentials in positive and negative electrode respectively, U_{ohm} the Ohmic overpotential, $U_{conc,pos}$ and $U_{conc,neg}$ the concentration over potentials in positive and negative electrode and U_{leak} the leakage overpotential.

Activation overpotential: Activation overpotentials in the positive electrode ($U_{act,pos}$) and negative ($U_{act,neg}$) are associated with overcoming the energy barriers at the active sites – the triple phase (see in Fig. 7) boundaries (TPB) – which prevent reactions taking place spontaneously. The larger the activation energy, the bigger the energy supply needed from the reactants to surpass these barriers. Due to the high operating temperatures, activation overpotentials are very low in SOCs [37].

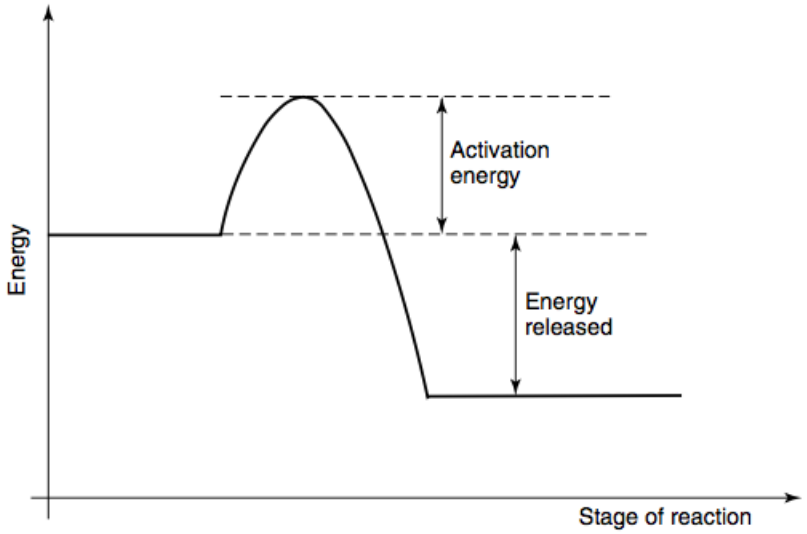

Figure 8. *Schematic diagram of the stages of reaction as a function of the energy [26].*

For electrochemical cells, the equation that relates the current density j to the overpotential generated at an electrode is the Butler – Volmer equation [38]:

$$j = j_0 * \left[\exp\left(\frac{\alpha F \eta}{RT}\right) - \exp\left(\frac{(1-\alpha)F\eta}{RT}\right)\right] \quad \text{(Eq. 10)}$$

where j_0 is the exchange current density, and α is the charge transfer coefficient at the electrode. The exchange current densities are in turn defined as follows, applying an Arrhenius-type equation for both positive and negative exchange current densities:

$$j_{0,neg} = j_{0,neg}^{pre}\left(\frac{p_{H2}}{p_{H2,ref}}\right)^{\gamma_{H2}}\left(\frac{p_{H2O}}{p_{H2O,ref}}\right)^{\gamma_{H2O}} * \exp\left(\frac{-E_{act,neg}}{RT}\right) \quad \text{(Eq. 11)}$$

$$j_{0,pos} = j_{0,pos}^{pre}\left(\frac{p_{O2}}{p_{O2,ref}}\right)^{\gamma_{O2}} * \exp\left(\frac{-E_{act,pos}}{RT}\right) \quad \text{(Eq. 12)}$$

where $j_{0,neg}^{pre}$ and $j_{0,pos}^{pre}$ are the exchange transfer current density pre-exponential factors in the negative and positive electrode respectively, $E_{act,neg}$ and $E_{act,pos}$ the activation energies for negative and positive electrode, $p_{i,ref}$ the reference partial pressures which can all be considered to be equal to the ambient pressure and γ_i is the reaction order of specie i.

When the exchange current density $j_0 \geq 4 * j_0^{pre}$, Equation (13) can be simplified and takes on the name of the Tafel equation, which expresses the activation overpotential as a function of the current density:

$$U_{act} = \frac{RT}{\alpha n F} \ln \frac{j}{j_0} \quad \text{(Eq. 13)}$$

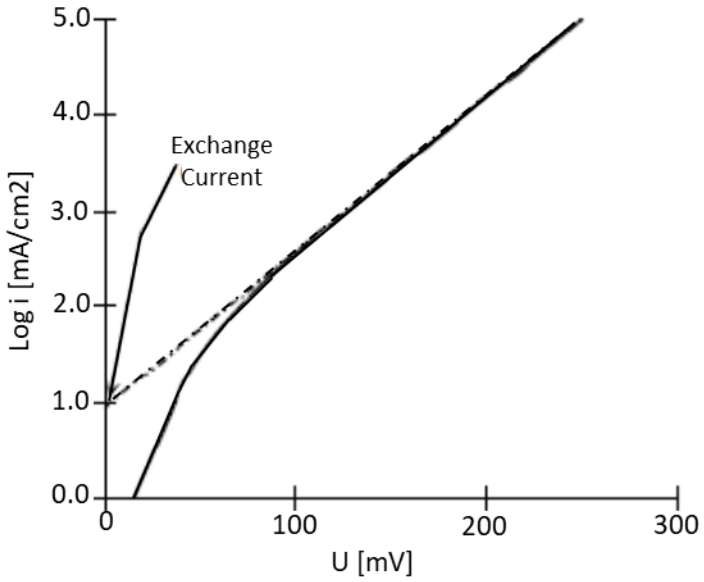

Figure 9. *Example of a generic Tafel plot [27].*

Since for a single electrode, the group $\frac{RT}{\alpha nF}$ can be considered as a constant, the Eq. (13) is simplified as follows:

$$U_{act} = A \ln \frac{j}{j_0} \qquad \text{(Eq. 14)}$$

Where A is the Tafel slope. With linearization it is possible to estimate the values of α and of j_0 from the slope and the intercept of the curve extrapolated for $U = 0$

Ohmic overpotential: The Ohmic losses are caused by the conduction of charge through the ionic and electric conductors within the cell, that in the specific case of Re-SOC are related principally to the transport of oxygen ions across the electrolyte and electronic transport in electrodes and interconnects. They are linearly dependent upon the current density and decreases with increasing temperature [39], and for the electrolyte and the electrode layers, they obey Ohm's law:

$$U_{ohm} = i * R_{ohm} \qquad \text{(Eq. 15)}$$

where i is the current and R_{ohm} contains the contributions of the ionic conduction, the electronic conduction and the contact resistance, so that:

$$R_{ohm} = R_{ion} + R_{el} + R_{cont} \qquad \text{(Eq. 16)}$$

However, in typical Re-SOCs with no contacting issues, the resistance associated to the conduction of O^{2-} ions through the electrolyte layer results the major contribution, so that it is generally valid to consider the Ohmic contribution to the voltage loss equal to that related to the electrolyte:

$$R_{ohm} \cong 2 * R_{ion} \qquad \text{(Eq. 17)}$$

Concentration overpotential: At high current densities or fuel utilizations, the requirement for reactants in the TPB exceeds the gas capability of diffusing through the porous electrodes to these active sites, resulting in an undersupply of fuel (negative electrode) or oxygen (positive electrode) causing a plummet in the cell voltage. Thus for example, during fuel cell operation if the request of

new H_2 in the negative electrode, at the TBP is higher than that provided by the diffusion of gas through the porous matrix of the electrode, the local undersupply of fuel results in a drop of the cell voltage.

The mass transfer through a porous electrode can be expressed by means of Fick's first law [38]:

$$j = \frac{nFD_i(C_i^{bulk} - C_i^{TBP})}{l} \quad \text{(Eq. 18)}$$

where D_i is the diffusion coefficient of the species i, C_i^{bulk} and C_i^{TBP} are the concentrations of the species i in the bulk of the electrode and at the three phase boundary respectively, and l is the thickness of the diffusion layer.

The maximum current, or the limit current, that can theoretically be obtained is when $C_i^{TBP} = 0$, so:

$$j_L = \frac{nFD_i C_i^{bulk}}{l} \quad \text{(Eq. 19)}$$

Combining Equations (18) and (19) this results in:

$$\frac{C_i^{TBP}}{C_i^{bulk}} = 1 - \frac{j}{j_L} \quad \text{(Eq. 20)}$$

By applying the Nersnt equation (Eq. 17), considering ideal gases at operating temperature, the concentration overpotential can be expressed as:

$$U_{conc} = \frac{RT}{nF} * \ln\left(\frac{C_i^{TBP}}{C_i^{bulk}}\right) = \frac{RT}{nF} * \ln(1 - \frac{j}{j_L}) \quad \text{(Eq. 21)}$$

Leakage overpotential: Actually, electrolytes are never perfect fully dense gas barriers, thus leading to fuel crossover from anode to cathode reducing the maximum theoretical voltage. Furthermore, these are never ideal electrical insulators, therefore internal currents appear which further increase the Ohmic losses. Both these losses can be lumped together creating the so-called leakage overpotential (η_{leak}), nevertheless these are neglected in many occasions as their effect is insignificant when compared with the rest of current-dependent overpotentials.

In electrolyte supported cells, activation and concentration overpotentials tend to be small relative to the Ohmic losses, thus the latter overpotentials dominate over a range of currents. This, in turn, results in the typical current-voltage curve for SOC's exhibiting a linear relationship over a wide range of currents. As shown in the representative current voltage characteristic in Figure 10, the relationship between current and voltage tends to be linear except at the extremes, where the reaction becomes mass-transfer limited and the concentration overpotential dominates only at the extreme of high current density [40].

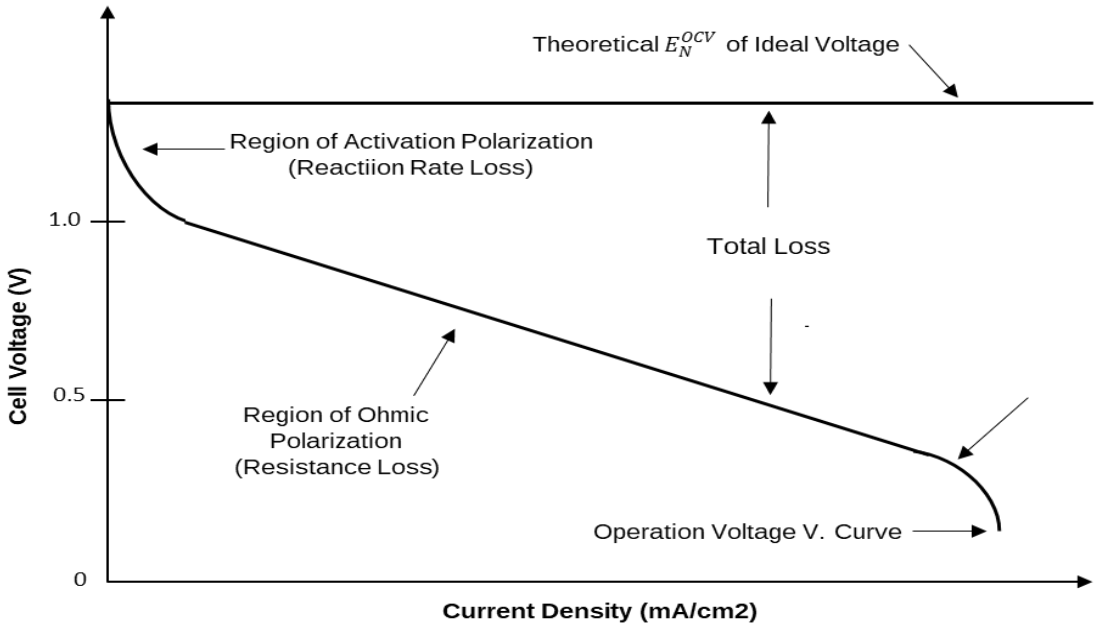

Figure 10. *Ideal and actual performance of a fuel cell with respect to the potential current response* [14].

The cell voltage in each mode of operation is calculated as a deviation from OCV by a current-dependent overpotential, *U*:

$$V_{SOFC} = E_N^{OCV} - \Delta U \quad \text{(Eq. 22)}$$

$$V_{SOEC} = E_N^{OCV} + \Delta U \quad \text{(Eq. 23)}$$

Inefficiency (i.e. overpotential) increases with increasing current density; however, it is essential to operate at reasonably high current density in order to achieve a power density that ensures an economical Re-SOC stack size.

2.3.3. Efficiency considerations

Efficiency is a measurable concept, described as the difference between the amount of produced energy and that put in. Considering an electrical device, the overall efficiency will be given by the product sequence of efficiency of each single part:

$$\eta_{OVERALL} = \prod_{i=0}^{n} \eta_i = \eta_1 * \eta_2 * \eta_3 * \dots * \eta_n \quad \text{(Eq. 24)}$$

Therefore, the efficiency of a Re-SOC system employed for energy storage/buffering (also referred to as overall roundtrip system efficiency) will depend on the efficiency of the cell-stack (overpotential) both in fuel cell mode and in electrolysis mode. The electrical efficiency in SOFC stack can be defined as the ratio of electric power output to the total enthalpy flow input (based on LHV of feed fuel gas) while the electrical efficiency of an SOEC stack can be defined as the ratio of enthalpy flow of fuel gases produced by the electrolyzer to the electrical power consumed by the stack for the electrochemical reaction:

$$\eta_{SOFC} = \frac{P_{el,SOFC}}{\sum_{i=1}^{n} LHV_i * q_{i,neg,in}} = \frac{(I*V)_{SOFC}}{\sum_{i=1}^{n} LHV_i * q_{i,neg,in}} \quad \text{(Eq. 25)}$$

$$\eta_{SOEC} = \frac{\sum_{i=1}^{n} LHV_i * q_{i,neg,out}}{P_{el,SOEC}} = \frac{\sum_{i=1}^{n} LHV_i * q_{i,neg,out}}{(I*V)_{SOEC}} \quad \text{(Eq. 26)}$$

$$\eta_{Re-SOC} = \eta_{SOFC} * \eta_{SOEC} \quad \text{(Eq. 27)}$$

where P_{el} is the electrical power, LHV_i is the lower heating value of fuel component i, $q_{i,neg,in}$ is the inlet flow rate of fuel component i in the negative electrode while $q_{i,neg,out}$ the flow in the output line.

For the specific case where that the charge transferred (oxygen ions) from air to fuel side during SOFC operation is equal to the charge transferred (oxygen ions) from fuel to air side in SOEC mode. and the duration of charge and discharge is equal, the current obtained during electrochemical oxidation (extent of electrochemical oxidation) must be equal to the current supplied during electrochemical reduction (extent of electrochemical reduction).

Thus, working with the same fuel gas composition at the negative electrode, the roundtrip efficiency η_{RT} reduces to a ratio of SOC reactor voltage in fuel cell operation and its voltage in electrolysis operation [41] [42]:

$$\eta_{RT} = \frac{V_{SOFC}}{V_{SOEC}} = \frac{E_N^{OCV} - \Delta U}{E_N^{OCV} + \Delta U} \quad \text{(Eq. 28)}$$

Consider a hypothetical ideal SOC reactor, which is assumed to have no electrochemical losses (Ohmic, activation or diffusion). For an ideal SOC reactor with complete usage of reversible heat, the roundtrip efficiency is the theoretical maximum that can be attained for a set of thermodynamic conditions of temperature, pressure and conversion ratio [43].[44]:

$$\eta_{RT,ideal} = \frac{E_N^{OCV}\,(T_{fc}, p_{fc}, \xi)_{fc,ideal}}{E_N^{OCV}\,(T_{ec}, p_{ec}, \xi)_{ec,ideal}} \quad \text{(Eq. 28)}$$

To achieve high roundtrip efficiency, it is desirable to operate at high cell voltage in SOFC mode and low applied voltage in SOEC mode (i.e. operate at low overpotential). However, it is necessary to consider all the auxiliary power required by the balance-of-plant (BOP) components which involves a BOP energy requirement in both modes of operation Thus in practice, the roundtrip efficiency will be affected by additional overpotential [45].

2.3.4. Thermoneutral voltage

The thermoneutral voltage, V_{TN}, (also referred to as thermalneutral voltage or reaction voltage) is a useful parameter for quantifying the heating and/or cooling requirements of a Re-SOC in electrolysis mode and has been employed previously in the literature in the context of thermal management for SOEC studies.

Strictly speaking, the thermoneutral voltage is equal to the cell voltage where the cell's consumed power is equal to the heat generated by all reactions (chemical and electrochemical) occurring inside the cell. The thermoneutral voltage is typically defined as the change in enthalpy (i.e. heat of reaction) associated with the electrochemical reaction per unit of charge transferred [46] [47] [48]:

$$V_{TN} = \frac{\Delta H}{nF} \quad \text{(Eq. 30)}$$

where ΔH is the molar enthalpy of the electrochemical oxidation reaction, n is the number of moles of electrons transferred in the electrochemical reaction per mole of reactant, and F is Faraday's constant. Thus, V_{TN} can be used to assess the heat removal or addition requirements for electrolysis at a given operating point (e.g. current/voltage).

In SOFC mode, heat is generated when the thermoneutral voltage exceeds the cell voltage because the energy generated by the exothermic fuel cell reaction (Eq. (1)) is greater than the energy removed

from the stack as electric power. In contrast, an electrolyser must be operated at a cell voltage greater than the thermoneutral voltage to generate net heat. Operating at the high overpotential required to generate net heat in a steam-hydrogen electrolyser is prohibitively inefficient for an energy storage application.

To generate net heat in both modes of operation without an external heat source, the following condition must be met:

$$V_{SOEC} > V_{TN} > V_{SOFC} \quad \text{(Eq.31)}$$

A general definition of the thermoneutral voltage is the cell voltage at which the net heat consumed by all of the cell reaction (both electrochemical and chemical) exactly balances the heat generated by the passage of current through the internal cell resistance, thereby resulting in no net heat evolution from the cell. In other words, it is the voltage at which the Re-SO operates both isothermally and adiabatically.

Nevertheless, in practice, a Re-SOC will not be strictly isothermal because of temperature gradients associated spatially varying driving potentials, related to processes such as species transport, charge transfer, heat transfer, and in-situ reforming reactions.

For a typical cell operating with H_2:H2O redox chemistry, the thermoneutral voltage in fuel cell mode is always above the operating voltage, due to the negative entropy associated with the electrochemical reaction ($V_{cell} < V_{TN}$). Thus, in fuel cell mode the cell is always exothermic and requires active cooling. In electrolysis mode, however, it is possible to have operating voltages that are below V_{TN}, which implies that the cell operates endothermically, extracting heat from the environment. In the absence of a high-temperature heat source, operating the cell below V_{TN} implies that the cell cools as it operates. If one wishes to operate exothermically, such that the cell produces more heat than it consumes, the operating voltage must be above the thermoneutral voltage [49]. Table 3 summarizes these relationships.

Figure 11 shows the behaviour of V_{TN} on a typical current voltage plot and the operating regions (voltages) where heat is generated or consumed.

Table 3. *Operating Voltage and Thermoneutral relationship.*

Voltage	Operating Mode	Result
$\boldsymbol{V_{cell} > V_{TN}}$	*Fuel Cell*	$Q_{net} > 0$. Cooling Required
$\boldsymbol{V_{cell} < V_{TN}}$	*Electrolysis*	$Q_{net} < 0$. Heating Required
$\boldsymbol{V_{cell} > V_{TN}}$	*Electrolysis*	$Q_{net} > 0$. Cooling Required
$\boldsymbol{V_{cell} = V_{TN}}$	*Electrolysis*	$Q_{net} = 0$. Isothermal Operation

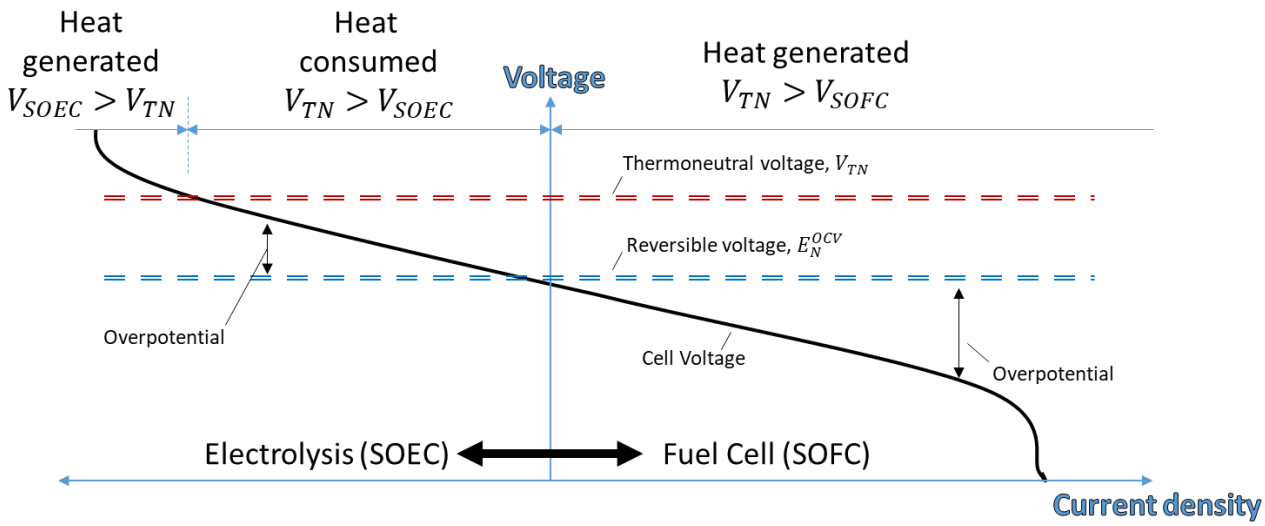

Figure 11. *Representative current-voltage characteristics for a Re-SOC* [49].

3. ANALYSIS TOOLs AND TECHNIQUES

In this chapter, a description of the basics behind the investigation tools and techniques employed is provided.

The first part of this section treats the most renowned electrochemical characterization techniques employed in the study of Re-SOC cells and stacks, namely Polarization Curves (or jV curves) and Electrochemical Impedance Spectroscopy (EIS).

In the second part of the following section instead, will be taken into consideration, the description of the fundamental principles of two different analysis techniques, which are more complex, nut powerful methods of analysis:

- The Distribution of Relaxion Times (DRT) method;
- The Differential Resistance Analysis (DRA) method.

The first one is based on the results achieved during EIS measurements while the DRA is a new approach based on jV measurements. The final outcome of these combined analysis tools (EIS-DRT on one side and jV-DRA on the other) will represent good means to evaluate all the degradation phenomena and understand the mechanisms occurring within a Re-SOC device.

3.1. Polarization curves (Current – Voltage Characteristics)

The polarization curve (also known as jV or I-V curve) is probably the most employed diagnostic technique used to characterize the overall immediate performance of a Re-SOC cell/stack [38][50].

It consists in the measurement of the cell/stack voltage varying the current generated on extracted from an external load, thus it provides information about the general electrical response of the cell over the range of currents investigated.

The I-V curve (see Figure 10) allows to comprehensively distinguish the irreversibilities in electrochemical devices for certain operating conditions (i.e. temperature, fuel composition, etc.), hence resulting in a useful technique for evaluating the operating window of the system. Additionally, it can also suggest hints about the effect of the different polarization losses by examining the different portions of the plot, as indicated below:

- First of all, the Open Circuit Voltage (OCV), measured at I = 0 A/cm^2, can be compared to the theoretical voltage calculated from the Nernst equation and the difference between them is a good estimation of losses related to gas leakage, since the Nernst voltage is the maximum voltage obtained in ideal conditions. Deviations of up to 5% from the theoretical OCV are acceptable for an adequate operation of the SOFC.
- The rapid decrease in the cell voltage in the low current density region is associated to the activation polarizations in the electrodes. Indeed, the relatively high energy needed to overcome the energy barriers in the triple phase boundary in order to thrust the electrochemical reaction induces distinct voltage loss in the cell. The acuteness of this slope can therefore be used to potentially pinpoint criticalities in the fuel cell charge transfer mechanisms.
- The flat central region of the current-voltage curve, having a linear response, can be linked to the Ohmic losses. Because the electrolyte is the layer presenting by far the lowest conductivity, this region is often exclusively associated to this element. The area specific

resistance (ASR) measured in Ω*cm^2, is given by the slope of this straight line and it is generally estimated in order to compare the overall performances of different cells.

- Finally, the fragment of the I-V curve in the high current density region is associated to gas transport losses in the porous structures of the fuel cell (i.e. anode and cathode). It should be highlighted that operation of the SOFC in this region should be avoided by all means because it induces rapid material degradation.

Therefore, this technique is a general characterization method that can be used in SOC research and development and for the quality assurance of SOC cell/stack. Furthermore, it can be used as a reference measurement for the qualification of a SOC in a given application [38][50].

A typical jV measurement profile for combined SOFC and SOEC operating mode is given in Figure 12. Here the example considers the same gas composition for negative and positive electrode gases in both electrolysis and fuel cell modes, leading to the same OCV, but it does not need to be the case.

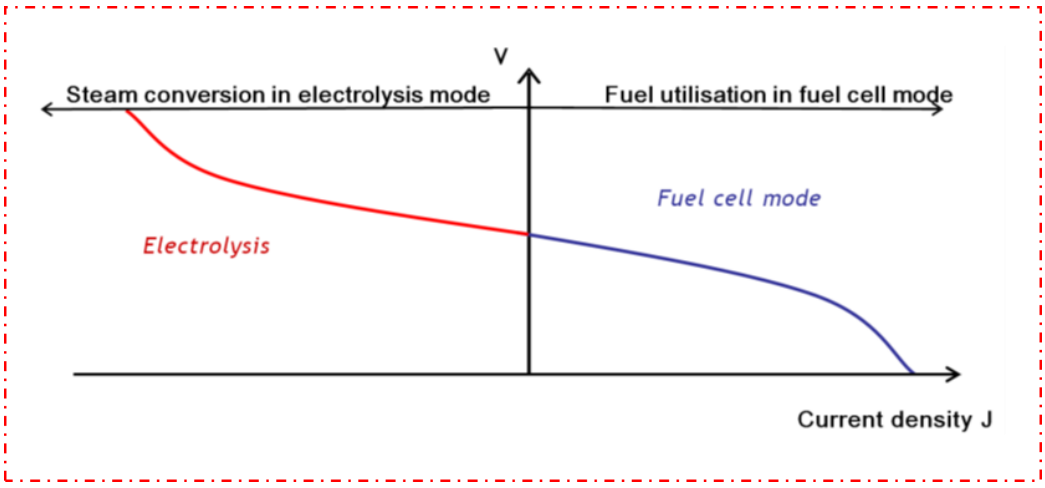

Figure 12. *Schematic representation of a j-V curve in both electrolysis and fuel cell modes*

Notwithstanding the fact that the I-V curve is somewhat a rudimentary technique, it still can provide inestimable information about the health of the reversible SOC and its components:

The test starts at open circuit voltage (OCV) conditions (zero current) up to the specified current or voltage and back to OCV. The current is changed in steps or using a ramp with a defined rate. The total number of steps and each step size should be the same in both the ascending part and the descending part.

At each step, the current is held constant for a specific time t_{dwell} (Figure 13). For each current step k, t_{dwell} comprises the period of equilibration time (t_{eq}) and of data acquisition time (t_{acq}). The equilibration times starts with t_{dwell} and ends with the starting of t_{acq}.

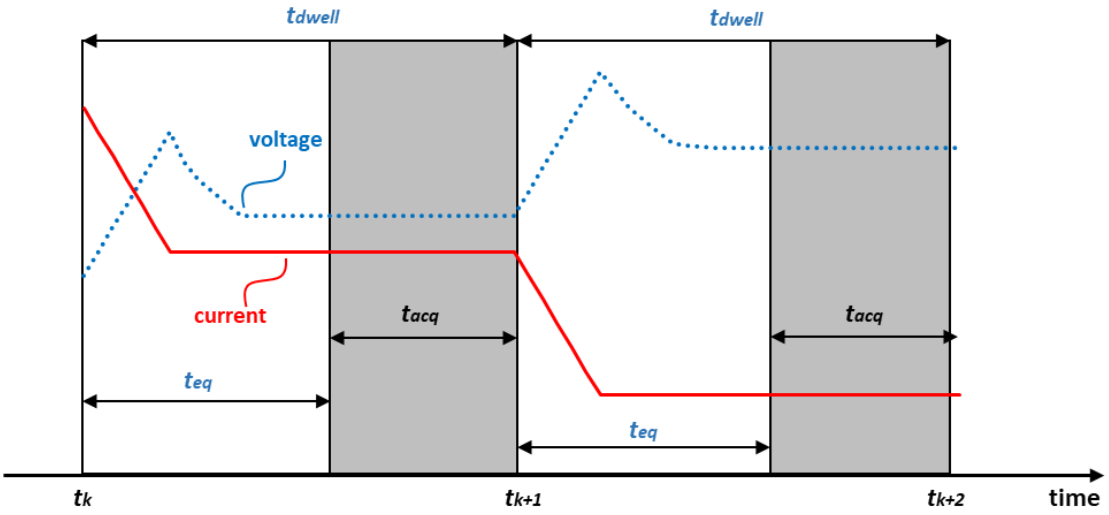

Figure 13. *Schematic of the current-voltage characteristics test for two consecutive set points k and k+1*

By convention the current density J is considered positive in fuel cell mode and negative in electrolysis mode. The fuel utilization is proportional to the current density since the inlet reactant flow rates and compositions remain constant over the duration of the measurement of the I-V curve. Therefore, it can be plotted as a secondary x-axis. As a function of the hold or dwell time, it is possible to effectuate two different methods of analysis:

- Method A – Long hold time data acquisition
  In this method, it is assumed that t_{dwell} is sufficiently long to attain voltage stability during teq and that the temperature variation at each current step is not too significant to strongly affect voltage or to significantly affect the area specific resistance (ASR). The drawback of this method is that it may lead to very long measurement times
- Method B – Short hold time data acquisition: I
  In this method the voltage measurement shall proceed as quickly as possible to prevent the temperature changes that to affect the SOC voltage and the area specific resistance (ASR). At each current step, t_{dwell} (see Figure 13) should be as short as possible to minimize too high temperature excursions but, at the same time, long enough to obtain sufficient representative measurement data.

3.2. Electrochemical Impedance Spectroscopy (EIS)

3.2.1. Principle of EIS

Electrochemical Impedance Spectroscopy (EIS) is a very sensitive technique to analyse processes taking place in electrochemical systems like fuel/electrolysis cells and stacks. It maps an electrochemical cell's response to the application of a periodic small Alternating Current (AC) signal carried out at different frequencies. In contrast to polarization curves, EIS measurements can shed light on the diverse physicochemical processes occurring in the active layers of the cell, as each process has associated a unique time-constant (relaxation time) and therefore each process is exhibited at different frequencies [51].

Thus, EIS analysis besides shows the different frequency dependent impedances of a test object which can either be a cell, a repeat unit of a stack or a complete stack. It is also used to understand the

behaviour of the resistance of the cell/stack test object, e.g. the Ohmic resistance, the polarization resistances of the electrodes and the gas conversion resistances [52].

The fundamental approach of electrochemical impedance spectroscopy is to apply a sinusoidal excitation signal with small amplitude to the system under investigation and measure the corresponding sinusoidal response signal (Figure 14). If the system satisfies contemporaneously the conditions of causality, linearity and time-invariance, the response to a sinusoidal current is a sinusoidal voltage and vice versa, both sharing the same frequency [53][54].

Input Signal: $I(w,t) = \bar{I} * \sin(wt + \theta)$ (Eq. 32)

with: $w = 2\pi f$

An electrochemical system, i.e. a fuel or electrolysis cell/stack assembly, usually consists of capacitive, inductive and resistive components, which create phase angles/shifts between the alternating excitation signal and the corresponding response signal. Thus, the output signal can be formulated as follows:

Output Signal: $V(w,t) = \bar{V} * \sin(wt + \varphi)$ (Eq. 33)

where f being the signal's frequency, w is angular perturbation frequency, $\bar{I}$ and $\bar{V}$ are the amplitude of the current and voltage signals respectively, whilst θ and φ are their initial phases [55].

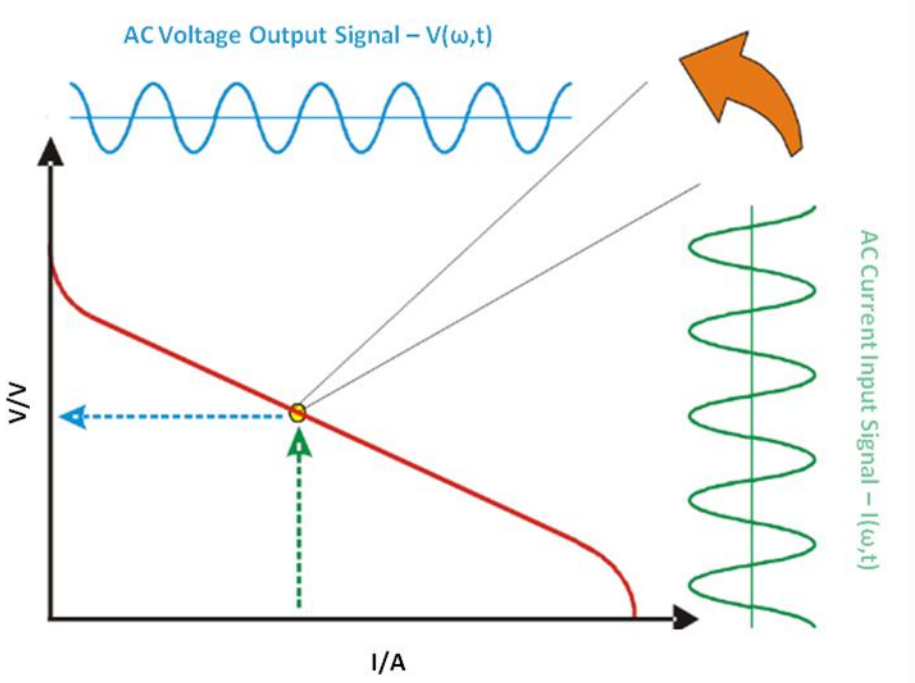

Figure 14. *Input/output signals during Electrochemical Impedance Spectroscopy (EIS) of a solid oxide fuel/electrolysis cell.*

The standardized parameter employed analysing EIS measurements is the impedance, which is defined as the ratio between the voltage and current signals:

$$Z(w) = \frac{V(w,t)}{I(w,t)} = \frac{\bar{V} * \sin(wt + \varphi)}{\bar{I} * \sin(wt + \theta)} = |Z| * \frac{\sin(wt + \varphi)}{\sin(wt + \theta)} \quad \text{(Eq. 34)}$$

Fourier analysis converts a signal from its original domain (often time or space) to a representation in the frequency domain and vice versa:

$$Z(w) = \frac{FFT\{V(w,t)\}}{FFT\{I(w,t)\}} = |Z|\exp[i(\varphi - \theta)] = |Z| * \left(\cos(\varphi - \theta) + isin(\varphi - \theta)\right) \quad \text{(Eq. 35)}$$

or simplified in:

$$Z(w) = Z' + iZ'' \quad \text{(Eq. 36)}$$

The magnitude or the modulus of the impedance can be expressed:

$$|Z(w)| = \sqrt{Z'(w)^2 + Z''(w)^2} \quad \text{(Eq. 37)}$$

$$tan\varphi(w) = \frac{Z'}{Z''} \quad \text{(Eq. 38)}$$

where Z' is the real part of impedance, Z'' the imaginary part of impedance.

From Equation 27 it can be observed how the impedance, being a complex variable itself, is composed of a real and an imaginary part, specifically:

$$Re[Z(w)] = Z'(w) = \frac{V}{I} * \cos(\varphi - \theta) \quad \text{(Eq. 39)}$$

$$Im[Z(w)] = Z''(w) = \frac{V}{I} * \sin(\varphi - \theta) \quad \text{(Eq. 40)}$$

The magnitude and the phase angle of the impedances change with the frequency. Therefore, by varying the frequency of the applied signal, the impedances of the studied electrochemical system can be determined as a function of frequency.

3.2.2. EIS measurements on Re-SOCs

Reversible Solid Oxide Cells couple very diverse mechanisms and processes each of them have a characteristic frequency at which they can be excited by the sinusoidal stimulus provided by a Frequency Response Analyzer (FRA) and the electrical response, measured in terms of amplitude and phase shift of the signal, is the response of that single process having its maximum intensity at that particular frequency. These physicochemical processes occur contemporaneously, making Re-SOC non-linear systems. Nevertheless if the excitation single is small enough ($V < 10mv$), the response can be assumed to be linear (see Figure 15), causal and time-invariant, therefore the mathematical properties above mentioned can be applied [55].

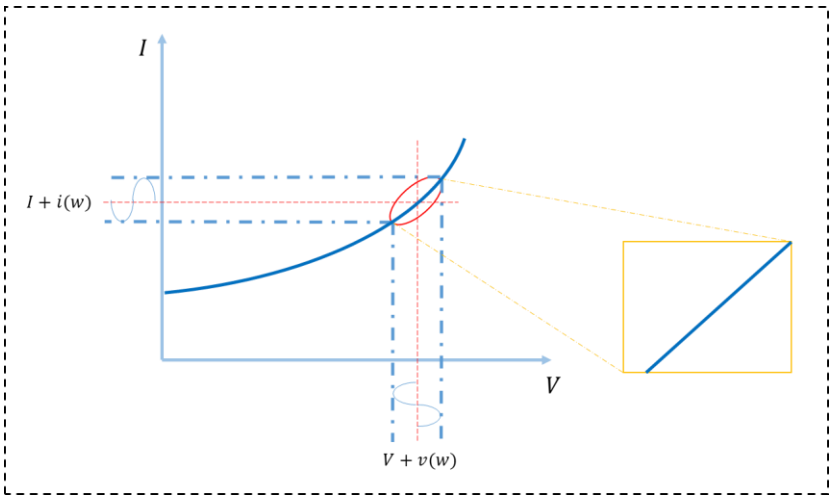

Figure 15. *Linear response to a small excitation input signal in an electrochemical device.*

Electrochemical impedance spectroscopy measurements are carried out in a defined range of frequencies and for a finite number of points, therefore in order to obtain the maximum possible information from the phenomena driving the operation of Re-SOCs, these measurements should be performed from very high frequencies (c.a. 100 kHz) to very low frequencies (10 mHz or below) at relatively short intervals (at least 10 points per decade on a logarithmic scale).

In an EIS spectrum the directly achieved output parameter is the sinusoidal voltage (in galvanostatic mode) or the sinusoidal current (in potentiostatic mode). Moreover, the phase shift between the excitation signal and the corresponding response signal is measured directly as an output parameter. It is possible to obtain an electrochemical impedance spectrum by calculation of the corresponding impedances (see equation 34). One way is to calculate the total impedance as a function of frequency. Another possibility is to divide the total impedance (Z) into the imaginary part (Z'') and the real part (Z').

There is more than one way to illustrate the results of impedance spectra in order to interpret the processes in the cell/stack. A Bode plot shows for example the phase angle and the modulus of impedance (see Figure 16) as a function of frequency. Another option is to plot the real and imaginary part (see Figure 17) as a function of frequency. Assuming the impedance reaches a constant level at low frequencies, the low-frequency resistance R_{LF} can be easily read from this graph. This represents the overall impedance of the test object, the ASR (Area Specific Resistance). The lowest point of the impedance shows the high-frequency resistance R_{HF} which can be seen as the ohmic resistance of the cell/stack. The changes of the phase angle and the slope of the impedance are related to the different loss processes appearing at different frequency ranges [56][57].

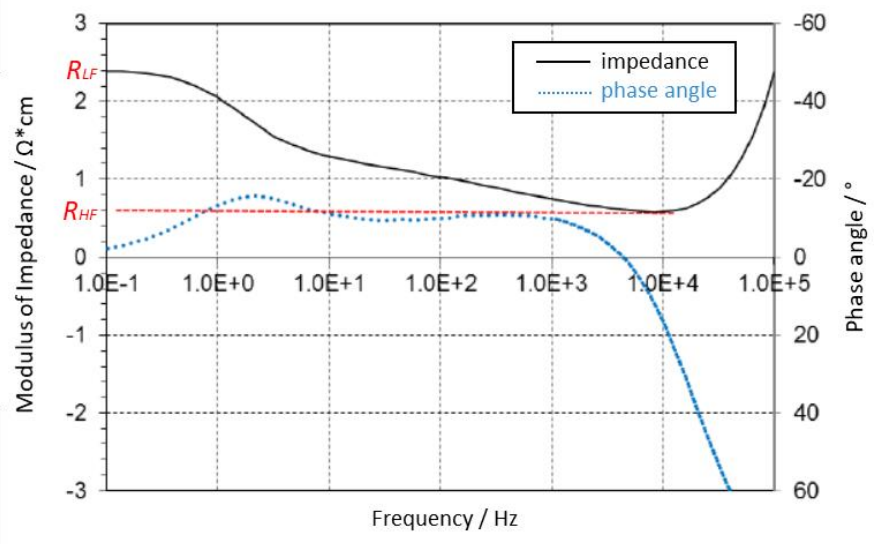

Figure 16. *Bode plot representing the modulus of impedance and phase angle vs. frequency.*

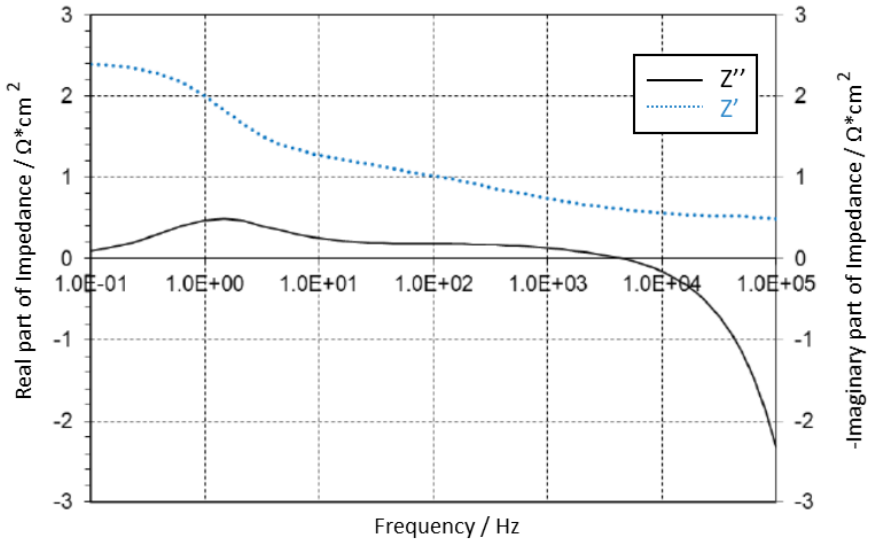

Figure 17. *Bode plot representing real and imaginary part of impedance vs. frequency.*

In a Cole-Cole diagram - often also called Nyquist diagram - the conjugated imaginary and real parts of the impedance are plotted (see Figure 18). In this case, the low-frequency resistance R_{LF} is given by the (second) intersection of the curve with the x axis. The intersection of the tangent drawn to the curve with the x axis shows the value of R_{HF} (or R_{ohm}). The difference of the high frequency resistance and the low frequency resistance gives the non-ohmic resistance of the cell/stack – often also called polarization resistance (R_{pol}). This value usually contains the polarization impedances and the gas conversion impedances of the positive and negative electrodes. In the Cole-Cole diagram the arcs are caused by frequency dependent processes, e.g. the electrochemical process at the electrodes and gas concentration processes of the electrodes.

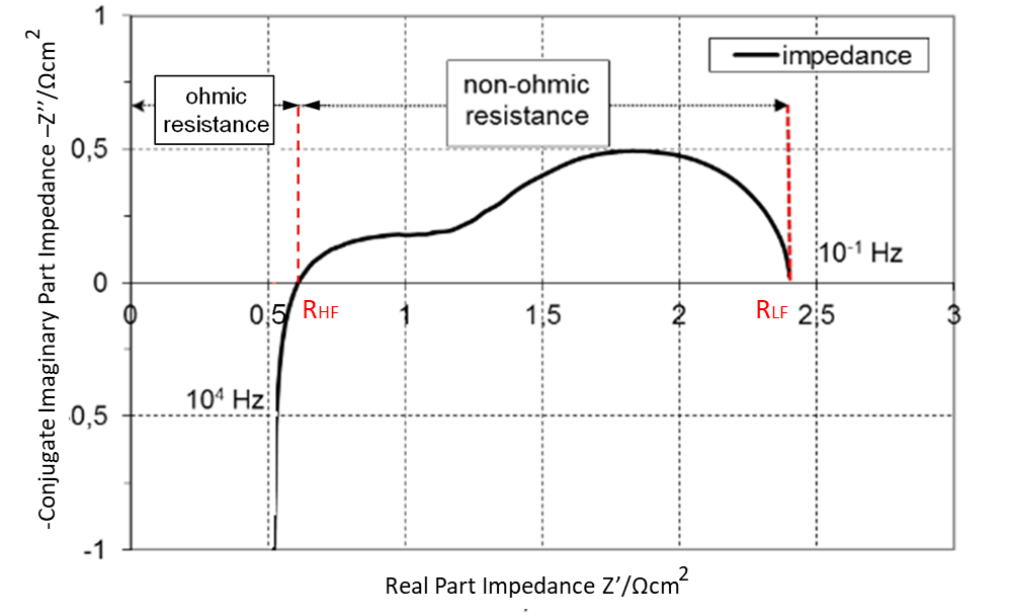

Figure 18. *Cole-Cole plot representing imaginary part vs real of impedance*

3.3. Distribution of Relaxation Times (DRT) method: deconvolution of signals

Even though the information obtainable from the analysis of Nyquist plots provides quantitative measurement about the polarization losses, nothing can be said about which process, anodic or cathodic, is predominant for a given amount of polarization loss; moreover, since the EIS response appears very broadened, it is difficult to clearly visualize the contributions of single physicochemical processes to the total polarization resistance, hence impeding a profound and complete comprehension of the evolution of these processes and their dependency on the operating conditions of the cell.

In this Section, a novel and reliable deconvolution methodology for the EIS spectra will be extensively explained.

As explained before, Re-SOCs are complex electrochemical devices, in which many processes occur at the same time, each of them characterized by a typical relaxation time. When two (or more) processes have a similar relaxation time, it is hard to separate and distinguish their contributions to the overall impedance of the cell, since the EIS spectra can clearly distinguish processes separated at least by two decades in the frequency domain. Furthermore, it is hard to identify small contributions, these being totally covered by processes with large polarization losses.

The Distributed Relaxation Times (DRT) method, is a mathematical tool which allows to overcome this issue, by calculating the d relaxation times of the processes from the experimental data [58].

It is based on the validity of the Kramers-Kronig equations for the cell studied [59][60]:

$$Z'(w) = R_{ohm} + R_{pol} * \sum_m \frac{1}{1+(w\tau_m)^2} * \alpha_m \quad \text{(Eq. 41)}$$

$$Z''(w) = R_{pol} * \sum_m \frac{-w\tau_m}{1+(w\tau_m)^2} * \alpha_m \quad \text{(Eq. 42)}$$

where τ_m is the relaxation time of the process m and α_m is the contribution of the process m to the total polarization loss.

The DRT function can be calculated either from Eq. (41) or (42). Considering the Eq. (42) expressed in its matrix form and introducing the constant value of the polarization resistance into the distribution vector $b_m = R_{pol} * a_m$, it results:

$$Z'' = \boldsymbol{K} * \boldsymbol{b} \quad \text{(Eq. 43)}$$

To solve Eq. 43, the Tikhonov regularization algorithm has been employed [61][62]. This algorithm allows to obtain the distribution vector $\boldsymbol{b}$ as:

$$\boldsymbol{b} = (\boldsymbol{K}^{-1} * \boldsymbol{K} + \lambda^2 \boldsymbol{I})^{-1} * \boldsymbol{K}^T * Z'' \quad \text{(Eq. 44)}$$

where $\boldsymbol{I}$ is the identity matrix, and λ is the self-consistent regularization parameter that must be optimized: too small values result in artificial meaningless peaks, while too large values excessively smooth out the shape of the distribution function.

NOTE 1: The symbols in bold correspond to the matrices.

The solution of the Eq. (44) is governed by λ. Depending on the value of λ, fluctuations in proximity of the peak may appear; however, the optimal value of λ, which minimizes the fluctuations related to the calculation process, can be estimated from the L-curve of the Tikhonov regularization method [63]. Various method have been developed for the selection of optimal regularization parameters (e.g.

Discrepancy principle, Generalized cross validation method) but the L-curve is the most used due to its robustness and ability to treat perturbations consisting of correlated noise [64].

The L-curve is basically a trade-off curve between two quantities that ought to be controlled contemporaneously: data fitting and contribution from data errors. On the one hand too large values of λ tend to over-smooth the shape of the solution curve not fitting well with the given data and hiking the value of the residual $\|Kb - Z''\|$. On the other hand too small values of the regularization parameter result in a good fit but artificial meaningless peaks will be present in the solution due to the excessive contribution form data errors making $\|b\|$ too large (see Figure 19). The optimum value of λ corresponds to the angle of the L-shaped curve, which is the point where the residual norm and the solution norm have a minimum value contemporarily. Attending to the particular example in the figure below, the optimum value is in the proximities of λ = 0.01.

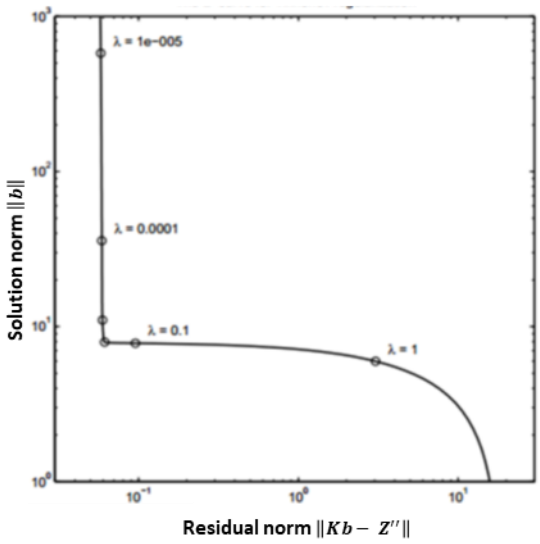

Figure 19. *L-curve for Tikhonov Regularization* [65].

Figure 20 and 21 are two typical examples of DRT analysis. The first shows the imaginary part of the impedance of a dummy-cell compared to the distribution function obtained from the DRT calculation as a function of the frequency while in the second one the imaginary part of the EIS spectrum of an IT-SOFC button cell with active surface of 2 cm^2 is shown. The two figures are both related to the DRT analysis as a fitting strategy but show different cases.

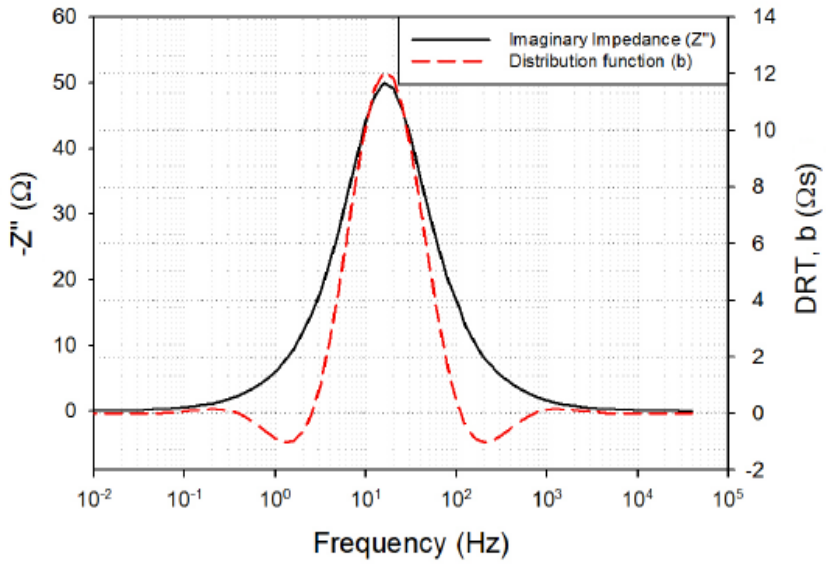

Figure 20. *DRT distribution function with the imaginary part of the impedance of a dummy-cell.*

Observing Figure 20, it shows that the DRT calculation does not affect the characteristic frequency at which the process occurs but marks it out more distinctly, while in Figure 21, 6 different peaks can be distinguished from the imaginary part of the EIS measurement

The nature of these peaks will be discussed in the next paragraph through a systematic experimental campaign conducted in the ENEA laboratories earlier than this work, in which the objective was to understand the anodic or cathodic process behind each peak according to the parameters set (charge transfer or mass transport phenomena).

The DRT method has been already successfully employed in the study of physicochemical processes occurring in anode-supported SOFCs operating in humidified hydrogen or in reformate fuel, in tubular SOFCs, and in the study of degradation effects, providing profound insights about the number, nature and behaviour of the diverse processes that determine the overall response of a SOFC, under a broad range of different operating conditions [66][67][68].

It is important to underline that the quality of the experimental data plays a fundamental role in the interpretation of the DRT plots. If the experimental spectra are affected by instrumental interference that cause a loss in the linearity of the EIS response, scattered signals appear in the EIS spectra that will be converted in ghost peaks into the DRT plots, impeding a correct identification and analysis of the processes [69][70].

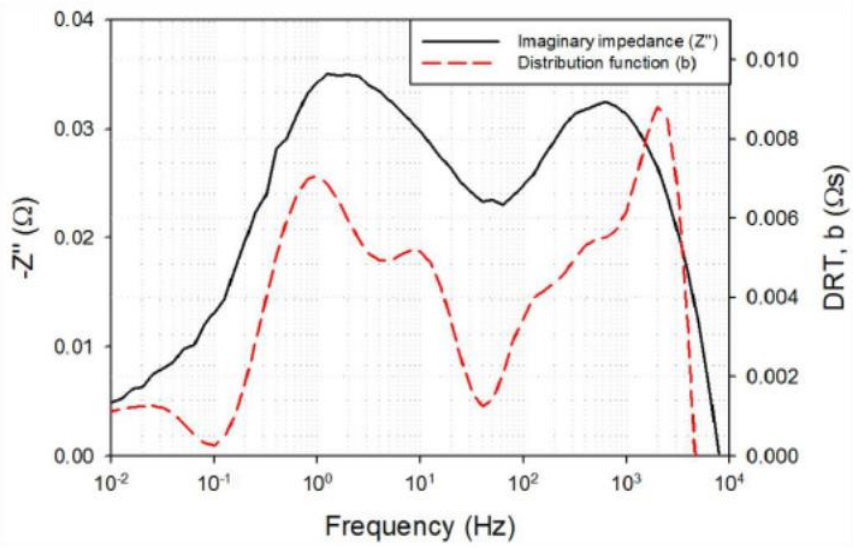

Figure 21. *DRT distribution function with the imaginary part of the impedance of an IT-SOFC button cell.*

In addition, it is important to know that the physicochemical and electrochemical processes taking place in a fuel/electrolysis cell or stack repeat unit can be modelled as an equivalent circuit consisting of passive elements such as resistors, capacitors and inductances. Factually, these processes are distributed in space and time hence special circuit elements describing these realistic phenomena are usually taken into consideration. For instance, the Warburg element is often employed to represent the gas diffusion impedance of the SOC electrodes while the generalized constant phase element (CPE) usually replaces the ideal capacitor. Each element of the equivalent circuit represents a physicochemical or electrochemical process taking place in the cell/stack layer and is excited at a particular characteristic time. There are many different equivalent circuit models (ECMs) which are described in literature, for example in [69][70], yet there is discrepancy on how these should be chosen/built. Different equivalent circuit models have shown to have virtually identical frequency dependent impedance behaviour.

After choosing a suitable equivalent circuit model, initial values are assigned to the elements in the model. These values can be determined in different ways. The starting values for the model can be read out from the Cole-Cole or Bode plot. The initial values are provided as input to the simulation model. Using complex nonlinear least squares (CNLS) algorithm, software can generate a curve (which is referred as a "fit") for simulating the experimental result. At the end of the simulation, the values for the various resistors, capacitors and the inductor are identified and they can be used in a computational model with the aim of generating a model that deviates as little as possible from the real behaviour.

EIS analysis, DRT methodology and the CNLS algorithm is typically used for study the response of the button/single cells when different parameters are continuously varied. The combination of these three instruments can be recognized as a powerful tool for analysing the behaviour of a single cell. Use of these can be useful for:

- characterize different materials used within the device in order to find the best that can replace existing ones;
- identify parameters such as Diffusion, Tortuosity and others in order to improve the quality of the computational models;

3.3.1. Process identification – Brief summary of previous works

During previous works carried out in ENEA's laboratory, an experimental procedure was conducted for the identification of the different operating processes on button cell samples with active area equal to 2 cm^2.

To identify all physic-chemical processes occurring in the cell which contribute to the overall polarisation losses and investigate their parameter dependency, a series of impedance measurements was carried out by varying one parameter at a time such as fuel and oxygen composition and operating temperature.

The higher resolution of the DRT analysis has allowed the identification of losses with characteristic frequencies separated by only half a decade as demonstrated by the comparison of a typical spectrum of an ASC and the corresponding DRT. Unlike the impedance curve where the processes overlap, at least five processes were clearly distinguished in the calculated DRT.

Depending on the changing parameters each process has showed a particular behaviour that permit to hypothesize its physical origin. The results of the process identification are addressed below (see Figure 22):

- At high frequency two processes “P1” and “P2” were identified. Both these contributions are barely affected by a change in the negative electrode composition but show a prominent dependency on the operating temperature. These behaviours suggest a fast, thermally activated negative electrode process underlying these peaks; with furthermore, the process P2 is also more sensitive to a variation of the fuel composition respect to the P1 process. Together with their high characteristic frequencies, they have been both ascribed to the electrochemical oxidation of the fuel occurring at the negative electrode side. In particular, the process P1 is related to the transport of O^{2-} ions within the YSZ matrix of the negative electrode functional layer. The process P2 is in turn identified with the charge transfer mechanism of the electrochemical oxidation of the fuel occurring within the negative electrode functional layer, in the triple phase boundary. This attribution perfectly agrees with other works carried out on YSZ-based negative electrode supported SOFCs reported in literature by other authors [66][70][71][72][67]. The two peaks present a squashed deflection-curve when the button cell works at 750°C with a composition in H_2/N_2 of 50/50%.

- Peak P3 appears around the frequency of 10^2 and it is unaffected by a modification of the negative electrode molar fractions, but shows an exponential dependency on the operating temperature, that allows associating this feature to the charge transfer mechanism related to the oxygen reduction within the positive electrode layer. The results are in agreement with other works [73][69][66][67][70]. Also in this case, working at high temperature, the peak results squashed.

- In the low-frequency region, two distinct peaks have been identified. One falling at c.a. 1 Hz and the other one around 10 Hz which shows similar behaviour when the negative electrode composition and the operating temperature are altered. They both showed a prominent dependency on the negative molar fraction variations and they are only marginally influenced by the increase of the temperature. Thus, it was reasonable to ascribe these two peaks to a single mass transport phenomenon (P4) associated with the diffusion of species through the porosity of the negative electrode supporting layer of the cell [71][72][74][67].

- Finally, the process P5 falls at very low frequency. This peak does not change with a change in the negative electrode composition thus it was hypothesized to be the contribution of the gas diffusion through the porosity of the positive electrode layer in the MIEC porous structure [73]. In addition, Leonide et all showed a visible new process evolves in the frequency range below 10 Hz. It is reported in literature that significant and coherent variations of the positive electrode processes are achievable only for a very low oxygen content in the positive side (for a partial pressure of oxygen ≤ 0.21 atm) [69][71].

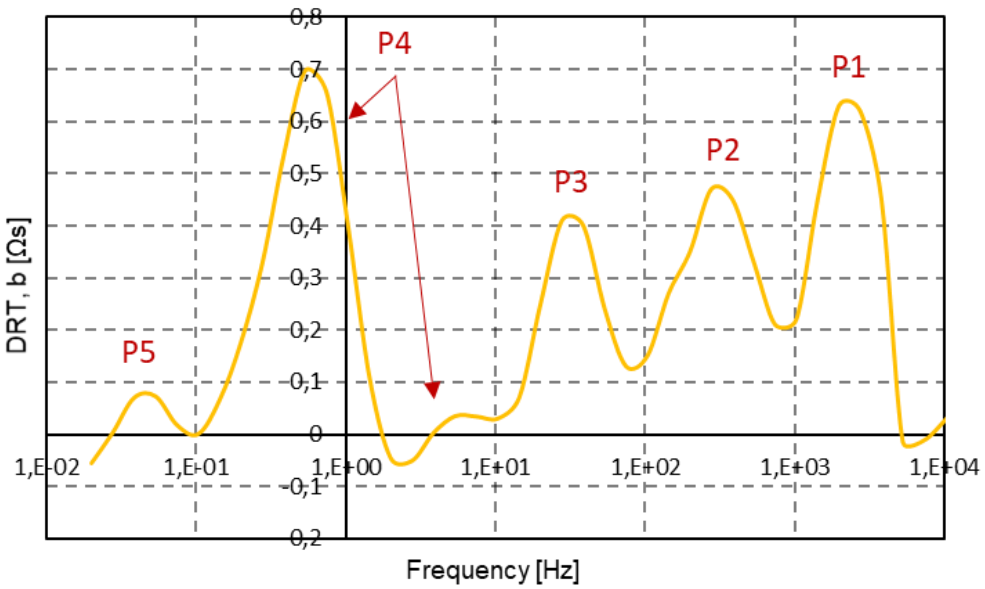

Figure 22. *Example of DRT distribution function. 5 processes are visible in the distribution curve.*

During the experimental campaign also changing in current was investigated but unfortunately in all the measurements carried out under constant current a very poor resolution of the experimental EIS spectra was obtained. When the experimental points result largely affected by noise, the incoherent signals produce scattered points in the EIS spectra, that in turn greatly affect the DRT response, which then loses its effectiveness.

However, from the expression of the Butler-Volmer equation it is expected that during the change in current through the cell, both peaks related to the charge transfer process should show a significant variation in their intensity; moreover, the current generation is correlated to the oxidation of the fuel in the negative side, which causes a reduction in the fuel content and an increase in the content of the product at the negative electrode, thus influencing the processes associated with gas transport.

Based on the results obtained by other authors in the literature, an increase in current should correspond to a decrease in intensity and a slight shift towards high frequency. Moreover, peak 4 related to the diffusion of the gas in the negative electrode should be the one most influenced [75][76].

3.4. Differential Resistance Analysis

Differential Resistance Analysis (DRA) is a new analytic tool based on the current-voltage characteristics. Two performance indicators with differing selectivity can be extracted:

- $R_{d,min}$, sensitive to transport hindrances;
- ΔV^*, sensitive to activation losses;

Both performance indicators can be extracted by analysing the IV-curve as shown in Figure 23.

Via combination with impedance measurements and numerical modelling, the two DRA parameters can give deeper insight about the origin of the degradation phenomena sources and improved understanding of ageing factors and their interactions within the cell.

The idea arises from the consideration that the IV-curve can be used as performance indicator since its shape is sensitive to conditioning parameters and level of degradation. Thus a periodic measurement of IV-curves during testing of cells and stacks life at constant external operating conditions can ensure quantitative estimation of those deviations reflecting degradation and its rate [77].

3.4.1. Methodology

As mentioned in the previous paragraph (4.1), the IV-curve is usually used to describe the cell/stack performance and different parameters can be extracted such as:

- the open circuit voltage E_N^{OCV};
- the maxim power density P_{max};
- the internal (secant) resistance R_i at P_{max} ($R_i\ P_{max} = E_N^{OCV} - {}^{E_{P_{max}}}\!/_{I_{P_{max}}}$);
- the area specific resistance ASR;

Figure 23 show an example of IV curve with its relative Power Density trend expressed in W.

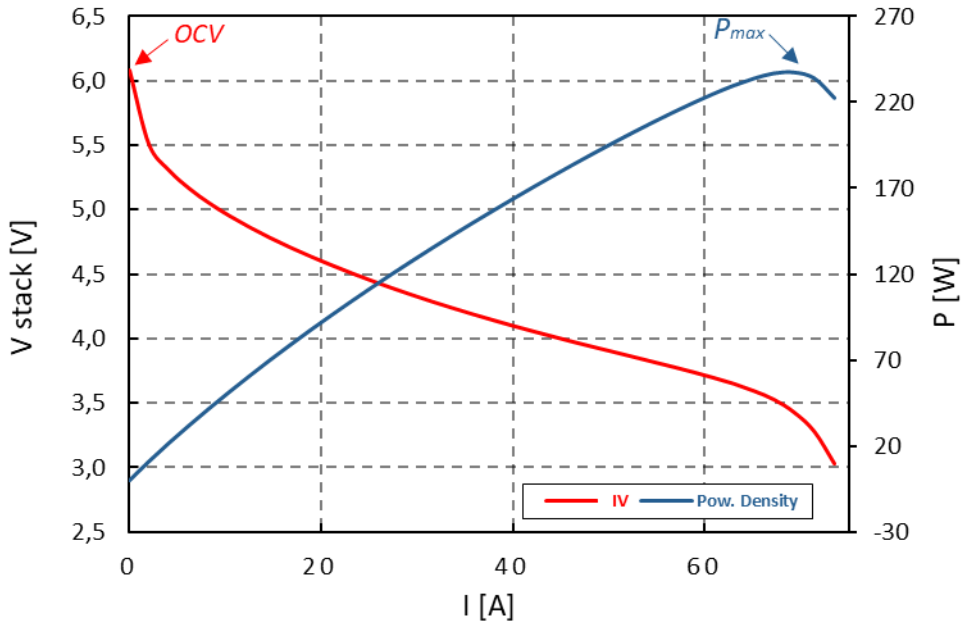

Figure 23. *Example of current-voltage and the relative power density dependence expressed in W.*

However, depending on the current density value, the internal resistance can be calculated also as differential (tangential) resistance $R_d$defined as the derivative of the voltage V in respect to the corresponding current I [78]:

$$R_d = dV/dI \qquad \text{(Eq. 45)}$$

The method includes several steps, starting with the calculation of the differential resistance for every point of the IV-curve (its change correlate to the current-voltage shape) and the determination of the minimum value of $R_{d,min}$ which can be considered as an important indicator related to the state of

health at given condition since it only depends on the intrinsic properties of the system i.e. its response characteristics and not on the external conditions [77].

Figure 24 illustrates an example of current-voltage curve with the new functional R_d both in response to a change in current density *j:*

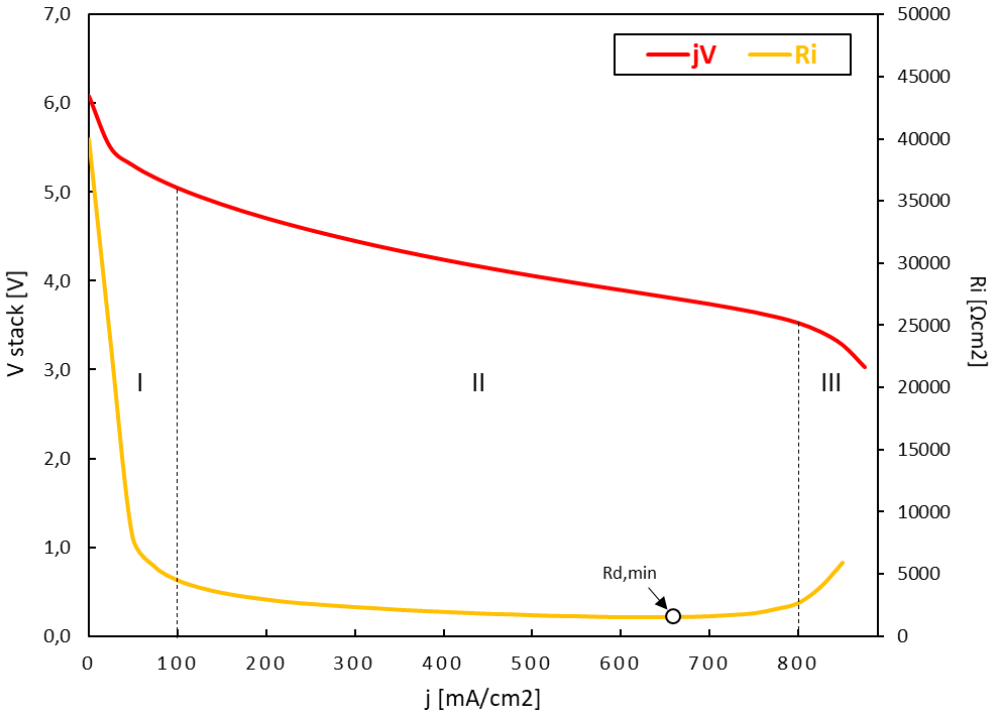

Figure 24. *An example of current-voltage and the relative Rd/I dependence* [77].

As stated before, DRA allows the extraction of an additional performance indicator ΔV^* which is equal to the difference between the open circuit voltage E_N^{OCV} and the voltage V_{00} calculated as the intercept at J=0 of the tangent at $I_{Rd,min}$ (relates to $R_{d,min}$) as shown in Figure 25.

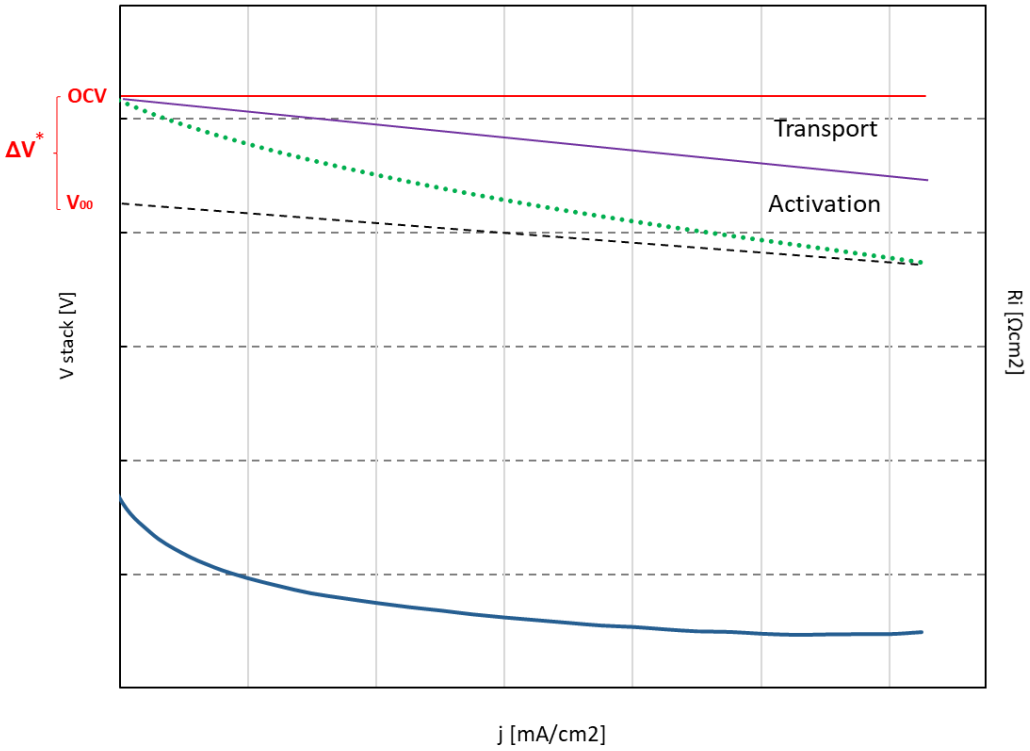

Figure 25. *Schematic presentation of the procedure for definition of the performance indicator ΔV^** [77].

Although connected with the position of $R_{d,min}$ in the current-voltage, the new parameter ΔV^* is related more closely to the non-linear losses which are dominated by the activation hindrances (Region II shown in Figure 25). As already marked, the two new indicators can be supposed to be characteristics for the Re-SOC state of health. Figure 26 presents impedance diagrams for a button cell during SOFC mode measured in different working points. The diagram marked as "3" is measured close to the state corresponding to $R_{d,min}$. As it is possible to see the spectra 3 is the smaller among those analysed, which corresponds low values of impedance. Thus based on the DRA analysis, working in a point close to the $R_{d,min}$ should means test the cell/stack in a "comfort" zone in terms of degradation.

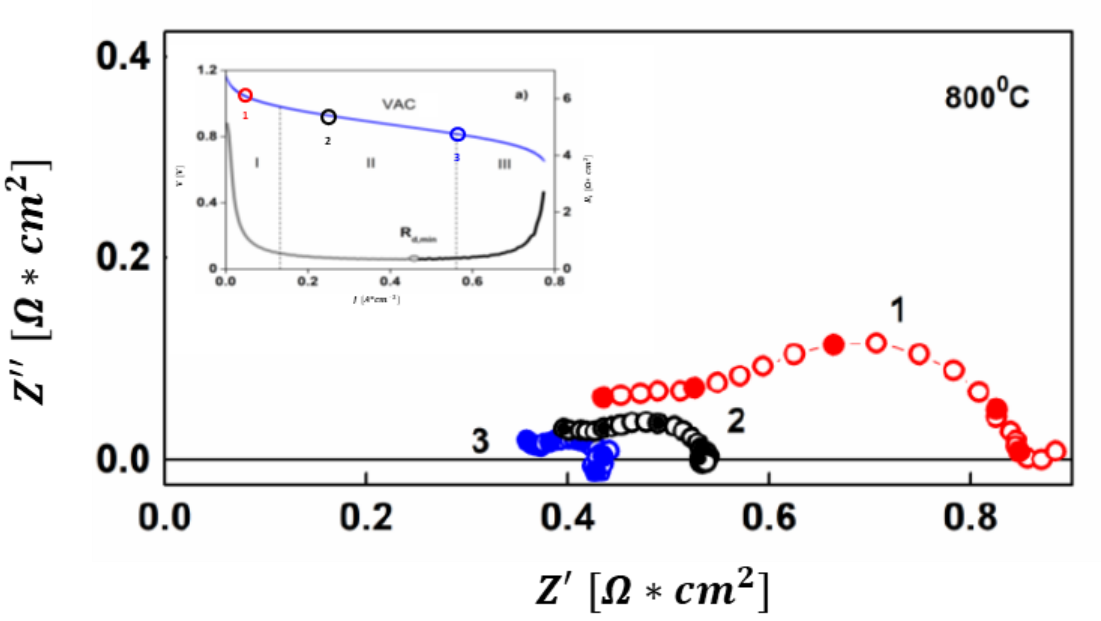

Figure 26. *Impedance diagrams comparison of three different working points* [77].

Summarizing, the simple measurement of the voltage at a constant current under constant conditions, produces a voltage/time curve that cannot give a lot of information for early diagnostics. The development of DRA is a step forward toward in this issue. The definition of the Differential Resistance as expressed above, represents a derivative of the cell voltage, while the defined value of $R_{d,min}$ corresponds to the zero point of the R_d derivative, i.e. it can be regarded as a second derivative. As a result, the changes in $R_{d,min}$ become observable much earlier than those of the other Re-SOC performance parameters. The introduction of $R_{d,min}$ and ΔV^* increases more than 10 times the sensitivity with respect to performance changes and degradation. Therefore, new "performance indicator" enables early recognition of Re-SOC degradation and thus to support an adequate and early diagnostic. [79].

In this work, the results generated from DRA have the intent as for the DRT analysis to:

- give more information on the performance of the stack;
- confirm the high reproducibility among the different stacks tested in the frame of SOCTESQA Project;

Additionally, being a new tool, the analysis on the SOCTESQA results have to demonstrate the feasibility of the approach also in the SOEC operating mode, since DRA presented in the literature refers to the SOFC mode. Therefore, the study will contribute to the improvement of the state of the art.

4. THE TEST SYSTEM: AN OVERVIEW OF THE EXPERIREMTNAL MATERIALA

In this chapter, the technical details for the realization of the experiments presented in this work are addressed.

During the experimental campaign carried out in the frame of SOCTESQA, four validation campaigns were performed, in each of which a new stack of the same type and from the same manufacturer was used, in order to obtain comparable results. An initial test bench validation among the testing project partners was carried out to figure out possible test station differences. The review of the test bench validation focused on the harmonization of the test benches among the different partners by minimization of the possible differences. The other two validations represent specific test programs applied to the SOC cell/stack assembly, while a final round robin test was performed and reviewed to ensure comparability of the results obtained in different test laboratories.

The main objective of the Project was to develop uniform and industry wide test procedures for SOC cell/stack assemblies. To achieve this goal, the different partners that took part in the project had to show high reproducibility and repeatability in terms of results, addressing operating mode, performance, durability and degradation.

The test procedures include and specify the complete testing system, the different operating modes, the test conditions and the preliminary electrochemical characterisation methods, based on current-voltage curves and electrochemical impedance spectroscopy analysis.

Part of the SOCTESQA results, more specifically jV and EIS data, are the basis for a deeper study, where more powerful analysis techniques, as the Distribution of Relaxation Times (DRT) and Differential Resistance Analysis (DRA) are taken into account in order to obtain more accurate information for improving the performance of the SOC cell/stacks. Last but not least, the contribution of these two techniques can validate the comparability of results obtained in SOCTESQA. The single results achieved in each test module, are therefore investigate in detail with the aim of finding performance indicators, critical issues and possible correlations between the different variables.

Thanks to the contribution of these two different but linked campaigns, a complete testing protocol consisting of standards and specific parameters is developed with the aim to characterize any type of cell/stack system giving a final Feedback Report which includes summarized information pertaining to performance and degradation rate.

In the first part of this section, after the description of the test system (5.1), the characteristics of the tested samples (5.2) and the description of the equipment of the test stations (5.3), modifications on the system (5.4) and safety subsystem (5.5) are presented.

In the second part of this chapter, the definition of test modules and test program are given and at the end all the testing conditions adopted for the realization of SOCTESQA are summarized in paragraph 5.5.

4.1. Test System

The fuel cell test system, called also test bench or test environment can be understood as a series of subsystems and interfaces (for example, safety equipment, mechanical load control equipment, measurement and data acquisition equipment, fuel and gas control equipment and other) where the reversible solid oxide cell module represents the core of the system.

Figure 27 shows a complete test system which consists of the solid oxide cell/stack assembly unit (test object) and the corresponding test and control subsystems. The test object is exposed to test inputs or operational conditions and delivers test outputs or performance results. Each subsystem can be associated to a specific set of physical quantities that are handled and has a specific role in the overall control of the experiment. The subsystems can be classified according to their physical properties, which are of media, electrical, heat, mechanical and data type. Especially for high temperature solid oxide systems, the temperature control subsystem and the gas control subsystems (flow rate, pressure) play an important role for the test output results

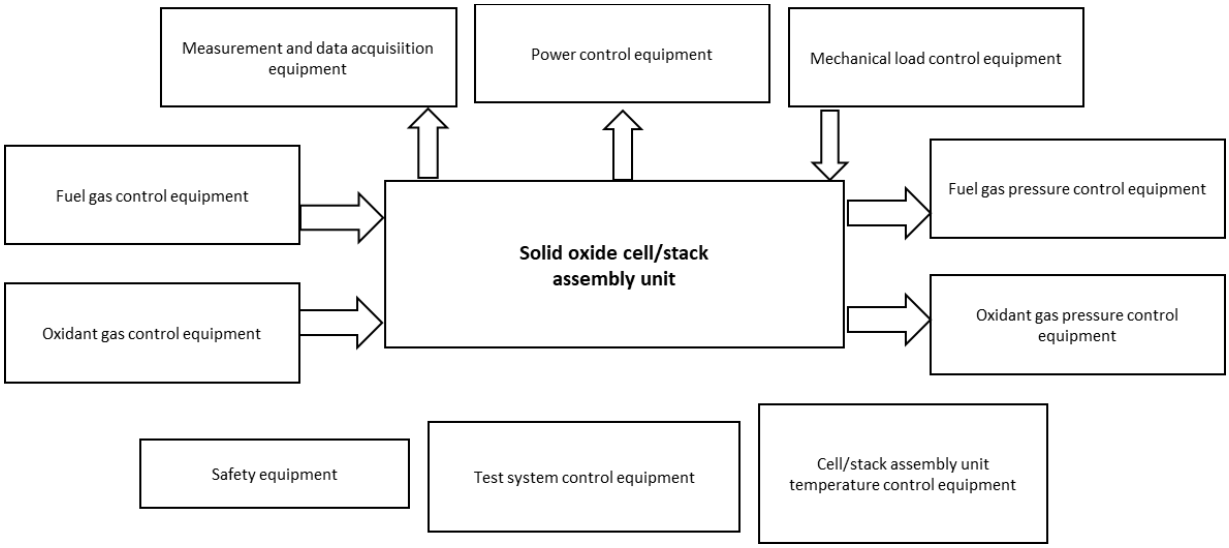

Figure 27. *Schematic graph of a test environment for high temperature solid oxide cell/stack assembly unit.*

Figure 28, instead, shows the physical interfaces between the SOC stack test object and the test environment. The physical interfaces between the test environment (test station) and the SOC cell/stack test object can be separated in media, electric, heat and mechanic interfaces. Media interfaces are the reactants inlet and outlet; electric interfaces are the load and power supply and voltage wiring; heat interface is the furnace and the mechanic interface is to mount the cell/stack on the test station which may supply compression force to the cell/stack. These interfaces will be defined by different physical parameters. Depending on the test program these physical parameters can be either of input nature (TIP) or of output nature (TOP).

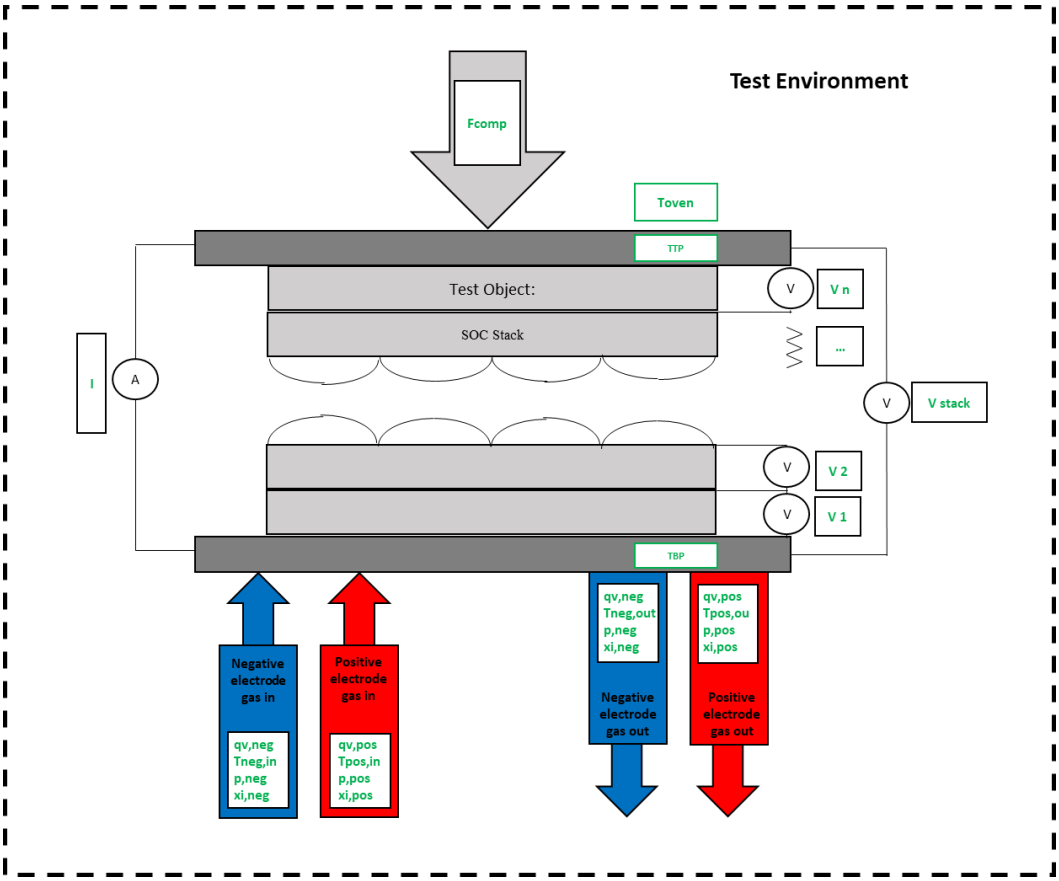

Figure 28. *Interfaces between SOC stack and test environment.*

For the reactants at cell/stack inlet and/or outlet these parameters are:

- Temperature, T
- Flow (mass or volume), q_v
- Pressure, p
- Gas composition, x_i

The electric interface parameters are:

- Cell/stack current (common synonym is stack load), J
- Stack voltage, V_{stack}
- Voltages of cell or the individual repeating units, V_{cell} or $V_{RU,i}$

The heat interface parameters are:

- Furnace temperature, T_{furn}
- Stack top plate temperature, T_{TP}
- Stack bottom plate temperature, T_{BP}
- Cell or stack internal temperature T_{cell} or $T_{stack,intern}$

Considering the fact that a temperature gradient in the stack is unavoidable and depends on various factors such as gas flow rates, current, thermal exchange rate with the furnace, it is difficult to determine the stack temperature. In practice, depending on the stack design, temperature sensors mounted at different locations in or around the stack (e.g., in endplates, in gas inlet/outlet channels, or just in close proximity to the stack) can be used to estimate the stack temperature. It is however important to identify the one that represents the best the real stack temperature. In order to make

results comparable among different test facilities, it is necessary to agree prior to the test on which temperature is used to represent the stack temperature. For the results presentation, it is recommended to show also other temperatures measured in order to have an idea of the temperature distribution in the stack.

The mechanic interface parameter is:

- Cell or stack compression force, F_{compr}

Ideally, the positions for the setting/monitoring of the input/output parameters are as close as possible to the boundary of the test object and the test environment.

4.1.1. Tested Samples

All the stacks studied in this work are planar, anode supported, Reversible Solid Oxide Cell (Re-SOC), manufactured by ElringKlinger (Dettingen an der Erms, Germany). The test object consisted of five single Repeating Unit cells assembled in series, each of them with a specific working area of 84 cm^2. The cell employs a porous Ni-8YSZ anode, a dense 8YSZ electrolyte and a LSCF cathode. The stack is also equipped with:

- Voltage wires for each single RU and for the stack (including top and bottom plates), insulated to avoid electric short-circuit;
- Two current collector cables to connect the stack to the power load, one fixed to the top plate and one to the bottom plate of the stack;
- Two bore holes for thermocouples (one in the top plate and another one in the bottom plate);

The test object is mounted on a Gas Distribution Plate (GDP), which provides gas connections between the test object and the inlet/outlet flow piping. The temperatures of the inlet and outlet gas supplies are measured with four thermocouples, each placed in the corresponding inlets/outlets for negative/positive electrodes of the gas distribution plate. Figure 29 shows a photo of the test object when it is mounted in the furnace core.

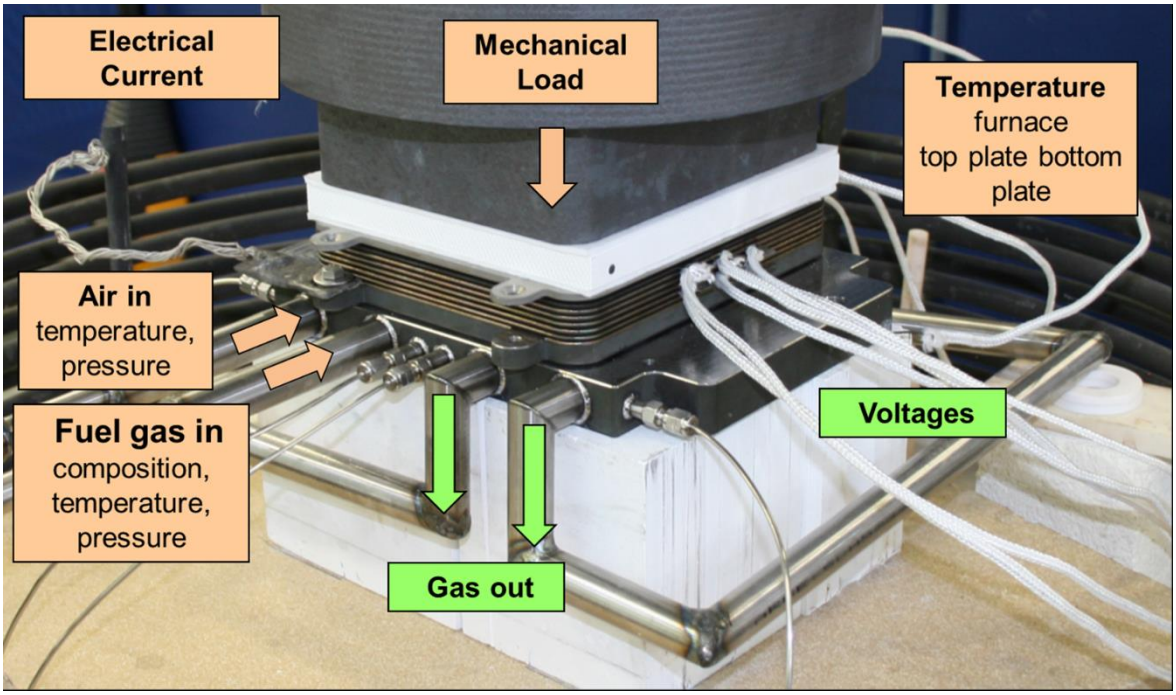

Figure 29. *Re-SOC short stack in test station.*

The test object and the gas distribution plate are placed inside an insulated furnace, constituted of refractory bricks with the aim of minimizing heat dissipation. The pipes in the gas distribution plate are made of Inconel to avoid thermal or chemical decomposition effects of the piping, in particular chromium evaporation, which may influence the local test conditions in the stack.

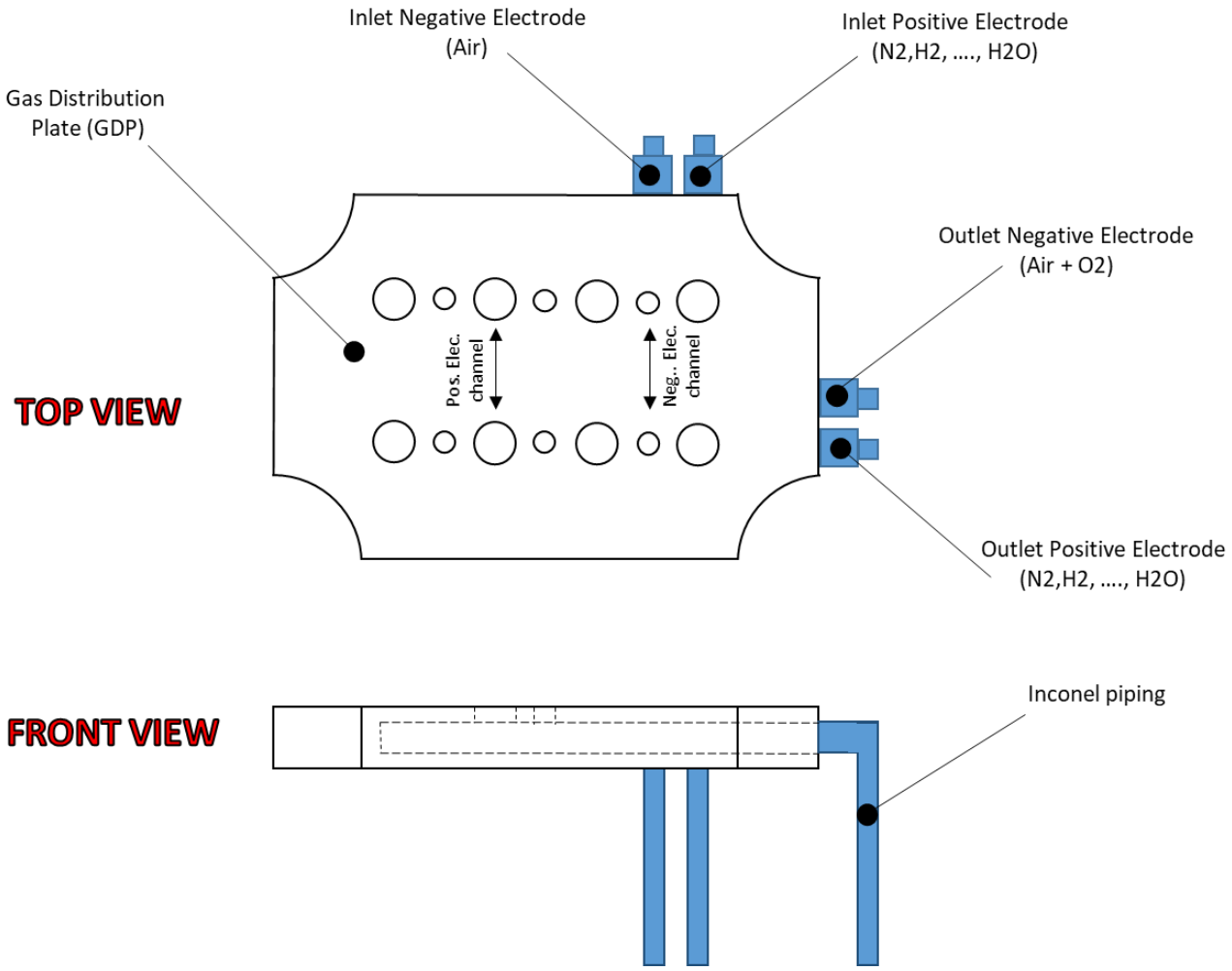

Figure 30. *The Gas Distribution Plate (GDP) design. Top and front view.*

4.1.2. Test Station

The test station, also called test bench, consists of the solid oxide cell/stack unit and the corresponding test and control subsystems. These interfaces between test environment and the Re-SOC stack can be classified according to the physical properties that are controlled/monitored:

Media interfaces - related to inlet and outlet reactants, such as:

- mass flow controllers (MFC) used to set and monitor gas flow rates;
- thermocouples placed in the gas stream line and as near as possible to the item under test;
- pressure sensors used to measure differential pressures of gases upstream and downstream of both positive and negative electrodes in order to monitor the drop-pressure (ΔP) into the two lines of the stack;
- controlled evaporator mixer (CEMs) on the SOFC/SOEC lines in order to provide the necessary steam for the operation of the system;

Electric interfaces- the electrical equipment, such as:

- electrical load in SOFC mode;
- power supply in SOEC mode;
- voltage wiring placed as close as possible to stack terminals to prevent that the measure is affected by losses over the wiring;

Heat interfaces – consisting primarily of a fully automatized furnace that via radiation heat exchange enables to achieve high operation temperatures. Besides, pre-heating systems of the inlet gas streams are indispensable to ensure a uniform temperature and avoid steam condensation in the piping

Mechanical interfaces - the compression force applied on the stack top plate to ensure good electrical contact and gas tightness between the stack layers. The mechanical load ideally is uniform over the complete stack top plate. This can be realized by a flat ceramic plate on top of the stack, which also has a lower heat transfer coefficient compared to metal plate. A possible unevenness of the stack top plate and the ceramic plate can be equalized by an additional ceramic fleece sheet between the two components. Figure 31 shows the ceramic plate on the fleece. Both components distribute the mechanical load over the whole stack area and also minimize the heat transfer from the stack to the weights on the stack. To apply the required compression, force a quantified metal weight is placed on the ceramic plate. It is very important that the position of it is in the middle of the stack to make sure there are no shear stresses.

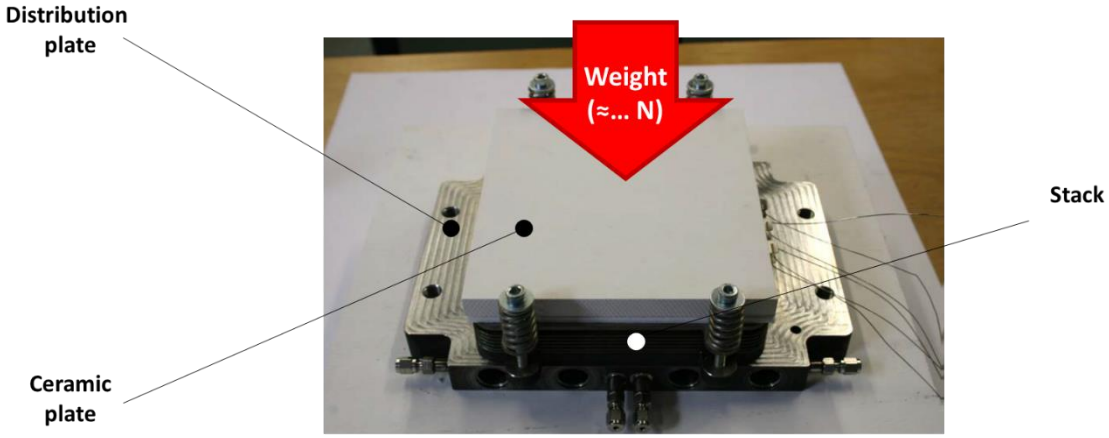

Figure 31. *Ceramic plate and weight placement on the stack.*

The different parts of the whole system are summarized below in detail.

4.1.3. Furnace

The furnace is one of the most important parts of the test environment because its geometry, volume, heating system and thermal insulation must guarantee a uniform and stable temperature depending on the principle of operation of the stack. The selected furnace has a cubic shape and consists of:

- Fire brick, or refractory brick is a block of refractory ceramic material used in lining furnace, kilns, fireboxes, and fireplaces. They have an aluminium oxide content that can be as high as 50-80% to withstand high temperature, but usually also have a low thermal conductivity for greater energy efficiency. They are weaker, but they are much easier to form, and insulate far better than dense brick. Their strength should hold well during rapid temperature changes and they should not spall;
- Ceramic base plate, made in alumina and silica to avoid thermal losses;
- Four heaters to achieve high operation temperatures;

- An automatic Temperature Control System where the controlled variable is measured by a suitable sensor such as a thermocouple (located in a thermal resistance) and converted to a signal acceptable to the controller. It is possible to set working temperature (max 1200°C), heating rate and working time (max 999 h);

4.1.4. Gas Distribution Plate + Gasket

The gas distribution plate promotes uniform gas distribution inside the stack. It is made of Crofer® 22H, enables co-flow and four thermocouple holes (two for inlet and two for outlet) are present. The thermocouples are type K (chrome-alumina), located inside the pipe, near the gas distribution plate.

The gasket is a mechanical seal which fills the space between stack and gas distribution plate, generally to prevent leakage into the joined test object while under compression. It is made of Mica material, excellent alternative in high temperature critical applications without failing due the presence of oxygen. In addition, Mica gasket resists fire without burning and it acts as an electrical insulator.

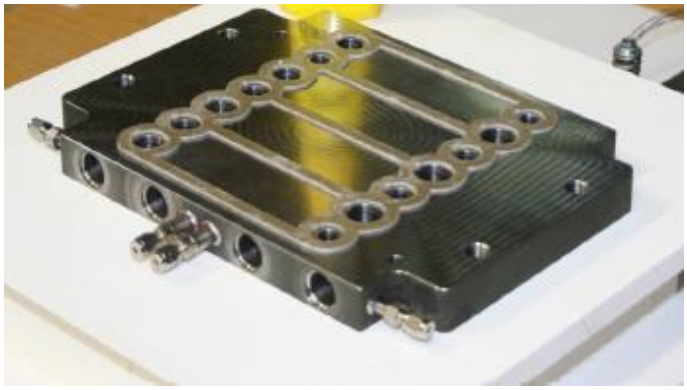

Figure 32. *Gasket mounted on the GDP.*

4.1.5. Steam Stability – The role of Controlled Evaporator Mixer (CEM)

In SOEC mode, the stability and quality of the steam generation play an important role in the resulting performance of the SOEC short stack, especially for what concerns the control of a stable steam supply and accurate and stable steam-to-H_2 ratio monitoring. This warrants therefore particular attention towards the equipment for steam generation. There are several methods for steam supply:

1. Steam can be produced by direct combustion of feeding oxygen into an upstream combustion chamber where it reacts with hydrogen in a stoichiometric mixture producing superheated steam. The resulting gas mixture is then fed to the negative electrode [19],[16].
2. Deionized water evaporates in a heated sand bath and is mixed with N_2, that is used as sweeping gas. H_2 is combined with the steam/N_2 stream and the resulting mix feeds the negative electrode of the stack flowing beforehand through heated pipes to avoid steam condensation. Even if it is possible to control effectively the steam-to-H_2 ratio through the N2 carrier flow, H_2 cannot mix completely in the pipe and the ratio varies continuously [16].
3. H_2 is mixed with N_2, as inert gas, and steam by means of a heated humidifier. Through a dew point sensor, it is possible to monitor the dew point temperature of the gas mixture exiting the humidifier. This is the most extended method for humidity control, unfortunately, the dew point temperature always fluctuates; this means that the absolute humidity characterizing the steam-to-H_2 ratio can fluctuate more than 10%, consequently making the voltage fluctuate during SOEC mode due to unstable steam-to-H_2 ratio [17],[80].

4. Steam can be produced directly injecting liquid water with a peristaltic pump in the gas channel and evaporation using the heat provided at the pipe trace heating.
5. Steam gas fogged mixer (SGFM) is a device that includes a water suction device and heat exchanger. H_2 is fed into the water suction forming a negative pressure in the device. At the same time, deionized water is transported in the same device by a High Pressure Liquid Chromatography pump (HPLC pump), where successively it is sucked and mixed with hydrogen by means of a negative pressure gradient. The mixture is then transported to the heat exchanger (working at 400°C) where water evaporates. Finally, the steam and hydrogen feed to the stack. The peculiarity of this system is that the flow rate of water is controlled accurately by the HLPC pump and the steam and hydrogen mix completely in the SGFM, so steam-to-H_2 ratio is stable all the time [81].
6. A Controlled Evaporator Mixer (CEM) is a device able to set up a precisely controlled injection rate of a liquid source (in vapour state) creating a humid/vapour condition both accurately and repeatedly, thanks to an evaporator and a 3-way mixing valve. At room temperature, the liquid is drawn from a container (with an inert gas blanket, or membrane) and measured by a liquid meter. The required flow rate is controlled to the set point value by a control valve forming an integral part of the patented liquid flow and carrier gas mixing valve. The gas is applied to the mixing chamber from a Gas Controller accurately supplying the required gas to be mixed with the liquid. This mixture is then directed to the heating module of the system where the mixed gas and liquid are vaporized with a controlled heating range. Different form the other systems, the CEM is able to handle sufficient quantities of liquid with a low vapour pressure, creating accurately and repeatedly the required humid-vapour condition.

After several discussions it was decided to consider the CEM as a steam generation system for its cost, capacity and reliability of the product under the Bronkhorst label, same brand used for mass flow controllers (MFC).

Table 4 shows the technical characteristics of all the equipment:

Table 4. *Technical characteristics of the measurement tools.*

Measurement Tools	Flow (l/min – g/h)
H2 MFC	0 – 10 l/min
CH4 MFC	0 – 10 l/min
CO2 MFC	0 – 10 l/min
CO MFC	0 – 10 l/min
N2 MFC	0 – 10 l/min
AIR MFC	0 – 20 l/min
CEM1	0 - 10 l/min H2; 0 - 1000 g/h H2O
CEM2	0 - 1000 ml/min H2; 0 - 36 g/h H2O

As it is possible see, in Table 4 also appear the mass flow meters of CH4, CO_2 and CO, which not used in the SOCTESQA campaign. The inclusion of these mass flow meters is to make the test bench complete for other possible future studies such as for example validating the stack when it is fuelled with biogas or syngas.

4.1.6. Electrical Load / Power Supply

An Electrical Load/Power Supply is a device that can set a precisely controlled current in both SOFC/SOEC operating modes thanks to a switch that allows changing in polarization and therefore the direction of the current.

The model KIKUSI PLZ1004W with a maximum operating current of 80 A is used.

4.1.7. Piping

For the flow setting outside the furnace normal steel piping with a normal pipe size (NPS) of 1/4 "is used. For security reason two lines were built, one for SOFC mode and one for SOEC. The juncture between piping and GDP was designed directly in ENEA and produced by RMP Srl (Rome, Italy), consisting of two channels realized in INCODEL (D_{ext} = 16 mm, D_{int} = 12 mm, L = 1 m each channel), one for fuel and one for air needed to the GDP. The idea was to optimize the gas path inside the furnace in the smallest possible volume but maximizing the heating. For improving turbulences and internal thermal flux a corrugated rod of 2 mm was welded inside the pipes.

4.1.8. Mounting of SOC-stack on gas distribution plate

In this paragraph an overview for the most important steps for the installation of the ElrinKlinger SOC stack on the gas distribution plate is given. After insulating all the voltage wires with ceramic tubes or ceramic cloth tubes and placing the gasket on the GDP fixed with 3-4 glue points to be sure it will not slip away during stack placement, the stack is ready to be mounted on the GDP. For the next step that concerns the positioning of the stack, 2 standard socket screws (with the relative M6 nuts) and 2 locating pins have to be used in order to fix the stack in x and y direction as shown in Figure 33. With the pins inside the plate and the screws at the stack, there are four fixing points to locate the stack in the gas distribution plate. It is recommended to be careful not to move the gasket during the positioning.

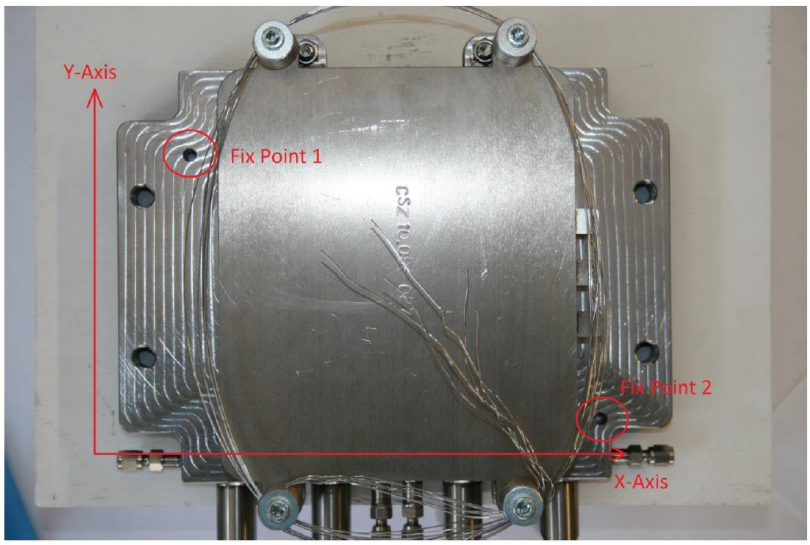

Figure 33. *Placement of the stack on GDP.*

Then, after loading 50 kg of weight on the stack, in the middle of the stack to make sure that there are no shear stresses, the transportation bracings can be removed completely. At this point, the stack can be connected to the power supply to fix one current cable to the top plate and one to the bottom plate. It is recommended to use flexible current wires and silver or platinum paste between the current cable connectors and the stack plate in order to reduce the contact resistance. Then the voltage wires are connected to the test station. Altogether 6 probes for the voltage of the RUs and two for the stack voltage are needed. The 5 voltages of the single repeat units will be measured as shown in the Figure 34. For the measurement of the total stack voltage connect the two additional wires on the stack top

plate and the stack bottom plate. The stack voltage probes can be mounted in the same way as the stack current wires, but not in the same position are connected.

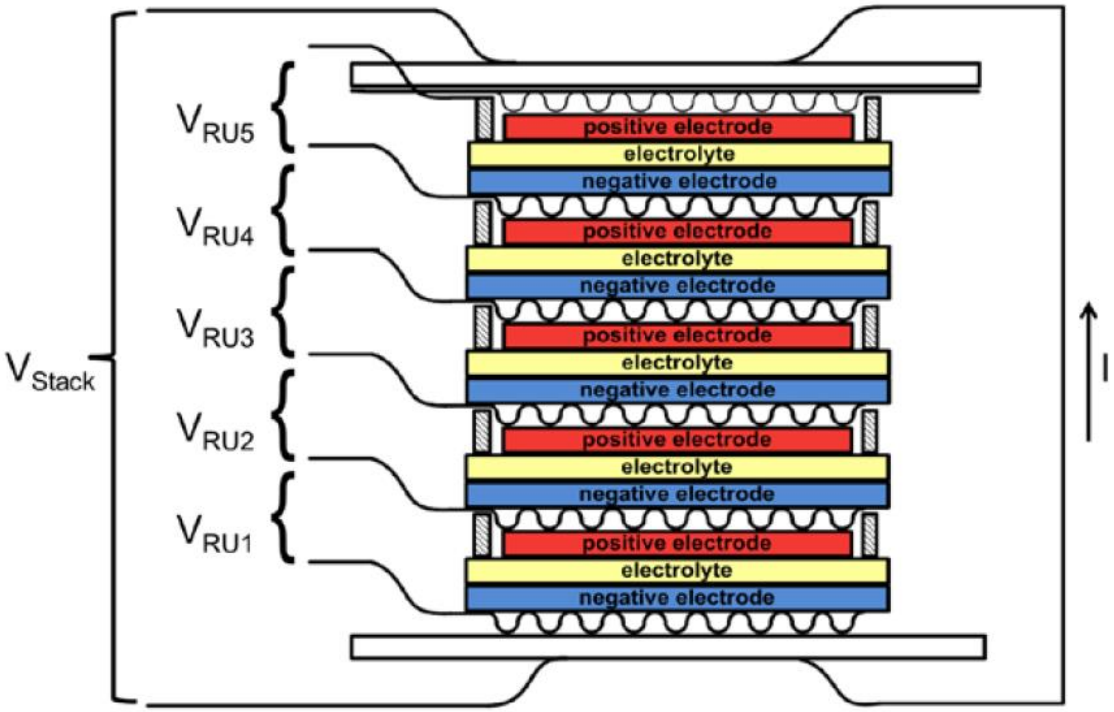

Figure 34. *Schematic overview for the voltage and current wire connection at the stack.*

At the end, after insulating the two thermocouples regarding the measurement of the top and bottom temperature with a ceramic tube, they can be fixed to the stack.

When mounting a cell within a cell test fixture, some general considerations have to be made to assure that the influence of the test setup on the results is minimized:

- Electrical contact to both the negative and positive electrodes has to be assured; this is done by ensuring actual mechanical contact of the cell to the contact components, and by having sufficient contact points to avoid current restrictions.
- A well-defined or masked geometric area of an electrode has to be defined as the geometric cell area.
- The cell has to be sufficiently leak-tight to avoid significant mixing of the test gases with other gases, before passing over the negative or positive electrodes.
- Any potential pollutants (sulphur, phosphorous, etc.) from components used in the cell test fixture have to be avoided.
- Mechanical stresses from the cell test fixture components have to be avoided, to prevent any potential cracking of the cell during testing.
- Furthermore, flow fields at the electrodes have to distribute the gas evenly, and without a potential turbulent flow, to avoid gas starvation and mass transport limitations at the electrodes.

In addition, when the cell/stack assembly has to be mounted in the test setup, it has to be securely positioned, to avoid accidental movement during testing. Electrical connections have to be properly done and gas connections securely tightened, while sharp bends of the gas tubes should be avoided.

Electric insulation between the repeating units in the stack should be checked to avoid a short circuit. Gas tightness of the gas supply subsystem of the test station, of the stack itself and of the interface between stack and test station should also be checked. Furthermore, the gases fed into the cell test fixture/stack assembly have to be preheated to the ambient furnace temperature, to avoid a significant temperature difference at the gas inlet. The mechanical load applied on the cell/stack should be uniform. In some cases, the compression mechanism required for stack transport may need to be removed after mounting the stack into the test station.

4.1.9. Leak test

Leak testing is the process of checking for leaks (or defect) along the pipelines. In this specific circumstance compressed inert gas was used (as air) under carefully controlled conditions. The test method requires the closure of the two gas lines (positive and negative line); and only after the test bench is pressurized.

The method consists of:

1. Close the line with a pipe plug;
2. Pressurize the system (normally 20 mbar, but a pressure of up to 0.5 bar could be used);
3. Wait at least 10 minutes, checking the gauge for pressure drop and if necessary "walk" the route of the piping under test checking for leaks using leak detecting fluid such as soapy water;
4. In the presence of bubbles along fittings, tighten bolts;
5. Once the leak test is passed, release the air pressure and then open slowly the pipe plug;

4.2. Modification of the test system

After the test bench validation, comparing the results of the different laboratories, it was necessary to modify the test system in order to ensure harmonization of test benches.

The improvements to the system consisted in:

- A better insulation of the furnace by an enveloping thermal coating around the refractory bricks that make up the furnace, in order to diminish heat dissipation;
- Improvements of preheating systems in order to guarantee an inlet temperature as close as possible to the nominal operating temperature of the stack and so as to avoid thermal difference inside the stack which can cause internal damage;
- Avoiding the accumulation of water in the pipes which causes harmful back pressure. In a fuel cell, there is no significant differential pressure between the anode and the cathode, while in an electrolysis cell the presence of water can lead to considerable counter pressure due to condensation in the output line, which leads to mechanical stress and pronounced degradation. For the same reason, also the performance stability can be affected by the water condensation, due to resulting instability of the voltage;
- Improvement of stack position inside the furnace by placing the stack in perfect alignment with the heating elements in order to obtain a more homogeneous temperature distribution;
- Improved insulation of both positive and negative electrode piping outside the furnace in order to avoid heat dissipation.
- Substitution of the ceramic cloth tubes with ceramic rings to avoid vitrification and disintegration of the former due to the high temperature inside the furnace;
- Positioning the current collectors in such a way as to diminish the effects of parasitic magnetic fields with the aim of improving the quality of EIS spectra;

Figure 35 shows a schematic representation of the test system employed after test validation, highlighting the modifications carried out during the second validation. The complete test system consisted of the solid oxide stack assembly unit, defined test object, and the corresponding test environment, defined also as test station.

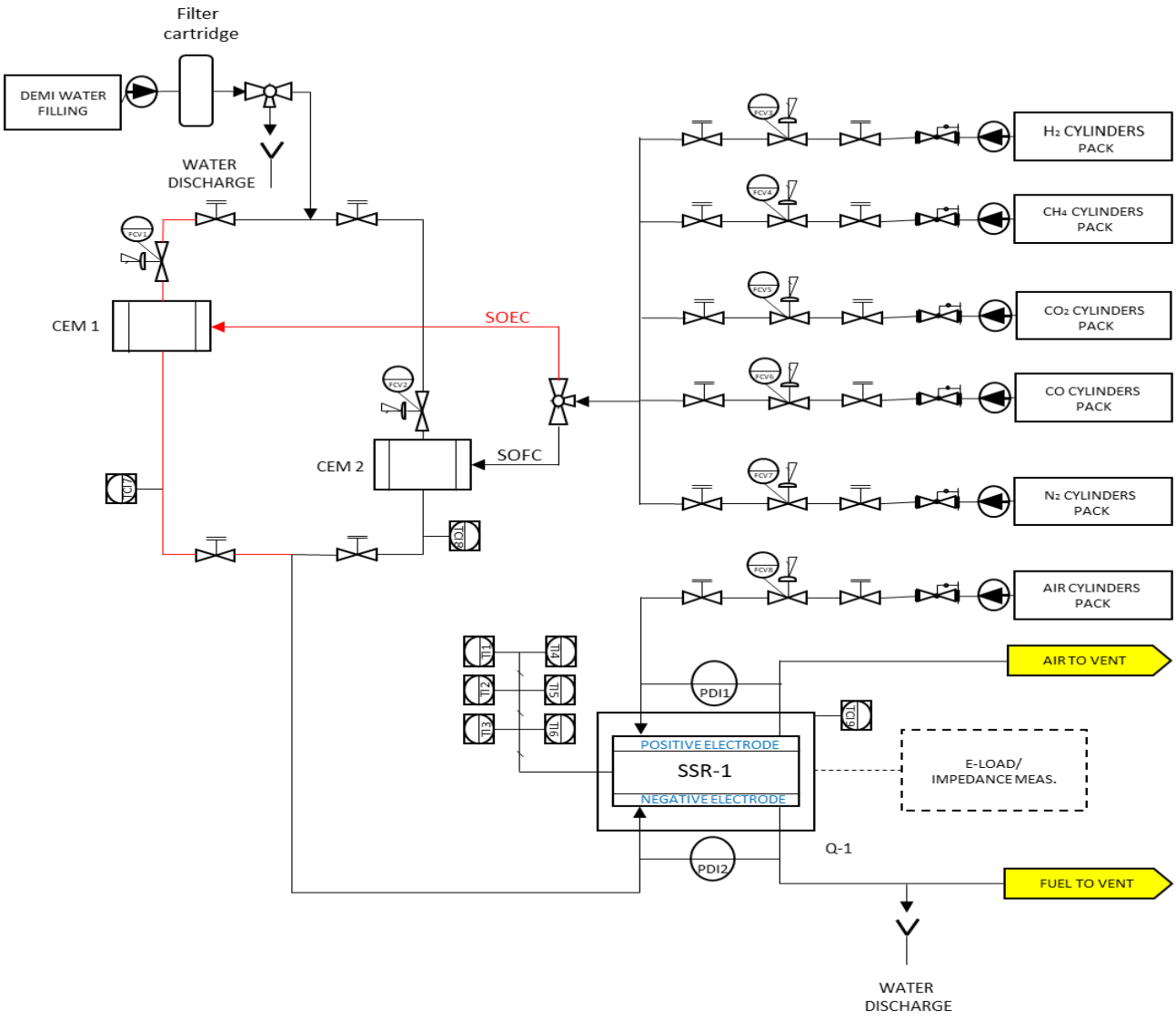

Figure 35. *Schematic representation of the test system for high temperature solid oxide assembly unit after first validation.*

4.3. Safety subsystem

Re-SOCs operate at high temperature, typically above 700 °C, that is higher than the spontaneous ignition temperature of hydrogen (565°C); it is important for the system to have a specific safety subsystem for explosive atmospheres, fire protection, electrical equipment and reactive, compressed gases. Therefore, the operating conditions of the Re-SOC assembly unit have to be carefully monitored to prevent safety issues through an appropriate emergency shutdown system.

The safety subsystem should include:

- Gas sensors in close proximity to the test station (in particular for H2, CO and CH4), connected to an automated emergency shutdown system that cuts off the fuel feed to the test station if hazardous concentrations of said gases are measured;
- Protection gas (e.g. 4% hydrogen in a nitrogen matrix) emergency supply that, in case of emergency shutdowns, expels flammable reactants from the system and at the same time protects the fuel electrode from re-oxidizing, which may otherwise compromise the performance of the Re-SOC assembly;
- A system to monitor the stack voltage, since low open circuit voltage (OCV) could indicate the presence of gas leakage;
- Redundant temperature sensors placed into the furnace to ensure that igniting gas leaking from the stack assembly may be detected from the measurement of high local temperatures;
- Pressure sensors to control overpressures in the Re-SOC stack assembly unit to prevent a break in tightness.

5. THE SOCTESQA PROJECT – METHODS AND PROCEDURES

All the testing procedures and modules that refer to the SOCTESQA Project are discussed in this paragraph.

At first, the definition of Test Module, Test Program and the difference among TIPs, TOPs and derived quantities are given while in a second moment, each specific Test Program will be discussed with the aim of showing the potential applications and the benefits of using Re-SOC devices. Successively, all the operating procedures for the analysis of each Test Module will be reported. Graphic examples will help readers understand better.

5.1. Definition of test module and test program

In the SOCTESQA project, test programs have been defined for different objectives and purposes. The test programs consist of a series of test modules, in which the actual test parameters, the specific conditions and the test setup are described in detail. The test program describes the objective and scope of the test as well as the test operating conditions (TOC), in which the general application provides specific parameters, such as reagent composition, operating temperatures, etc.

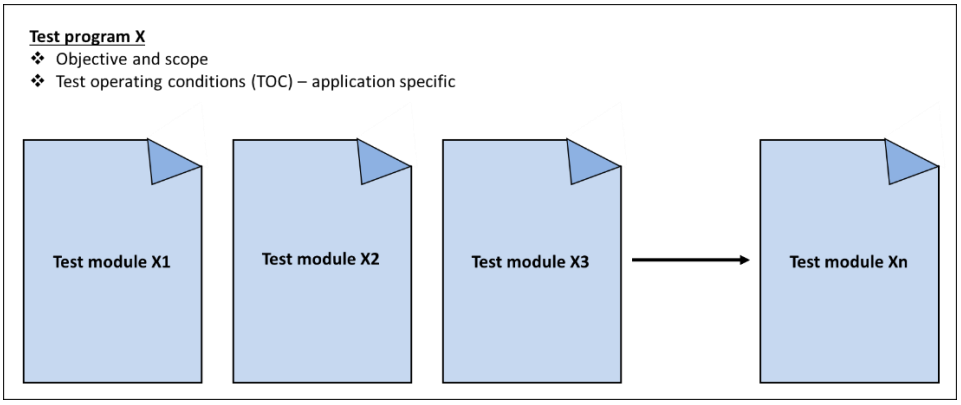

Figure 36. *Scheme of a test program consisting a series of test modules.*

The suggested test programs, chosen during the SOCTESQA project, refer to three different operation modes: solid oxide fuel cell (SOFC), solid oxide electrolysis cell (SOEC) and combined SOFC/SOEC operation. Each of these cases includes both performance and durability. The purpose is to cover many potential application requirements, e.g. micro-combined heat and power generation (micro-CHP), auxiliary power unit (APU), SOEC for H_2 production (power-to-gas) or combined

SOFC/SOEC energy conversion systems (power-to-gas-to-power). Nevertheless, there is no limitation for others to create their own test programs as needed.

Before describing all the important concepts concerning the objective of the test and the other definitions, three important recommendations are given:

- Most test programs will comprise a start-up and a shutdown module to safely start up the stack and document the initial and final performance of the SOC cell/stack.
- More than one test program can be run in sequence, whereby time and thermal stress from start-up and shutdown in test programs can be minimized.
- Each of these test programs may contain several test modules for characterization, e.g. current-voltage characteristics, electrochemical impedance spectroscopy (EIS) and performance and durability testing, with e.g. dynamic operating profiles or long term stationary operation.

Thus, test programs can ideally be placed in sequence to investigate several objectives, and thus the shutdown and start-up in between can be omitted.

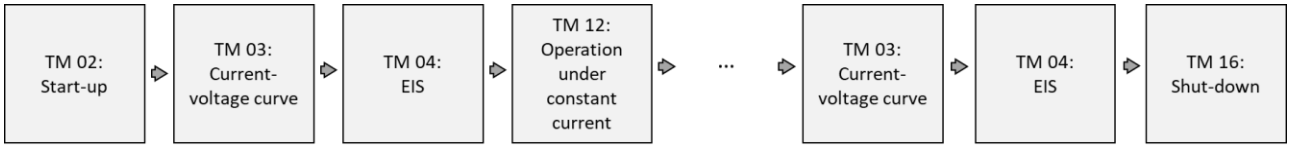

Figure 37. *Example of a test program structure, comprising several test modules for characterization and performance evaluation.*

5.2. Test module

A test module is a confined test procedure in which a minimum of test input parameters is changed to achieve a desired effect. The test module is carried out under the general test operating conditions set in the test program, unless stated in the module.

The test module describes input and output to be controlled and/or measured.

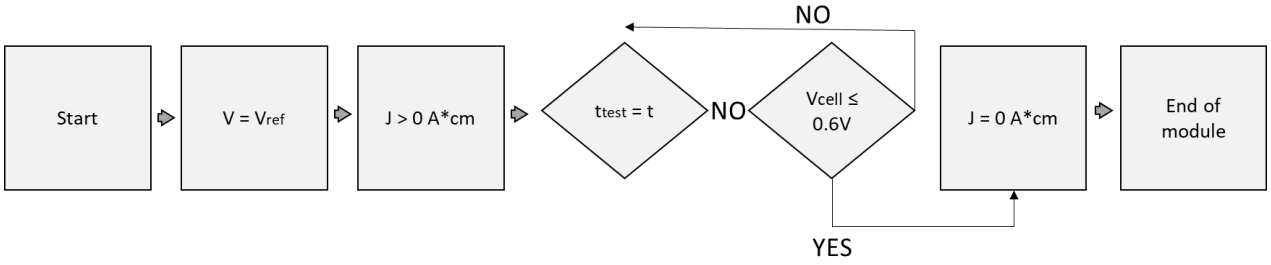

Figure 38. *Example of a test module, for durability testing under constant current in SOFC operation.*

5.3. TIPs, TOPs and Derived quantities

Depending on the test program, there are several Test Input Parameters (TIPs) and Test Output Parameters (TOPs) are available.

Test input parameters (TIP) are physical quantities whose values can be set to define test conditions for the test system, including the operating conditions of the stack. Therefore, TIPs must be controllable, regulated and measurable; TIP values are known before conducting the test. They can be classified as static, when the TIPs remain constant, or as variable when the values vary during the test.

On the other side, Test output parameters (TOPs) are measurable physical quantities that indicate the response of the test system/test object as a result of variation of TIPs. Values of TOPs are unknown before conducting the test and will be measured during the test. They must therefore be measurable.

Therefore, TIPs correspond to test settings (for example flow rate and current for long term operation test) that - in order to compare test objects -must be the same during each test depending on the SOFC/SOEC work mode, while TOPs correspond to test outputs that, once analysed, indicate how good the test object response is

The process of determining the precision, accuracy and uncertainty of TIPs setting and TOPs measurement is an extensive process. More details can be found in the ISO Guide to the Expression of Uncertainty in Measurement (GUM).

- Precision is the closeness of agreement between independent measurements of a quantity under the same conditions. It is a measure of how well a measurement can be made without reference to a theoretical or true value and depends only on the distribution of random errors.
- Accuracy is the closeness of agreement between a measured value and the true value. Error is the difference between a measurement and the true value of the quantity being measured.
- Uncertainty is the component of a reported value that characterizes the range of values within which the true value is asserted to lie. An uncertainty estimate should address error from all possible effects (both systematic and random) and, therefore, usually is the most appropriate means of expressing the accuracy of results.

Based on the aforementioned definitions it is clear that the most appropriate means of expressing the values of TOPs is the Uncertainty of the measured values, while for the TIPs, the Control Accuracy (which is usually instrument specific) should be reported.

Having set the TIPs and measured the TOPs, after a normal test it will be possible to calculate the derived quantities, defined as values that can be derived or calculated from test input parameters and/or test output parameters (e.g. current density, reactant utilization, electrical efficiency). In comparison to test output parameters, derived quantities are not directly measurable.

5.4. Test Procedure

The objective of the project SOCTESQA was to develop uniform of industry-wide test procedures for high temperature solid oxide cells/stacks. The test procedures address three different operation modes which are SOFC, SOEC and combined SOFC/SOEC operation. Each of these modes will include both steady state and dynamic operating conditions, focusing on the following application specific operating combinations:

1. Stationary application of SOFC: micro-CHP and distributed power generation;
2. Mobile application of SOFC (APU);
3. SOEC for H_2 production in a power to gas system (P2X);
4. Combined SOFC/SOEC for electricity storage in a power-to-gas-to-power system;

For each application, a test program consists of a series of generic test modules. Each test module has its own test objective and contains specific procedures to be followed. They will be discussed in the next chapter, are a brief description of each Test Procedure will be given. In order to check the applicability of the as-developed test procedures, laboratory tests of state-of-the-art solid oxide cells/stacks had to be performed. For this purpose, three rounds of test campaigns were planned in the project. The application-specific test programs and generic test modules were reviewed and optimised after each round test campaign.

The four application-specific test programs were defined as:

TP01: Test program for the stationary application of SOFC in a micro-CHP system
TP02: Test program for the mobile application of SOFC in a APU
TP03: Test program for the application of SOEC in a power-to-gas system
TP04: Test program for the application of combined SOFC/SOEC in a power-to-gas-to-power system

In these four test programs, ten test modules were integrated:

TM02: Start-up
TM03: Current-voltage characteristics
TM04: Electrochemical impedance spectroscopy
TM07: Reactant utilisation
TM08: Reactant composition
TM09: Temperature sensitivity
TM12: Operation under constant current
TM13: Operation under varying current
TM14: Thermal cycling
TM16: Shut-down

Table 5 gives a list of test modules which have been integrated into each test program.

Table 5: *Test programs TP01, TP02, TP03 and TP04 and corresponding test modules.*

Generic Test Modules		TP01	TP02	TP03	TP04
TM02	Start-up	✓	✓	✓	✓
TM03	Current-voltage characteristics	✓	✓	✓	✓
TM04	Electrochemical Impedance Spectroscopy	✓	✓	✓	✓
TM07	Reactant utilisation	✓	✓	✓	✓
TM08	Reactant gas composition			✓	
TM09	Temperature sensitivity	✓	✓	✓	
TM12	Operation under constant current	✓		✓	✓
TM13	Operation under varying current			✓	
TM14	Thermal Cycling		✓		
TM16	Shut-down	✓	✓	✓	✓

Following the feedback coming from the three rounds of test campaign and revision of test modules and test programs, a final round robin test was suppled:

TP05: Test program for the final round robin test

TP05 was performed to check the robustness of these test procedures. Through the first and second test campaigns, the first four test programs were validated. In comparison to the first campaign, more application-relevant operating conditions were implemented in the second test campaign. For instance, for the durability testing, the current density was increased from 0.3 to 05 A cm^{-2}, and the reactant utilisation was increased from 35% to 59%. In order to keep the total test duration realistic according to test capacities of all partners, yet to conduct the durability test for long enough to reveal meaningful degradation rates of the stack, it was decided to perform the most time-consuming test module (TM12 and TM13) for 500 hours.

5.4.1. TP01: Test program for the stationary application of SOFC in a micro-CHP system

Micro combined heat and power or micro-CHP or μ-CHP is an extension of the idea of cogeneration to the single/multi family home or small office building in the range of up to 50 kW. Local generation has the potential for a higher efficiency that traditional grid-level generators since it lacks the 8-10% energy losses from transporting electricity over long distances. It also lacks the 10-15% energy losses from heat transfer in district heating networks due to the difference between the thermal energy carrier (hot water) and the colder external environment. The most common systems use natural gas as their primary energy source and emit water and carbon dioxide.

Several small heat engines have been developed for micro-CHP systems as stirling engines, gas turbines, diesel engines. Between them, particular interest in fuel cell system is recorded. SOFC fuel cell μ-CHP operates at a high temperature (600 – 900 °C) and can handle different energy sources (as natural gas, LPG, biomass and also hydrogen) but the high temperature requires expensive materials. Due to the high efficiency of the CHP process, cogeneration has still lower carbon emissions compared to energy transformation in fossil fuel driven boilers or thermal power plants. The majority of cogeneration systems use natural gas for fuel, because it burns easily and cleanly, it can be inexpensive, it is available in most areas and is easily transported through pipelines which already exist for over 60 million homes. Because of the higher temperature SOFC in general has a longer start-up time and needs continuous heat output even in times when there is no thermal demand.

As can be seen in Figure 39, considerable amounts of primary energy input can be saved by producing power on the spot and utilizing the excess heat for heating purposes, rather than relying on centralized production of power and separate heat generation.

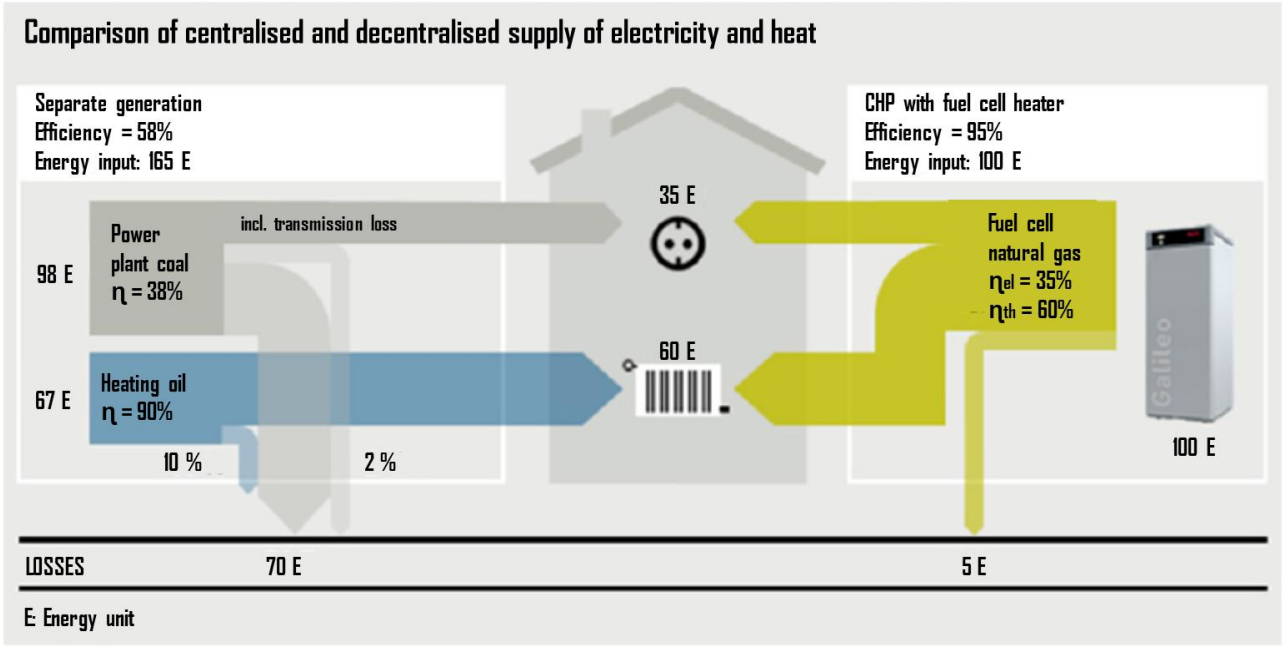

Figure 39. *Comparison of overall primary energy consumption between centralized supply on-the-spot micro-CHP, for given household power and heat requirements.*

5.4.2. TP02: Test program for the mobile application of SOFC in an APU system

An Auxiliary power unit (APU) is a device on a vehicle that provides energy for functions other than propulsion. They are commonly found on large aircraft and naval ships as well as some large land vehicles. SOFCs can be employed in APU for on-board generation of electricity on vehicles of any kind. The main scope for application is that of electricity supply while a vehicle is at a standstill,

ranging from caravans stationed overnight to aircraft parked at an airport gate. An SOFC-based APU also improves electricity generation efficiency during the vehicles' journeys and can supply back-up power during emergencies.

Many large vehicles run on diesel today, and SOFCs offers the advantage of being able to operate on diesel reformate without the necessity of further gas processing steps that would be required to purify the reformate to hydrogen. It is the ideal APU unit from a size of 500 W_{el} up to several tens of kW_{el} for road vehicles or even several hundreds of kW_{el} as required by aircraft and marine vessels.

The efficiency of electricity generation on board vehicles, using a conventional generator coupled to the engine, is in the range of 10 to 15% today. The system net efficiency of an SOFC APU could reach above 30%, which would more than double the power yield from the same amount of fuel. Additionally, on-site emission of diesel fumes, noise, and other pollutants would be reduced to near-zero. Utilisation of the heat produced by the SOFC for heating or cooling (via adsorption coolers, for instance) on the vehicles would further increase the overall efficiency.

Figure 40 shows the comparison of overall electric efficiency between a conventional engine and a SOFC-based APU.

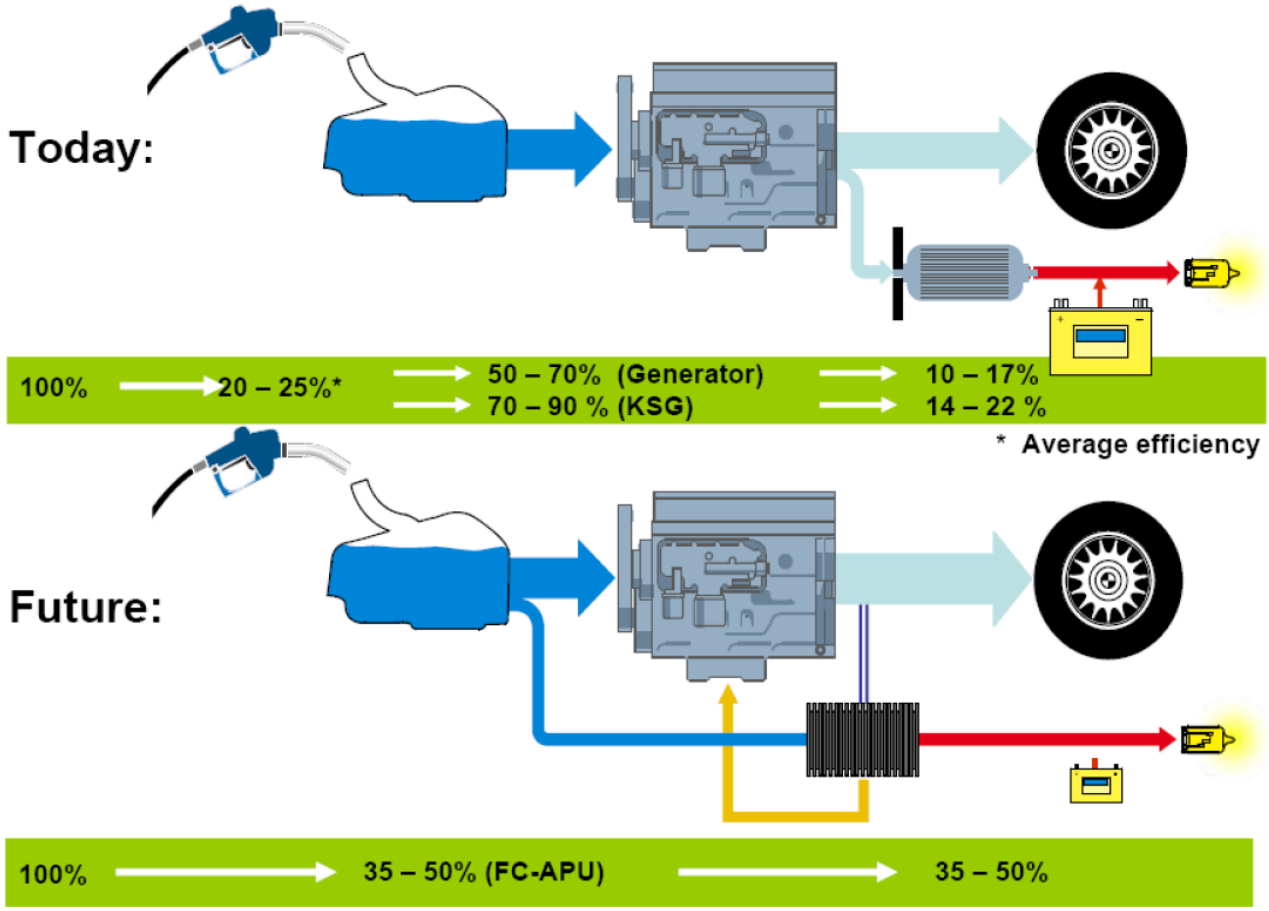

Figure 40. *Comparison of overall electric efficiency between a conventional engine-base power train (fuel-engine-generator-load) and a SOFC-based APU (fuel-SOFC-load).*

5.4.3. TP03: Test program for the application of SOEC in a power-to-gas system

Power-to-gas (often abbreviated P2G) is a technology that converts electrical power into chemical energy (fuel) using the surplus from wind or solar panels power generation.

In this case, the Re-SOC system can be seen as an Energy Storage System (EES) classified as Chemical which allows storage of large amounts of energy, up to the TWh range, and for greater periods of time – even as seasonal storage.

There are currently three methods in use where electricity is split into hydrogen and oxygen by means of electrolysis. The hydrogen gas produced can then be used energetically (as fuel) or also chemically (in industry). In the first method, the resulting hydrogen is injected into the natural gas grid or is used in transport or industry. The second method is to combine the hydrogen with carbon oxide and convert the two gases to methane using a methanation reaction such as the Sabatier reaction or biological methanation. The methane/syngas (SNG) may then be fed into the natural gas grid or further converted to LPG. The third method uses the output gas of a wood gas generator or a biogas plant, mixed with the hydrogen produced from the electrolyser, to upgrade the quality of the resulting biogas.

Another advantage of hydrogen and SNG is that these universal energy carriers can be used in different sectors, such as transport mobility, heating and the chemical industry as seen in Figure 41 below.

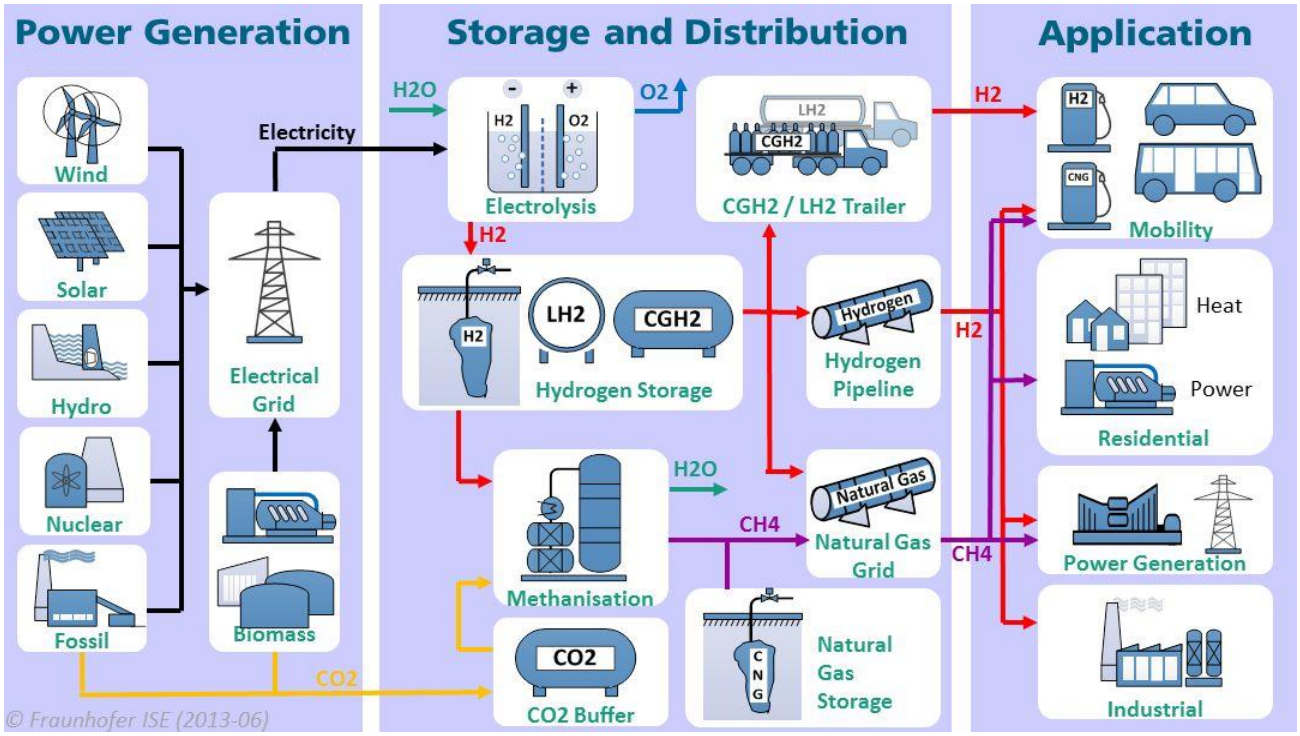

Figure 41. *General principles of the power to gas concept.*

5.4.4. TP04: Test program for the application of combined SOFC/SOEC in a power-to-gas-to-power system

The advantage of switching operating modes guarantees different applications to the Re-SOC system as power conversion to gas and gas to power following wind energy or solar power profiles. In this case, according to the demand / supply trend, the cell/stack will work in one of the two modes, avoiding waste of energy (in terms of electricity or chemicals) that instead would have in traditional systems.

In this test program, the SOC cell/stack runs in SOFC mode for a certain period for power generation, and then switches to SOEC mode for a certain period for gas production. In order to make the test procedures as applicable as possible and achieve an implementation throughout the industry, a test

program was suggested that allows for switching operation modes during daytime only. When used for real life evaluation of stack performance in this application, it is recommended having automatic SOFC/SOEC mode switching and longer operation time, e.g. 5000 hours. For SOCTESQA test program validation, initial j-V and EIS characterization in both SOFC and SOEC mode was performed, followed by pre-conditioning of the stack in SOFC mode for 120 hours. After that, the stack was tested in combined SOFC/SOEC mode by following an artificial/virtual "wind profile" for around 500 hours.

Figure 42 shows a typical scenario where a Reversible Solid Oxide Cell system is expected to support the growth of wind and solar energy by providing grid balancing services. In an excess of electricity, the Re-SOC will produce hydrogen (blue line), which can be stocked and used for future applications as mobile (as fuel) or industry (as chemical) while when the electricity supply is lower than the demand, converted into power (orange line).

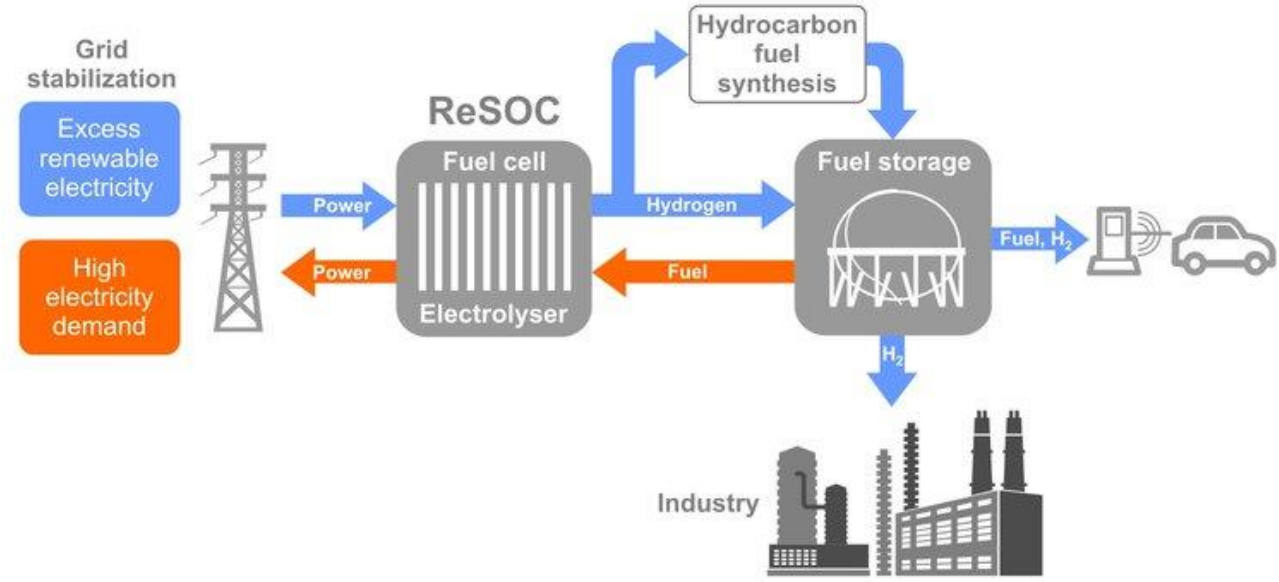

Figure 42. *General principles of the power to gas to power concept. The blue line directs the SOFC operating mode while the orange regards the SOEC operation.*

5.5. Test Modules

The experimental procedure and the testing conditions for the evaluation of the immediate performances of the Re-SOC samples studied are reported in this section.

5.5.1. Test Module 02 – Start-up

The objective of this test module is to define the start-up procedure needed to achieve operating conditions. Start-up includes the heating step and if needed, the tightness and electrical contact optimization, the reduction and the conditioning of the SOC cell or stack. It allows to make the SOC cell/stack operational to be tested properly on a test station.

The start-up procedure is given by the manufacturer. It is very important to distinguish between start-up of a "reduced cell/stack" and a "non-reduced cell/stack". A "reduced cell/stack" needs a reducing atmosphere at the negative electrode during start-up otherwise the nickel in the cells will re-oxidize and the cells will be destroyed. After start up, the manufacturer recommends a period of stabilization, or initialization before the cell/stack assembly unit is ready for characterization.

Since the ElringKlinger Test Stacks are classified as in "non-reduced cell/stack" after the heating step a particular procedure for reducing the cells was needed. The entire procedure consisting of start- up from cold state plus cell reduction is described below:

1. Set the flow for the negative ($f_{neg,in}$) electrode to N_2 or Ar (inert gas)
   Set the flow for the positive electrode ($f_{pos,in}$) to air.
2. Preheating of inlet gases to $T_{PH,\ neg}$, $T_{PH,\ pos}$, if applicable.
3. Increase cell/stack temperature $T_{cell/stack,\ intern}$ by setting $\dot{T}_{furnace}$ with defined temperature changing rate $\Delta T_{furnace}/\Delta t$. Gas inlet temperatures $T_{neg,\ in}$ and $T_{pos,\ in}$ are equally increased (if possible) by adjusting $T_{ph\ neg}$, $T_{ph\ pos}$.
4. Hold at temperature according to Re-SOC requirements.
5. Change $T_{cell/stack,\ intern}$ by setting $\dot{T}_{furnace}$ to the reduction temperature required by the SOCs. Hold at the targeted value until $T_{cell/stack,\ intern}$ is stabilised. Change the negative electrode gas feed to H_2/N_2 (Ar) (either in a single step or through step by step increase of H_2 in N_2 (Ar) content) and increase $f_{neg,\ in}$ required for reduction. Change the positive electrode feed to air/O_2 and $f_{pos,\ in}$ required for sintering of the electrode (if needed).
6. Hold at temperature according to the SOCs requirements.
7. Change $T_{cell/stack}$, intern by setting $\dot{T}_{furnace}$ to the operating temperature.
8. Change the reactant flows $f_{neg,\ in}$ and $f_{pos,\ in}$ to nominal values and $x_{i,neg,in}$ to nominal composition.
9. Change the reactant pressures (both at the same time) $p_{neg,\ in}$ and $p_{pos,\ in}$ (if applicable).
10. Wait until cell/stack/temperature $T_{cell/Tstack,intern}$ reaches its set-point (nominal temperature).

A large temperature gradient between the gas inlets and the cell/stack itself should be avoided to reduce the risk of cell/stack damage. All relevant temperatures like T_{cell}, $T_{stack,\ intern}$, T_{TP}, T_{BP}, $T_{neg,\ in}$, $T_{pos,\ in}$, $T_{neg,out}$, $T_{pos,\ out}$ were monitored precisely in order to be able to determine the maximum temperature difference ΔT_{max} (Eq. (46)) during start-up and measure an average temperature of the stack T_{av} (Eq.(47)) at the end of this Test Module.

$$\Delta T_{max} = \left| \frac{(T_{neg,in} + T_{pos,in})}{2} - \frac{(T_{TP} + T_{BP})}{2} \right| \qquad \text{(Eq. 46)}$$

$$T_{av} = \frac{T_{pos,in} + T_{pos,out} + T_{neg,in} + T_{neg,out} + T_{TP} + T_{BP}}{6} \qquad \text{(Eq. 47)}$$

Figure 43 illustrates an example of start-up procedure for a non-reduced SOC stack. During heating up of the SOC stack, N_2 was supplied to the negative electrode compartment and air was supplied to the positive electrode compartment. Stack reduction starts after the sintering of the stack with a step increasing of H_2 concentration in the N_2 at the negative electrode compartment, and the increasing of Air flow at the positive electrode. After reduction, the stack is ready for pre-conditioning or testing.

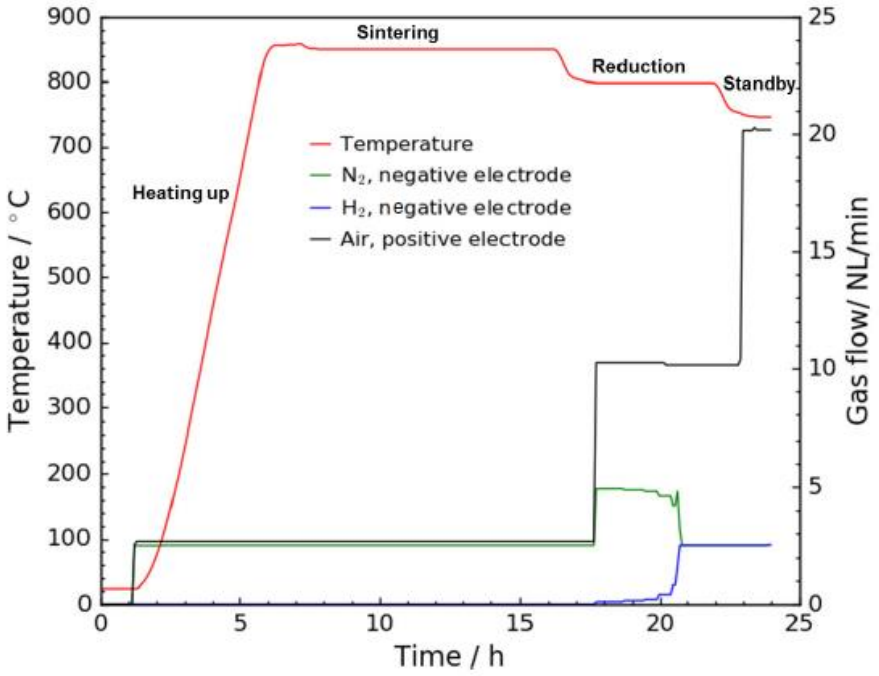

Figure 43. *Schematic example of start-up procedure for non-reduced SOC cell/stack.*

5.5.2. Test Module 03 – Current-voltage characteristics

The purpose of this test module is to characterize the performance of a SOC cell/stack while operating at different current density conditions either in fuel cell (SOFC) mode or in electrolysis (SOEC) mode. The module is used for measuring the voltage of the SOC as a function of the current, as a baseline measurement for the qualification of an SOC.

The j-V curves were measured in galvanostatic mode, which means that a defined electrical current is applied to the test object and the corresponding voltage is measured. This was done by connecting both current and voltage probes of the test object to an electronic load. The test was carried out by changing the current stepwise (at a specified settings), and recording the cell/stack assembly unit voltage. Measurements were taken when the cell/stack assembly unit reached the stable state in each step, for a specified duration time

From this test, the electric power P_{el} and/or the power density P_d were calculated, according to Equation (48) and (49).

$$P_{el} = V_{stack} * I \quad \text{(Eq. 48)}$$

$$P_d = \frac{P_{el}}{A*N} \quad \text{(Eq. 49)}$$

Note: with the active electrode area, A and N, the number of repeating units.

The Area Specific Resistance (ASR) is defined by the slope of the current-voltage characteristic curve at a specified SOC voltage or current density, depending on the test objective and test conditions. It is determined by linear regression of at least three data points around the target voltage or current density value, obtained during the current density ascending part of the curve. Thus, two specific points are selected and the ASR calculated:

$$ASR(j) = \left|\frac{\Delta V(j)}{\Delta j}\right| \quad \text{(Eq. 50)}$$

Figure 44 below presents an example of j-V curve measurement (ascending and descending) in SOFC operation mode for a stack with 5 repeating units (RUs) including its (top plate) temperature. This diagram displays the performance in terms of voltage at various current densities with hysteresis between the ascending and descending curves. The presence of hysteresis effect that occurs in the cells is due to several reasons such as for example the water management and temperate that affect the stack electric performance even if they have little effect on the system. The stack (top plate) temperature increases with increasing current density from 750 to 770°C due to the exothermal electrochemical reaction and the generated heat of the internal resistances of the repeat units (Joule heat). The reverse happens with subsequent decrease in current density.

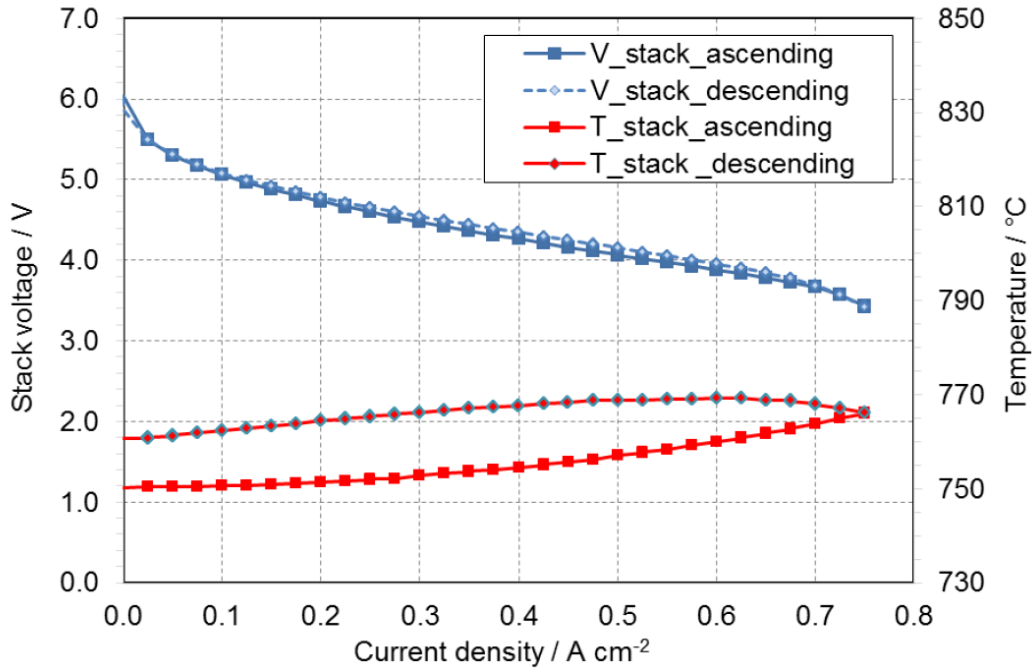

Figure 44. *Example of a j-V curve for an SOFC stack including its top plate temperature.*

5.5.3. Test Module 04 – Electrochemical Impedance Spectroscopy

Electrochemical impedance spectroscopy (EIS) is an important tool to analyse processes taking place in electrochemical systems like fuel/electrolysis cells and stacks. It shows the different frequency dependent impedances of a test object which can either be a cell, a repeat unit of a stack or a complete stack. Moreover, it is used to understand the behaviour of the resistances of the cell/stack test object, e.g, the ohmic resistance, the polarization resistances of the electrodes and the gas conversion resistances. The principle was described in Chapter 3.

Impedance spectra can either be measured with alternating current (galvanostatic) or alternating voltage (potentiostatic) excitation input signal. If tests have to be performed in potentiostatic mode, an AC voltage waveform generator is needed. Otherwise, for galvanostatic test conditions, an AC current waveform generator is used. In this work, galvanostatic mode was used.

The main action of the test is to determine the dynamic response of the cell/stack assembly unit to oscillating electric perturbations at the reference state, allowing to determine the ohmic resistance and the total polarization of the unit.

The following recommendations are given for this test method:

1. Direct current (DC)

EIS can be carried out at open-circuit voltage or under electric load. It is recommended to carry out measurements in DC to understand the different processes occurring under load. For electrolysis measurements the external current must be negative. Therefore, a DC source is needed.

2. Amplitude of excitation signal
   The recommended perturbation amplitude for an AC signal is about 1 to 3% depending on the system noise. For example, an AC voltage excitation signal is 10-30 mV per cell, and an AC current excitation signal is 3-30 mA.cm-2at DC current density of 1 mA.cm-2.
3. Sweep mode
   It is recommended to start the measurements with high frequencies to get output quickly and see directly if the measurement is giving reasonable results. Continue to sweep to lower frequencies.
4. Number of measuring points
   Four to twenty points per decade of frequencies (to be distributed evenly as logarithms, if possible) are required; they shall be numerous enough to identify clearly the geometry of impedance plots. If possible, avoid the fundamental and harmonics of the electrical grid frequency.
5. Number of measuring periods
   The measurement of the input signal is the average over more than one sine period. If the number of periods is chosen very high the measurement needs a lot of time. It is recommended to find a compromise between acceptable measuring time and precision (4-20 periods are feasible).

In electrolysis mode, special attention was paid to the noise of voltage signals caused by insufficient stability in steam supply, especially in small, low-power test environments. The operation parameters of the steam generator have been optimized to reduce the noise resulting in the impedance measurements. For this test an AC voltage/current waveform analyser or frequency response analyse, (FRA) is required for recording the response of the cells. For measurements under DC operating current, an electrical load (fuel cell) or an additional power supply (electrolysis) is necessary. Figure 45 shows the generic set-ups for the testing of either cells or stack in fuel cell (SOFC) or electrolysis (SOEC) mode.

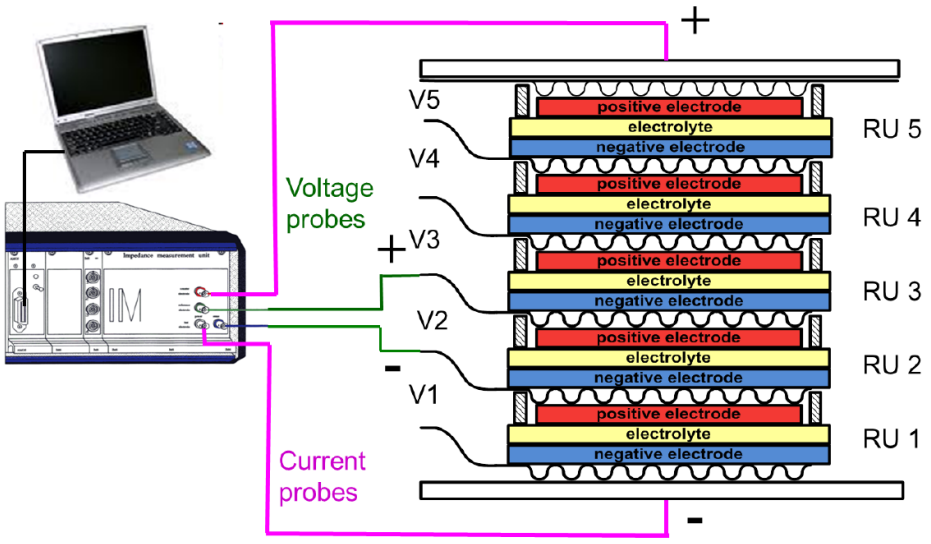

Figure 45. *Set-up for electrochemical impedance spectroscopy of an Re-SOC stack.*

In SOFC mode for single cell and short stacks an additional voltage supply may be needed, e.g. to overcome voltage drops in the hot current wires. In SOEC mode the voltage supply is necessary in order to impose the electrolysis voltage on the SOEC cell/stack object. In this case the polarity of the cell/stack has to be reversed in the test setup compared to the SOFC mode in order to reverse the current direction. For stack measurements the current is always applied to the whole stack whereas the voltage probes can either be connected to the complete stack or are just taken from the repeat unit of interest. The latter case has the advantage to examine the electrochemical behaviour of individual repeat units of the stack. It is advised to minimize all kinds of high frequency artefacts, e.g. use twisted wire pairs both for current and voltage probes, make sure that the voltage probes are perpendicular to the current probes etc.

The test was conducted using the following procedure:

1) Connect the cell/stack test object to the EIS system.
2) EIS can be measured at open-circuit voltage and/or under DC electric load. In the latter case increase the current stepwise to the set point. Precondition the cell/stack in order to achieve thermal equilibrium.
3) Verify that a steady state of the cell/stack in the test station has been reached. Moreover, voltage fluctuations should be kept as low as possible by ensuring stable input parameters, e.g. gas flow rates and electrical current load.
4) Superimpose AC sinusoidal waves of current or voltage at a characteristic (middle) frequency (e.g. 100 Hz) and make sure that a corresponding sinusoidal output signal is generated.
5) Start the measurement. Sweep the AC sinusoidal waves within the prescribed frequency range and measure the impedance at each selected frequency.
6) Save the measured data on a reliable data storage medium.

Other more detailed information on this technique is presented in Chapter 4.

5.5.4. Test Module 07 – Reactant Utilisation

The purpose of this test module is to characterize the influence of the reactant utilisation on the performance of a Solid Oxide Cell (SOC) cell/stack in both operation modes. The parameters governing the reactant utilisation are the current generated (SOFC) or consumed (SOEC) by the cell/stack, the gas composition and the volumetric flow rate of the fuel/oxidant gas stream.

This test procedure has no specific target application. However, this test module describes a general characterization method that can be used in research and development of the SOC and for quality assurance in cell and stack production.

The reactant utilisation of the negative and positive electrodes gas streams can be calculated according to Eq. (51) and Eq. (52).

$$U_{gas,neg} = \frac{I*N}{71.74*\sum_{i=1}^{n} z_i*f_{i,neg,in}} * 100\% \qquad \text{(Eq. 51)}$$

$$U_{gas,pos} = \frac{I*N}{71.74*\sum_{i=1}^{n} z_i*f_{i,pos,in}} * 100\% \qquad \text{(Eq. 52)}$$

Note 1: I is the electrical current, N is the number of repeat units, zi is the number of electrons of reactant i participating in the electrochemical reaction and fi is the flow rate of reactant i of the gas stream at cell/stack inlet expressed in l/min.

Note 2: The number 71.74 is given by the ratio between the Faraday's constant (equal to 96485 A*sec/mol) and the molar volume of an ideal gas at normal temperature and pressure (equal to 21.414 l/mol).

In SOFC mode the reactant components at the negative electrode are H_2, CO, CH_4 and at the positive electrode O_2. In SOEC mode the reactant components at the negative electrode are H_2O (and CO_2). There is no reactant utilisation at the positive electrode in SOEC mode.

In order to evaluate the effect of the flow rate of the (negative or positive) electrode gas stream at cell/stack inlet, the molar fraction of the reactant was kept constant. Hence, in the case of the negative electrode for example, the gas composition must be kept constant, i.e. the molar composition must be kept constant. The operating conditions of the cell/stack, including the temperature, the electrical current and the reactant gas composition were kept constant throughout the whole TM07. Only the volumetric flow rates in the negative or positive electrodes have been varied, being this variation discrete and only happening in one electrode at a time. The test started with low fuel utilisations (i.e. high volumetric flows) and care was taken not to surpass the maximum reactant utilisation recommended by the manufacturer, as shown in the example in Table 6.

Table 6. *Test matrix example of Test Module 07.*

$U_{gas,neg}$ (%)	I (A)	$f_{neg,in\ (nlpm)}$	$x_{H2,neg,in}$ (-)	$f_{pos,in\ (nlpm)}$	$x_{O2,pos,in}$ (-)	$U_{gas,pos}$ (%)
29	50	**10**	0.6	20	0.21	21
39	50	**7.5**	0.6	20	0.21	21
58	50	**5**	0.6	20	0.21	21
83	50	**3.5**	0.6	20	0.21	21

In order to avoid reactant starvation, the reactant flow has to be increased prior to an increase of the current density while the current density has to be decreased prior to reactant flow reduction.

In SOFC mode the reactant utilisation can be used to calculate the volumetric flow of steam being produced in the negative electrode. If steam can be condensed in the experimental set-up, then the difference between the measured volume of water over a predetermined period of time and its theoretical value can give an insight of the gas losses inside the stack.

Additionally, in SOEC mode the reactant utilisation can be used to calculate the volumetric flow of hydrogen being produced in the negative electrode and of oxygen in the positive electrode.

Figure 46 is an example of how to correlate graphically the TIPs and TOPs of this test module. In this particular example the average cell voltage has been the chosen TOP; nevertheless, others could be plotted, such as the various temperatures in the stack or the pressure differences in the positive and negative streams.

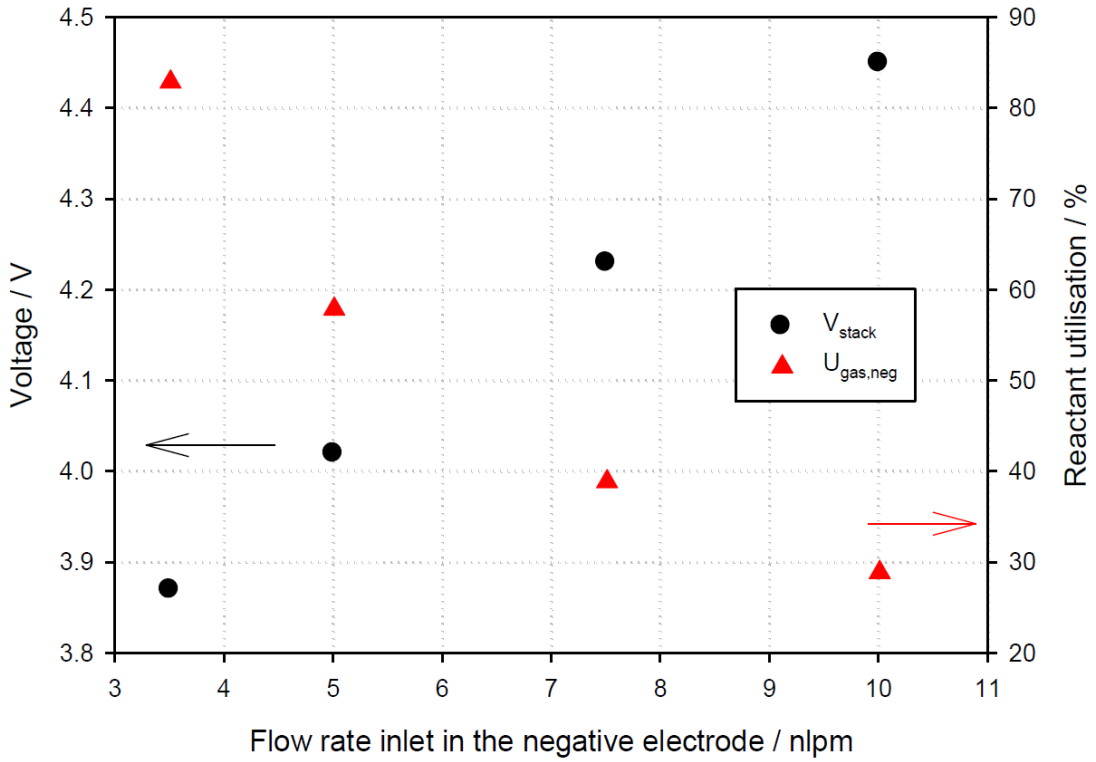

Figure 46. *Example graph of representation of results in SOFC mode when varying $f_{neg,in}$ and keeping constant I, $x_{H2,neg,in}$ and $f_{pos,in}$.*

5.5.5. Test Module 08 – Reactant Gas Composition

In this test module, the effect of the reactant gas composition on the performance of a cell or stack is determined, relevant for both operations. More specifically the test module can be used to investigate how changes in reactant gas compositions, such as inlet fuel-to-steam ratio or concentrations of impurities (e.g. sulfur compounds or other sources of catalyst poisoning impurities), affect the performance of the cells or stack, and their sensitivity.

Possible negative-electrode gases in fuel cell mode could be H_2, H_2/N_2, CH_4/H_2O, simulated reformate gases derived from natural gas or diesel using different reforming processes or other fuel mixtures such as biogas and syngas. In electrolysis mode reactant/negative-electrode gas compositions could be H_2O/H_2, H_2O/CO_2 or H_2/CO_2 or more complicated mixtures involving CO or CH_4.

To investigate performance under gas compositions where the quality of the fuel is relevant, impurities can be added separately, such as hydrogen sulfide in a hydrogen source, or similar for other sources of poisoning.

At the positive electrode, the influence of oxygen concentration on the stack performance can be examined; also for some types of electrodes, sensitivity to steam content could be investigated. An example of objectives can be found in Table 7, where also key parameters are described.

Table 7. *Possible objectives for gas variations, key parameters on the cell or stack.*

Objectives	Description	Key Parameters
Coking/carbon deposition	Carbon/steam ratio (specifically C:H:O ratios) – SOFC Effect of steam concentration on fuel electrode – SOEC/Co-Electrolysis	Inlet steam and carbon containing gas on fuel electrode; X_{steam} reactant conversion
Poisoning by reactant gas impurities	Performance loss due to impurities in reactant gases such as H_2S, e.g adsorption on TPB.	Inlet impurities: type and concentration
Oxygen diffusion	Sensitivity investigation of different oxygen concentrations on SOFC oxygen electrode performance.	Oxygen partial pressure
Humidification effect on negative electrode performance	Negative electrode, steam Concentration	Steam partial pressure
Humidification effect on positive electrode performance	SOFC positive electrode, steam concentration.	Steam partial pressure
Oxidizing/reducing conditions on negative electrode side.	SOEC; H2 and CO Concentrations	Inlet H2 and CO contents

The best practice of this module was to study the effect of each component by changing the mole fraction of all the components, one at a time. To keep the total flow and the mole fraction of the other components constant, the variation will be balanced by an inert. The cell/stack assembly unit voltage was recorded when the device reaches a steady-state condition.

Same recommendations of TM07 are given. Figure 47 shows an example of the influence of H_2O concentration on the RU voltage of a 5 RU Re-SOC stack tested in SOEC mode at 0.3 A/cm^2.

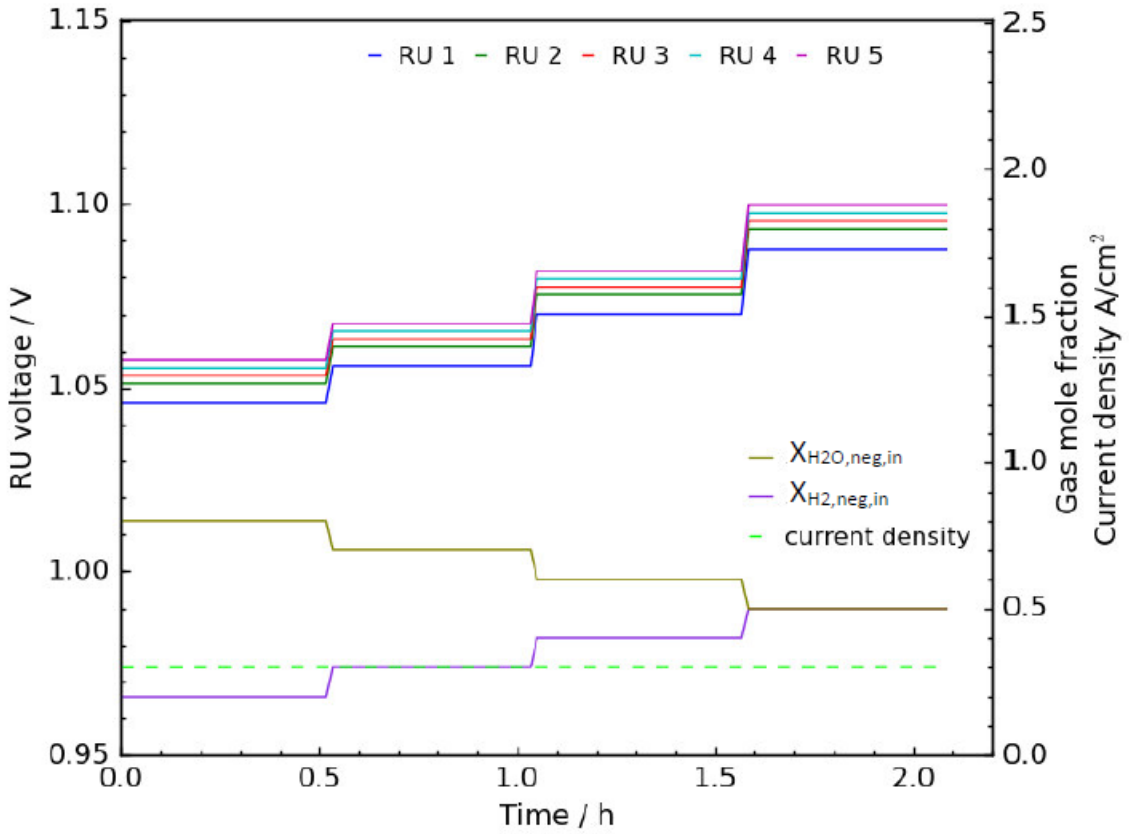

Figure 47. *Example of influence of gas composition on the RU Voltage under current in SOEC mode.*

5.5.6. Test Module 09 – Temperature Sensitivity

The purpose of this test module is to investigate the influence of the cell/stack nominal operating temperature on the cell/stack performance. The parameters that have a predominant role in this test are: furnace temperature, reactant preheating temperatures, current and, optionally, the flow rate of the positive electrode gas stream at cell/stack inlet. The latter is often used in real-life systems for the thermal management of the stack.

This test procedure has no specific target application. However, this test module describes a general characterization method that can be used in research and development of the SOC and for quality assurance in cell and stack production. This module should be applied in combination with other test modules in a test programme. The test programme will be application-specific and also describe the operating conditions of the SOC in more detail.

The main action of the test was to record the cell/stack assembly unit voltage in steady-state operation, at specific conditions, as a function of different unit operating temperature levels. It could be reasonable measure the cell/stack temperature at a fixed location as close as possible to the geometric centre of the cell/stack. However, this temperature could be inaccurate since the heat map of the device strongly depends on different factors such as the cell's dimension, operating conditions, and others. In addition, it is not always possible to place a thermopile (or similar temperature sensor) in the core of a stack. To overcome these problems, the best practice is to study directly the heat map thanks to the contribution of a modelling approach, but in the absence of the necessary equipment, a mean stack temperature it is recommended as test indicator.

In the second case, a mean temperature could be defined as the arithmetic average of the top and bottom plate temperatures (Eq (53)):

$$T_{stack,av} = \frac{T_{TP}+T_{BP}}{2} \quad \text{(Eq. 53)}$$

After stabilization of the cell / stack temperature, the test begins with increasing the current to a specific value. Since the aim of the test is to determine the influence of the cell / stack temperature on the performance, changes in the cell / stack temperature caused by electric power variation have to be taken into consideration.

The tested cell/stack temperatures have to be chosen considering the allowable operating conditions specified by the cell/stack manufacturer. Based on these parameters the test point matrix is prepared. Table 8 shows an example of this test module considering the behaviour of the stack under 25, 50, 75 and 100% of the nominal load when the nominal operating temperature is varied by multiples of 50°C and $f_{neg/pos,in}$ remains constant.

Table 8. *Test Matrix example of Test Module 09.*

$T_{cell/stack}$ (°C) @ I nominal	I(A)	$f_{neg,in}$ (nlpm)	$f_{pos,in}$ (nlpm)
700	30.1	10	20
700	40.2	10	20
700	60.2	10	20
700	80.3	10	20
750	30.1	10	20
750	40.2	10	20
750	60.2	10	20
750	80.3	10	20
800	30.1	10	20
800	40.2	10	20
800	60.2	10	20
800	80.3	10	20

Figure 48 represents the results of an analogous case where the three temperatures studied were $T_{stack,av-}$= 720, 750 and 780 °C and the current densities drawn from to the short stack were 300, 500 and 700 mA/cm^2.

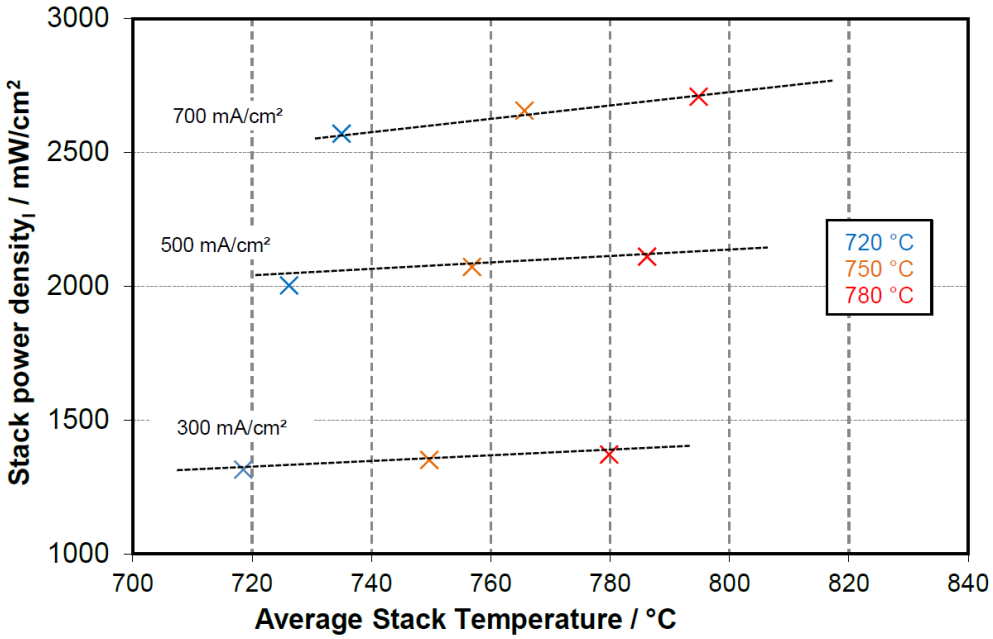

Figure 48. *Example of temperature trends during the temperature sensitivity analysis.*

5.5.7. Test Module 12 – Operation under Constant Current

Test module 12 deals with solid oxide cell (SOC) operation under constant current (i.e. galvanostatic conditions) either as a fuel cell (SOFC) or as an electrolyser (SOEC). The aim of this test module is to establish method for SOC long term steady-state operation. The test is also linked to the calculation of the SOC degradation rate through the SOC voltages recording as a function of time. For a long-term endurance test, the degradation rate is reported as the change in Area Specific Resistance (ΔASR), power density (ΔP_d) and/on voltage (ΔV_{cell}, ΔV_{stack} and $\Delta V_{RU,i}$) over a given duration (t_1-t_0) which has to be clearly mentioned (Eq. (54)). For instance, the first hundred hours are generally disregarded because the cell/stack assembly unit goes through a stabilization phase.

$$\Delta X_{rel} = \frac{X(t_1) - X(t_0)}{X(t_0)} * 100\% \qquad \text{(Eq. 54)}$$

Note: X is used to represent a generic degradation quantity among those indicated above.

The particular interest of this method consists in achieving the voltage evolution/dependency over time and so to know if SOC performance evolves steadily or not. This test is one of the most important because its results together with others, such as those given by TM03 and TM04, could provide information to help research developing test protocols for accelerated stress tests.

This test module addresses SOC cell/stack assembly units, and it is applicable to the four different SOC applications selected in the SOCTESQA project:

- Stationary and distributed power generation (SOFC-µCHP);
- Mobile (SOFC-APU);
- H2 production in power-to-gas (SOEC);
- Electricity storage in power-to-gas-to-power (SOEC/SOFC);

The test prescribes to:

1) Check the stability of the static TIPs ($T_{furnace}$, $p_{neg,out}$, $p_{pos,out}$, $f_{neg,in}$, $f_{pos,in}$, $f_{i,neg,in}$, $f_{i,pos,in}$);
2) Set a current I

3) Let operation last for t_{op}. The evolution of V_{cell}, V_{stack} and $V_{RU,i}$ voltages is measured and of T_{cell} or T_{stack} as a function of time. If a leak is suspected at any moment during the test (unexpected temperature evolution, signal instabilities), stack operation can be interrupted by decreasing the current absolute value to zero and OCV value checked, or an automatic cut-off voltage threshold may also be set, bringing immediately to zero the current density even if the foreseen duration t_{op} is not achieved yet.

Figure 49 shows an example of durability test in SOEC mode. A strong temperature evolution is observed during the operation under constant current that largely influence the determination of the degradation rate. In this case a temperature correction can be applied:

- either by adapting the furnace temperature at the end of TM12 in order to bring the stack temperature back to the initial value and take the obtained voltage as the final one,
- or by performing TM12 at a constant *Tstack* through constant adjustment of the furnace temperature which can be automatically realized through the temperature regulation unit.

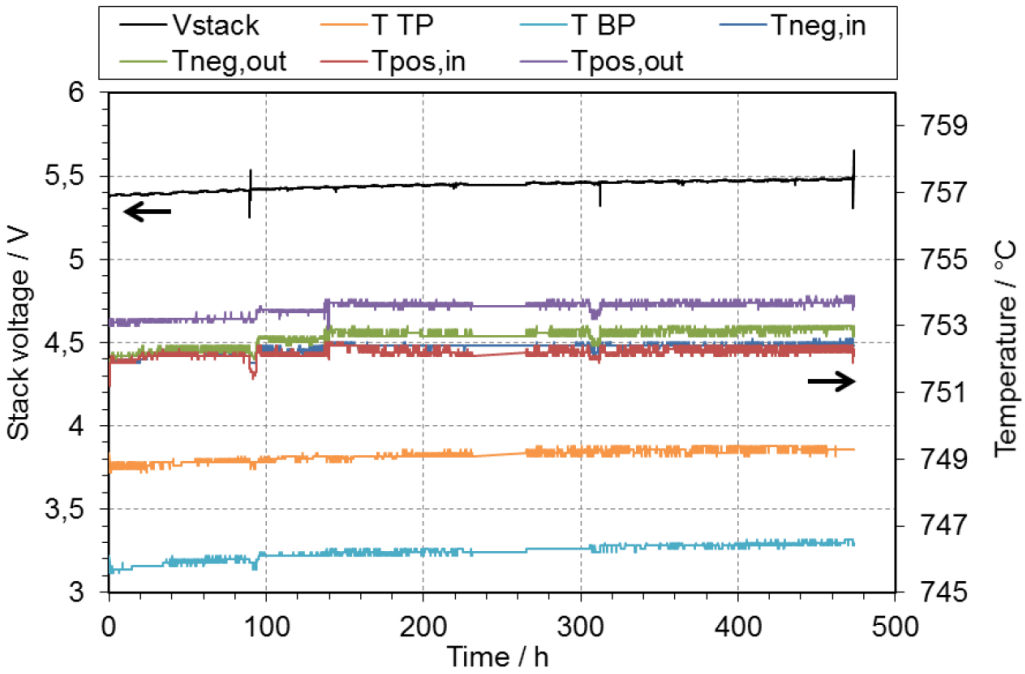

Figure 49. *Example of data representation in SOEC mode during TM12: stack voltage and temperatures as a function of time for a constant current.*

5.5.8. Test Module 13 – Operation under Varying Current

Test Module 13 deals with solid oxide cell operation under varying current when in galvanostatic conditions. The present test is valid for both fuel cell and electrolyser modes of the cell/stack and as seen above in TM12, it is also applicable to the four SOC applications and same Equation 51 was used for calculating degradation rate. SOC assembly units are expected to operate under various loads depending on the electrical, thermal and/or gas demands. The test aims to measure the response of the cell/stack assembly unit under quasi-dynamic operation, i.e. under varying current levels but in generally galvanostatic conditions (at a constant current for a given operating point).

The main action of the test is to record the evolution of the cell/stack assembly unit voltage at various current levels. A cycle can comprise several plateaus at different current values or continuous current ramps and can be repeated a number of times. The reactant utilization shall be kept constant

throughout the test. For the test, realistic currents, plateau durations and ramp rates for switching from one current to the other have been defined, reflecting the target application selected for the test though also taking into account manufacturer recommendations.

TM13 prescribes to:

1) Check the stability of the static TIPs ($T_{furnace}$, $p_{neg,out}$, $p_{pos,out}$, $f_{neg,in}$, $f_{pos,in}$, $f_{i,neg,in}$, $f_{i,pos,in}$);
2) Increase I from zero to the first targeted value progressively in accordance with the chosen rate of current application $\Delta I/\Delta t$
3) Let operation last for $t_{op,1}$, then vary I from the first to the second target current value with the chosen rate of current change $\Delta I/\Delta t$ for $t_{op,2}$ operating and so on.
4) The evolution of the V_{cell}, V_{stack} and $V_{RU,i}$ voltages was measured and of the T_{cell} or T_{stack} were carefully recorded as a function of time during the overall duration of TM12. If a leak is suspected at any moment during the test (unexpected temperature evolution, signal instabilities), stack operation can be interrupted by decreasing the current absolute value to zero and OCV value checked or an automatic cut-off voltage threshold may also be set, bringing immediately to stop the current density even if the foreseen duration t_{op} is not achieved yet.

Figure 50 below shows an example of TM13 for mobile SOFC-APU application where a typical usage profile of a truck APU system is supplied:

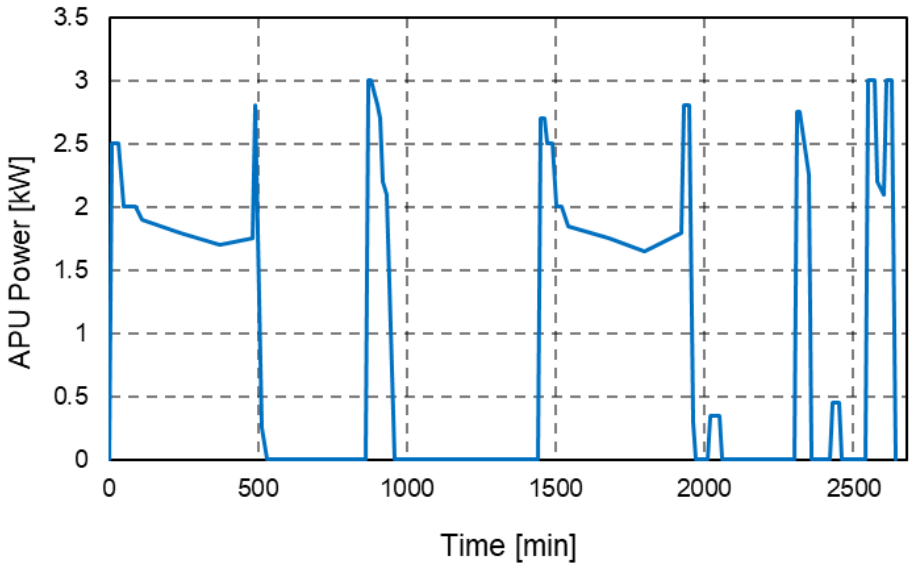

Figure 50. *Load profile of a SOFC truck APU.*

5.5.9. Test Module 14 – Thermal Cycling

Test module 14 deals with thermal cycling of a solid oxide cell/stack assembly unit. SOC assembly units, whether in fuel cell, electrolysis or regenerative modes, are expected to bear thermal cycling during service, due to sequential start-ups and shut-downs of varying periods, depending on the application. The objective of this test is to evaluate the stability of a SOC cell/stack assembly unit when thermally cycled. This test is carried out by cooling the cell/stack from the operating temperature (T_{cell} or T_{stack}), to a lower value T_{min} at a constant rate of temperature change during a number of cycles *m*. The dwell times at the operating and minimum temperatures respectively is defined beforehand.

Realistic thermal profiles have been defined for each application. For example, for stationary and distributed power generation (SOFC-µCHP), a profile between the operating temperature and room temperature (<50°C) with 25 thermal cycles is proposed in reference [82].

The procedure of TM14 consists of two phases depending on the nature of the thermal cycle:

1) In the first case that includes all the thermal cycles that do not drop below 600°C, the inlet positive and negative electrode gas flow rates ($f_{neg,in}$ and $f_{pos,in}$) and the inlet negative and positive electrode gas compositions ($x_{i,neg,in}$ and $x_{i,pos,in}$) are kept constant. The electrical current is kept at zero. Without electrical current load, it is not possible to determine any electrochemical performance data but only the OCV of the cell/stack assembly unit;
2) With regards to thermal cycles which drop below 600°C instead the inlet positive and negative electrode gas flow rates and the inlet negative and positive electrode gas compositions are changed. Below this temperature the H_2-concentration in the fuel gas has to be decreased to less than 4% to avoid consumption of hydrogen Usually, at high temperature the electrical current is increased and then kept at a constant level for a system relevant period. This period for mobile applications is very often in the range of several hours and much shorter compared to the long operating period for stationary applications.

An example of thermal cycling, is proposed in Figure 51 where the general TIP's evolution are shown:

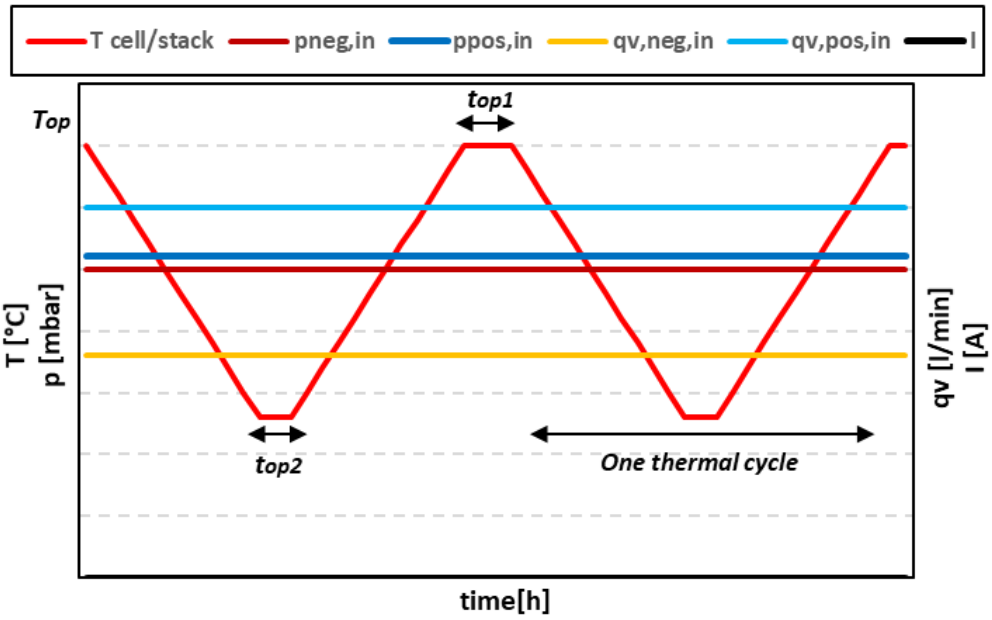

Figure 51. *General evolution of TIPs during Tm14: continuous thermal cycling above 600°C (in this case with electrical current at zero).*

Figure 52 shows an example of data post-processing consisting in the analysis of the OCV voltage evolution during the overall duration of the TM 13. Usually degradation rates are the most interesting results of thermal cycling experiments. About the results achieved in Figure 52, better explanations will be given in Chapter 6.

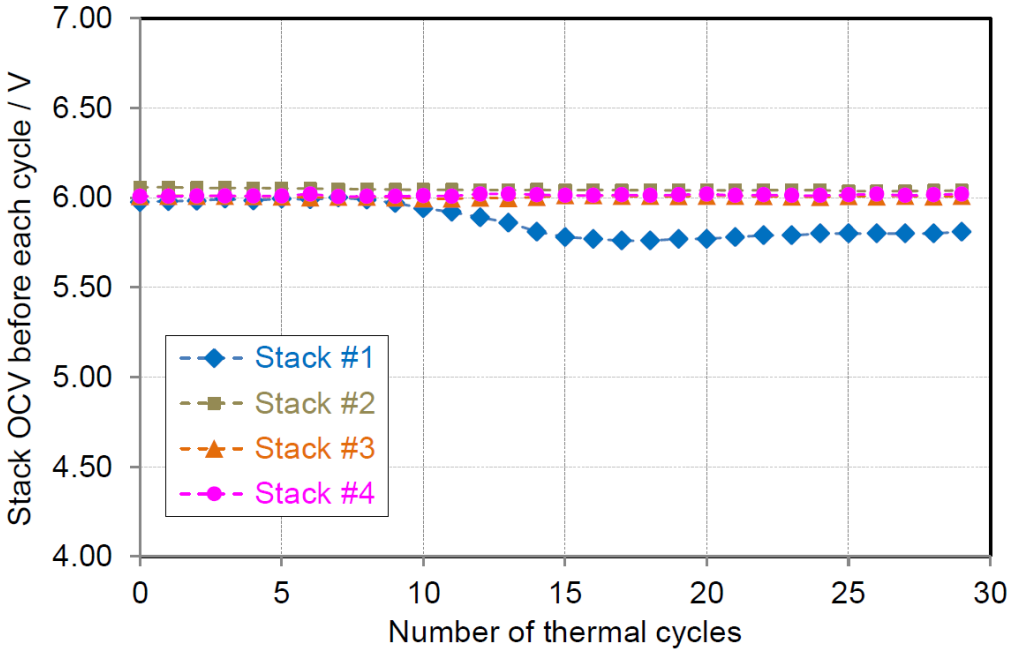

Figure 52. *Stack OCVs at 750°C during 29 thermal cycles between 50°C and 750°C.*

5.5.10. Test Module 16 – Shut-down

The objective of this test module is to define the shut-down conditions needed for ending SOC cell/stack operation and coming back to ambient temperature. The shut-down procedure normally is given by the manufacturer. However, if no shut-down procedure is available a recommendation is given below:

1) Decrease the current I (voltage V) stepwise to zero current (OCV) in locally galvanostatic (or potentiostatic) mode if applicable;
2) Disconnect/switch off the electronic load and power supply;
3) Change the reactant flow $f_{neg,in}$ and $f_{pos,in}$ to nominal values and $x_{i,neg,in}$ to nominal composition;
4) Decrease the reactant pressures (both at the same time) $p_{neg,in}$ and $p_{pos,in}$ to ambient pressure, if applicable;
5) Set negative electrode and positive electrode flows to H_2/N_2 (Ar) and air respectively;
6) Reduce cell/stack temperature $T_{cell/stack}$ by the predefined temperature change rate of $\Delta T_{furnace}/\Delta t$. The gas inlet temperatures $T_{neg,\,in}$ and $T_{pos,\,in}$ are decreased to ambient temperature by adjusting $T_{ph\ neg}$ and $T_{ph\ pos}$;
7) At ambient temperature reduce gas-flows of negative and positive electrodes to zero.

Figure 53 shows an example of an SOC stack shut-down procedure. During shut-down, the negative electrode gas is switched from H_2 rich gas mixture (in this example, 60% H_2 + 40% N_2) to protection gas (e.g. 5% H_2 in N_2). The air supplied to the positive electrode is kept at 10 nlpm. All the gases are cut off after the stack cooling down to ambient temperature.

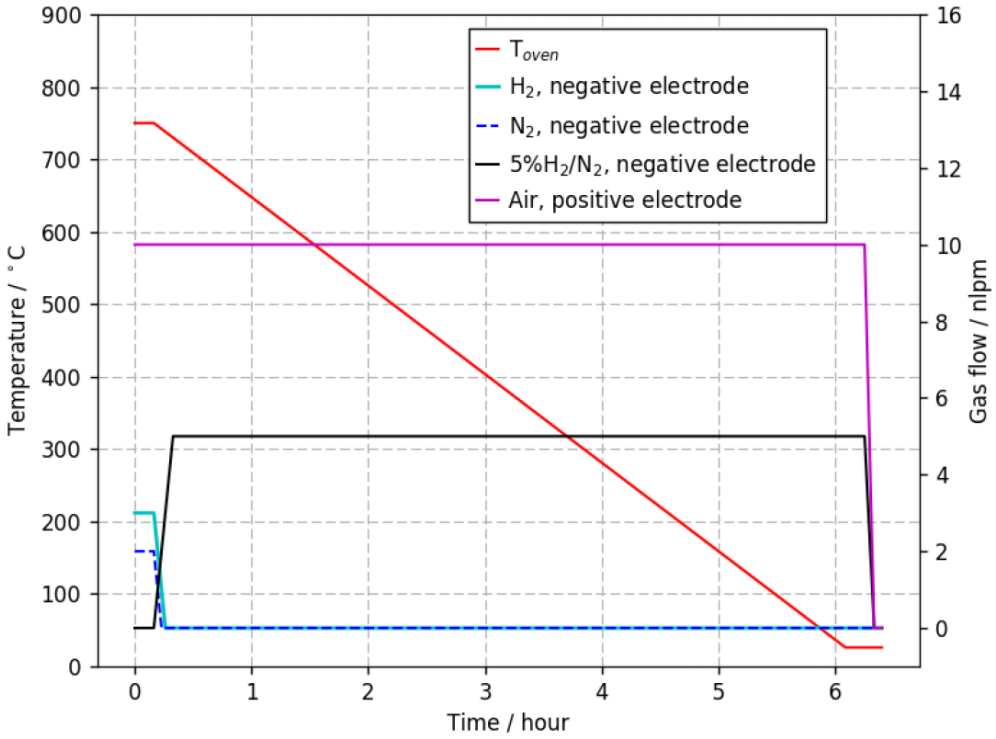

Figure 53. *Schematic overview of a possible shut-down for a SOC stack (from SOFC conditions).*

6. RESULT AND DISCUSSIONS

In this chapter, the results of the experimental campaign described in Chapter 5 are presented.

In the first part, the investigation on the quality of the ENEA's test bench architecture undertaken identify which improvements are needed to narrow the gap is measurements among the different partners. The final objective of the SOCTESQA project in fact depends mainly on the quality of the results produced which have to be compatible in the different test set-ups otherwise the tested stacks cannot be easily compared.

After having demonstrated that the modifications improve the system, reaching values close to those prescribed by the manufacturer, the second phase is aimed at developing robust uniform and harmonized test procedures. The attention has therefore focused on all the variables that influence the performance of the stack in the different test modules with the aim of finding a linearity among the results achieved by the different partners.

The purpose of this thorough analysis is highlight the pros and cons of the test modules and at the same time identify any critical issues and draft a list of recurring errors in order to generate improved, validated test protocols.

During the analysis, the results concerning I-V curves and EIS spectrums will be treated by DRA and DRT analysis in order to evaluate which variables play a more significant role and to find connections between the results of first characterization and degradation phenomena.

6.1. Test bench validation

The results presented here focus principally on the performance improvements achieved after test bench validation. To help the reader understand better, "Stack A" is used to designate the test specimen characterized prior to the test bench modifications while "Stack B" refers to the specimen tested after the aforementioned modifications.

During the test bench validation, it was immediately clear that modifications on the system were needed in order to reach a uniform temperature target among the gases and top/bottom plates close to 750°C (nominal operating temperature). Temperature distribution is one of the most important factors to take care of, because the presence of temperature gradients between stack and gas inlet flows may cause differences in the performance of the stack, measured in different set-ups and a higher rate of degradation in case of long-term operation.

It can be observed in Figure 54 how the modifications made to the test system after test bench validation, clearly improve the average temperature of inlet flows (shown in Stack B), to be comparable with $T_{av,stack}$.

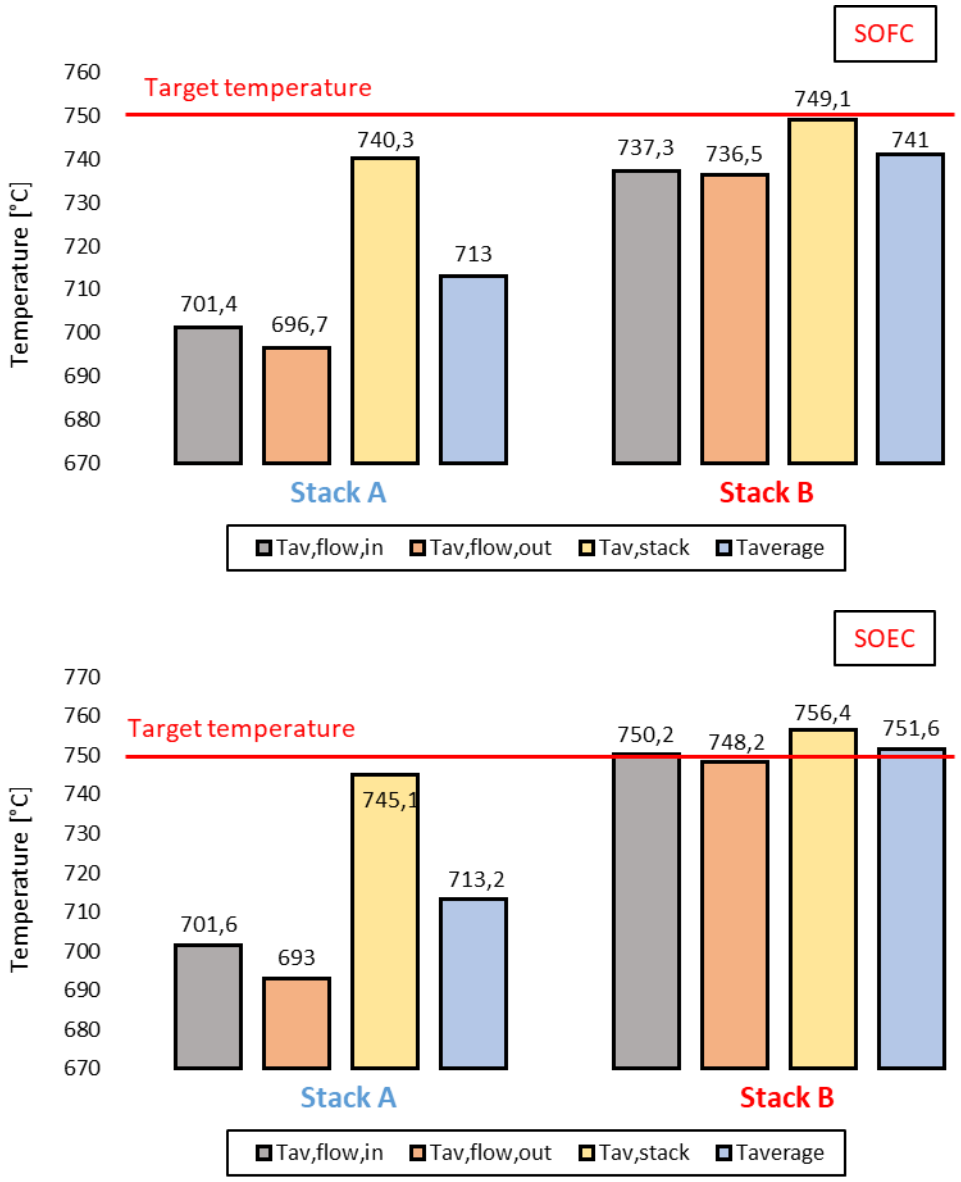

Figure 54. *Comparison of temperatures for each validation in both SOFC/SOEC modes.*

Unlike SOFC mode, the target temperature of 750 ° C in SOEC is achieved more easily, as less gas is supplied on both the negative and positive electrodes sides, which allows the gas preheaters to work more effectively.

Figure 55 shows the performance of both stacks, in terms of polarization curves, in SOFC and SOEC modes respectively:

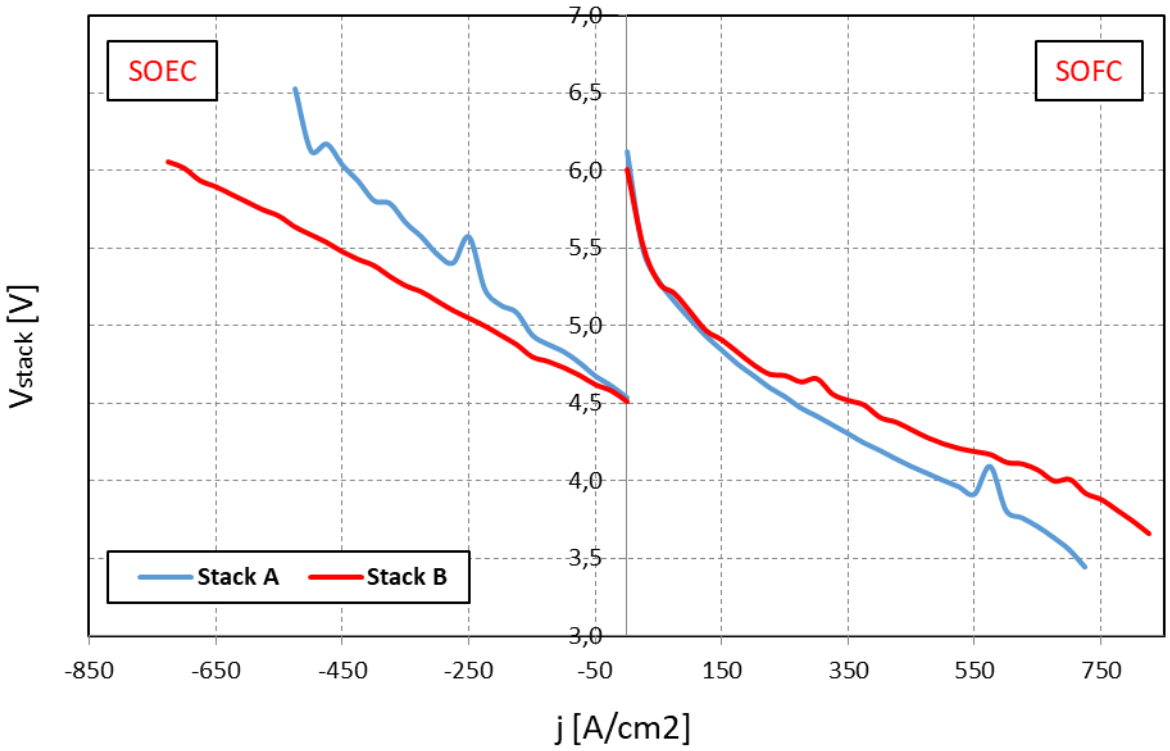

Figure 55. *Comparison of polarization curves in both SOFC/SOEC modes.*

The plot shows that, in SOFC mode, the performance obtained in the two validation tests are similar, close to a value of I_{MAX} of 775 A/cm2, while considerable improvements are obtained in SOEC mode where the performance in Stack B shows a higher value of V_{max}. In order to safeguard the stack during SOEC mode, the jV test was interrupted before reaching V_{max}. Drawing a trendline of the curve it was calculated an I_{min} of 825 A/cm^2 for a stack voltage of 6.5 V (obtained considering the product of the voltage threshold values of each single cell).

The trend of the jV-curve in SOEC mode is worth noting, where unlike a linear trend (obtained after modification) before improving test system, it presented irregularities. This behaviour did not appear to be connected with temperature but rather to a poor steam stability or to water condensation in the output line, providing important indications on the necessary changes to the system. In SOEC mode, the stability and quality of the steam generation play an important role in the resulting performance of the SOEC short stack, especially for what concerns the control of a stable steam supplying and accurate and stable steam-to-H_2 ratio monitoring. This warrants therefore particular attention towards the equipment for steam generation. There are several methods for steam supply:

It is not really possible to correlate voltage trends and steam flow stability, because the steam flow could not be directly measured. Whatever happens, during the experimental campaign, the use of CEM shows good steam stability. This mixture, before exiting the device, is led into a spiral-shaped evaporator to achieve total evaporation. Other reasons to encourage the choice of CEM were the peculiar features this device presents:

- a lower working temperature than conventional systems that guarantee less energy consumption;
- an accurately controlled gas/liquid mixture.

Nevertheless, also the CEM needs to be optimized in terms of settings, since better results were achieved thanks to a higher temperature setting of the evaporator to 150 °C and due to a more efficient thermal insulation that avoids water condensation and improves steam production stability.

These results were confirmed by EIS results in SOEC mode too. The presence of CEM in the test bench which ensures better stability of steam-H_2 ratio, and the absence of water accumulation in the output negative electrode pipes provide an improvement in the quality of the spectra as shown in Figure 56. Unlike the plot before modifications where it was impossible to define a real EIS spectrum, the second one (after modification) shows a tendency similar to a normal galvanic cell (with the 2 semicircles) even though the instability problems seem to reappear at low frequency due to mass transfer mechanism.

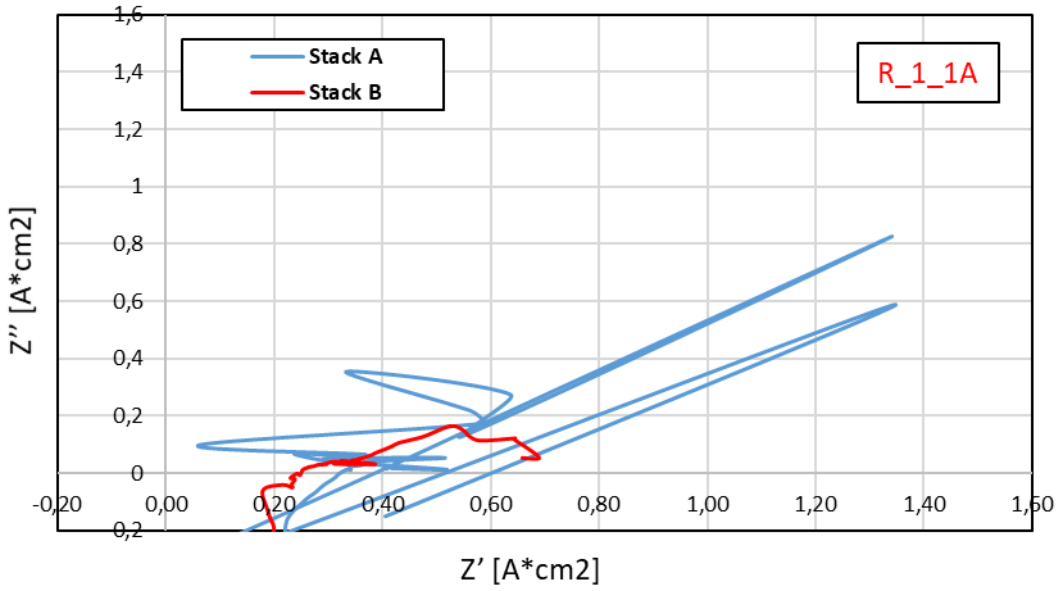

Figure 56. *EIS spectra of RU1, before and after modification, at 12 mA/cm² – SOEC mode.*

Trace heating may be a good option to avoid water condensation, but only if the heating system will cover the entire line including the vent. Otherwise it needs to be actively tapped from an expansion vessel as in our case in the second and third validation rounds.

With regards to the Nyquist plot in SOFC mode, it can be noticed from Figure 57 that the changes of the position of current collectors improved the quality of the spectra in terms of reduced scattering of the measurement points.

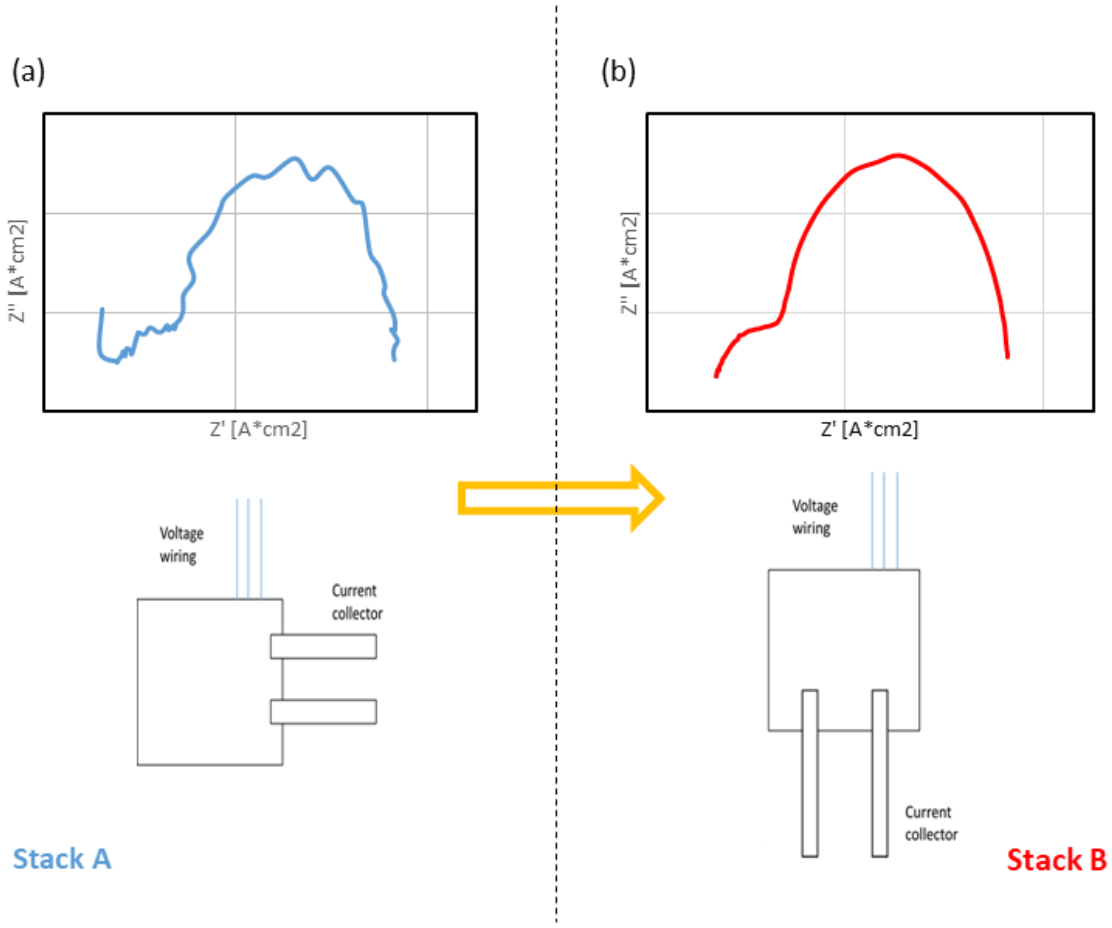

Figure 57. *Position of the current collectors and the respectively EIS at 12 mA/cm^2 in SOFC mode. In the specific (a) is the configuration before modification and (b) with modifications.*

The effect of the experimental set-up has been evaluated also in a long term test at constant current in SOFC mode.

Figure 58 shows the voltage characteristics of the involved stack at continuous operation under constant current in SOFC mode and the corresponding degradation rate for 500 h of testing. As it is possible to note in the figure, the stack after modification (red line) was tested at a higher current than the before (blue line), which should mean a more pronounced degradation rate due to greater thermal and thus mechanical stresses. In this case, instead, comparing the two trends, after modifications of the test bench, a better performance occurred due to a more homogeneous temperature of the inlet gases with the actual stack temperature.

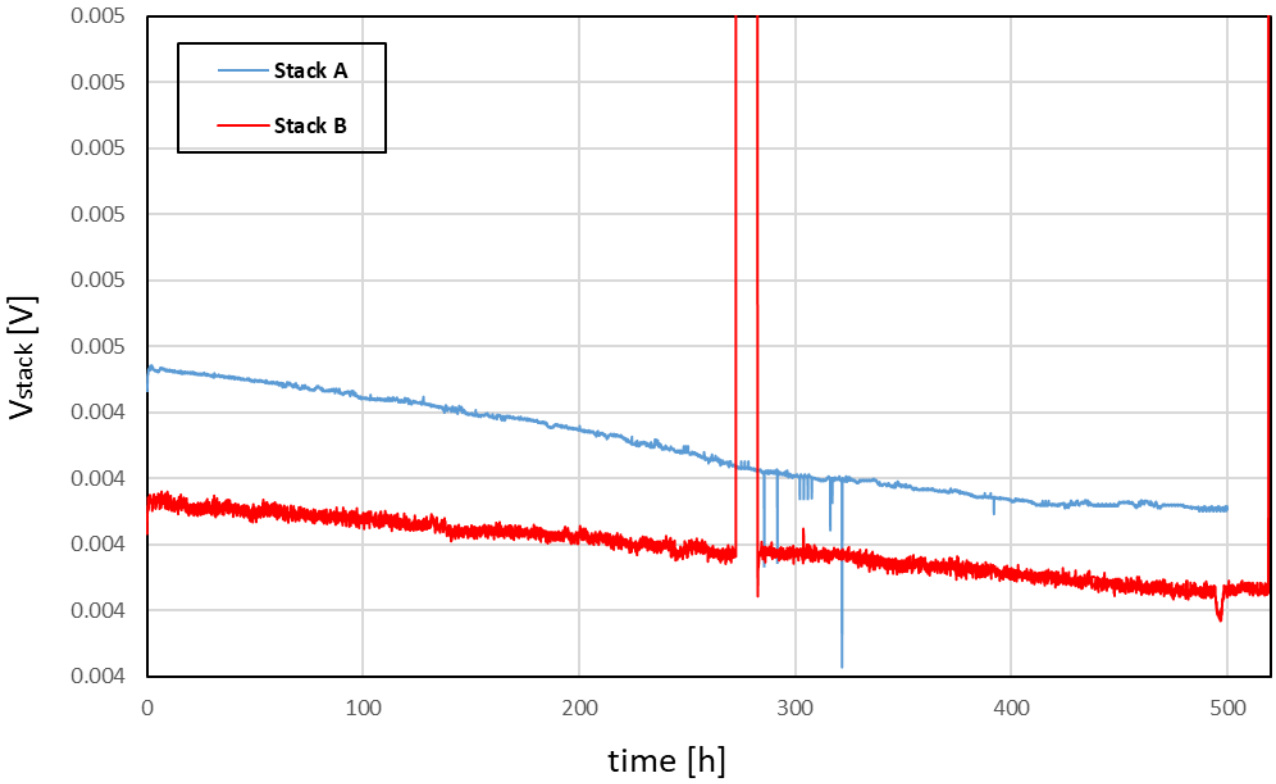

Figure 58. *Voltage profiles during long term operation under constant current (500 h) in SOFC mode with the respective degradation rates. In the specific, the Stack A (the line-up) was tested with 0.3 A/cm2 of current while the Stack B with 0.5 A/cm2.*

To ensure good stability of the system to work in SOFC/SOEC modes, stack B was also tested in cycling operation in combined mode following a symmetrical load profile to study the influence of electrical and/or thermal effects on degradation and voltage stability. The aim was to emulate a possible power-to-gas-to-power profile when operating the Re-SOC assembly unit with an archetypical PV profile where power is stored as H_2 and re-generated as electricity in a 24-h cycle.

Figure 59 shows the results of the stack run in combined SOFC and SOEC mode after modification of the test bench. The duration was 3 hours in SOFC mode and 20 hours in SOEC mode (per day) of operation, including twice 0.5 h for switch from one mode to another.

Voltage degradation rate in stack B was observed during the SOEC mode operation. The degradation trend appears rather uniform after each cycle probably due to a not perfect quality of the steam even if the recorded voltage increases again in the 8th cycle peaking a value close to the initial value. This final behaviour seems to be connected at the presence of condensed water in the output line that has caused voltage drop. These results are linked to Stack B. Without the test bench changes, was impossible test stack A due an immediate failure.

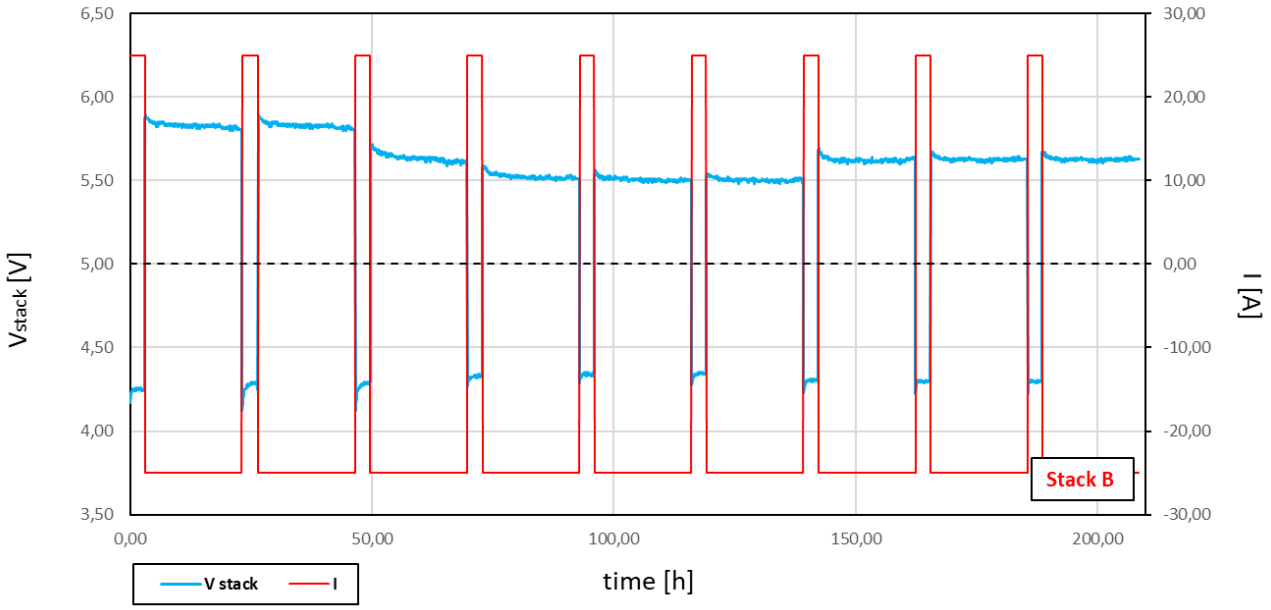

Figure 59. *Stack voltage B evolution with time in combined SOFC/SOEC modes after modification of the test bench.*

6.2. A meticulous analysis of selected test modules

Only results related to key test modules will be taken into consideration. From the "final round robin test" will be examined TM02, TM03, TM04, TM07, TM09, TM12, TM13, TM14and TM16 as these have been tested by all SOCTESQA project partners both in SOFC and SOEC mode.

6.2.1. TM 02: Start – Up

Figure 60 shows the heating-up and reduction process of a stack characterised at ENEA. Figure 60 includes the temperature of the top plate T_{TP} and the 5 repeating unit voltages.

The T_{TP} of the stack was defined as set point for the stack temperature on which the operating temperature is controlled.

As it is possible to see in the graph, during the heating-up stage, even if the amount of H_2 fed into the negative electrode is equal to 0 l/min, all the cell voltages start to increase up to a maximum point between 0.3 and 0.6 V, thereafter they decrease and remain virtually constant until the reducing stage around 26 hours in which hydrogen is supplied.

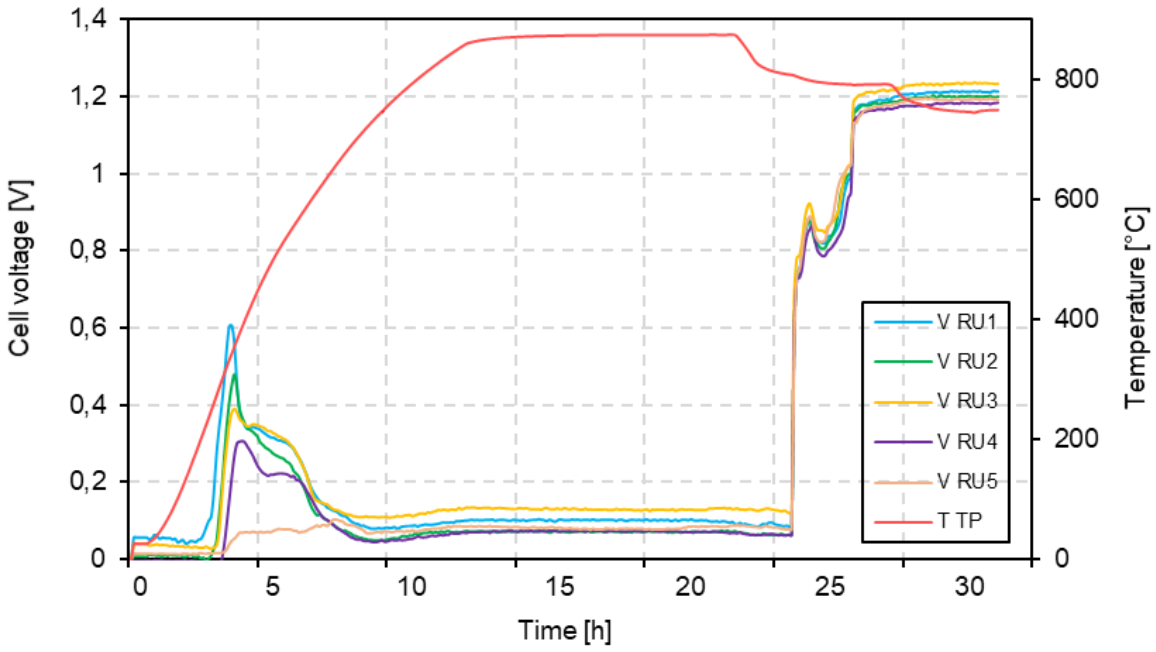

Figure 60. *Start-up of the stack of ENEA with a heating rate of 3 K/min.*

In order to verify the influence of the maximum temperature difference (ΔT_{max}) on the tightness of the stack, the OCVs of all the partners was compared and the results are shown in Figure 61 and 62. During the second validation, the influence of ΔT_{max} has been investigated more detailed by reducing the heating rate at ENEA's test station from 3 to 2 K/min. Nevertheless, no additional benefit of lower ΔT_{max} was found.

The temperature differences of the tested stacks vary between 27 K (stack ENEA and CEA) and 70°K (stack DLR) with a difference from the lowest to the highest value equal to 53 K, comparable to the other test validations.

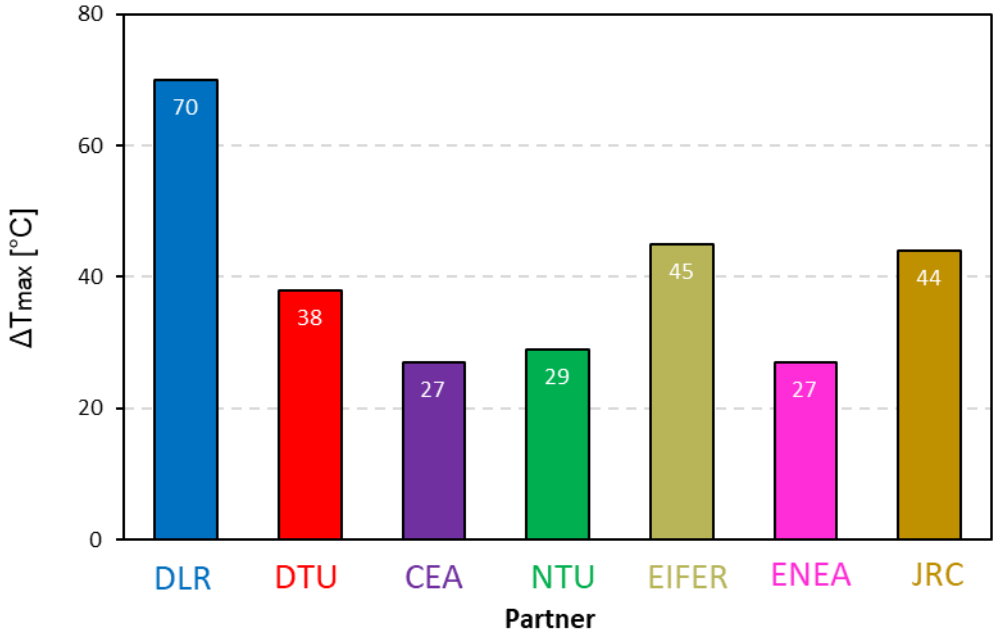

Figure 61. *Maximum temperature differences during heating-up.*

The influence of these temperature gradients on the stack tightness is shown in the following diagrams.

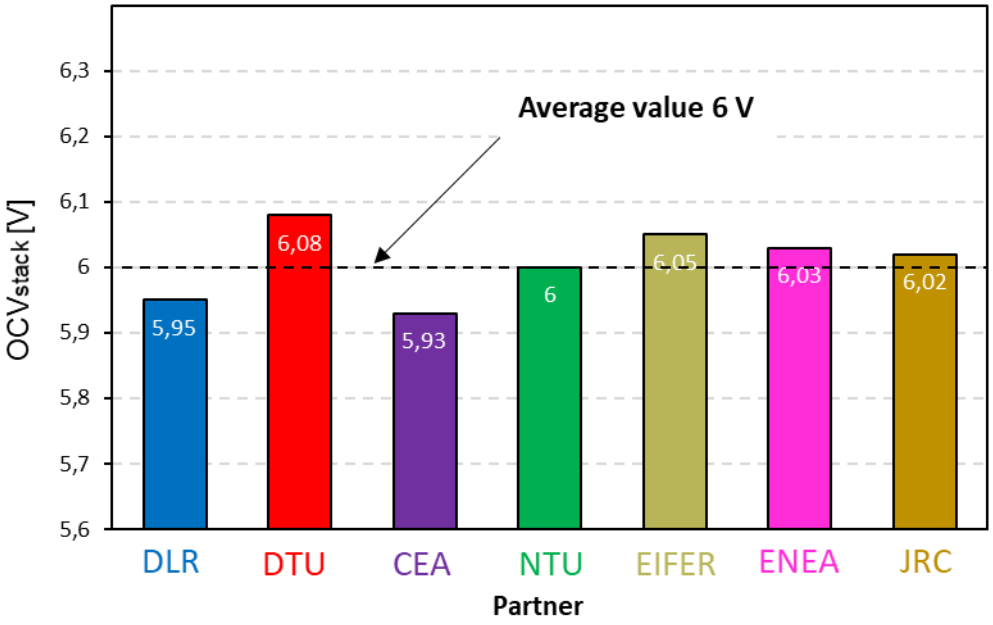

Figure 62. *OCV's stack at the end of the start-up procedure.*

The average stack OCV of the tested stacks is 5.997 V (± 0.061 V for standard deviation) which is slightly lower than the theoretical calculated value of 6.0 to 6.25 V. The values are in a range of 5.93 (stack CEA) and 6.08 V (DTU).

In order to find a possible reason for the lower OC measured at DLR and CEA, also the single repeat units have been investigated. Figure 63 shows the OCVs of the RUs of all tested stacks at the same operating conditions.

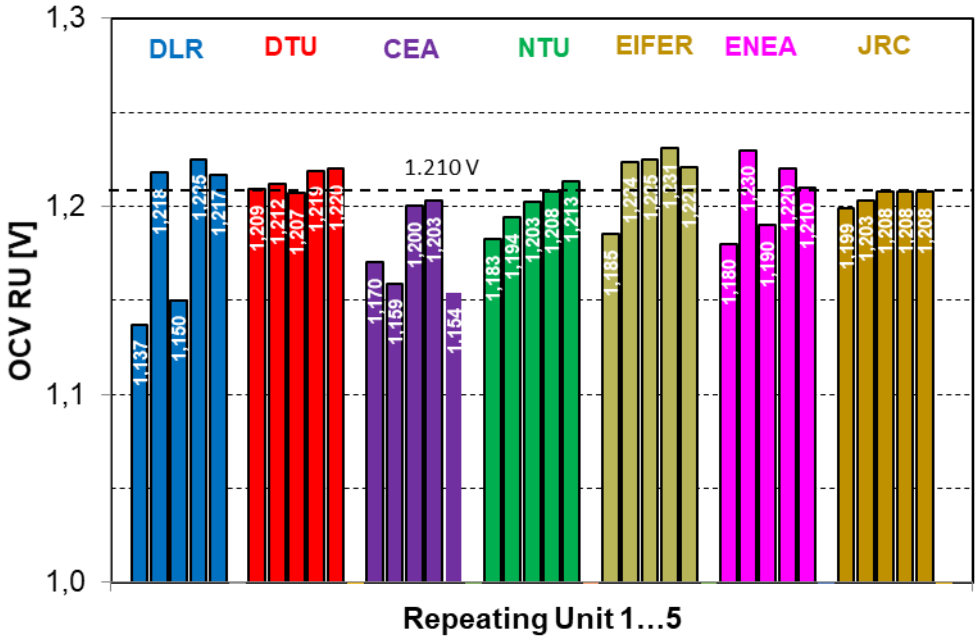

Figure 63. *OCVs of single RUs at the end of the start-up procedure.*

The average OCV of all RUs is 1.210V (± 0.018 V) with similar standard deviations close to the theoretical value of 1.2 to 1.25 V/RU. It is clearly shown that the lower OCV of DLR stack is caused by RU1 and RU4, while for CEA stack is caused by RU1, RU2 and RU5. Therefore, the other OCVs value proving that the performed ΔT_{max} have not significant influence on the gas tightness of the single RUs and the whole stack. The assumption is also confirmed by CEA and ENEA stacks that, even if present comparable ΔT_{max}, show different OCV values. Since the OCV is not dependent on ΔT_{max} it is assumed that slightly higher pressure levels of the operating gases in the stack are responsible for the different value of OCVs. In any way it has be considered that the sealing between gas distribution plate and stack may be the reason for this difference- At the same time the deviations in OCV of the other cells can be explained by oscillating cell voltages caused by the software and the resulting coarse resolution of the cell voltage measurement.

In order to harmonize the temperature measurement among the different test stations of the partners, different solutions can be applied e.g. focusing on the positioning of the thermocouples. However, the discrepancy in maximum temperature difference will be always dependent on various factors such as different preheating gas subsystems, a non-optimal positioning of the stack inside the furnace and furnace design, which can be comprehensively recognized as the main cause.

However, the results of the different stacks tested during the five validation rounds show a high consistency which proves the high quality and reproducibility of the test module 02.

Therefore, in order to optimize the test module, the following recommendation should be integrated:

- Before the start-up a high gas tightness of the gas supply subsystem of the test station, of the stack itself and of the interface between stack and test station has to be guaranteed;
- Detailed monitoring of the test input and output parameters at the interface is obligatory;
- In order to obtain information of the real temperature of the stack it is recommended to install several thermocouples at characteristic reference positions om, in or near the stack;
- ΔT_{max} should be kept as low as possible during the heating-up process in order to minimize thermo-mechanical stresses;
- The temperature distribution inside the stack during the whole start-up procedure should be as homogeneous as possible.

Thus, in conclusion, when it is not possible to directly measure the internal temperature of the stack, T_{av} (Eq. (47)) is recommended as the best parameter to access the temperature of the real stack since it takes into account all temperatures, such as those relating to the endplates, the two inlets and the two outlet gases. A good preheating system is required that can reach the operating temperature. To keep ΔT_{max} as low as possible, it is advisable to set the temperature of the preheating system following the evolution of the furnace temperature. In so doing, the discrepancy between the temperature of the stack and the gas inlet shall be avoided.

This TM topic is quite common and usually described by the cell/stack manufactures. The use of this TM also depends on the specific test facilities. Similar start-up test procedure can also be found in references [87][18]. However, the current test module gives an additional descriptive start-up sequence, which may be used for both SOC single cell and stack testing, also detailing the relevant TIPs, TOPs and derived quantities with their associated formulas and their evolution.

Based on the literature, in order to optimize the test module, a future step could be to test several heating-up stage increasing the heating rate. Even if usually the start-up and shut-down procedure are left as secondary tasks to be solved, however they may be events that happen quite often and thus,

may be quite important in the creative process of developing system. This is especially true for small power units used in transportation applications or for domestic energy supplies, where the load demand changes frequently and peaks in load of short duration are common. In addition, start-up and shut-down may also significantly affect the life span of the system due to thermal stresses on all system components and a procedure in as short a time as possible can reduce the costs of fuel consumption [88][89][90].

In that case to really investigate the thermal stress increasing the heating rate, an I-V curve test would be appropriate beside the OCV measurement.

6.2.2. TM 03: Current-voltage characteristics

To help the reader for a better understanding of this important test module it was decided to split the results report in two parts, one concerning the SOFC and one the SOEC operating mode.

SOFC mode

The initial current-voltage characteristics of all tested stacks for the round robin test are shown in Figure 64 along with the variation of the average endplates temperature which is considered the one that increases the most by varying the current. due to the heat generated whenever current is passed through resistive material for the Juele-Thomson's law. Therefore, as the current increases, the thermoelectric effect will induce heating of the system.

The test input parameters were 750 °C with 0.5 H_2 + 0.5 N_2 // 4 air NLPM/RU.

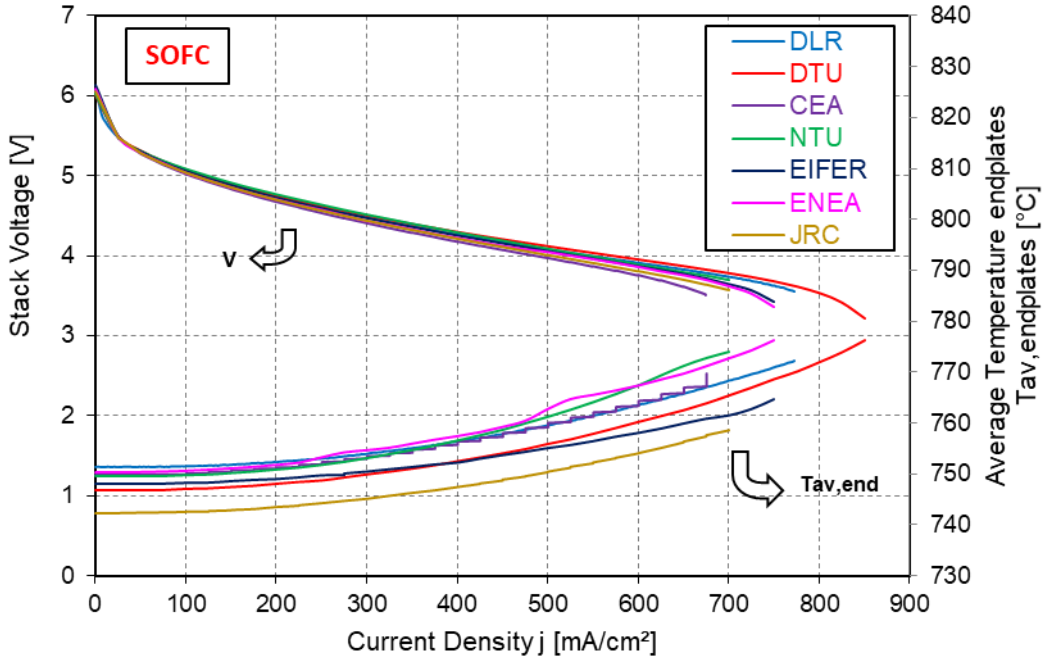

Figure 64. *Initial current voltage behaviour and average stack temperature of all tested stacks in SOFC mode.*

Figure 64 shows a high uniformity of the jV-curves among the different partners. The performance of all tested stacks is very uniform and the variation of the stack voltage at 500 mA/cm^2 among the single jV-curves is around the 5% that is exactly in line with the defined tolerance range of 5% given by the stack supplier. The variance becomes more obvious with increasing current densities. At a current density of 700 mA/cm^2 the deviation is 8.2%. This value is quite acceptable taking into account that this might be an influence of the disposal of stacks from different manufacturing batches,

as well as of different test bench hardware with differing thermal inerzia. After 700 mA/cm$_2$ the deviation increases more and more as the current increases and in the end only DTU and DLR are able to reach the maximum current density point equal to 850 mA/cm^2 while partners as ENEA and EIFER drop at the minimum voltage permitted at 750 mA/cm^2.

The shape of the temperature curves is also very uniform among the partners (during the jV-curve the temperature increases with increasing of the electrical current). With increasing current density, the average temperature of endplates, increases gradually with a maximal difference of 16 K at 700 mA/cm^2.

Calculating the voltage difference at 500 mA/cm2 of the others partners with respect to that achieved in DTU (as the best in performance), and comparing these values as a function of the average temperature of endplates, it is possible for this test to notice in Figure 65 that:

- the stack tested at CEA reaches the lowest stack voltage despite the fact that the measured temperature is the same as that of DLR;
- the stack tested in JRC which would be expected to reach the lowest performance since it had the lowest average temperature instead shows the same voltage as DTU;
- the stack performance in ENEA, which should reach the maximum performance, is about 1.9% lower compared to the stack of DTU;

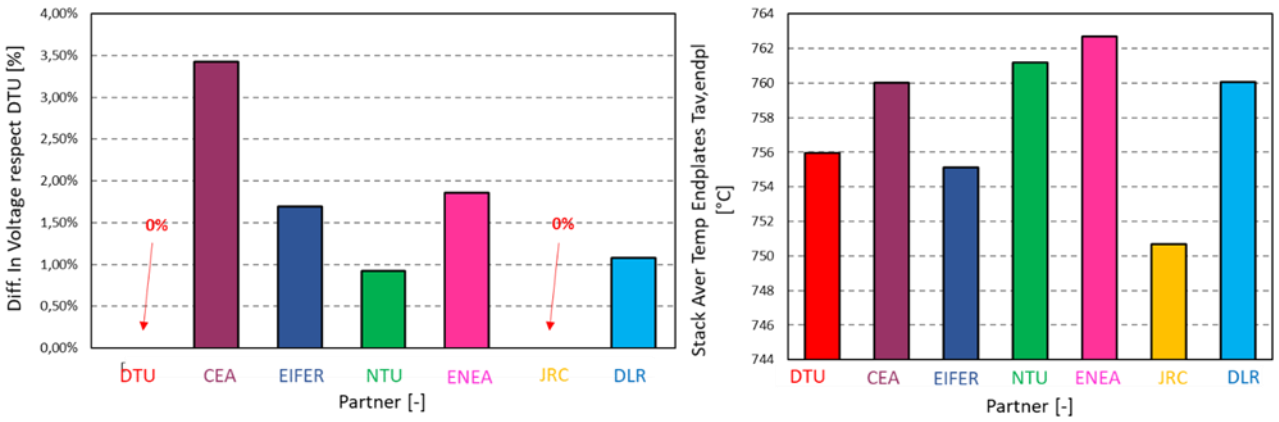

Figure 65. *Comparison between Voltage Different and Average Stack Temperature among the partners.*

Similar results were achieved in the other validation confirming that the dependency between temperature and stack performance is much more complex. For this reason, additional influences have to be responsible to accurately explain the behaviour. In order to validate reproducibility and repeatability, the stacks of the same partner of the different campaigns have been also correlated to the gas inlet temperature. The choice of this assessment parameter is linked to the preheating systems since the value of preheater outlet temperature is highly dependent on $T_{av,gas,in}$ and $T_{av,endplates}$.

Figure 66 shows the stack power densities of all stacks at 500 mA/cm^2 as a function of average gas inlet temperature of all four testing campaigns.

Nearly all of the tested stacks, except JRC in the 2nd validation, are in range of 1980 to 2090 mW/cm^2 which corresponds to a variation of 5.1% between all stacks (highest and lowest value). This value is very close to the quality variation threshold value given by the stack supplier. By optimization of the gas preheating systems in previous campaigns the average gas inlet temperature in a range of 741 to 753 °C can be reached by all partners except of ENEA and JRC. Nevertheless, as it is possible to see in the graph, a real dependency between gas inlet temperatures and stack performance is not visible.

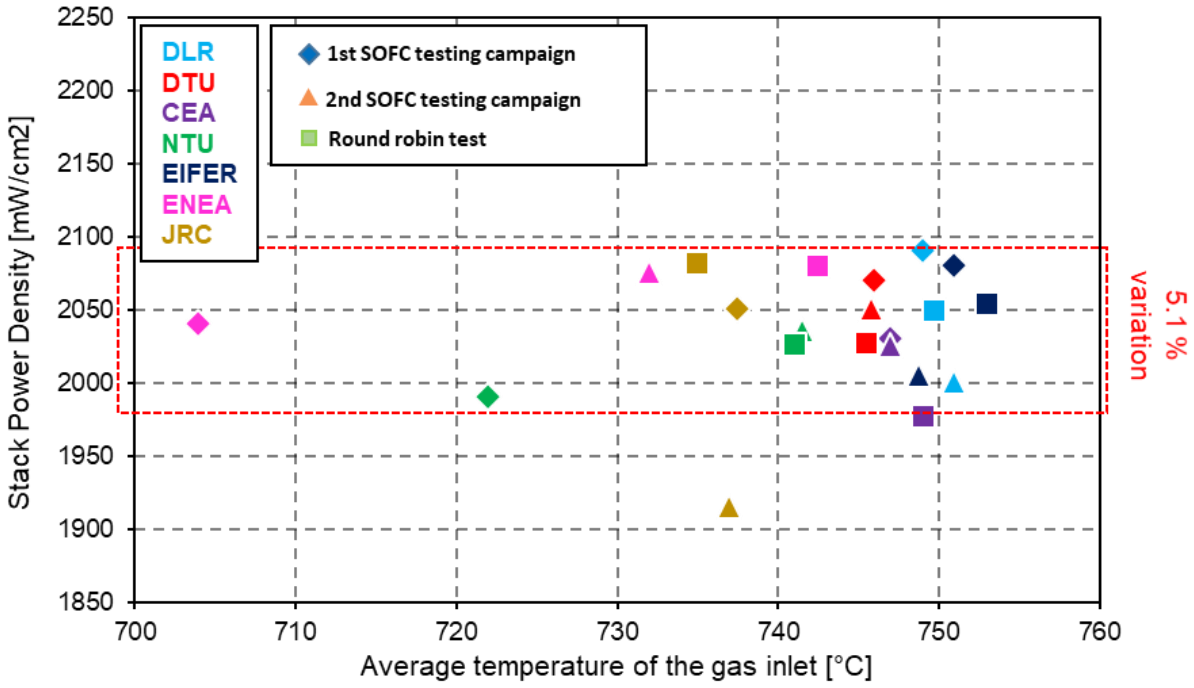

***Figure 66**. Stack power density calculated at 500 mA/cm2 as a function of the average temperature of the stack inlet gases ($T_{av,gas,in}$).*

With these results it can be concluded that the variation in power density is within the defined values of the stack supplier and probably rather related to stack reproducibility than to the influence of gas inlet temperatures.

Considering that the most commonly applied parameters that can be extracted from jV-curves are the open circuit voltage *OCV*, the maximal power density Wel_{max}, the internal resistance R_i and the corresponding area specific resistance *ASR*, in order to find a correlation among the results also the *ASR* value was taken into account in this critical analysis.

Figure 67 confirms that the ASR values determined at 238 mA/cm^2 and 500 mA/cm^2 in SOFC mode are comparable among the partners, except for the stack tested in ENEA which shows different ASR compared to the other partners for a density current of 238 mA/cm^2. As it is possible to see, the calculated ASR values do not always correspond to the measured jV-curves shown in Figure 64.

For example, the ASR values of the stacks measured at CEA and NTU determined at 500 mA/cm2 are the same observed (1903 mΩ*cm2) but the jV-curves of both stacks differ from each other. Moreover, stacks tested at ENEA and EIFER should have the same value of ASR since the jV-curves achieved are very close to each other but instead they differ by 130 mΩ*cm2 while the stack tested at DLR should have a lower value of ASR compared to that achieved in JRC comparing the jV-curves visually.

Based on the theory (Eq. (50)) the ASR value changes in correlation with the jV-curves shape and these show that their shape is sensitive to conditioning parameters, thus the ASR can yield quantitative estimation of those deviations reflecting the characterization among the different partners. However, the ASR calculation depends strongly on an accurate measurement and recording of the voltages. Since the ASR value is expressed as the ratio between voltage and current, the presence of voltage scattering alters the correct measurement. Therefore, the determination of the ASR calculation must be improved. For example, in ENEA the globally higher ASR might be associated to the scattering of the voltage.

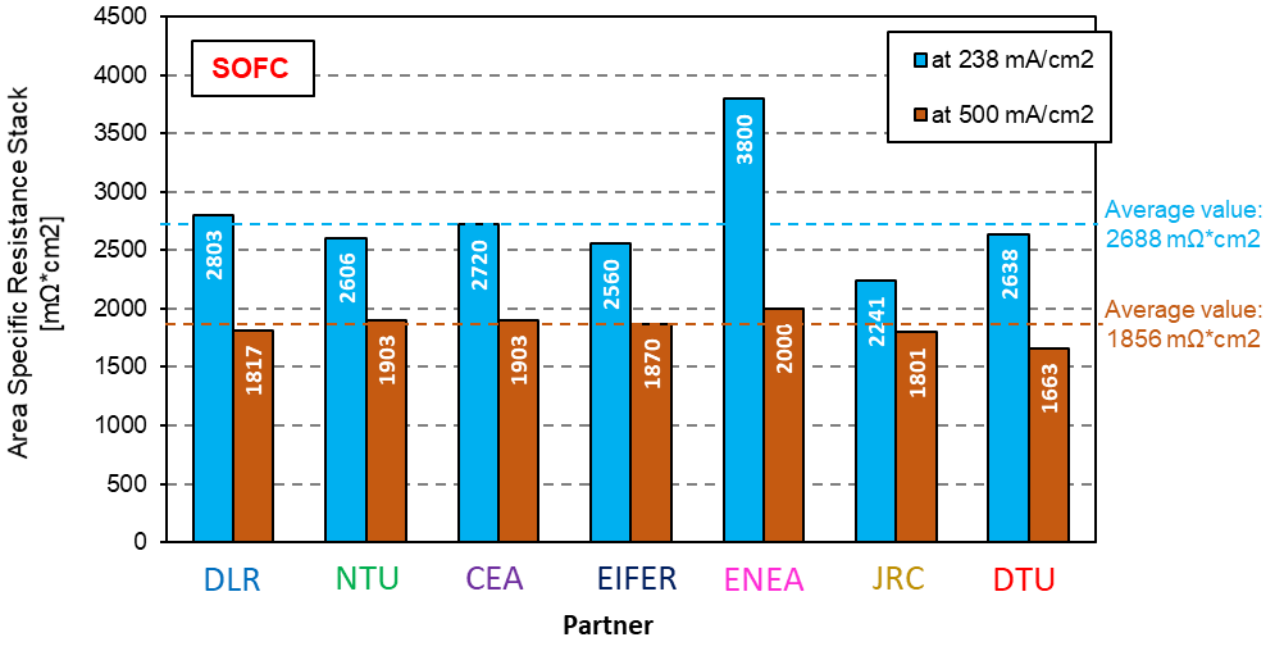

Figure 67. *Comparison of stack ASR values for initial jV-curves calculated at 238 mA/cm² and 500 mA/cm².*

Despite the slight differences Figure 68 demonstrates a good reproducibility of the results showing the *ASR* for every experimental point of the jV-curve. The average *ASR* trend (labelled "media") has also been determined and plotted in Figure 68.

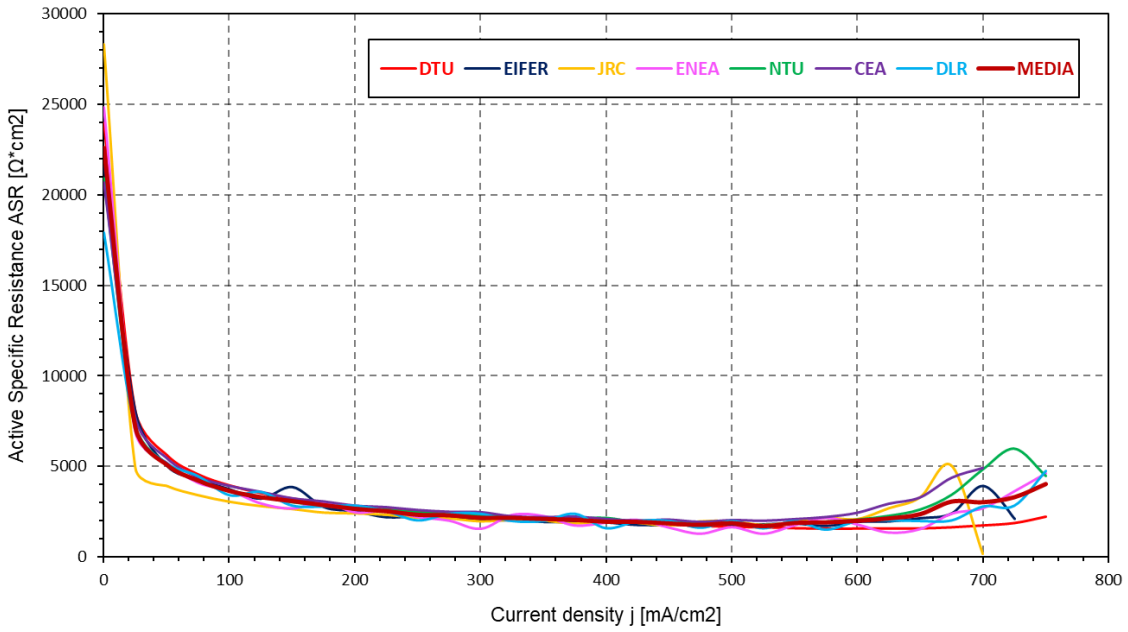

Figure 68. *Comparison of all ASR trend calculated for every experimental point vs the average ASR trend.*

Starting from the theoretical OCV value equal to 6 V it is possible to extrapolate from the "media" trend a reference jV-curve. Since the tested stacks are composed of 5 repeating units, it is possible to determine the single cell voltage trend "V_{cell}*" as a function of the current density at 750°C.

The resulting V_{cell}*, represents benchmark to evaluate the initial performance of similar stacks. In the event that a cell shows for a current density of 500 mA/cm2, a voltage trend of less than 2.5%

compared to V_{cell}*, for example it is possible to apply an acceptance/criterion for the rejection measured stack.

Figure 69 shows, together with the V_{cell}* trend, two initial cell voltage trends of stack tested in CEA and DLR respectively. Both stacks present at least a cell with a difference in voltage higher than 2.5% compared to the *Vcell**. Both stacks showed irregularity during the test program: one collapsed and the other showed a fast degradation rate during the long term test.

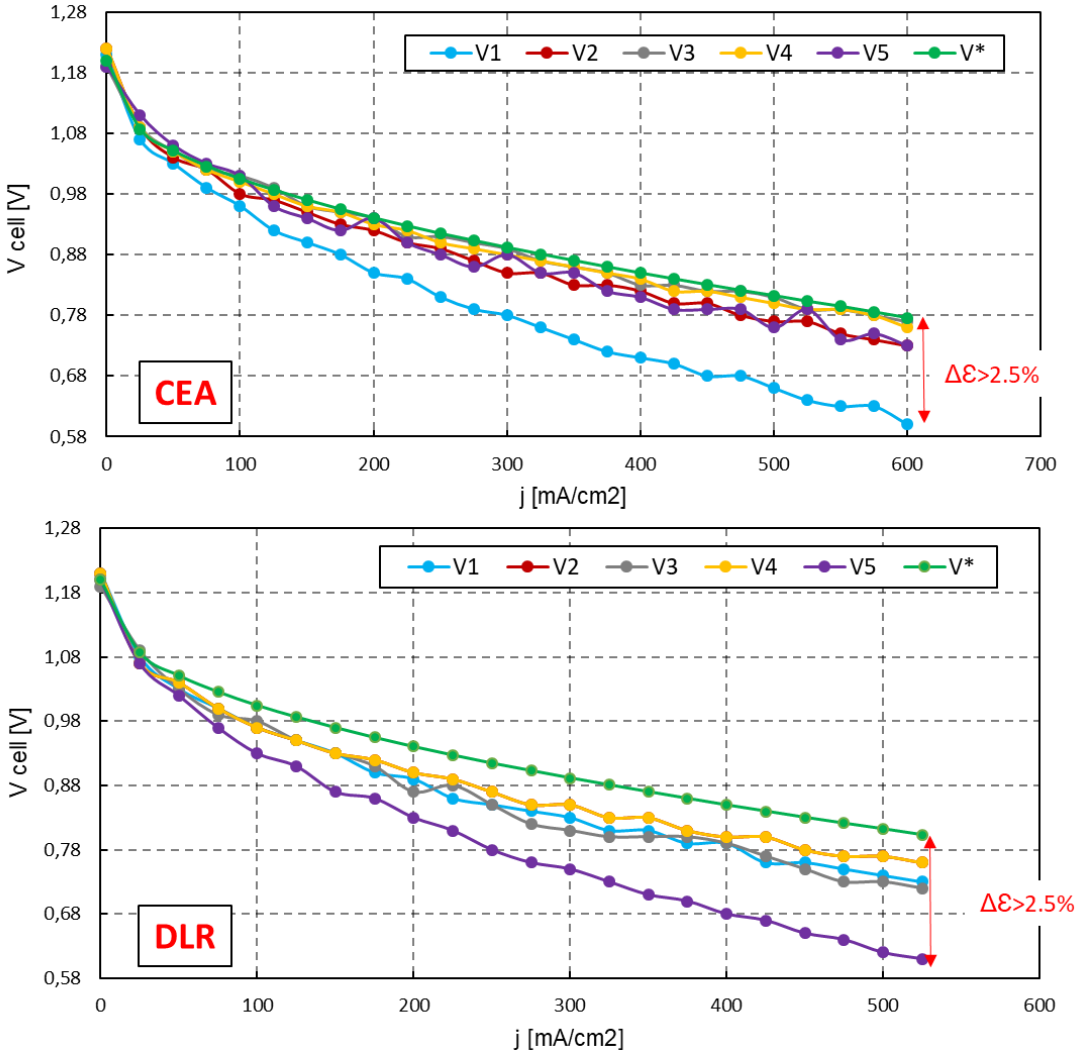

Figure 69. *A first evaluation of the initial performance based on the calculation of Δε according to the Vcell * for the stacks tested in CEA and DLR.*

Figure 70 shows the behaviour of the stacks tested at CEA and DLR during the operation under constant current. As it is possible to see, based on the irregularities present in the Figure above, both stack during the test showed problems. In particular, the stack at DLR after showing voltage stability at the beginning of the test, collapsed around the first 75 hours while the stack tested at CEA showed a very fast degradation rate.

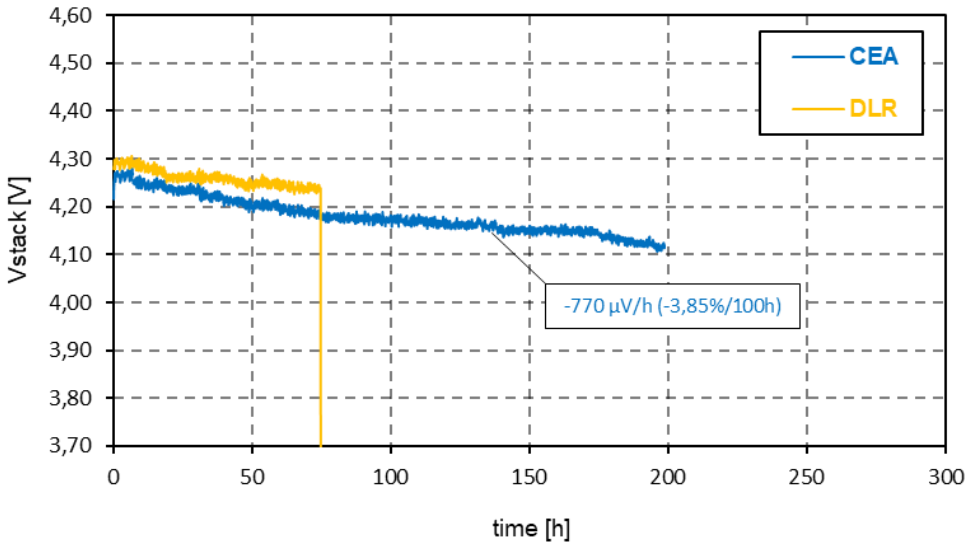

Figure 70. *Voltage trends of stack tested at CEA and DLR which showed problems during operation under constant current.*

Starting from *Vcell**, on the basis of the open circuit voltage (OCV), the total loss has been calculated. Assuming a linear proportion between the total loss and the active area, a first estimation of the voltage trends as a function of the current I for different active area has been determined. The idea behind this processing is related to the large amount of data collected during the entire project that, in addition to providing advice to improve each individual test module, can provide an estimate of the performance expectation.

Figure 71 shows an example of voltage trend for a cell with an active area of 120 cm^2 extrapolated from the *Vcell**. At the same time, once known the *Vcell**, based on the number of the repeating units within the stack, it is possible to calculate the total voltage trend directly by multiplying each values of *Vcell** with *n*, number of cells. In Figure 72, some examples are shown:

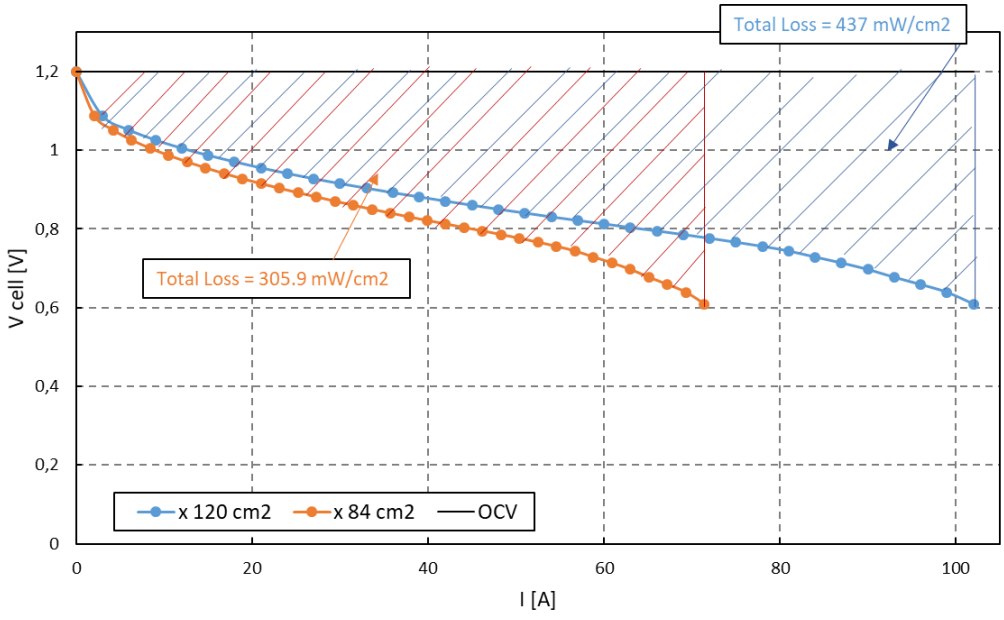

Figure 71. *jV-curve comparison between two cell with different active area.*

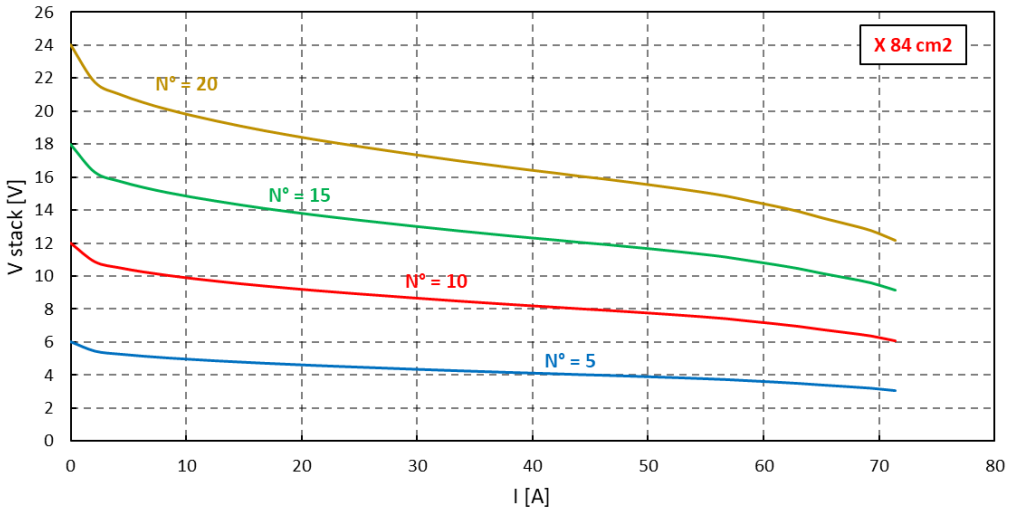

Figure 72. *Examples of different voltage trend depending on the number of the RU.*

All the new trends have been built based on theoretical reasoning and on the big amount of results collected. More results are necessary, to validate them, but as first evaluation can be considered acceptable.

SOEC mode

The same critical analysis done in SOFC mode has been repeated in SOEC operating mode.

Figure 73 below presents the initial performance of the EK stack tested in SOEC mode in each partner's laboratory and the evolution of the average temperature T_{av}. The test input parameters were 750 °C with 0.63 H_2 +2.52 H_2O // 1 air NLPM/RU.

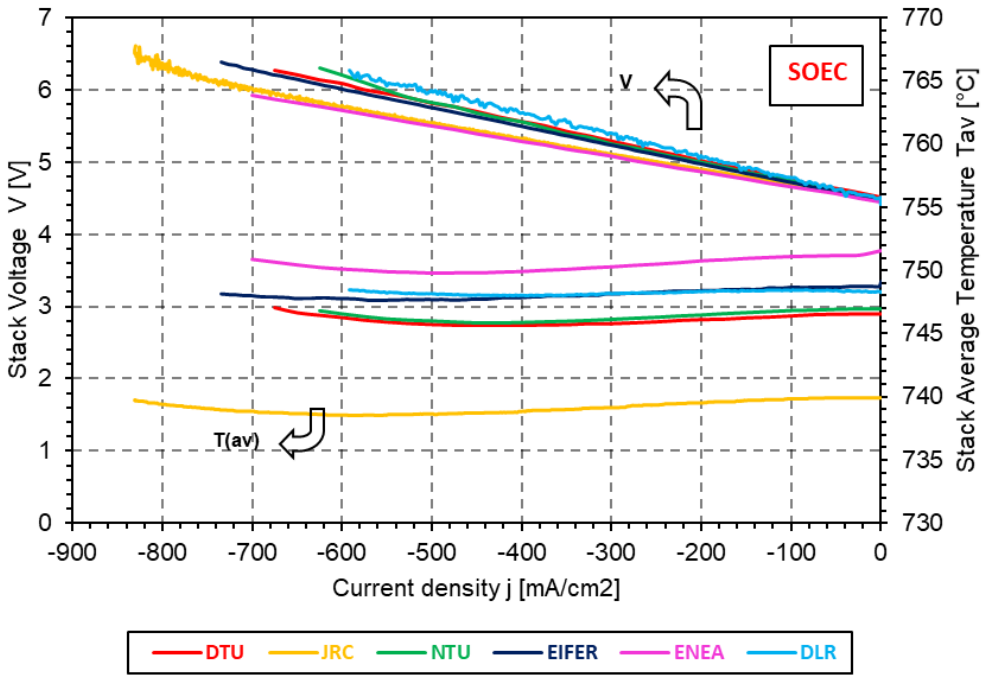

Figure 73. *Initial current voltage behaviour and average stack temperature of all tested stacks in SOEC mode.*

Differently from the SOFC mode, the experimental results appear more dispersed with fluctuations observed on the voltage signal for DLR and JRC. The variation of the stack voltage between the highest (ENEA) and the lowest (DLR) performance at -300 mA/cm^2 is around 6% and increases with current density for a maximum of 16% at -600 mA/cm^2.

As in SOFC mode, even in this case, thermal aspect does not seem to give a clear explanation of the results achieved since JRC and ENEA reach the highest performance even if ENEA was the hottest stack while the JRC the coldest one in terms of average temperature.

The ASR values at -238 and -500 mA/cm^2 in Figure 74 confirm the results above observed. However, by consulting the two plots, it can be noticed a direct link between the ASR values and the jV slope. The angular coefficient of the curve increases as well as increases the value of ASR.

Differently to the SOFC mode, where all the jV-curves have been recorded with a 2.1 A per 30 s current density increase, in SOEC instead the current density increase with a step of 0.07A/s. The new measurement leads to an identical jV curve with a higher number of points recorded but with a very low voltage fluctuations and thus a better precision of ASR determination.

To confirm the improvement in terms of less voltage scattering via reducing the current step size, in ENEA the jV-curve in SOFC has been repeated changing the step size from 2.1 A per 30 s to 0.07A/s. The benefit in the ASR measurement are shown in Figure 75. As it is possible to note, changing the current/time step, for the same power density, the difference in ASR reduces.

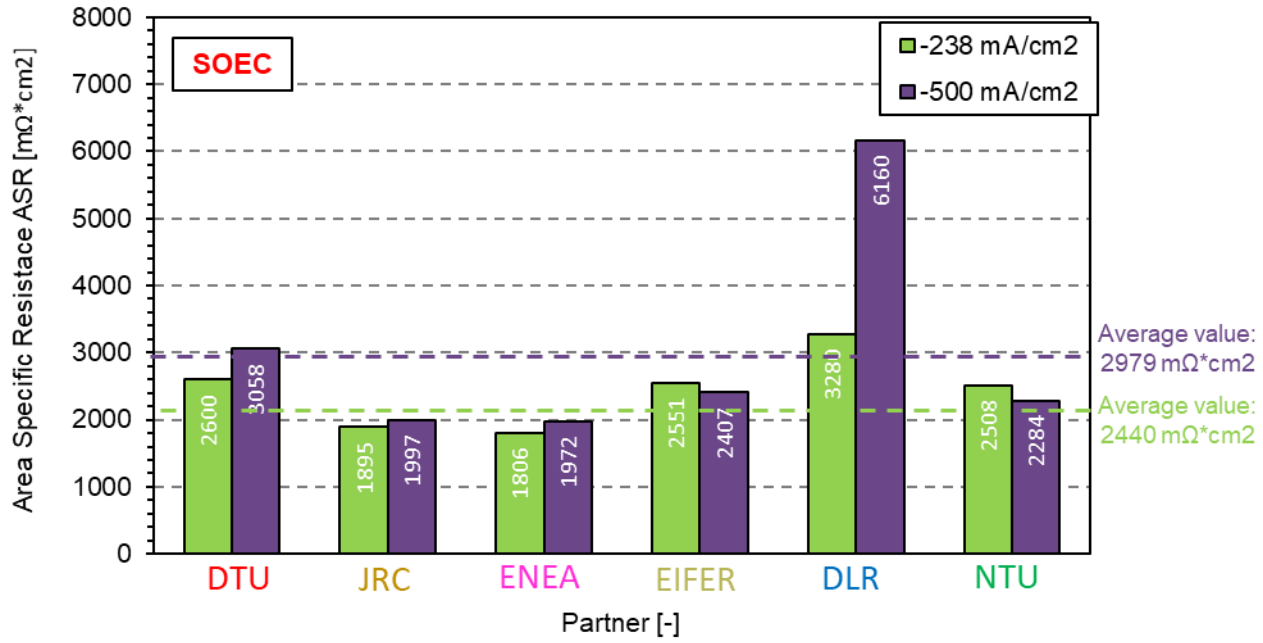

Figure 74. *Comparison of stack ASR values for initial jV-curves calculated at -238 mA/cm^2 and -500 mA/cm^2 for SOEC mode.*

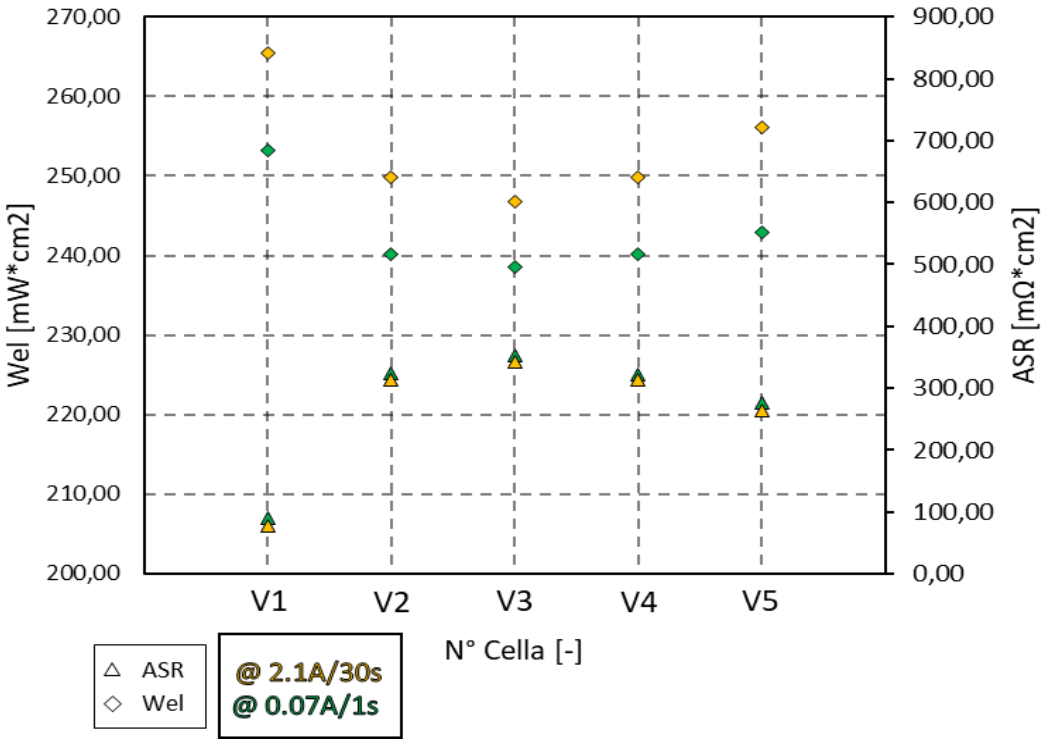

Figure 75. *Comparison of stack ASR values changing the step size from 2.1A/30sec to 0.7A/30sec.*

This results confirm that as well as to the rate of electrical current change also the current/time step is a fundamental input parameter. The current change rate has an influence on the hysteresis but not the current/time step. On the other hand, the smaller the change rate of the current, the longer the duration of the measurement and the smaller the hysteresis. Thus it is recommended to choose a current change rate which compromises between these two parameters.

The higher results scattering could be attributed to the fact that tests were performed on stacks from different batches due to the lower robustness of the stacks.

In addition, comparing the jV curves in SOFC / SOEC modes, it can be noted that there is no direct connection between the performances obtained since especially in the case of the DLR which had achieved the best performance in fuel cell mode together with DTU, in electrolysis mode it shows instead the lowest. As just mentioned in chapter 6.1, the problem related to the stability and quality of the steam generation are critical in order to have fully comparable results.

The jV analysis alongside that EIS is known as the best test module to characterize the initial performance of a Solid Oxide Fuel Cell. Different parameters can be extrapolate depending on the shape of the curve such as the power of the cell/stack or as mentioned above the active specific resistance which is a good parameter indicator for comparing different behaviours of cells/stacks. Thus, nowadays, this test method is rather common and easy to find it in the literature. Nevertheless, none of them deals with SOEC, or at cell or stack level, and in addition any existing procedures does not specify a cut-off voltage to terminate test or provides a detailed measurement method.

On the basis of this scrupulous analysis, the following recommendations are proposed in order to optimize the test:

- The calculation of the ASR values is strongly influenced by measurement errors or fluctuations of the voltage. High resolution enables a precise determination of ASR values. Thus, before a jV-curve can be performed, the measuring device should be checked in terms

of accuracy, waiting for the stability of the OCV and of all temperatures is obligatory. It is also recommended to adapt the width of the current interval at which the voltage values are recorded in order to get reliable results in terms of ASR calculation. Even the data acquisition rate should be small to get more data points (for example 3 s);

- The most common method for the determination of the ASR is classified as the "interval method", i.e. the specific points are selected in the current-voltage curve in order to calculate the slope of the curve around a specific current density. For a specified current density, the magnitude of the ASR is given by dividing the difference in SOC voltage with the difference in current density. However, in the case of fluctuations of the voltage which to not allow an exact determination, an alternative method is an enlargement of the interval so that the influence of the fluctuations is minimized or using a linear regression which fits well, to the jV-curve. A polynomial regression enables to describe also the non-linear jV-curves but in this case the measurement of ASR starts to be complicated and introduces uncertainty as regards the fitting criteria. Anyway the next bullet point is considered a right solution to avoid mathematical model or algorithms to solve the regression;
- The rate of electrical current change, the step size and the recording time are very important variables which have to be defined and specified at the beginning of the analysis. Even if reducing the current/time step size means a longer duration of the measurement, it is recommended to choose a current change rate as small as possible;
- Performing different jV-curves after each other, the stack should be kept for an adequate time without electrical current in order to ensure a homogeneous temperature for each measurement before starting a new jV-curve. This is obligatory in SOFC mode but also in SOEC, it is recommended;
- It is recommended to record also the current descending part of the jV-curve even if it is not fundamental. In case of opting for this solution, to which part the values are referred to should be indicated;
- An additional voltage supply is needed to overcome voltage drops in the hot current wires. Compare the two values (one from the voltage supply and the other one given by the sum of the voltage of any single repeating unit). In case of, they are different, choice the first one for drawing the current-voltage characteristics. It is more accurate and it is not affected from instrumental artefacts;
- In SOEC mode, special attention should be paid to a stable supply of steam in order to limit fluctuations in the voltages. The SOC voltages should not vary by more than a specified value at open circuit voltage (OCV) conditions. A threshold value of ± 10 mV per cell is recommended as stability criterion;
- In SOEC mode, voltage supply is necessary in order to impose the electrolysis voltage on the SOEC cell/stack object. In this case the polarity of the cell/stack has to be reversed in the test setup compared to the SOFC mode in order to reverse the current direction.
- For stack measurements the current is always applied to or taken from the whole stack whereas the voltage probes can either be connected to the complete stack or are just taken from the repeat units of interest. The latter case has the advantage to examine the electrochemical behaviour of individual repeat units of the stack;
- Opt for a system which ensures stability and quality of the steam generation. It is very important to be sure that the steam flow fed to the stack is controlled. Furthermore, it is critical to install a good preheating subsystem placed right downstream of it;

- For SOFC, a value of 0.6 V per cell is recommended as cut-off voltage while for SOEC, is recommended to quit the test when a cell achieves a voltage value of 1.4 V. For stack measurement the cut-off voltage is related to the worst repeating unit value;
- It is advisable to increase or decrease the current (according to the SOFC / SOC operating mode) until reaching the cut-off point with the aim of recording a complete measurement of the jV curve. Sudden drop in performance may occur in the region of gas transport loss thus pay attention on each single cell in order to avoid to overcome the cut-off point above mentioned;
- The V_{stack}* trend as elaborated seems to be a good estimate to compare the initial performance of a generic cell/stack. shows a high uniformity;

In conclusion, the results achieved in both SOFC/SOEC modes are homogeneous and the all partners shows a high uniformity. In electrolysis mode anyway some improvements are needed where the discrepancies are more relevant than the fuel cell mode. The test module as elaborated can be considered complete. However, the test can give just an initial information about the performance of the stack to immediately understand which cell/stack does not work well comparing it with the characterization extrapolated in Figure 71 or 72 depending on the active area of the cell. Thus, alongside this module, other tests are needed to have a precise check-up of the system.

6.2.3. TM 04: Electrochemical impedance spectroscopy

To help the reader for a better understanding of this important test module it was decided to split the results report in two parts, one concerning the SOFC and one the SOEC operating mode.

SOFC mode

Figure 76 shows the initial electrochemical impedance spectra at 1 A (corresponding to 12 mA/cm^2) of RU 3 of all tested stacks of the round robin test in SOFC operation. As shown in paragraph 6.1, one big issue was the improvement of the quality of electrochemical impedance spectra. Magnetic interferences between the voltage probes of the RUs themselves and also between the voltage and the current probes could be minimized in order to eliminate high-frequency artefacts. The improvements on the test benches given in paragraph 5.2 and emulates by the other partners have allowed to minimize the instabilities also in the low frequency range which led more reliable results for the total resistances.

The choice of analysing RU3 depends on the results achieved in the previous validation which showed that the cell located in the middle of stack delivers spectra with lower instabilities and lower artefacts.

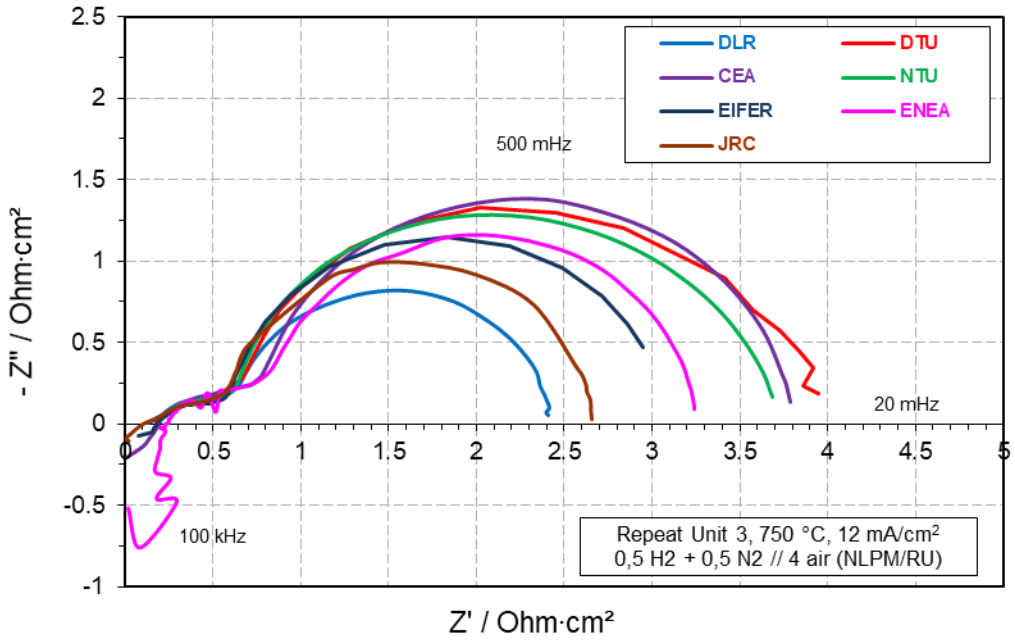

Figure 76. *EIS of RU 3 of all tested stacks as Nyquist plot, DC current 12 mA/cm², 0.5 H2 + 0.5 N2 // 4 air (NLPM/RU), 750 °C*

In the final round robin test all partners were able to determine the ohmic resistance and overall resistance for most of the measured RUs (with low current density) (Fig. 76). Nevertheless, the precise determination of the single resistances is still difficult as a lot of parameters influence the test results and the test system has a high sensitivity to disturbances

Looking on the high frequency range, 8 out of 8 spectra have a clear intersection with the x-axis where the ohmic resistance (R_{HF}) can be determined in a range of 0.12 Ω·cm² to 0.24 Ω·cm², showing a satisfying quality which confirms the successful implementation. The difference in terms of R_{HF} can be explained by differences in the stacks itself, by different temperatures and/or by existing high frequency artefacts caused by the wire inductances.

In the middle frequency range the polarization impedance arcs for the negative and positive electrode re almost the same, which proves a high reproducibility.

The low frequency impedances (R_{LF}) vary more strongly among partners. The total resistance strongly depends on the size of the gas concentration arc and therefore is influenced by the water content on the negative electrode although in this case, since the current density is 1 A, almost zero water formation can be considered. The discrepancy may occur due to small leakage between the stack and the gas distribution plate connected to unevenness or unequal weight placement during stack installation which may cause a relocating of the sealing during the test.

However, the instability only occurs for spectra recorded at low current densities and therefore has only a minor effect on the interpretation of the spectra.

The situation for the spectra at 20 A is quite different. Figure 77 shows the corresponding initial electrochemical spectra of RU3 of all tested stacks. No data are available for ENEA`s stack as their EIS equipment for high-current measurement was damaged.

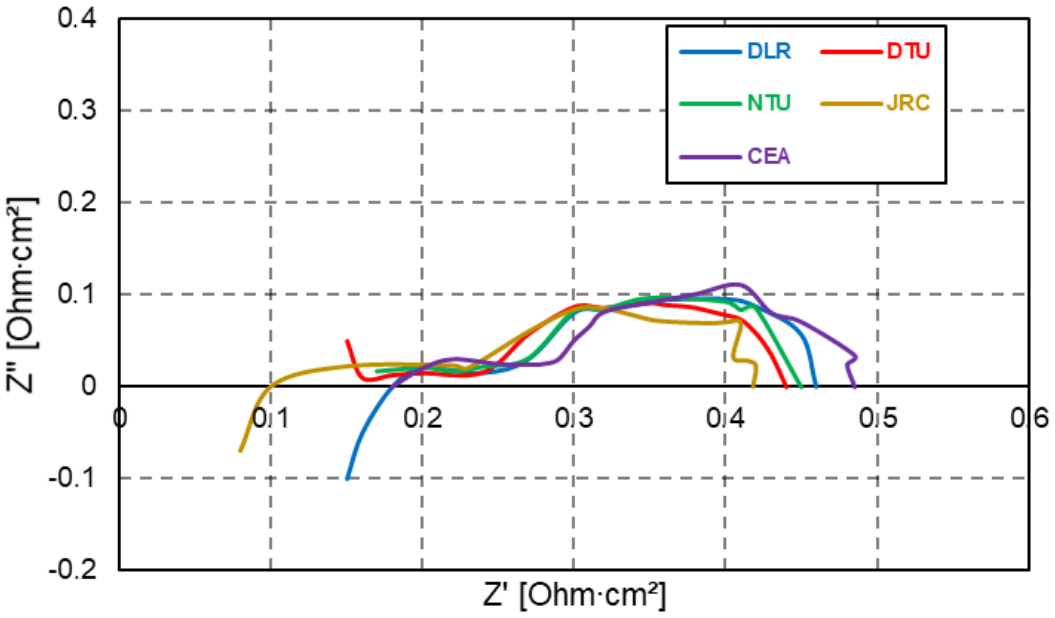

Figure 77. *EIS of RU 3 of all tested stacks as Nyquist plot, DC current 238 mA/cm², 0.5 H2 + 0.5 N2 // 4 air (NLPM/RU), 750 °C*

The spectra are very uniform among the partners, however, only some spectra at 20 A have clear intersections with the x-axis in the high frequency range. The high frequency impedances are in the range 0.09 Ω·cm² (JRC) to 0.18 Ω·cm² (DLR). Therefore, a precise determination of the ohmic resistances (R_{HF}) is quite difficult.

In the low frequency range only minor disturbances occur. Hence, the low frequency resistances (R_{LF}) can be determined with good quality. The values are in between 0.42 Ω·cm² (JRC) to 0.49 Ω·cm² (CEA).

Thus based on the results it is possible to suppose that at higher current densities, the electrode polarization resistances and the gas concentration resistance on the fuel gas side decreases. This leads to very low overall resistances in the low frequency region. In comparison to the measurements at 1 A, the determination of the overall resistance is easier and more precise, due to the fact that all spectra have an intersection with the x-axis or at least a point of contact in the low frequency region. This phenomenon can be related by increasing of the steam content at higher current densities which strongly minimizes the gas concentration impedance.

In order to investigate more deeply the processes in the cell/stack that influence the EIS spectra, all the stack results obtained by the different partners have been analysed using the DRT method.

Based on the strong knowledge gained in the ENEA laboratory [67][91][92][70][93][94] in recent, DRT was conducted starting from EIS spectra measured at 1A with a 50-50% mixture of H_2/N_2 in the negative electrode side and with pure air in the positive side. Observing Figure 78 related to the stack tested at ENEA, 5 peaks can be recognized each one referring to a physical-chemical process. The nature of each single peak is explained in paragraph 4.3.1

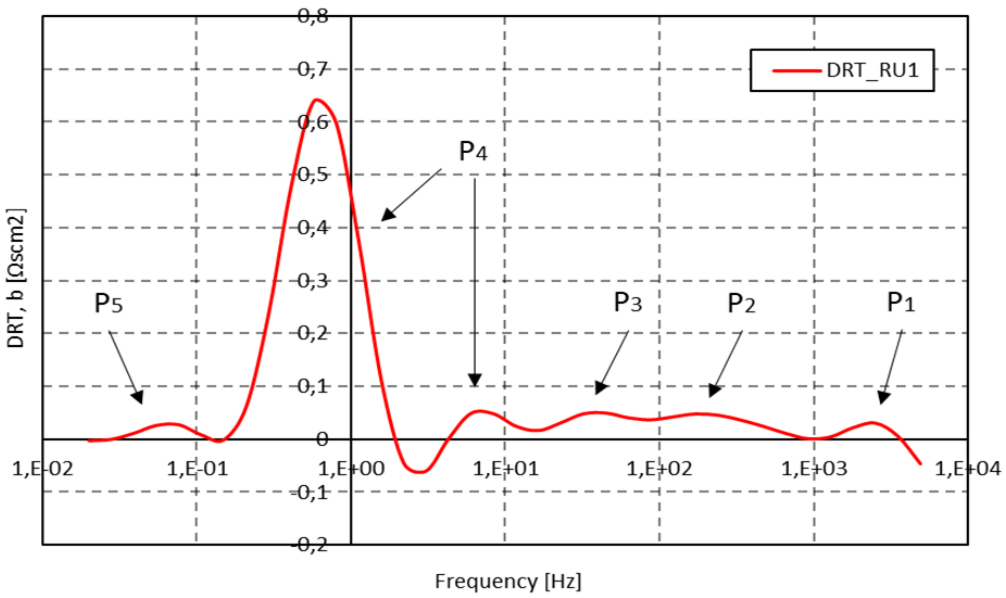

Figure 78. *DRT function of the experimental stack tested at ENEA.*

Differently to the results achieved and shown in paragraph 4.3.1, the presence of P5 is related to the flow of current through the stack which, even if small, reduces the partial pressure of oxygen to a value lower than 0.21 atm. P1, P2 and P3 are very squeezed due to the high operating temperature while P4 is the most pronounced peak.

Figure 79 shows the EIS spectra of all the cells within the stack tested in NTU and their corresponding DRT functions. As it is possible to observe, only peak 4 of DRT changes while the others remain unvaried. This peak as explained in the theory, is related exclusively on the gas diffusion in the fuel side thus, the observed discrepancy among the DRT trends may be correlated either to a different distribution of the gases among the cells within the stack or to a different difficulty of the gases to cross the negative electrode layer. In addition, in Figure 79 although there seems to be a tendency between the EIS spectra with respect to cells number, other partners did not show the same relationship. Instead following the dotted line n Figure 79 what can be confirmed is the presence of a direct link between the RLF and the peak's height that all partners have showed but instead all the partners showed a direct link between the R_{LF} and the peak's height.

Summarizing the overall polarization resistance (showed in paragraph 4.2.2) described as the sum of the resistances of the 5 different processes occurring in the cell based on the results achieved by means of DRT analysis, seems dependent exclusively on the gas diffusion in the fuel side as it is possible to see. In addition, analyzing the DRT function between the starting EIS spectra at 1 A and that measured at 20 A in Figure 80, it is possible to see as all the peaks, especially the peak 4 are feeling the effect of the current density confirming the expectations proposed by Butler-Volmer equation already mentioned in paragraph 4.3.1.

This is an important result since during the SOCTESQA Project, often the temperature has been mentioned as one the parameter that mainly cause difference in terms of performance among the partners. The DRT analysis instead tells us that beside the temperature, also the gas distribution/diffusion have to be taken into consideration as parameter that can affect the performance of the stack.

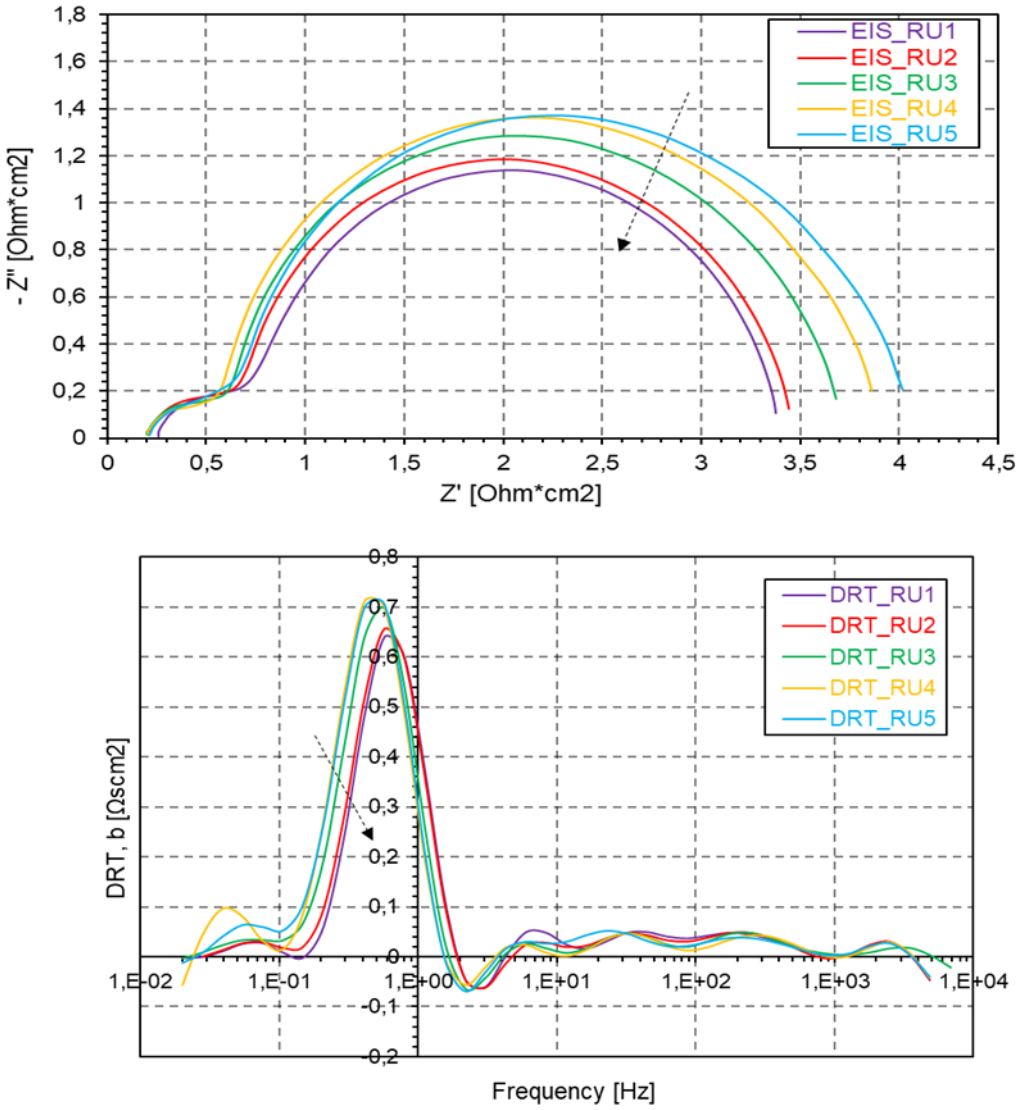

Figure 79. *EIS spectra and the corresponding DRT functions of all the cells of the stack tested at NTU.*

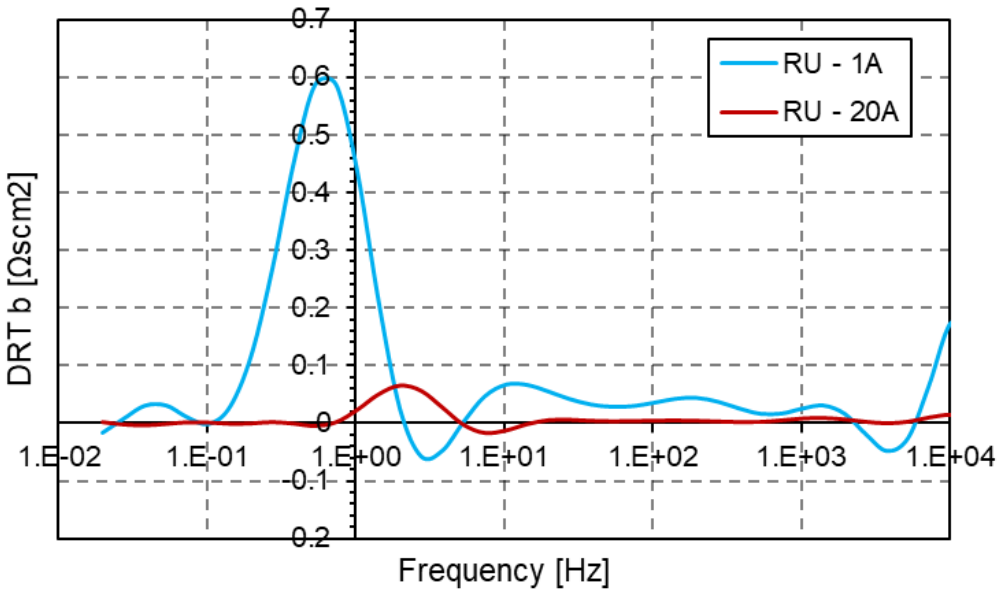

Figure 80. *DRT comparison of the same cell tested at 1 A and 20 A.*

In order to better analyse the reproducibility, the total resistance R_{LF} of the impedance spectra in the low frequency range at 1 A have been compared with the ASR calculated from the initial jV-curve measured at the same current density. In Figure 81, the correlation between R_{LF} and ASR of all RUs of the stack tested in CEA shows a direct link between these two values since R_{LF} increases with the increase in ASR.

However, taking into account the results obtained in Figure 76 and comparing the ASR value between the partners, it is possible to see in Figure 82 how this relationship does not work because, with the exception of DLR, no one partner respects the increasing order according to R_{LF}.

Furthermore, comparing the R_{HF} as a function of the average temperature in Figure 83, it is possible to notice that, no correlation occurs between R_{HF} and average temperature. The results achieved during this test module, show as exist a direct dependency between ASR and R_{LF} that is respected when cells within the same stack are analysed but no when different stacks are compared even if they are from the same manufacturer. Assuming that the difference in performance does not depend on the problems related to the different production batches, a possible parameter that can play an important role on the presence of correlation between the stack tested in different test benches, may be the pressure of the supply gases. However, this evaluation was not possible because none of the partners recorded the pressure during the whole project. It is therefore suggested to study any cells response by modifying the pressure in order to support or deny this hypothesis.

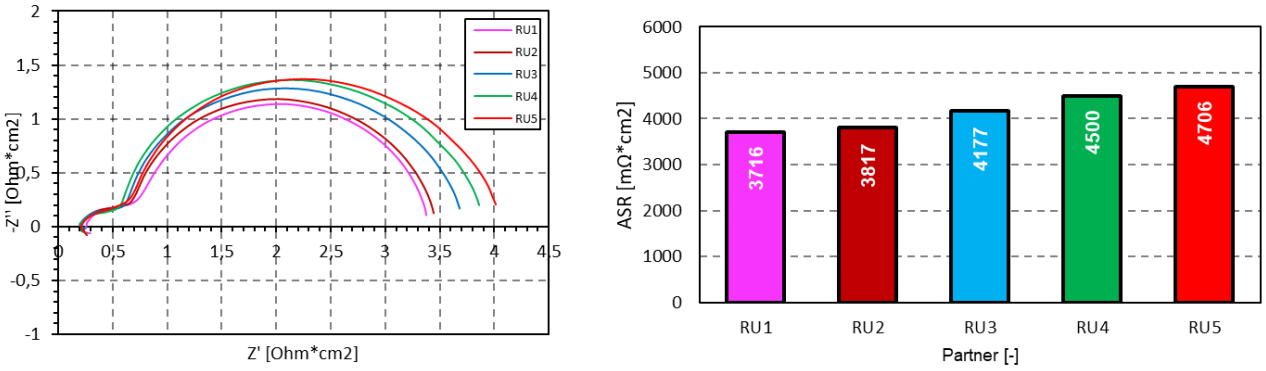

Figure 81. *Comparison between EIS spectra measured at 1Aand ASR values taken form the jV curve in order to find a possible direct correlation.*

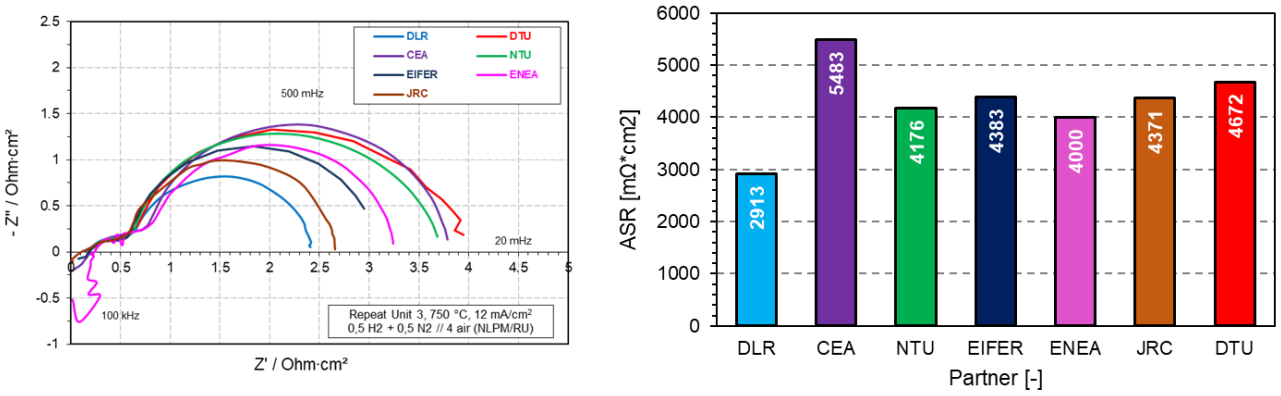

Figure 82. *ASR values measured at 1 A for each partner.*

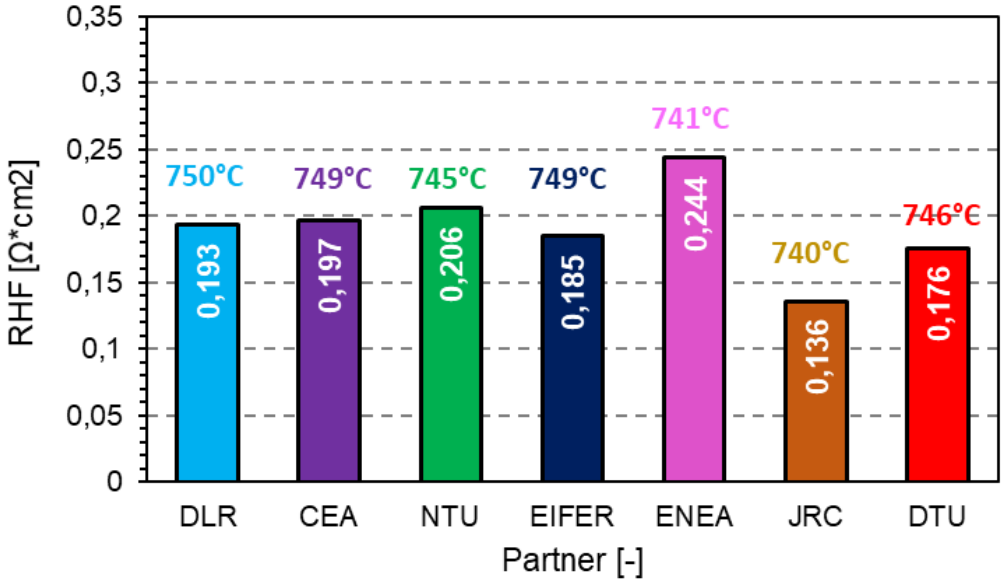

Figure 83. *The R_{HF} values extrapolated for each partners with the corresponding T_{av}.*

SOEC mode

Regarding EIS spectra in SOEC operation, impedance diagrams were measured under 1 and 20 A. Figure 84 below shows the EIS spectra measured at -1 A. The values of EIS spectra in SOEC mode

are a little bit more dispersed (around ± 17%) compared to the SOFC mode which could be attributed to the significantly larger presence of water in the negative electrode. The several modifications on the test benches during the preceding validations improved the measurement of EIS spectra, but as it is possible to notice, all the spectra are still affected by perturbation due to steam presence. At high-frequencies signal disturbance was limited as much as possible working on the way to apply current as well as on the relative position of current leads and voltage probes, however the difference in R_{HF} among the partners is still very high.

At low frequencies some improvement was also made. Noise has been significantly reduced on several diagrams after improvement of the humidification subsystem stability, but still for some partner the serial resistance R_{LF} was impossible to determine due too much noise and no intersection with the x-axis. In general, more low frequency disturbance is observed under polarization which is coherent with the increasing steam consumption and so the increasing effect of steam production stability as current density increases.

At DLR, the low frequencies disturbance was limited by replacing a part of hydrogen by nitrogen for a same total flow on the negative electrode side. The nitrogen dilution can be a first solution for low frequency disturbance reduction. This kind of nitrogen "dilution" can be a solution for low frequency disturbance reduction but seems very dependent on the steam supply subsystem. However, the increase of nitrogen amount can be affected. Although the increase of the amount of nitrogen would reduce the stoichiometry of the reaction, since the amount of hydrogen substituted will be less than 5% of the total flow, there should be no problems.

Some progress has been achieved also at DTU by increasing the number of measuring points per order of frequencies from 5 to 150 resulting in a better spectrum but with much longer analysis times (around 3 hours for each cell).

Overall, the results achieved can be considered similar and comparable, nevertheless the high and low-frequency disturbances make the analysis difficult.

The results achieved in the final round robin, confirm the most important points highlighted during the previous testing campaigns:

- Current leads and voltage probes relative position on which depend the electromagnetic interferences/disturbances occurring in the high-frequency (HF) domain of the EIS diagrams;
- Steam supply stability on which depend the disturbances observed in the low-frequency (LF) region of EIS diagrams;

It is important to work in these directions with the aim of improving the EIS spectra otherwise whatever possible assessment will be superfluous.

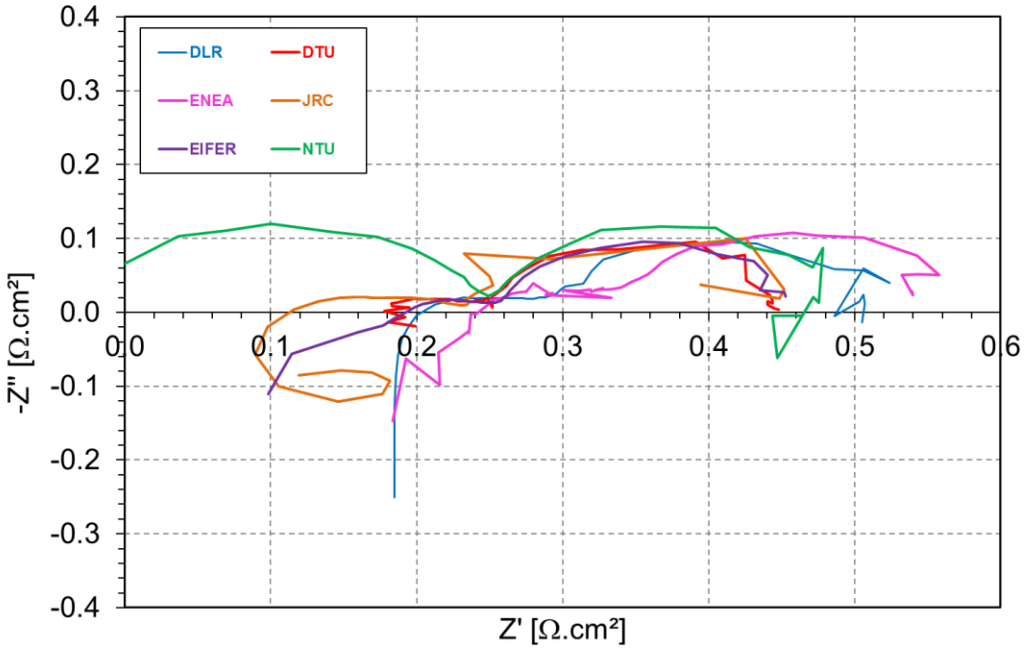

Figure 84. *EIS of RU 3 of all tested stacks as Nyquist plot, DC current 12 mA/cm², 2.5 H2O + 0.6 H2 // 5 air (NLPM/RU), 750 °C*

The various analyses carried out show a difficulty in interpreting the data obtained since even if the results in both operating modes are reproducible, the behaviour of the spectra between the different partners varies from cell to cell, from stack to stack. The results do not seem to follow a particular trend so they can be considered unreliable.

In summary, the EIS analysis shows several weaknesses:

- Unlike the jV curve, performance information cannot be extrapolated;
- The lack of homogeneous data can be related to a difference in the measurement tools used between the partners. Depending on the choice made, the instrument can induce a different electrical resistance, modifying the results, making it incomparable with respect to the others. Furthermore, the equipment is very expensive;
- The analysis seems to suffer greatly the presence of electrochemical interferences/disturbances so every time in order to have a good spectrum, the stack need to be isolated from all the electrical devices;
- The spectra are usually very sensitive to measuring conditions such as temperature, current and gas composition;
- Compared to the jV-curve, the EIS analysis is longer especially in SOEC mode where a large numbers of measuring points per each frequency are needed to obtain a good spectrum;
- Between one measurement and the other, the stack needs a lot of time for the voltage to return to a stable state because the sinusoidal input greatly stress the device;
- The analysis suffers greatly from the presence of water resulting in a very scattered spectrum.

However, unlike jV-curve, the EIS analysis shows several advantages such as the ability to study individually the response of a cell without considering the entire stack or to perform the measurement in-operando namely without stopping the test when the stack is under current during long-term analysis, if the impedance measurement can be carried out at the given current load.

Up to now only a brief description for measuring electrochemical impedance spectra on SOFC cell/stacks is given in the IEC document *"IEC 62282-7-2, Part 7-2"* [81]. This document describes the procedure for measuring EIS spectra very briefly and the presentation of the results with Cole-Cole plots. Another document describes several test methods for polymer electrolyte membrane stacks [82]. This document instead introduces the setup of the test, how to proceed and the data representation specifically for low temperature fuel cell stacks.

In contrast, TM04 describes much more detailed the electrochemical impedance spectroscopy for solid oxide cells and stacks which includes the basic principle of EIS, the test equipment and setup, the relevant test input and output parameters, the derived quantities and the test procedure for measuring EIS spectra. In addition, the document explains how to elaborate the data post processing how represents the results and how to interpreted it. Finally, the test module document addresses both the fuel cell (SOFC) and the electrolysis (SOEC) operation modes.

To optimize the test module and make it complete, some recommendations in order to obtain clear spectra especially in SOEC mode are necessary. Since the presence of water is considered to be the main cause of strong fluctuation, together with the advices given in Chapter 5, one solution could be to increase considerably the number of the recorded points for any single frequency in a way that the test will result a bit longer but the final spectra more accurate.

6.2.4. TM 07: Reactant utilization

The test module consists of three different parts in order to characterize the influence of the reactant utilization at the negative and the positive electrode ($U_{gas,\ neg}$ and $U_{gas,\ pos}$) on the performance of the tested stacks:

- Negative and positive electrode gas utilizations by varying current:
  Increase of electrical current stepwise while the other test input parameters like gas flow rates and temperature are kept constant.
- Negative gas utilization by variable gas flow:
  Decrease of gas flow rate on the negative electrode stepwise while the other parameters like electrical current and temperature are kept constant.
- Positive gas utilization by variable gas flow:
  Decrease of gas flow rate on the positive electrode stepwise while the other parameters like electrical current and temperature are kept constant.

Figure 85 shows the stack power density as a function of the negative gas utilization by varying the electrical current. The gas flow rates were kept constant at 0.5 H_2 + 0.5 N_2 NLPM/RU on the negative side and 4 NLPM/RU of air on the positive side. The operating temperature was 750 °C. After temperature stabilization for about 30 minutes the current was increased in steps of 0.1 A/cm² from 0.3 A/cm² to 0.7 A/cm². The test results are very homogenous concerning both fuel gas utilization and stack power density. No variations in fuel utilization are observed which shows a very high accuracy of the electrical current control systems in the test stations.

The deviations in power density among the partners increase with higher current densities and result in a maximum difference of ~5.5% at 0.7 A/cm^2 while the variation at 0.5 A/cm^2 is around 3.3%. This is in good accordance with the results achieved in TM03. The lower difference in variation compared to the current voltage characteristics depend on stable temperature conditions.

Measuring "Negative and positive gas utilizations by variable current" is nothing more than a different way to represents the jV-curve in which voltage is recorded at certain electrical current. The pro and cons of this test can be summarized in:

- Stable temperature conditions which allow to record the real voltage measures (PRO);
- Longer test than jV-curve (CONS);

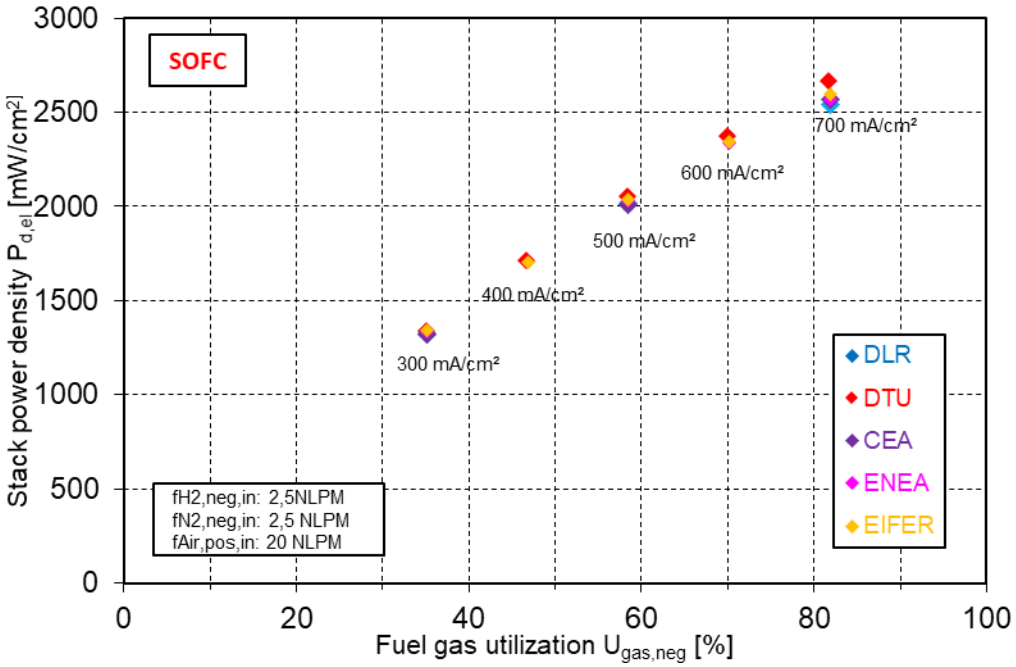

Figure 85. *Stack power density calculated at different current densities as a function of fuel gas utilization 0.5 H_2 + 0.5 N_2 // 4 air (NLPM/RU), 750°C.*

The results achieved in the second step of TM07 are summarized below.

Figure 86 shows the behaviour of the stack power density by varying the fuel gas flow rates at constant current load of 500 mA/cm^2. The operating temperature was kept constant at 750 °C just as the air flow rate on the positive gas side with 4 NLPM/RU. The fuel gas flow rate consisting of H_2 and N_2 was reduced stepwise from high gas flow rates per RU (0.5 H_2 + 0.5 N_2 (NLPM/RU)) to lower ones (0.45 H_2 + 0.45 N_2 to 0.4 H_2 + 0.4 N_2 to 0.35 H_2 + 0.35 N_2 (NLPM/RU)). Between every step a hold time of 30 minutes is applied in order to reach stable temperature conditions.

Figure 87 shows instead the behaviour of the stack power density by varying the oxygen gas utilization at constant current load of 500 mA/cm^2. The aim is to study the influence of decreasing supply of O_2 on the positive electrode. The air flow is varied between 4 and 2 NLPM/RU in steps of 0.5 NLPM/RU while the gas supply on the fuel was kept constant at 0.5 H_2 + 0.5 N_2 (NLPM/RU).

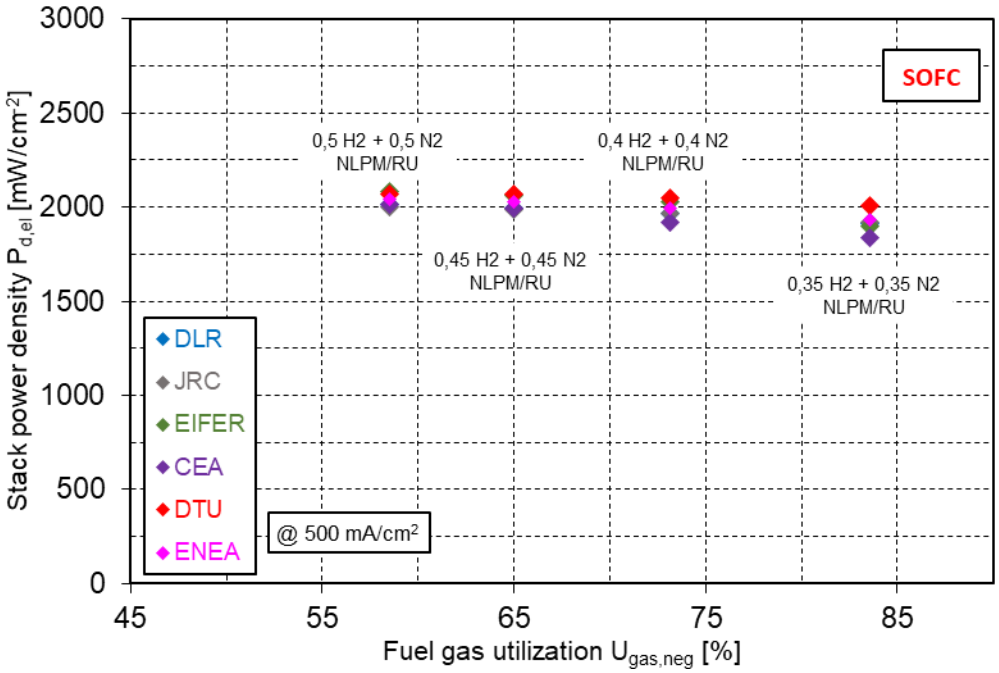

Figure 86. *Stack power density calculated as a function of fuel gas utilization calculated at constant current density of 500 mA/cm² and varying fuel gas flow rates at 750°C.*

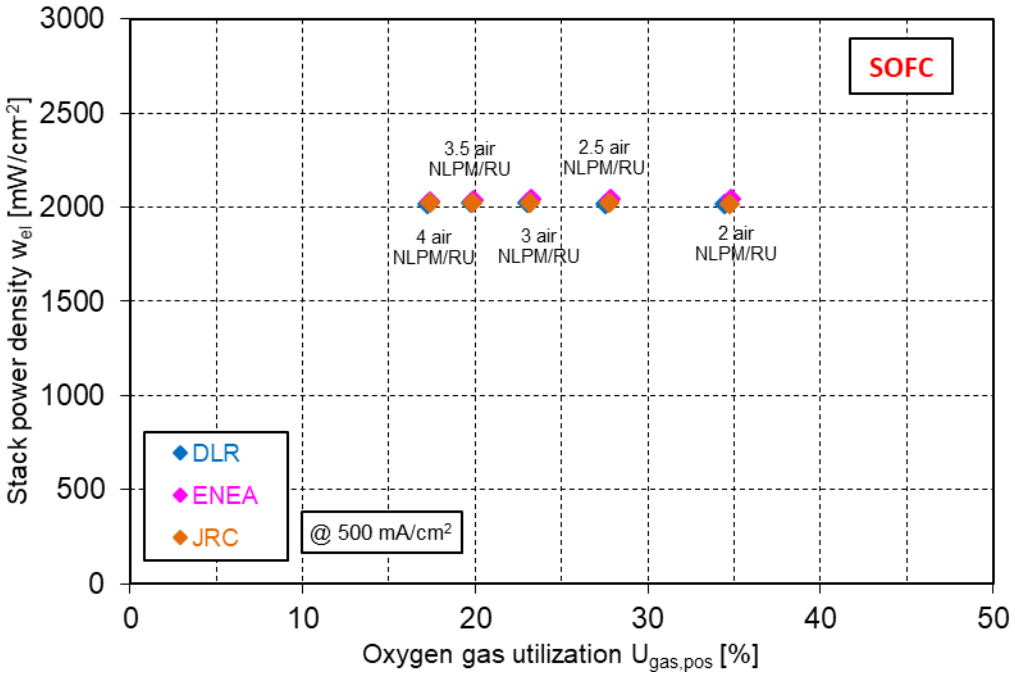

Figure 87. *Stack power density as a function of fuel gas utilization calculated at constant current density of 500 mA/cm²and varying air flow rates at 750°C.*

The results in both case are very uniform among the partners. As it is possible to note, the difference in stack power density reducing the O_2 on the positive gas side is much lower compared to that achieved when instead it is the fuel gas that changes because in the second case the stack works always in an excess of oxygen (also at 2 NLPM/RU).

This is the reason why there is no influence of the oxygen supply on the power density of the tested stacks within the range of oxygen utilization values measured.

Figure 88 below presents the effect of reactant utilization in SOEC mode when gas utilization on the negative electrode side decreases at a constant current density of -500 mA/cm^2. According to the theory, the difference in stack power density of all the stacks with increasing fuel gas utilization. The deviation among the partners is in accordance with the results achieved in TM03. However, the results of the stack can be considered very close together which proves a high reproducibility. Minor deviations can be explained by steam instability influencing the obtained results.

The second part of the TM07 in the form in which it was processed can be considered incomplete because the few results that can be extrapolated do not provide relevant information on the quality of the stack in terms of performance. So, the test module must be optimized to make it better, to make it efficient. For improving the test, two new methods are proposed.

Based on the idea behind the "Negative gas utilization by variable flow" test, a new graphical format could be to study the influence on stack performance by varying the flow rates of the fuel gas to three different constant current load and represent the results according to the evolution of the stack voltage.

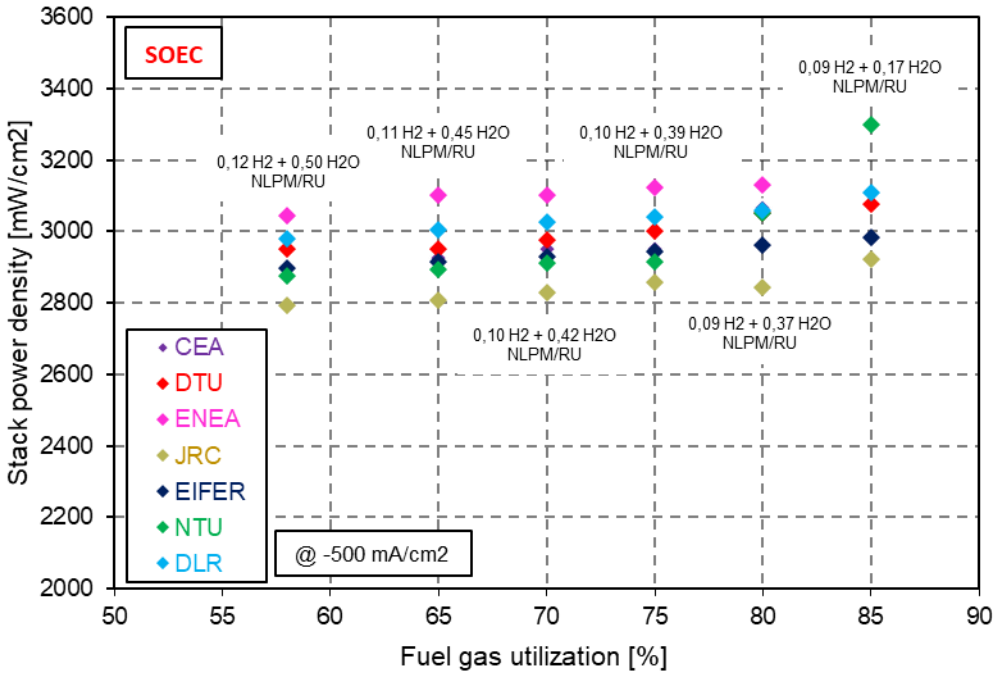

Figure 88. *Stack power density calculated as a function of fuel gas utilization calculated at constant current density of -500 mA/cm^2 and varying hydrogen and steam flow rates at 750°C in SOEC mode.*

The new data post processing and representation are shown in Figure 89. Different from the old version of the test module, in the new one, the behaviour of the stack voltage has to be measured at a constant current load of 300, 500 and 700 mA/cm^2 by varying the fuel gas utilization. In addition, since the results achieved during the project have showed that the temperature/voltage stabilization can be reached in less than 30 minutes, the hold time, can be halved. The new approach provides for the definition of a set of test in which for 3 different fixed current density points by varying the fuel gas utilization, the cell voltage must to be recorded. Subsequently, after plotting the data collected on a graph in function of stack voltage and current density, more trend lines will be trace. Usually 9 points recorded can be considered as satisfactory.

The new approach thus elaborated allows to trace directly only the central part of a standard jV curve, that is the area of the trend that mainly depends on the ohmic polarization avoiding a huge number of recording points.

Since the Region of the Ohmic losses, as written in the theory, are related principally on the transport of oxygen ions across the electrolyte and electronic transport in electrodes and interconnects, a reduction in the fuel gas utilization will lead only to a lower trend as Figure 89 depicts without changes in slope. Thus, since the central part is not depending on other factors, if the three trend lines show the same angular coefficient (they will be parallel among them), then the stack may be considered well operating, otherwise additional tests are recommended. Since the test regards the gas flow composition, if some discrepancies are present in terms of angular coefficient, the problems should regard either a difference in gas distribution among the single repeating units or diagnostic problems. In this case, it is recommended to identify which among the cells suffers more the variation in voltage when the gas flow is changed and carry out a EIS analysis at the lowest gas flow rate.

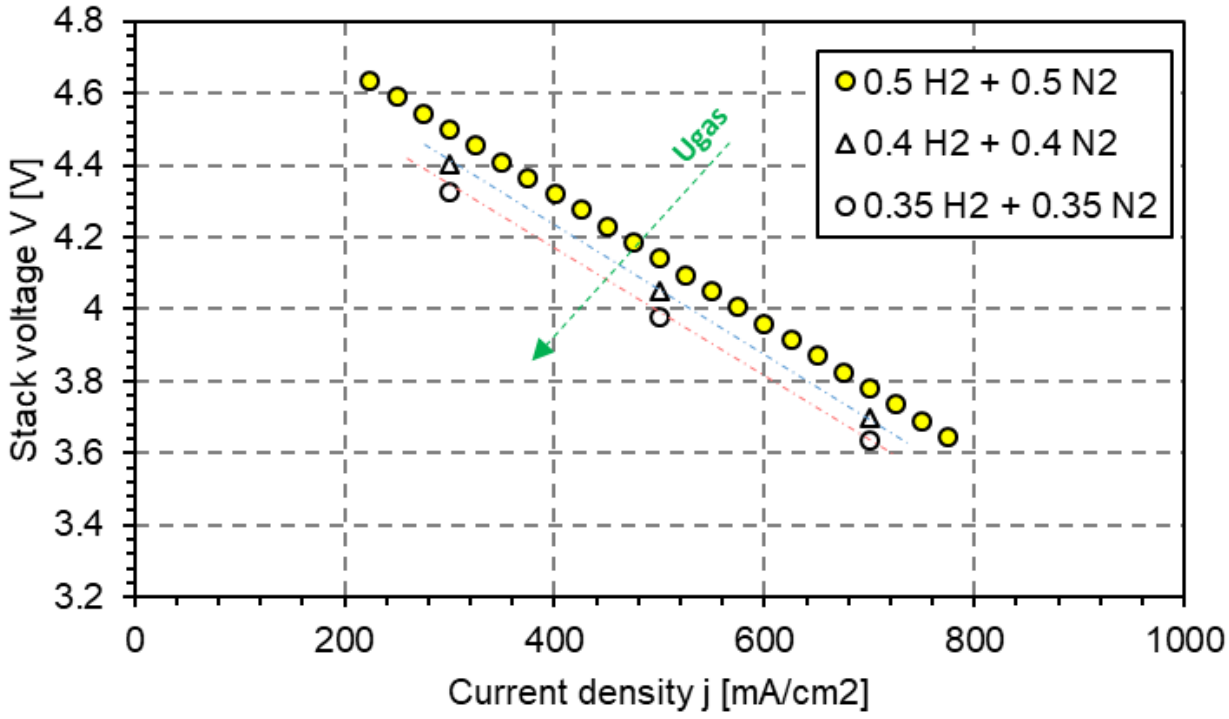

Figure 89. *Example graph of representation of results in SOFC mode based on the first new approach.*

Another approach could be that to record the stack voltage directly in the region of high fuel gas utilization. Thus, considering a fixed value of $U_{gas,neg}$ by varying the fuel gas composition, different operating current densities have been calculated and plotted in Figure 90. Based on the results achieved and taking into account a potential error of 2.5%, the voltage at each individual working point was measured. A stack can be considered excellent in terms of performance if for any single operating point, the voltage falls within the red line marked in Figure 90 for each operating points or in alternatively as already mentioned when for different fuel gas utilization values, the straight lines passing through the various current density points show the same slope.

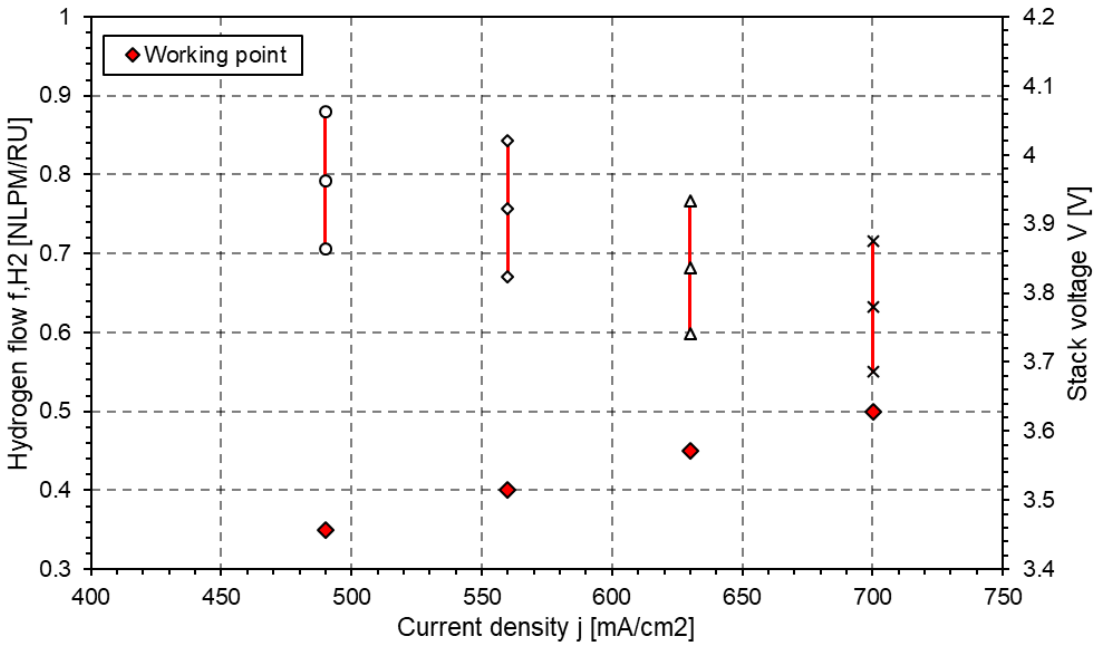

Figure 90. *Example graph of representation of result in SOFC mode based on the second new approach.*

These two new processes do not provide additional information compared to those obtained from the old version of the test, however, the data post-processing has been improved and in this way it would avoid unnecessary measurements The second approach has the advantage of being faster but less information can be obtained than the other one. In addition, it is important to remember that if the first is applicable for any stack configuration, the values in terms of voltage shown in Figure 90 are strongly depend on the active area of the cell that in this case was 84 cm^2.Thus for other areas, the voltage range for a fixed value of $U_{gas,neg}$ in which is suppose that the stack should fall need to be calculated again.

This Test Module is quite new since the existing procedure only takes into consideration operation in SOFC mode. The version as elaborated during the SOCTESQA Project, not seems to ensure all information required to verify the quality of the tested stacks. Some modifications have to be adopted in order to make it valid.

Anyway both approaches can substitute easily the currently version thus making it the module slimmer and complete. Recording the voltage stack by varying the oxygen gas utilisation seems to be totally useless unless the decision is made to test the stack voltage directly to very low values of oxygen composition with the risk of not having relevant information or destroy the device. During the test in fact it is recommended to pay attention not of not pushing the device too hard by decreasing the fuel/oxygen flow and therefore always falling within a certain safety range.

6.2.5. TM 09: Temperature sensitivity

The test was applied at three different operating temperatures 720 °C, 750 °C and 780 °C. After temperature stabilization the current density was increased from 0 A/cm^2 to ±0.3 A/cm^2 and ±0.5 A/cm^2 up to ±0.7 A/cm^2. depending on the operating mode. At each temperature step the stack was operated until a stable behaviour in terms of temperature and voltage was reached. Figure 91 and 92 show the power density of all tested stacks at the applied current densities as a function of the average stack temperature at the corresponding set point operating temperature and current density.

It has to be mentioned that due to the lower performances some stacks could not reach the operating point at 0.7 A/cm^2 in SOEC mode. Depending on the operating mode, the stack power density increases/decreases almost linearly with increasing current density as can be seen following the dashed line. The temperature dependency among the partners is nearly the same since most of the data points are very close together. In SOFC mode, due to the exothermal reaction the average temperatures increase with increasing current densities (up to 18°C). Nevertheless, the increasing in temperature is very similar between all stacks (e.g. ~ 8 to 12°C from 0.3 A/cm^2 to 0.5 A/cm^2 at 720°C). In SOEC mode instead it is worth noticing that the temperature dependency of the stack voltage does not change a lot as a function of current density. It could be explained by the stack thermal evolution in relation to the electrochemical reactions firstly endothermal and then exothermal at higher current densities.

Also in this case, the results of test module 09 confirm high reproducibility among the different stacks. The observed deviations are related to differences in test input parameters, e g. gas inlet and stack temperature set point.

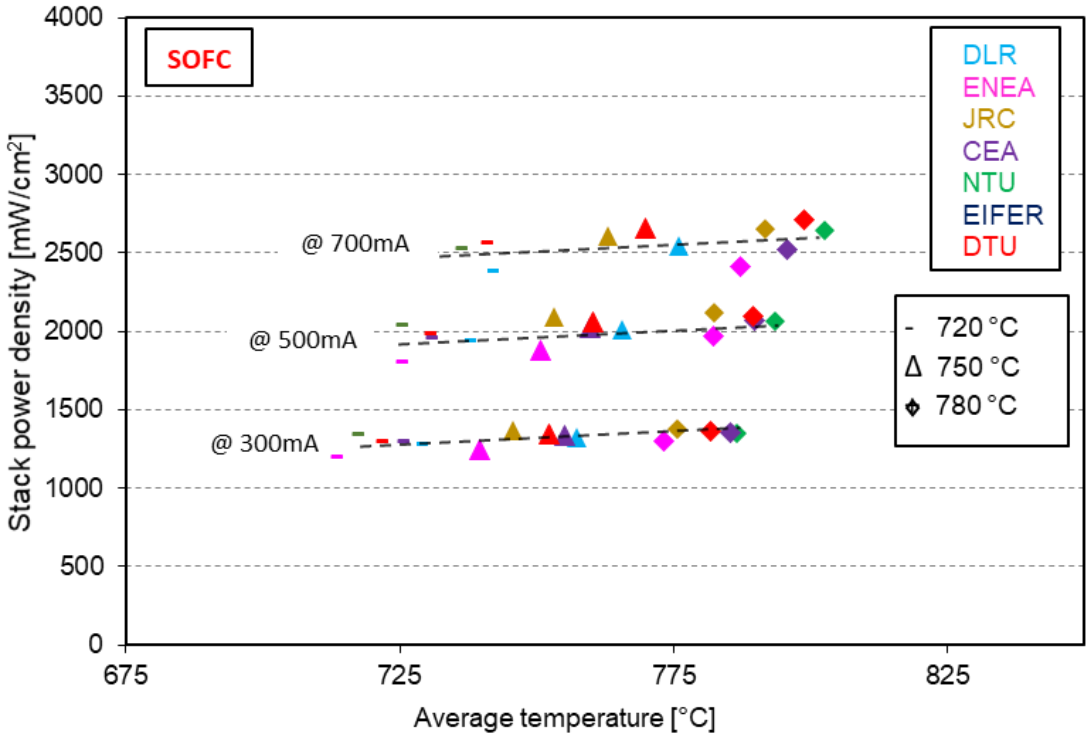

Figure 91. *Correlation between stack power densities and average stack temperate at varying current densities with operating gases of 0.5 H_2 + 0.5 N_2 // 4 air (NLPM)RU)*

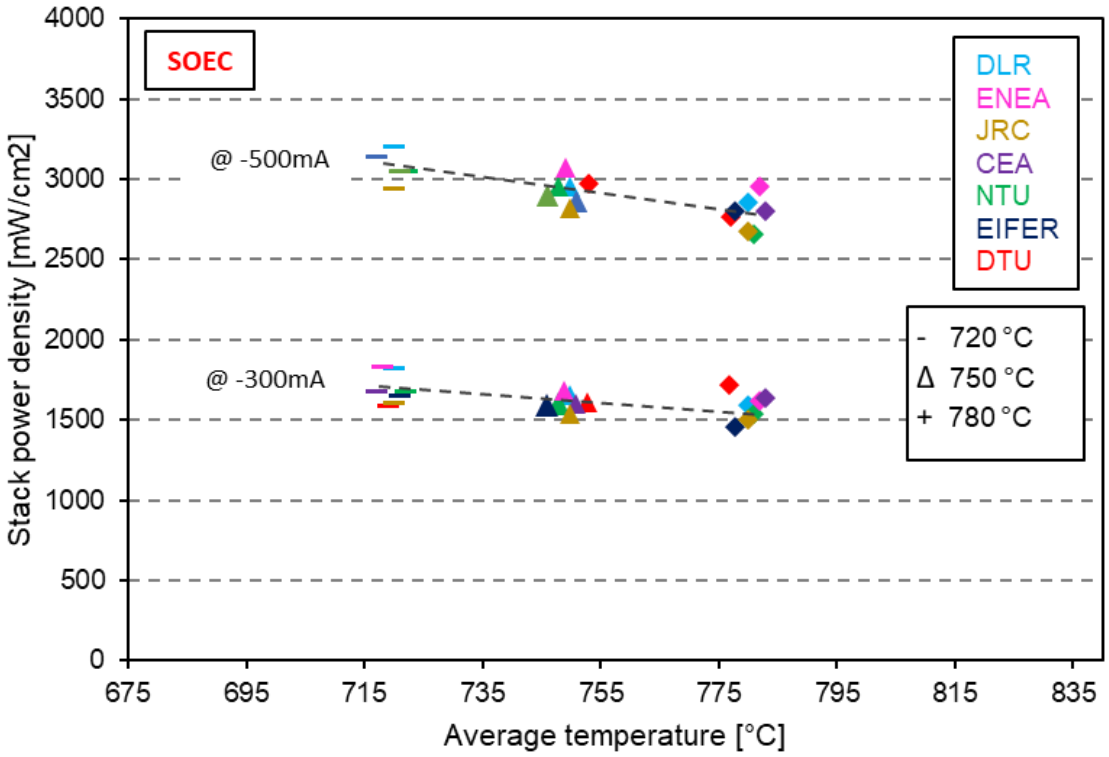

Figure 92. *Power density evolution as a function of average temperature in SOEC mode at -300 and -500 mA/cm2 under 80% H2O/20% // 1 air (NLPM/RU).*

Studying the results in greater detail and taking into consideration only the stack tested in DTU which showed the best performance during the jV-curve measurement, it is possible to see in Figure 93 that the recorded points at 720 and 780°C are laid along a linear trend which presents the same angular coefficient of the trend at 750°C corresponding to -0.0017. Also the stack tested in DLR have showed the same match (with an angular coefficient of -0.0018) while the other partner no, especially between 720°C and 750°C.

As already mentioned in the test module 07, also in this case, the slope of the straight line passing through different points can be considered good assessment criteria to evaluate the robustness of the stack and the quality of the test bench. Therefore, by varying the operating temperature, if all the trend lines have the same angular coefficient, the stack can be considered well otherwise additional tests are required.

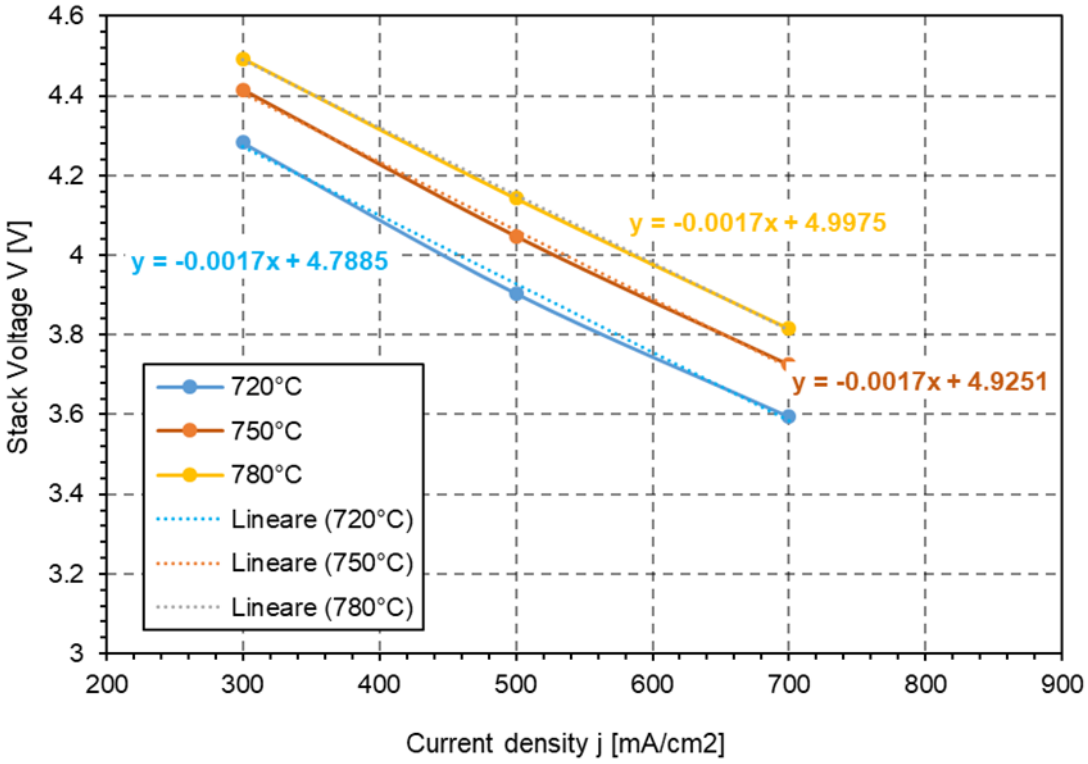

Figure 93. *Results achieved at DTU showing the same angular coefficient at the operating temperature of 720, 750 and 780°C.*

The test module 09 as it has been done can be considered complete. The use of this test in combination with other characterization methods such as the test module 07 mentioned above, can guarantee a set of data, parameters and range of values useful for the research and development of the SOC and for quality assurance in cell and stack production.

In any case, it is important to remember that different parameters play an important role on the performance of the stack as well as some problems are directly related to the production of the cells and other components so a degree of uncertainty must to be always included.

In order to improve the reproducibility of the results and optimize the test, some recommendations are given below:

- The measurement of the cell/stack temperature should be as close as possible to the geometric centre of the cell/stack. Since usually it will not be possible to place a thermocouple in the heart of a stack, it is suggested to measure the temperature in direct contact with the centre of the end plate(s) of the cell/stack assembly and take the arithmetic average of the two values;
- If direct measurement of the cell/stack temperature is not possible, the fuel/oxidant outlet temperature should be taken as reference, measured as close as possible to the cell/stack outlet since it is the resultant between the top/bottom plate temperature and that related to inlet gas;

No test procedures have been defined and elaborated in the international standardization literature specifically on the temperature sensitivity of a SOC cell/stack at the time of writing, thus this test module is particularly relevant as it can address the effects of temperature on the performance of the SOC when operating in power generation mode (SOFC) and electrolysis mode (SOEC).

During operation in SOFC mode, the electrical load variation always influences the operating temperature of the cell/stack resulting in a change of performance so a next step to improve the test

module could be to record also the effective temperature that the cell/stack achieves at a given current density, and indicate it on the data post processing. In addition, in order to avoid that, based on the geometry and size of the furnace system, the effect of the increasing temperature linked to the electrical load variation could affect the voltage stack, may be appropriate after recording the first dataset, set the furnace temperature in such a way that the electrical effect is void. In this way all the test benches will be actually comparable and a new dataset is provided.

6.2.6. TM 12: Operation under constant current

In this paragraph will be reported the behaviour of the stacks under constant current in SOFC/SOEC mode. The electrical current load was adapted to a more application specific mode of operation and for this reason it was set at 0.5 A/cm^2 (corresponding to 42 A) applied for 500 h of testing with gas flow rates of 0.5 H_2 + 0.$_5$ N_2 NLPM/RU on the negative side and 4 air NLPM/RU on the positive side, at a constant furnace temperature of 750°C.

Figure 94 shows the voltage characteristics of the involved stacks at continuous operation under constant current of 0.5 A/cm2 in SOFC mode. For the whole test duration voltage fluctuations occurred for the stacks tested at ENEA and JRC. Due to the overheating of the electronic load the test station at ENEA stopped after 270 h of operation. At the end of the test (494 h) a second interruption occurred. A short circuit of the relay of the preheating system caused the temperature decrease of the gas inlet to 10°C. In order to reach the specified operation time, it was decided to fix the problem and finish the test at 520 h. Also JRC had to interrupt the long term operation after 454 h for 2 h as the pressure of the gas inlet decreased. After solving this failure, the test was continued until the end.

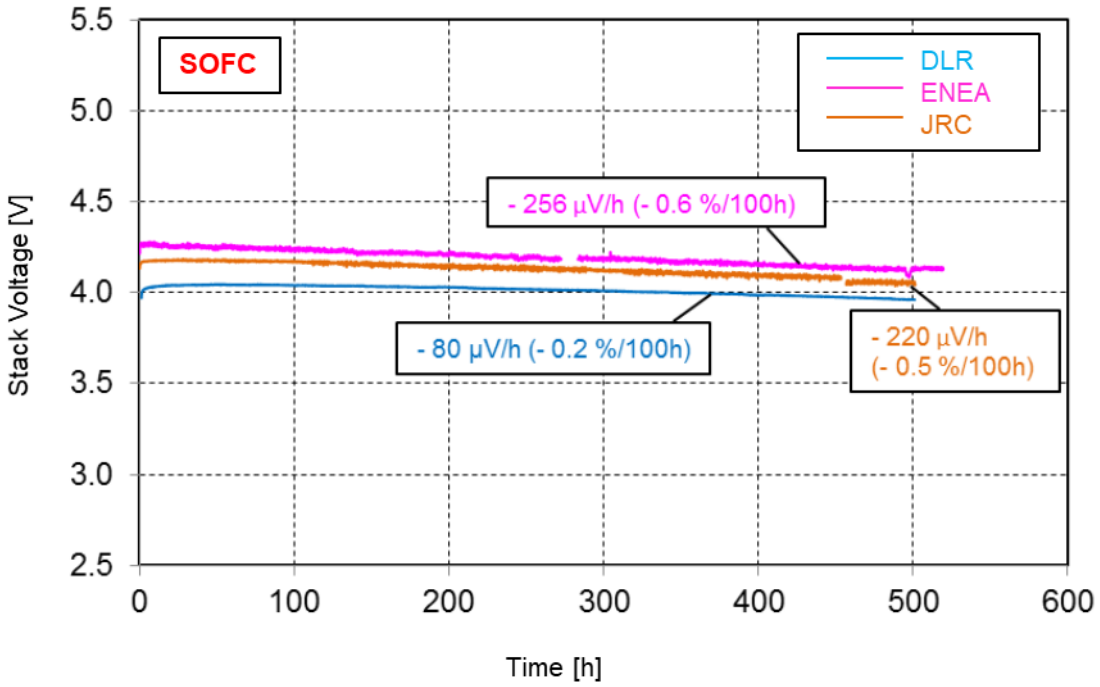

Figure 94. *Voltage trends (ENEA, DLR, JRC) during operation under constant current of 500 mA/cm^{2}with 0.5 H_2 + 0.5 N_2// 4 air (NLPM/RU), 750 °C in SOFC mode.*

The stacks started with different voltage from 4.0 V (DLR) to 4.19 V (ENEA) due to the different stack behaviours. The degradation rates are in range from -80 µV/h (DLR) to -256 µV/h (ENEA). These values correspond to -0.2 to 0.6 % / 100 h. The deviations between the partners are mainly related to the short duration time which had to be limited to 500 h due to the termination of the project. Former experiences with this kind of stacks showed that it is difficult to achieve similar degradation

rates within the first 1000 h of operation. Even stacks form the same supplier and the same manufacturing batch show different behaviour during the initial operation time. Thus, in order to optimize the test a first recommendation should be that to increase the operation time up to minimum 1000 h to avoid influences of the initial hours of operation. Anyway, the degradation rate of the different stacks is quite similar. Also the voltage fluctuations which occurred for the test stations of ENEA and JRC influence the determination of the degradation rates.

The precise recording of the voltages is a general requirement and all the test modules. However, for operation under constant current, the calculation of the degradation rate is less sensitive because the slope is low and there are many data over many hours, thus a second step of improving the test could be to modify the sampling rate from seconds to minutes or by using the average of the data recorded. The voltage values measured can be plotted directly every five minutes. Unfortunately, the existing literature is not able to provide accurate explanations regarding the degradation processes that take place within the cell. In order to do this, it is advisable and opportune to investigate the degradation event, so far unknown, relying on the results recorded during the test.

At the beginning T_{TP}, T_{av} and $\Delta T_{endplates}$ were taken into consideration as parameters of analysing. Nevertheless, after different assessments a new parameter "$\Delta T_{end\text{-}inlet}$" was analysed, defined as the difference between the T_{plates} average and $T_{inlet,gas}$. The 4 parameters were chosen because they should be those that most influence or a god indicators of the degradation rate. In Figure 95, 96 and 97 the trend of T_{TP}, T_{av}, $\Delta T_{endplates}$ and $\Delta T_{end\text{-}inlet}$ among the partners are shown. Looking at the graphs it is possible to notice that starting from the same operating temperature of 750 ° C:

1) The top plate of the stack tested at ENEA is the one most subject to increase in temperature due to the electric heating. Moreover, during the test, the trend undergoes a significant drop in temperature from 773 ° C to a minimum point of 769 ° C due to fluctuations in the furnace temperature. However, the stack voltage seems to decrease with a constant degradation rate.
   Both stacks tested in JRC and ENEA at the end of the 500 hours of testing showed an increasing temperature of 1/2 °C different from DLR, where instead the temperature is always the same. If there was a relationship between the stack degradation and the top plate's temperature, the DLR stack trend would be between the ENEA one and the JCR one. However, from the analysis carried out, the presence of such relationship is absent.

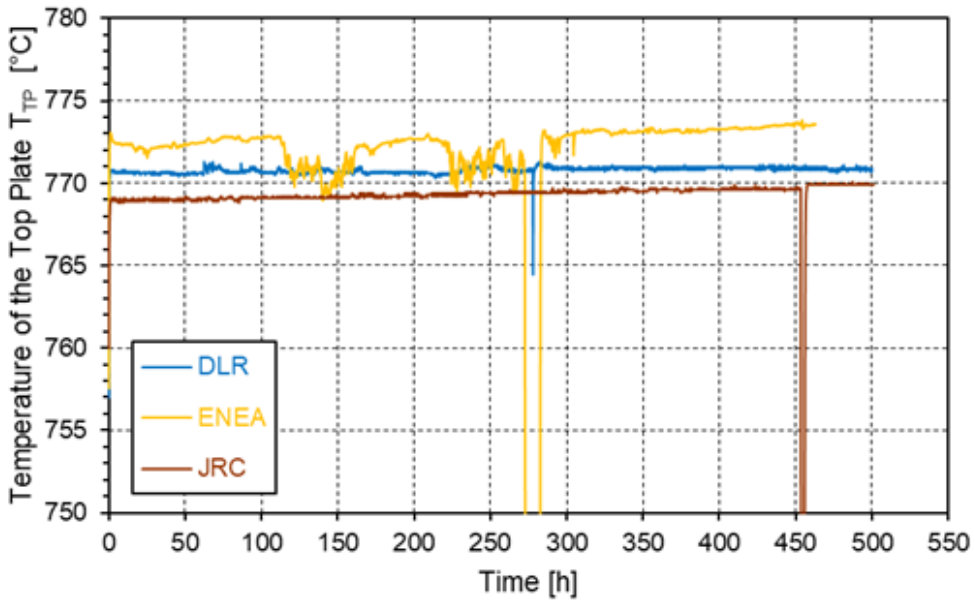

Figure 95. *T_{TP} comparison of stacks (ENEA; DLR, JRC) during operation under constant current of 500 mA/cm².*

2) The average temperature of the stack tested at the DLR is the highest with a difference of 8°C compared to the JRC stacks and 15°C compared to ENEA stack. The strange trend measured in ENEA is always due to fluctuations in the furnace temperature.
Based on these results there seems to be a connection between the degradation rate and the average temperature, but in this case DLR should be the one most subject to degradation due to the highest average temperature, so it can be concluded that T_{av} does not directly influence the degradation rate.

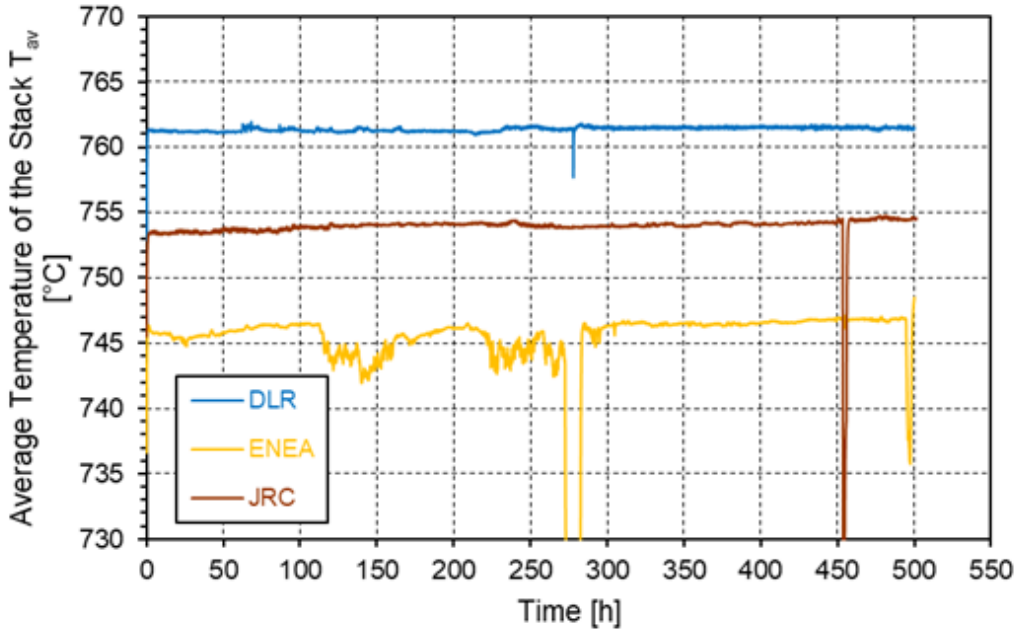

Figure 96. *T_{av} comparison of stacks (ENEA; DLR, JRC) during operation under constant current of 500 mA/cm².*

3) $\Delta T_{endplates}$ can be immediately excluded from the analysis because otherwise on the basis of the results obtained the stack tested at JRC should be that with the highest rate of degradation. Going to study the dependence of the parameter $\Delta T_{end\text{-}inlet}$, the results obtained seem to show a possible connection with the degradation rate.

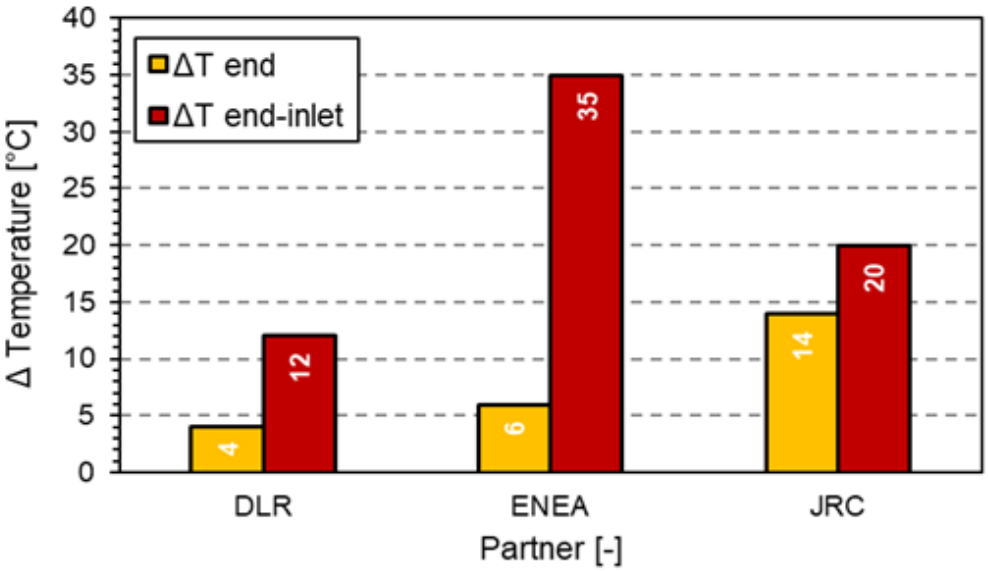

Figure 97. *$\Delta T_{end\text{-}inlet}$ comparison of stacks (ENEA; DLR, JRC) during operation under constant current of 500 mA/cm².*

For long-term endurance test, the degradation rate is reported as the change in voltage over a given time. However, this parameter is very sensitive because it changes a lot depending on the selected points for its measurement.

The degradation rate of DLR group was calculated using the first voltage point namely that measured once the current collector has reached the value of 42 A, but as can be seen in the graph, only after the 25th hour the stack reaches the maximum voltage point and only after this time, the stack voltage has started to decrease. Therefore, by calculating the degradation rate again at this voltage point and not at 4 V, a rate of 200 µV/h can be obtained. For both stacks tested in ENEA and JRC, it was not necessary to wait 25 hours to record the initial voltage point useful for measuring the degradation rate. However, the results obtained in DLR show the importance of having a fixed waiting time before measuring the first voltage point to be sure that the device reaches its stabilization.

By tracing this new value of degradation rate together with the others as a function of $\Delta T_{end\text{-}inlet}$, it is possible to see in Figure 98 how a linear tendency passes perfectly through these points. Nevertheless, more results are needed before confirming the any existing dependence. For this reason, the results obtained during the first validation were also taken into consideration.

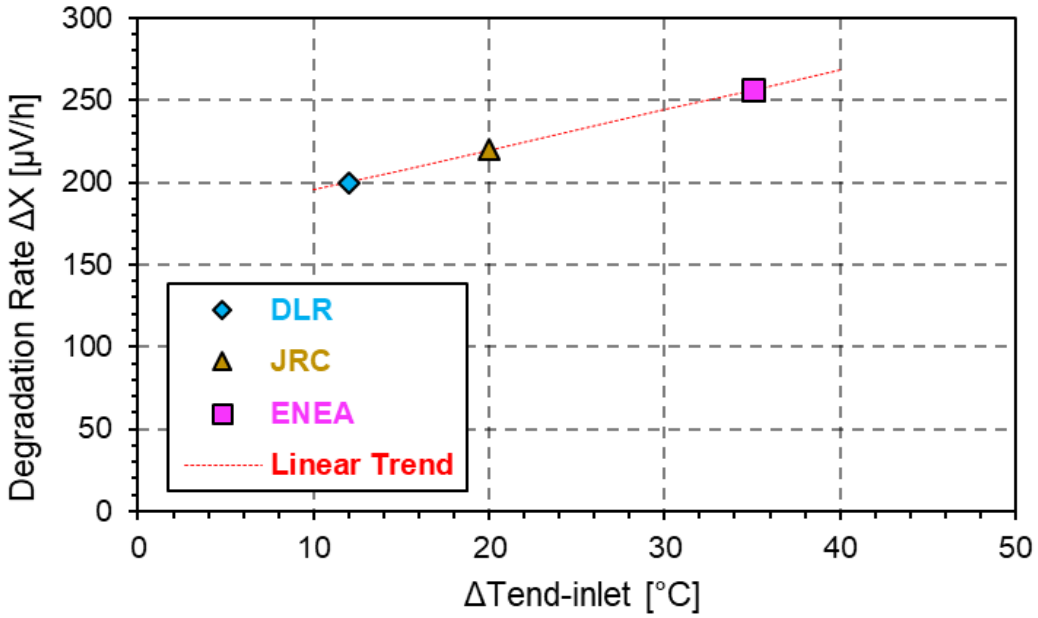

Figure 98. *Correlation between the degradation rate and the new parameter defined as $\Delta T_{end\text{-}inlet}$ during operation under constant current of 500 mA/cm².*

During the first validation TM12 was applied two times with an operation time of 500 h for each test so that the total operation time under constant current adds up to 1000 h. Between both applications jV-curves and electrochemical impedance spectra were performed. Figure 99 shows the stack voltages measured at DLR, DTU, JRC and ENEA during operation under constant current for the first 500 hours of test. Unlike the round robin test, the current was set at 25.2 A while the stacks were always at 750 ° with the same gas flow composition. In order to avoid an overlapping in presenting the voltages of all the stacks the results have been split in two different plots: one for DTU and DLR and the other one for JRC and ENEA.

Both DTU and DLR stacks show very homogeneous and stable voltage trends during the 500 h operation time. The stack at JRC shows a strong voltage fluctuation starting at 170 h that grows with increasing operation time while the stacks tested at ENEA show several reversible voltage drops.

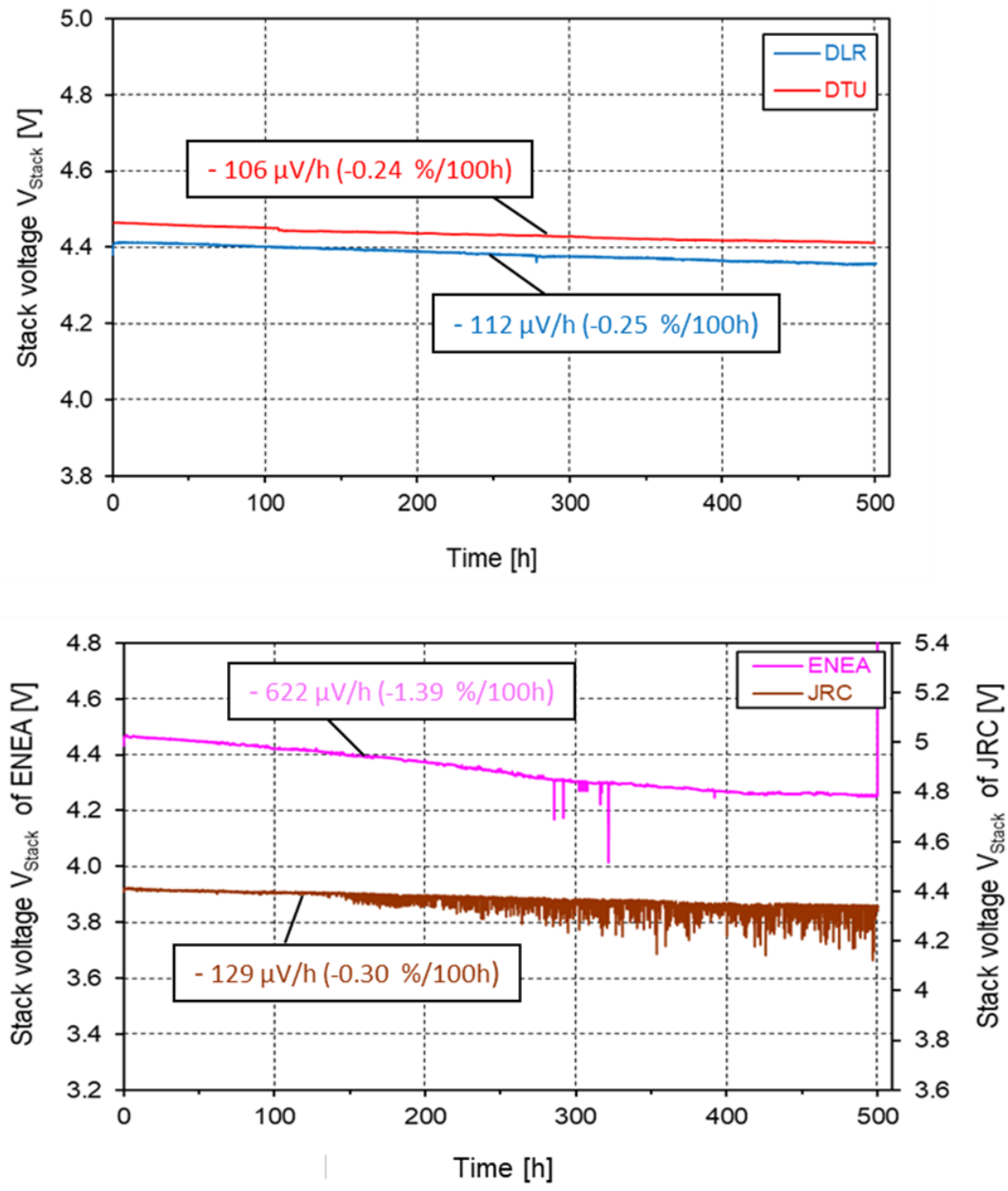

Figure 99. *Voltage of the stacks (DLR, DTU, ENEA and JRC) tested during the first validation under constant current of 300 mA/cm^2.*

Figure 100-A shows the degradation rate as a function of $\Delta T_{end\text{-}inlet}$. The other 500 h of test have been analysed and the results were plotted in Figure 100-B. The results are very close to those achieved during the first 500 hours, but again ENEA shows a very high rate of degradation. Unfortunately, due to strong fluctuations, the stack tested at JRC was not able to continue the test and for this reason its degradation rate as a function of $\Delta T_{end\text{-}inlet}$ does not appear.

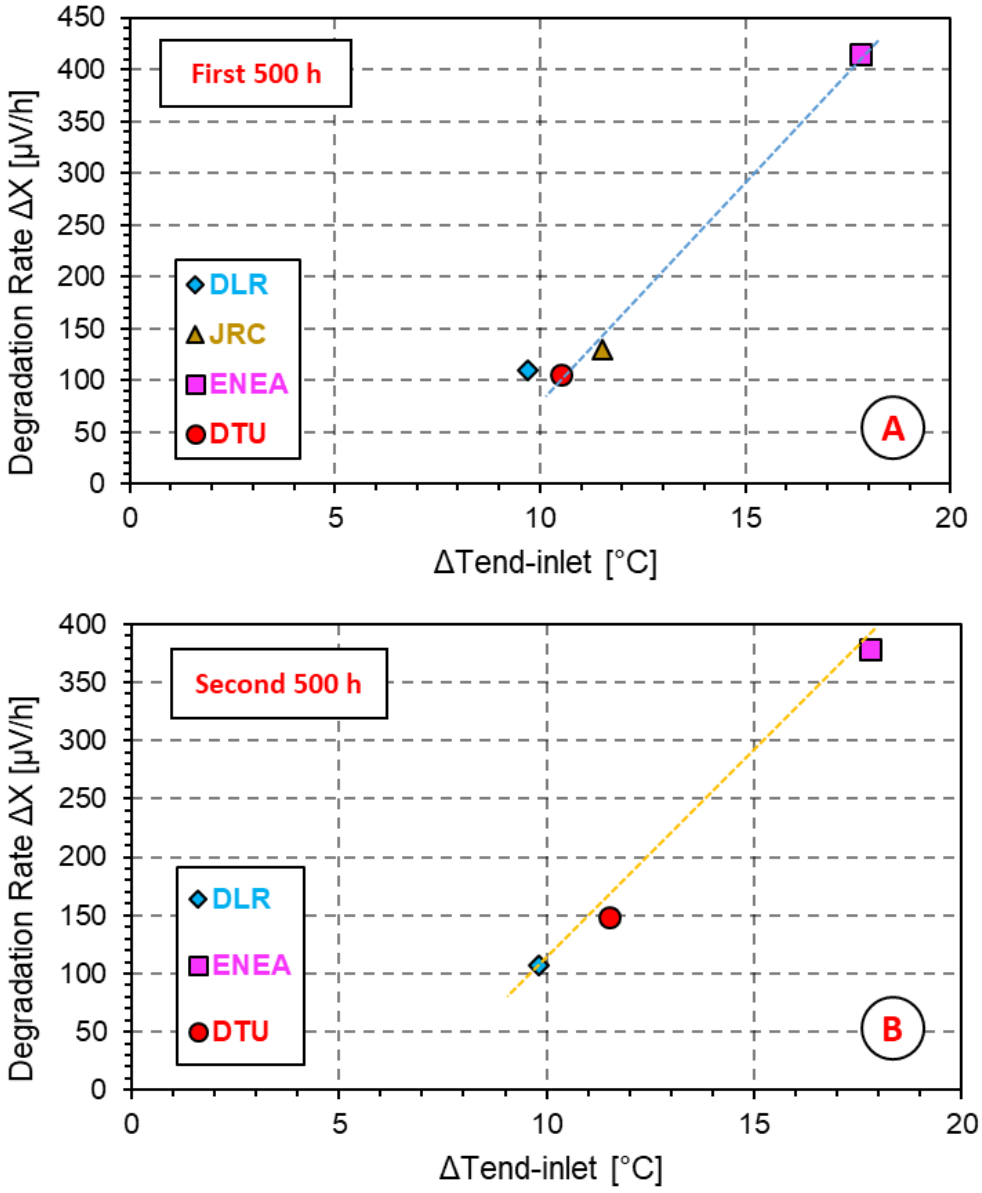

Figure 100. *Correlation between Degradation Rate and $\Delta T_{end\text{-}inlet}$ based on the data achieved during the first validation.*

Also in this case, as in Figure 98, there seems to exist a linear tendency. However, observing the results obtained between the first and final validation, it is noted that the degradation rates of DLR and JRC at 42 A are higher than those achieved when the current was 25 A, while the stack tested at ENEA showed at 25 A, a degradation rate 2 times higher than that obtained at 42 A. Due to the lack of other data to analyse and considering that the stacks from the same supplier and the same manufacturing batch show different behaviour during both test, nothing else can be said about the degradation rate. By the various evaluations carried out, $\Delta T_{end\text{-}inlet}$ can be recognized as a good starting point to analyse the degradation phenomena which occur within the cell. However, the results achieved show that together with $\Delta T_{end\text{-}inlet}$ other parameters are responsible for the degradation rates since $\Delta T_{end\text{-}inlet}$ is not enough to depict all the degradation phenomena.

The next step was to study a possible correlation between EIS results and the degradation rate of each individual cell. The aim was to investigate whether it is possible to immediately understand which of the cells suffers a faster degradation starting from R_{LF} and R_{HF}. The initial EIS spectra collected at 1

A of the stack tested in JRC and ENEA were taken into account for this analysis and their results are shown in Figure 101. Close to each single indicator (triangle or rhombus), the number of the specific repeating unit cell was inserted in order to show as no relationship exists between the degradation rate and R_{LF} (Figure 101-A) or R_{HF} (Figure 101-B).

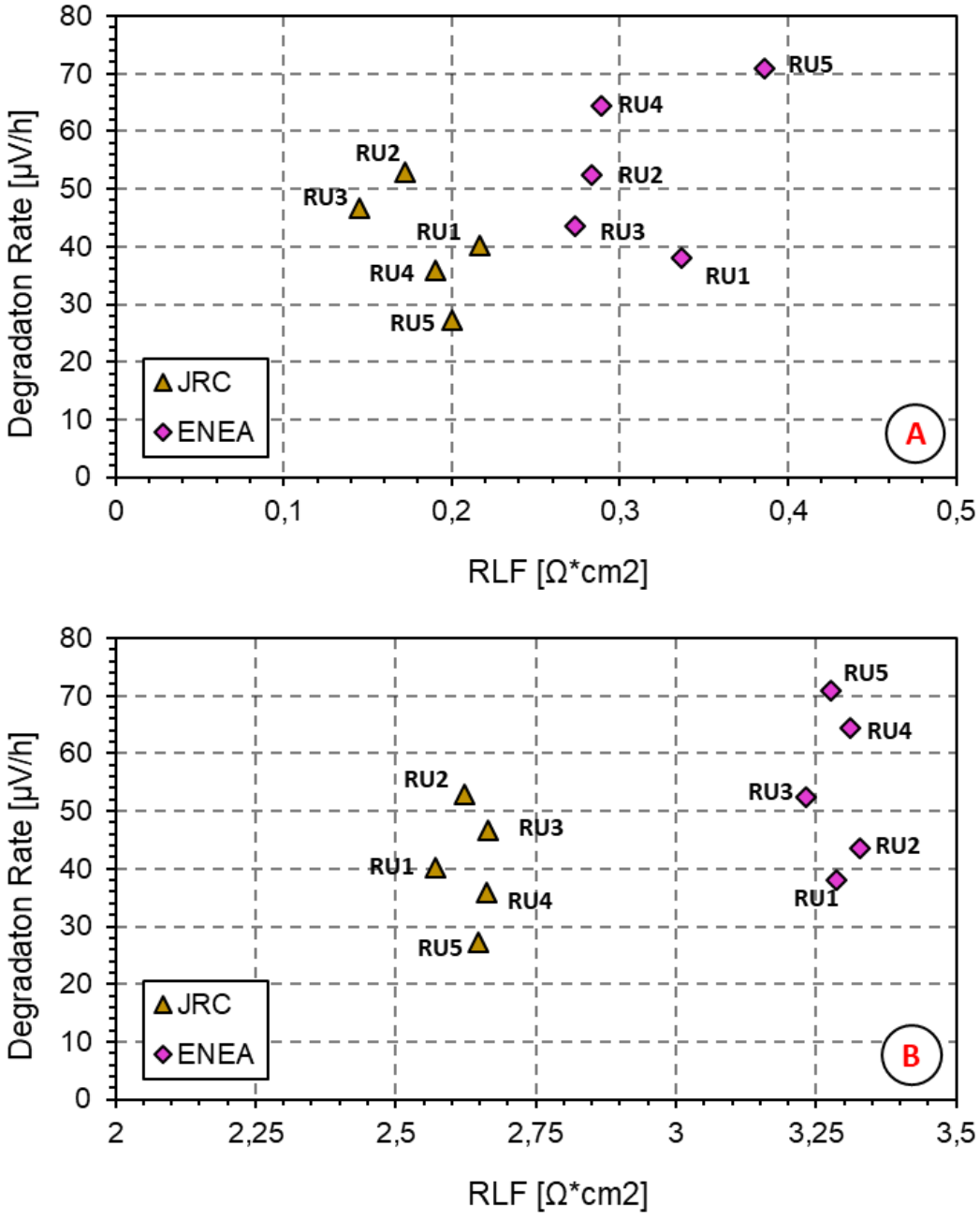

Figure 101. *Correlation between Degradation Rate and R_{LF}.(A) or R_{HF} (B).*

The only way to find possible correlations would be to repeatedly apply an EIS analysis when the stack is tested under constant current in long term operation without unplugging the current load. In fact, the EIS is an assessment of instant performance and can say something about degradation if it taken over time. Unfortunately, during the SOCTESQA Project this opportunity has never been taken into consideration. Nevertheless, it could be an idea to improve the overall analysis in future studies.

The last phase of the study involved the use of the DRA analysis in order to find a parameter that can help to better understand the phenomena of degradation or that can be used as a proxy variable.

The most commonly applied electrochemical test for quantitative evaluation of Re-SOC performance over time is long term operation at a given load which is presented with the Voltage-time characteristic and the periodically measured current-voltage curves which give integral picture of the system for a defined state. Remembering that the current-voltage characteristics are sensitive to operating parameters and degradation which reflects in the change of their shape, a quantitative estimation of the jV shape and thus of its change during operating at constant conditions can serve as degradation performance indicator. The parameter that reflects the shape is the internal resistance, which takes different values in different working point. Thus as already mentioned in paragraph 6.5 using the DRA analysis and starting from a jV curve, it is possible to extrapolate two new indicators which are $R_{d,min}$ and ΔV^*.

At the beginning, the study will focus only on the use of the first parameter while in a second moment also the second one will be taken into account. $R_{d,min}$, as defined, reflects the state of health at constant operating conditions. Since the slope of the current-voltage curve is a function only of the intrinsic properties of the system and therefore does not depend on external conditions, even the $R_{d,min}$ will have the same principles Thus, basically, the corresponding $I_{Rd,min}$ represents the working point at which the degradation rate during test under constant load is supposed to be the lowest.

Based on this concept and knowing the current under which the operation under constant load has been performed, the aim is to verify whether there is a dependency between the rates of degradation and the distance between this current value and $I_{Rd,min}$ calculated for each partner.

Starting from the jV measured for each partner, the new function R_d has been built and from it the. $R_{d,min}$ value has been determined. For the round robin test, refer to: Figure 64 with regards to $R_{d,min}$; Figure 94 for the degradation rate. Depending on the shape of the jV-curve, all the partners show a different value of $I_{Rd,min}$, presented together with their corresponding degradation rate in Table 9.

Table 9. *Correlation between Degradation Rate and $I_{Rd,min}$ during final validation for the stacks tested at DTU, ENEA; DLR; JRC. The current load applied was to 42 A (500 mA/cm^2).*

Partner	***$I_{Rd,min}$***	***Degradation Rate***
DLR	475 mA/cm^2	-200 µV/h
ENEA	575 mA/cm^2	-258 µV/h
JRC	600 mA/cm^2	-220 µV/h

For a better analysis also the data collected during the first validation were taken into account and presented in Table 10. As already mentioned before, during the first validation the partner DTU also took part in the operation under constant current, while JRC could not complete the test due to fluctuation problems. For the degradation rate, refers to Figure 99.

Table 10. *Correlation between Degradation Rate and $I_{Rd,min}$ during first validation for the stacks tested at DTU, ENEA; DLR; JRC. The current load applied was to 25.2 A (300 mA/cm^2).*

	First 500 h		**Second 500 h**	
Partner	***$I_{Rd,min}$***	***Degradation Rate***	***$I_{Rd,min}$***	***Degradation Rate***
DLR	642 mA/cm^2	-106 µV/h	639 mA/cm^2	-110 µV/h
ENEA	525 mA/cm^2	-420 µV/h	500 mA/cm^2	-140 µV/h

JRC	650 mA/cm^2	-129 µV/h		
DTU	649 mA/cm^2	-100 µV/h	599 mA/cm^2	-370 µV/h

The idea behind this study is that if $I_{Rd,min}$ really represents the best work point, then for a specific set load, the more $I_{Rd,min}$ is close to this value, the smaller the degradation rate will be.

Table 10 shows for each partner the corresponding $I_{Rd,min}$ value calculated directly from the jV-curves tested before TM12. Considering that the test under current was carried out with a constant load of 25.2 A which is equivalent to 300 mA/cm2, based on the hypothesis behind the DRA analysis, the stack tested at ENEA should have the lower degradation rate partners while that tested at JRC the highest compared with the others.

Unfortunately, as it can see by looking also the data presented in Table 9, there does not seem to be a direct correlation between the degradation rates and $I_{Rd,min}$. Thus, in order to bypass this problem then the analysis was focused only on the data collected at ENEA by investigating directly the single cells and not the entire stack.

During the analysis of the jV curve, RU1 and RU3 showed the same $R_{d,\ min}$ value in two distinct current density points, highlighting a first problem of the DRA methodology. As already mentioned in TM03, R_d is a very sensitive parameter and its calculation depends strongly on the current / time size to which the jV curve was measured. Thus, this first result confirms the importance to measure a jV-curve as accurately as possible in order to exploit the DRA methodology in the best possible way.

Table 11 shows the $I_{Rd,min}$ value calculated for each cells of the stack tested at ENEA and the corresponding degradation rate.

Furthermore, analysing the data, it is note that also comparing only the cells belonging to the same stack, it is impossible to find a direct link between the degradation rate and $I_{Rd,min}$ by using the DRA tool.

Table 11. *Correlation between Degradation Rate and $I_{Rd,min}$ during final validation of all the cells of the stack tested at ENEA. The current load applied was to 42 A (500 mA/cm^2).*

Repeating Unit	***$I_{Rd,min}$***	***Degradation Rate***
RU1	525 mA/cm^2	-38 µV/h
RU2	475 mA/cm^2	-52.4 µV/h
RU3	650 mA/cm^2	-43,6 µV/h
RU4	500 mA/cm^2	-64.4 µV/h
RU5	575 mA/cm^2	-70.8 µV/h

This additional result confirms that any cell behaves differently as whether it was a "foreign object" even if it is a part of the same stack due to the several variables that come into play in terms of degradation. Excluding cell production issues the different analysis carried out during this test module, confirm that, it is difficult to find a good parameter or a methodology that can help to understand the degradation phenomena.

Therefore, for this reason, from this point on, for the test modules concerning "operation under varying current" and "thermal cycling" only the results achieved will be present in order to

demonstrate the high reproducibility between the partners since, on the base of the recorded data set, nothing more can be added on the degradation rate.

However, starting from this in-depth study, a series of findings and recommendations will be listed in order to improve and optimize this test module. Before doing so and conclude this paragraph, also the results obtained in SOEC and in SOFC/SOEC mode will be presented.

Figure 102 below presents the stack voltage evolution as a function of time recorded during 500 h long-term operation at 750°C and -0.5 A/cm^2 in SOEC mode. It is worth noticing that initial stack voltages are very similar for the three partners. Temperature evolution during long-term operation has also been checked, showing stability all along the test module /variation of 1°C maximum for each thermocouple). EIFER shows good steam management differently from JRC and CEA where scattering occurred due to the presence of water in the output line.

The stack tested in JRC has already shown the same fluctuation problems in SOFC mode. Based on the results achieved in this operating mode and those that will be shown then in Figure 103 (regarding the operation under constant current in SOFC/SOEC modes) it is possible to state that together with the problems regarding the steam stability, also those concerning to the discharge of water produced must to be solved in order to minimize the problems related to the calculation of the degradation rate. It was observed in the course of this study that the presence of fluctuations certainly affects the calculation of the degradation rate since its measurement strongly depends on the choice of the voltage values and scattering problems make the identification of the correct value of stack voltage difficult. At the same time, the presence of water in the output line could be one of the main reasons why some stacks have suffered a fast degradation rate due to counter pressure which leads to mechanical stress as already explained in paragraph 5.2.

It is important to remember that in SOFC mode the presence of water in the output line which causes fluctuations is due to the formation of this molecule that it is together with electricity, one of the products of the electrochemical reactions occurred when the cells operate in fuel cell mode.

Anyway, also this time, the different stacks show good reproducibility even if it is recommended a longer test to establish similar degradation rate.

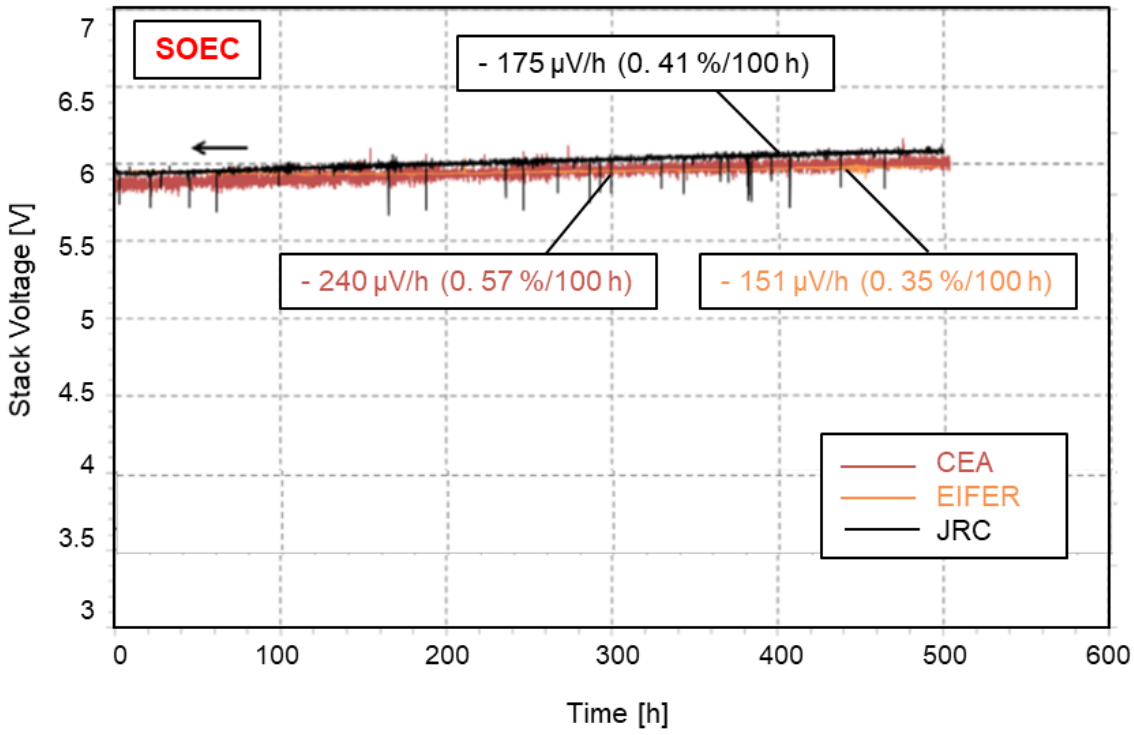

Figure 102. *Voltage trends (JRC, EIFER, CEA) during operation under constant current of -500 mA/cm² with 80% H2O/20& H2 // 1 air (NLPM/RU), 750°C, in SOEC mode.*

Different results have been achieved in combined mode. The operation condition for constant SOFC mode was at 750 °C with 2.5 NL/min H_2 + 2.5 NL/min N_2 supplied to the negative electrode compartment and 20 NL/min air supplied to the positive electrode compartment and the operation condition for constant SOEC mode was at 750°C with 0.64 NL/min H_2 + 2.5 NL/min H_2O supplied to the negative electrode compartment and 5 NL/min air supplied to the positive electrode compartment. The operation duration was 3 hours in SOFC mode and 20 hours in SOEC mode every 24 hours (per day).

Figure 103 shows the stack evolution with time of the two stacks (DTU and NTU) run in SOEC mode during the SOFC/SOEC combined mode. Due to the voltage fluctuation during the SOEC mode operations, the degradation rates were evaluated over the 500-hour operation using linear regression. The voltage degradation rates in the NTU stack appear rather uniform whereas relative large deviation is observed on the DTU stack which showed a fast degradation in the first 200 hours followed by a constant plateau. The degradation rates of all RU for both stacks are reported in Figure 104 where it is possible to note that the degradation rate of DTU during the last 200 hours is much lower than that of the overall degradation, and also lower than the stack tested in NTU. The strange behaviour at DTU, confirms along with the results provided in the first part of this paragraph, the importance to test the stacks for a time longer than 1000 hours in order to achieve similar and thus comparable degradation rates.

The results concerning SOFC mode during the SOFC/SOEC combined mode is reported in Figure 105. In the first plot, the evolution with time showed the same strong voltage activation for both stacks after switching to SOFC mode while in the second one, it is note a very similar degradation rate that is smaller than in SOEC mode, because of different operation mode. Also in this case, the

degradation rate of SOFC in DTU is much smaller compared to that achieved in NTU when considering the last 200 hours of test.

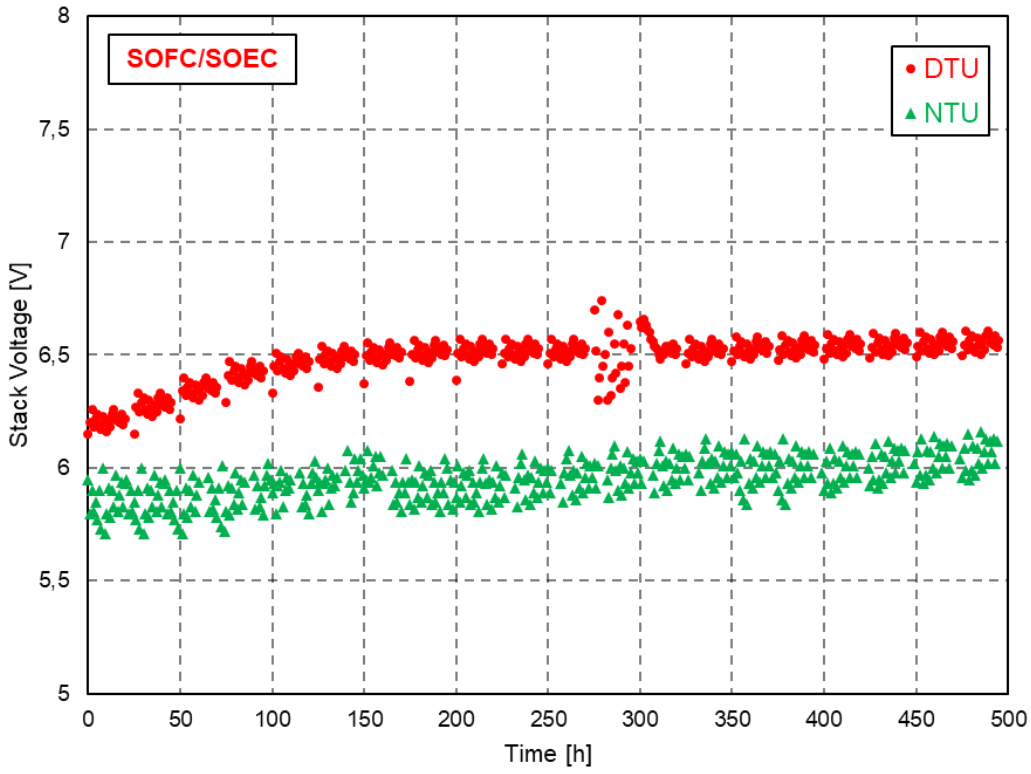

Figure 103. *Stack voltage evolution with time in SOEC mode during the SOFC/SOEC combined mode.*

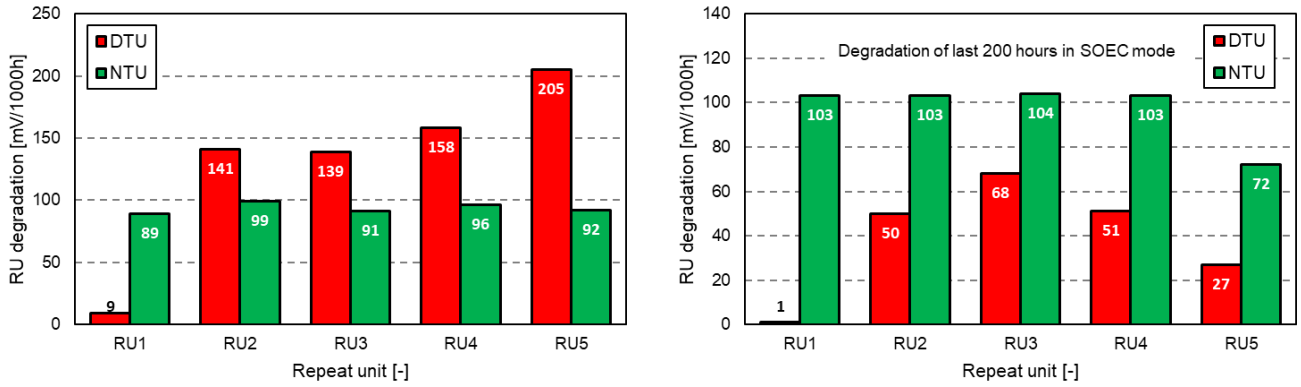

Figure 104. *RU voltage degradation in the SOEC mode during the overall operation (left) and the last 200 hours (right).*

This test module topic is quite common nowadays as shown by references found in literature [87] even if these procedures remain quite generic. Based on those references, the present TM12 fully dedicated to operation under constant current presents in details the relevant TIPs, TOPs and derived quantities with their associated formularies, their evolution, the test procedure to perform long-term operation in both SOFC and SOEC modes and the different ways to express degradation rates in order to achieve more comprehensive representation of the cell/stack assembly unit durability.

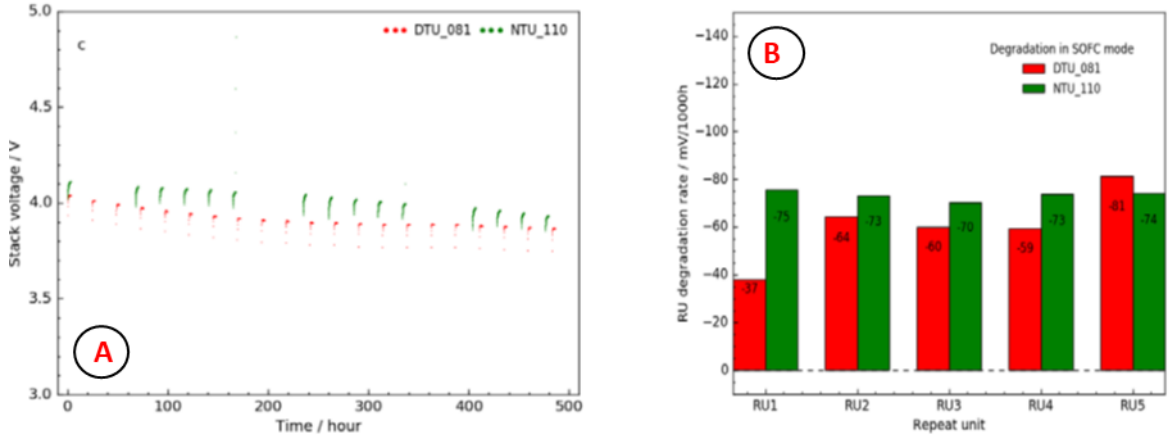

Figure 105. *Test results of stacks operated in SOFC mode during the combined mode operation. In particular, are shown the stack voltages evolution with time of stack tested at NTU and DTU (A) and the corresponding RU voltages linear degradation (B).*

Nevertheless, some recommendations in order to optimize the test are given below:

- The calculation of the degradation rates is very sensitive to the choice of voltage values. To optimize the measurement, the voltage must be noted at the third digit after the decimal place. Moreover, in case of scattering, a good way to get around this problem could be to use a linear regression or directly calculate the voltage using an average of the data points;
- The determination of degradation rates is also influenced by the choice of the initial voltage value. Especially in SOFC mode, the stack may take some time to stabilize the voltage, so use this value and not the initial value for calculating the degradation rate;
- Even stacks from the same supplier and the same manufacturing batch show different behaviour during the initial operation mode, thus the test should be performed for more than 1000 h in order to achieve reliable and comparable degradation rates;
- Unlike other temperatures, the new $\Delta T_{end\text{-}inlet}$ parameter is a good starting point for analysing the degradation phenomena that occur inside the cell by comparing several stacks;
- The DRA methodology can be recognized as a new useful tool with increased sensitivity towards degradation, since it works with derivatives of the measured parameters, which are in principle more sensitive to small deviations. However, this tool does not provide useful information on degradation rates when a stack is tested because each cell behaves differently from the others. It is recommended to use this tool, as for EIS analysis, only when studying a single cell to compare the change in results with the initial ones;
- Temperature is not the only parameter on which degradation rate depends. The stability of the steam and the discharge of water in the outlet line also significantly influences degradation. To overcome these problems, a first improvement will be to equip the test bench with a good steam generator, a heating sub-system in both inlet and outlet lines. Moreover, as regards the outlet line, in order to avoid pressure fluctuation, it is advisable to increase the exhaust section to avoid water condensation and extract the steam as far away as possible to the stack so that its absence does not influence total outlet gas pressure;
- However, on the basis of the results obtained, by comparing the various stacks and also separately the cells of the stack tested at the ENEA, the degradation rate seems to be influenced also by something else. A critical aspect of this test module was that during the operation under constant current, the partners have only provided the measurement of the voltage stack and not those regarding to the cells voltage. The critical analysis carried out in

this study showed in particular that since the cell / stack is a very complex device, together with the single test procedure, it is very important to be able to benefit from a large data package of standardized results, so it is highly recommended to record in detail all the variables in order to find a possible connection that can help science to take a step forward in the state of the art.

As already suggested in the paragraph concerning the "Temperature Sensitivity" Test Module, since the partners have showed a different temperature evolution due to different test benches (and in particular furnace design) during the SOFC mode, a next step in order to improve the TM12, may be to correct the strong temperature evolution by performing the test at a constant T_{stack} through constant adjustment of the furnace temperature which can be automatically realized through the temperature regulation or to calculate the degradation rate by adapting the furnace temperature at the end of TM12 step in order to bring the stack temperature back to the initial value and then record the obtained voltage as the final one.

6.2.7. TM13: Operation under varying current

At the beginning of the Project, the idea behind this test was to evaluate the stack durability under load cycling simulating a realistic profile that should have been defined for each application. Nevertheless, due to a delay in the SOCTESQA roadmap, the test was developed only to study the stack voltage evolution as a function of time in SOEC mode with the aim of simulating a simplified wind profile for electricity supply. For this reason, the results reported concern specifically the SOEC mode.

Figure 106 below presents the stack voltage and current evolution as a function of time recorded during 10 load cycles at 750°C between 0 and -0.5 A/cm^2 (left) and the stack voltage degradation (right). Each cycle consists of 3 hours at OCV and 20 hours under current. For a fair comparison between both partners carrying out this program, the data have been reported with the same time interval between two consecutive points, equal to 1 min.

It is worth noticing that in addition to the initial stack voltage also the evolution with time was similar for both partners with slightly higher voltage stability at EIFER. OCV values were very stable all along the step duration and the stack voltage increases during SOEC operation with a similar speed between both partners.

During the test also the temperature evolution has been checked showing an increase of 4-5°C for both partners at the end of the test.

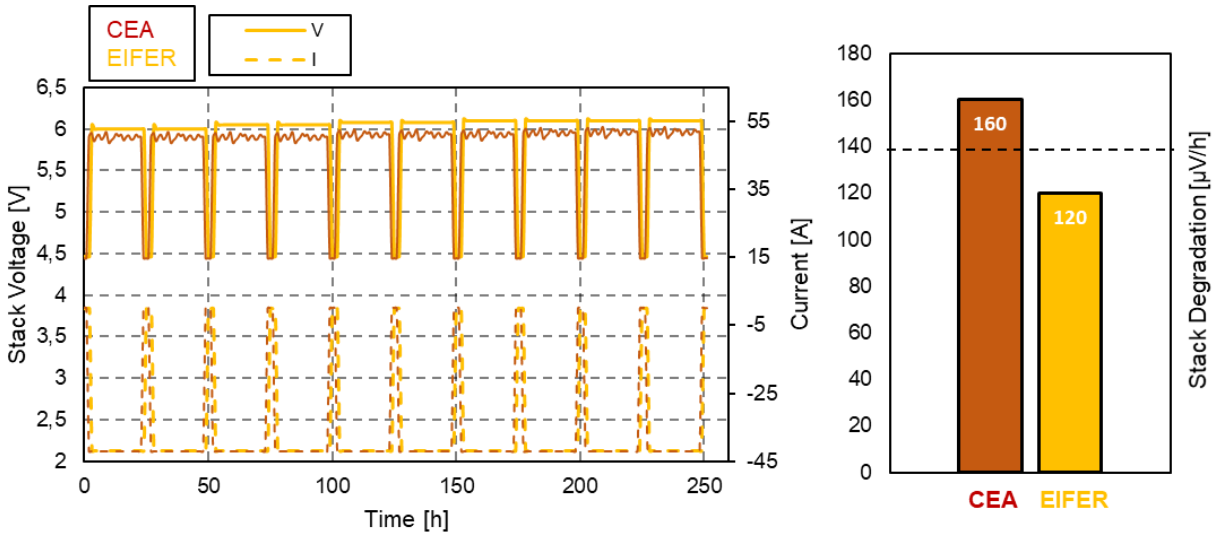

***Figure 106**. Stack voltage and current evolution as a function of time recorded in SOEC mode at 750°C under load cycling between 0 and -0.5 A/cm²(left) and stack voltage degradation (right).*

The degradation rates of the two partners during load cycling are quite similar with an average of 140 ± 20 µV / h. The higher degradation in CEA is due to the voltage signal that is a little bit noisier which compromises the determination of the precise rate of degradation.

During the first validation, the test was carried out using a time interval between two consecutive points of 5 minutes. The results are very similar compared to these, by resulting in a high reproducibility of the test.

This Test Module is quite new. Few test programs in transient operating conditions can be found in literature [2-4] but existing procedures as reference [1] do not take into account dynamic operation in both modes. The present TM13 fully dedicated to operation under varying current give in details all the relevant information necessary to perform stack tests in SOFC, SOEC and even combined SOFC/SOEC modes.

Not having many data to analyse and bearing in mind that it is difficult to give an explanations regarding the degradation rate, the only recommendations that can reported, together with those listed in TM12, regard the time interval between two consecutive points and the duration used for the calculation of degradation rates, which have to be clearly mentioned in the data post processing. In addition, it is advised to monitor all variables using a time interval as smaller as possible.

The next step should regard the study of the operation under varying current in SOFC and in combined SOFC/SOEC mode.

6.2.8. TM 14: Thermal Cycling

The Thermal Cycling test was specifically developed to examine the influence of different start-up and shutdown processes on the performance of the stacks tested especially for the SOFC mobile application in an APU device, where the behaviour of the stack during the thermal cycling is very important. For this reason, the only results that will be reported mainly concern this operating mode.

The aim of this test module is to establish a widely accepted method to evaluate stability of SOC when thermally cycled. The accurate monitoring of the voltages is essential for the determination of the degradation rates. Two phases with 15 thermal cycles for a total duration of 500 h each have been integrated. The 15 cycles include 12 so called “warm cycles” down to 200°C and three so-called “cold cycles” where the stack is cooled down to ambient temperature. The first cycle starts with the heating-

up from ambient temperature with a temperature increase of 3 K/min. After the set point temperature of 750 °C is reached a holding time of 60 minutes follows until the temperature is stable. Afterwards the current density is increased from 0 A/cm² to 0.5 A/cm² and kept constant for two hours. The following holding time at OCV lasts again 60 minutes before the stack is cooled down to 200 °C respectively ambient temperature.

The discussion of the thermal cycles concerns two types of degradation. First the degradation of the OCV and second the degradation under constant current. Figure 107 shows the OCV plus the degradation rate before each thermal cycle of the stacks measured at DTU, ENEA, DLR and JRC during thermal cycling. The stacks were operated at 750 °C with 0.5 H_2 + 0.5 N_2 NLPM/RU on the negative electrode and 4 NLPM/RU air on the positive electrode.

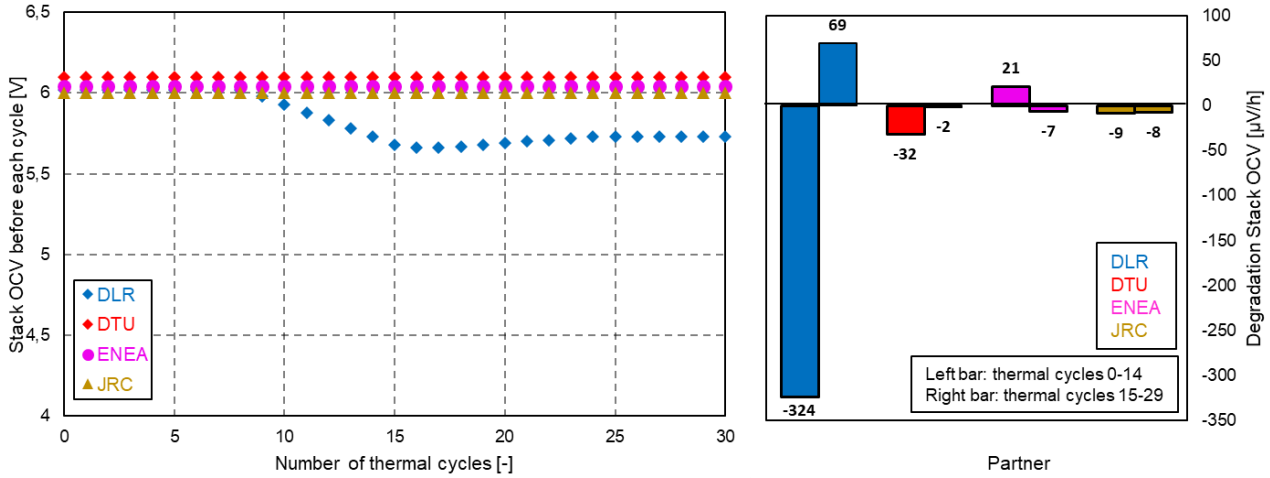

Figure 107. *Stack OCV before each thermal cycle (left) and the corresponding degradation rates (right).*

All partners were able to perform the required 30 cycles. At the beginning of thermal cycling all stacks show very homogenous and stable OCV behaviour. The OCV values are in a range of 5.98 V (DLR) and 6.06 V (DTU). Due to the lower gas tightness of RU 4 a lower value for the DLR stack was expected. Three stacks from ENEA, JRC and DTU are quite constant till the end of the 30th cycle. In contrast to that, the OCV of the stack tested at DLR starts to decrease at the 10th cycle. It is very likely that the higher leak rate of RU 4 is the reason for this behaviour. Due to the chemical reaction of H_2 with air the temperature of RU 4 rises resulting in non-uniform thermo-mechanical stresses. In general, the degradation of the OCV is strongly influenced by these thermo-mechanical stresses. It is also possible that the neighbour repeat units are influenced by this effect of RU 4. Especially during the start-up and cool-down the thermo-mechanical stresses might lower the sealing of the cells in the bipolar sheets of the DLR stack.

After the 17th cycle the voltage for the DLR stack becomes more stable and even increases a little bit. During the operation of the stack it is possible that the sealing between the stack and the gas distribution plate slightly improves, which leads to a higher OCV. The stacks of the other partners maintain their OCVs on a high level during thermal cycling, whereby the value from ENEA even slightly increases.

It is obvious that stack tested at DLR shows the highest degradation rate among all partners which is -324 µV/h for the first 15 cycles. Such a high value is very unusual for the OCV degradation. During the second 15 cycles the degradation is positive with 69 µV/h. For the other stacks the degradation rates are very uniform, whereby ENEA also shows a small positive degradation rate for the first 15 cycles. The impossibility of having a positive degradation rate highlights the importance of modifying

the sampling rate in order to avoid non-standardized and therefore incomparable results. The precise recording of the voltages is one of the steps forward to improve all general modules that regard tests under long term operation as already mentioned during Test Module 12.

Due to the positive values the OCV increases slightly. Three out of four stacks show a very uniform behaviour which is a good reference for the reproducibility of TM 14.

Besides the degradation of the OCV, also the degradation of the stack under electrical current load was examined. Figure 108 shows the stack voltage at 500 mA/cm² after approximately 90 minutes of operation. The stacks were operated at the same conditions.

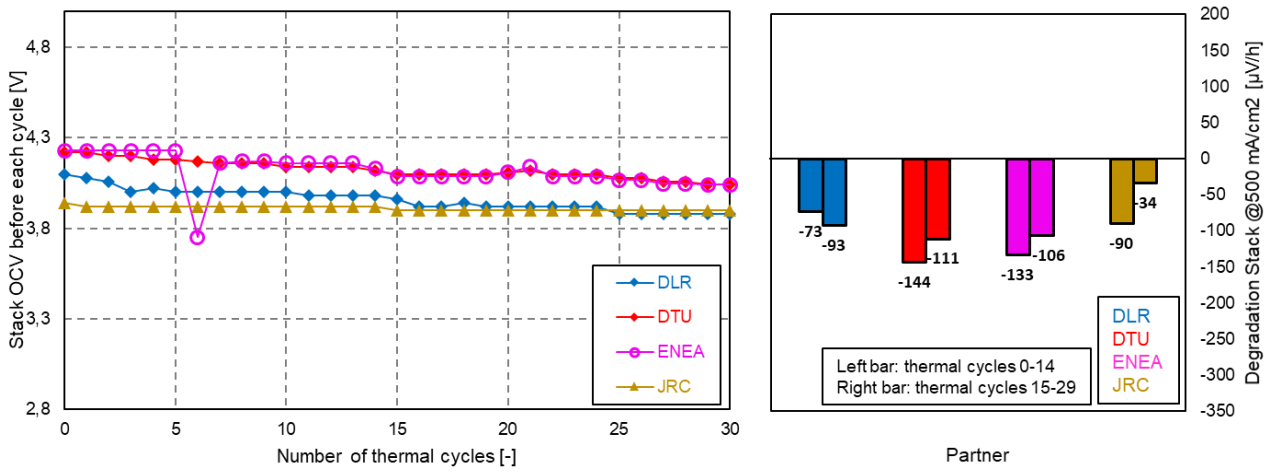

Figure 108. *Stack voltage for each thermal cycle after 90 minutes' operation at 500 mA/cm² (left) and the corresponding degradation rates (right).*

Stack tested at ENEA started with the highest stack voltage among the partners. The 6th thermal cycle of ENEA is an outlier and can be excluded. A disturbance of the voltage measuring transducer caused the recording of this inaccurate value. JRC had a similar problem at the 13th cycle, but in this case the voltage was not recorded at all. Independent of the differences in the voltage all curves show nearly the same characteristics. After the first 15 cycles all stacks exhibit a drop in the voltage even if the voltage degradation curves remain uniform. At the end of the 30th cycle ENEA still has the highest voltage with 4.052 V and JRC again the lowest one with 3.9 V.

It can be identified that the two stacks tested at DLR and JRC, as well as the two stacks tested at DTU and ENEA demonstrate a very similar degradation behaviour. It is conspicuous that all stacks, except DLR, degrade stronger during the first 15 cycles. Considering all 30 cycles DTU shows the highest degradation value which is -255 µV/h. Compared to that JRC has the lowest degradation rate of only -124 µV/h. Despite the high OCV degradation, the stack tested at DLR shows a rather stable thermal cycling behaviour under current. Therefore, it can be concluded that the strong degradation of the OCV does not influence the degradation rate under electrical load significantly.

In comparison to the initial value, the voltage decreased by -3.5 % for ENEA and -1.8 % for JRC. These different values demonstrate that the influence of the thermal cycles relating to the degradation of the stack is very complex and versatile. For a better understanding a higher number of thermal cycles is recommended. It is well known that the degradation rates are higher at the beginning and become more stable with progressive operating time. The degradation is primary caused due to the ageing of the components. In this context material and structure changes especially of the electrodes play an important role. This leads simultaneously to an increase of the polarization resistances. In

order to understand the degradation mechanisms during the thermal cycles better this issue should be investigated more precisely in the round robin test.

Considering the DLR problems during the test, the TM14 may be optimized by following these recommendations:

- Ensure high gas tightness of all repeat units before the thermal cycling. If this is not the case a less gas tight repeat unit in the stack may have a significant influence on the OCV of the other repeat units during thermal cycling.
- In order to monitor possible temperature gradients within the stack assembly, the proper positioning of the thermocouples and the accurate measuring of the temperatures is very important.

6.2.9. TM 16: Shut-down

Figure 109 shows the temperature of the top plate T_{TP} and the 5 repeating unit voltage during the shut-down process of stack tested at ENEA.

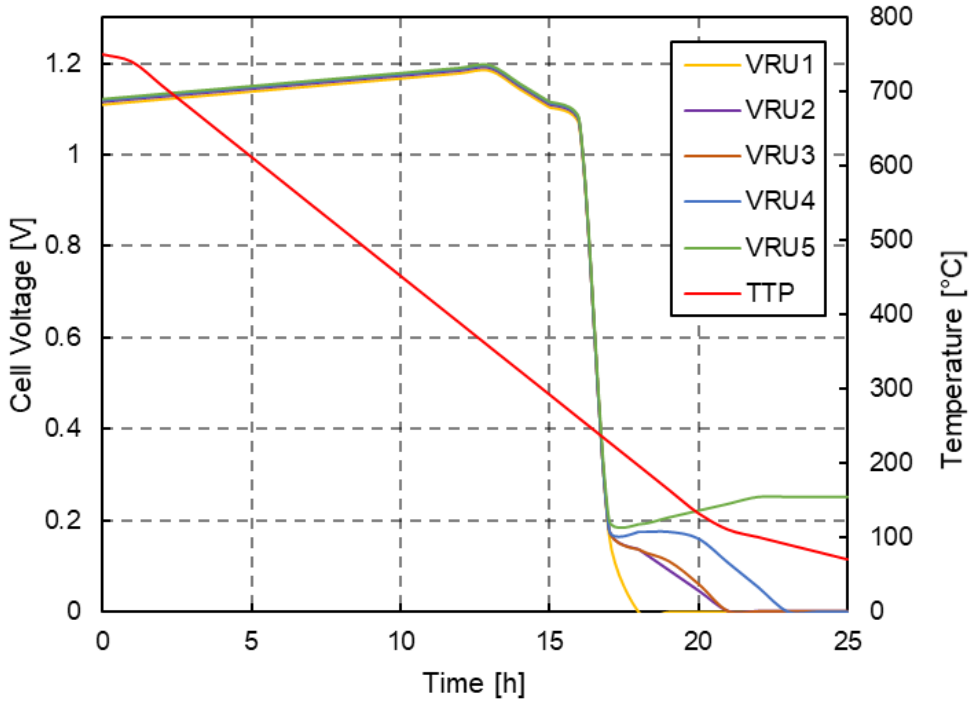

Figure 109. *Stack temperature and RUs' voltage during shut-down of a 5 cells SOC stack test.*

The figure 110 instead, shows the cooling rate for the individual partner together with the intended cooling rate of 2 K/min (dotted line). It can be seen that none of the partners can follow the intended cooling rate. CEA and DLR both have a significant slower cooling rate over the whole temperature range. The most obvious reason for that is the better thermal isolation of their furnaces which reduces the heat transfer with the surrounding environment, especially a lower temperature which becomes very low. However, this measure has no influence on the validation of TM16.

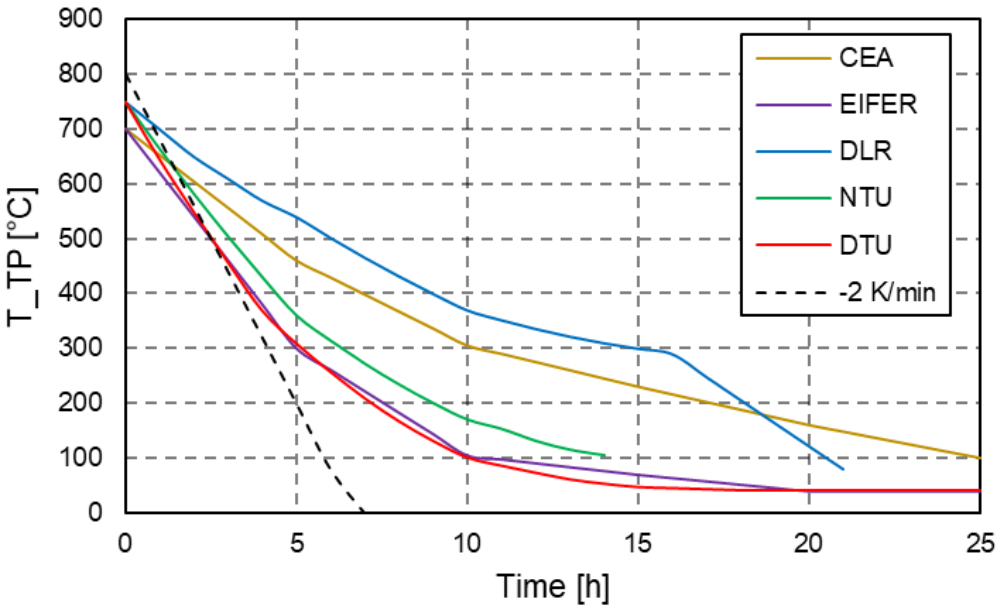

Figure 110. *Comparison of cooling rates between partners.*

7. CONCLUSION

After the last alarming news about the global warming due to the continuous increase of greenhouse gas emissions which will entail disastrous consequences for whole world such as sea level rise, the increase in heat waves, massive increase of drought period, of flood and other problems, the time to find concrete solutions has come. Reversible solid oxide cell technology comes as a promising possibility to tackle the energy poverty and environment pollution. Thanks its possibility to convert directly hydrogen in electricity by coupling with other systems such as solar or wind energy, Re-SOC can represent an important green energy solution for the next generation. In addition, thanks to its ability to work as electrical energy storage system, its trending is going upwards. Thus, there are many positive reasons to consider Re-SOC ready to be entered into the market.

The last gap to be bridged is to create a specific international standard that collected all the regulations, normative, procedures and test modules in order to allows consumers and producers to refer to the same specific regulation. There is a need for developing uniform test procedures for high temperature ceramic oxide cell/stack assembly units operating in both fuel cell and electrolysis mode. These test procedures usually consist of a combination of different test programs, each of which contains different test modules, which address the three different operating modes. Each of these cases includes both stable and dynamic operations. The test procedures will include and specify the complete test systems, the different operating modes, the test conditions and the electrochemical characterisation methods, e.g. current-voltage curves and electrochemical impedance spectroscopy, with the aim of providing robust and easy-to-use protocols for experimental characterisation of the specified SOC test items and the interpretation of measured data minimizing the possible differences in terms of end results when applying the same tests on equivalent stacks on different teste benches.

The SOCTESQA project has carried out pre-normative activity for the definition of validated Re-SOC test procedures. Successively, the critical analysis of all the data collected during the entire project has been the basis for a secondary elaboration with the aim of optimizing and improving all the teste modules and understand which will be the future steps to follow. At the end after an additional review, all information about the test protocols, they have been inserted into IEC standardization process.

All the step regards the entire work of the thesis has been as purpose that to accelerate the development and the market penetration of hydrogen and fuel cell energy system.

The experimental campaign has been divided in five parts. The first one aimed to identify the specifications and the definition of the overall test matrix which consists of test programs and test modules. The second one was aimed to obtain sufficient accuracy, reliability and repeatability of measurements among the different partners by modifying the test benches after an initial validation stage. The third was aimed at validating the stack in terms of performance and endurance following the guidelines of test programs created specifically to test the device in SOFC, SOEC and combined SOFC / SOEC operation mode. After collecting a huge data package and verified the comparability of the results among the different test laboratories, the fourth part was aimed to search the most important parameters and information to characterize and improve the performance of the stack. The fifth and final part was aimed at updating of the standard IEC 62282 with all the new information extrapolated from the whole work.

The chapter has the aim of summarizing only the most important results achieved during the work.

The test bench validation was aimed at highlighting the weaknesses of the different test systems and finding solution to improve them. The test bench is a crucial part of the whole work since its

modifications are indispensable to obtain reliable test results. Some of the most critical points of attention for obtaining accurate and reliable results have been identified and described below:

- Surely, the temperature is one of the most important variables to control, in order to mitigate the thermal stresses in the presence of temperature gradients across the stack which may cause a decrease in the performance of the stack, and a higher rate of degradation in the case of long operation. Thus, it is important that Average Temperature is as close as possible to Average Temperature of the stack;
- In order to obtain acceptable EIS spectra it is important to avoid all electromagnetic interferences of the equipment through specific positioning of the current cables;
- A suitably powerful preheating subsystem is very important to obtain good performance of the test object;
- In SOEC mode, the stability and quality of the steam production play a crucial role in the resulting performance of the SOEC short stack, especially the control of a stable steam supply and accurate and stable steam-to-H_2 ratio monitoring as shown in the I-V curve. Paying close attention to avoid the condensation of water in the output anode gas line is an important point since the presence of liquid water could mitigate the performance of the stack.

During the third phase, 4 test programs were performed, each of them focused on a specific application, defined as:

TP01: Test program for the stationary application of SOFC in a micro-CHP system
TP02: Test program for the mobile application of SOFC in a APU
TP03: Test program for the application of SOEC in a power-to-gas system
TP04: Test program for the application of combined SOFC/SOEC in a power-to-gas-to-power system

For each application a test program consists of a series of generic test modules. Each test module has its own test objective and contains specific procedures to follow. At the end of the SOCTESQA project, ten test modules were integrated that each partner performed at least once.

However, due to lack of time, during the project each partner focused only on 2 of the 4 applications. In particular, ENEA carried out the first and second test programs.

The test modules were differentiated in "characterization Test" (TM3, TM4, TM7 and TM9) and "endurance Test" (TM12, TM13 and TM14) in addition to TM02 and TM16 that concern the Start-up and Shut-down procedures.

All the tested stacks, except in some cases that can however be considered irrelevant, showed a high uniformity and reproducibility of the results in all the test modules in both SOFC and SOEC modes.

Thanks to the meticulous analysis of all the data collected during the entire Project, for each test modules have been provided:

1. TIPs, TOPs and Derived quantities;
2. The Test Methodology;
3. The Critical Parameters and Parameter Controls;
4. The most important parameters that can be extrapolate
5. Different and sophisticate ways to represent the results achieved;
6. The data post processing;
7. Recommendations to integrate in order to optimize the test;

Furthermore, again thanks to the critical analysis, other information can be provided, which set out below.

Regarding the characterization tests, TM03 together with TM04 are known as the best test modules to characterize the initial performance of a Re-SOC, while TM07 and TM09 can be considered new and relevant since they can address the effects of gas utilization and temperature on the performance of the SOC device. However, unlike the first two tests, TM07 and TM09 do not guarantee all the information necessary to verify the real quality of the tested stack.

For consumers, if the only purpose is to immediately qualify the performance of the stack to understand if the device is working properly or not, the only use of TM03 can be considered efficient. Unlike the EIS analysis, the jV curves are faster in response, the analysis does not undergo electrochemical interferences or the presence of water and the stack does not need time for the stable voltage state. Moreover, based on the strategy behind the DRA analysis and thanks to the many available jV curves, it was possible to extrapolate a *Vcell** trend useful for immediately comparing the performance of any similar stack. Considering that the *Vcell** trend has been built as a function of the current density *j*, this trend will be perfect for comparing any cell independently of the active area. However, if the intent is to continuously evaluate the performance of the stack when it is under constant current or during thermal cycles, it is better to use together with TM03, also the TM04, that unlike the jV curves, the EIS analysis has the ability to perform the measurement in-operando i.e. without stopping the test.

Instead for laboratory tests, it is recommended to perform all characterization tests that can provide useful information. It is also advisable to record all possible information over time because, as it was possible to see in the chapter regarding the results, more parameters play an important role on the performance of the stack. It should be added that the importance of using EIS analysis is related to the possibility of using the results for DRT analysis especially when the intent is to study a single component of the cell by testing it in a large number of different pre-defined operating conditions or during long-term tests.

In the fourth part of the experimental work, for the first time, methods as the Distributed Relaxation Time (DRT) and the DRA were performed on the experimental EIS spectra and JV-curves obtained from several stack samples tested in different test benches.

In particular, the experimental investigation has proved that regarding the first analysis, the observed response of DRT spectra respected all the electrochemical processes what they were expected based on the theory. In addition, the DRT analysis has proved that beside the temperature also the gas distribution plays an important role on the performance of the stack. Instead with regards to the DRA method, the different analysis has demonstrated that also the cells belonging to the same stack behave differently undermining any evaluation and comparison.

However, both methodologies can be considered innovative and useful when a single cell is taken into consideration, but nevertheless especially DRA being a new diagnostic tool needs more collected data and cell tested with the aim of improving its potential, since the method presents some gap which must be closed as for example the possibility to apply the analysis only for the SOFC mode and not for the SOEC.

As for the resistance tests, using all the available results and all methodologies at the disposal, unfortunately, no correlation was found between degradation rate and different parameters such as temperature. Every single cell seems to behave differently as if it were a "foreign object", even if it

is a part of the same stack probably due to the different variables that come into play in terms of degradation.

The overall meticulous analysis reported in the thesis permits to confirm that too many parameters play a key role on the performance of the cell / stack. Together with the temperature, which is usually considered the main cause of degradation rate, the whole study has shown how also other parameters such as the gas utilization, the water management, the gas distribution in some way interferes with the characteristics of the device. Further tests are needed to find a possible correlation that could help to understand all the processes that occur in the cell / stack and why some devices degrade faster than others depending on the operating conditions.

However, from the analysis of the long-term operation, the study emphasized the importance to:

1. Test the device for an operating time of over 1000 hours, since in this period every single stack behaves differently, otherwise the comparison has no value;
2. Use the real voltage reading in the calculation of the degradation rate to avoid errors that could affect the analysis, then make sure the stack reaches a stable state before recording the voltage;
3. Among the different temperatures evaluated, $\Delta T_{end\text{-}inlet}$ can be recognized as a good starting point to analyse the degradation rate since it contains all the temperatures without incorporating those related to the output since they are directly affected by the plates.

Since it is impossible to find correlations that can help science to understand the mechanisms underlying the degradation rate, further efforts are needed. The whole study, focusing mainly on the importance of creating robust test modules and procedures to develop a comprehensive guide for the management of the Re-SOC, globally recognized, has guaranteed a lot of important information but no response on the problems related to the degradation rate.

Considering all the operating conditions studied, a first solution could be that to propose a new test module in which the stack is tested by changing the pressure of the supply gases, since during the study it was the only parameter never took into consideration.

Anyway the entire work developed during the PhD period has contributed significantly to the progress of the state of art of Re-SOC devices. At the end they have been developed:

- 4 important test programs each of them focused on a specific application, have been performed and developed;
- 9 test modules have been developed and optimized, each of them containing all information necessary to be used as a complete guide such as the test input and output parameters together with those that can be calculated, test methodology in which all the operating steps to execute are summarized and data post-process in which the best way to represent the results is given.

Figure 111 shows 3 of the 9 test modules elaborated during this work. For each of them also a short description version is given.

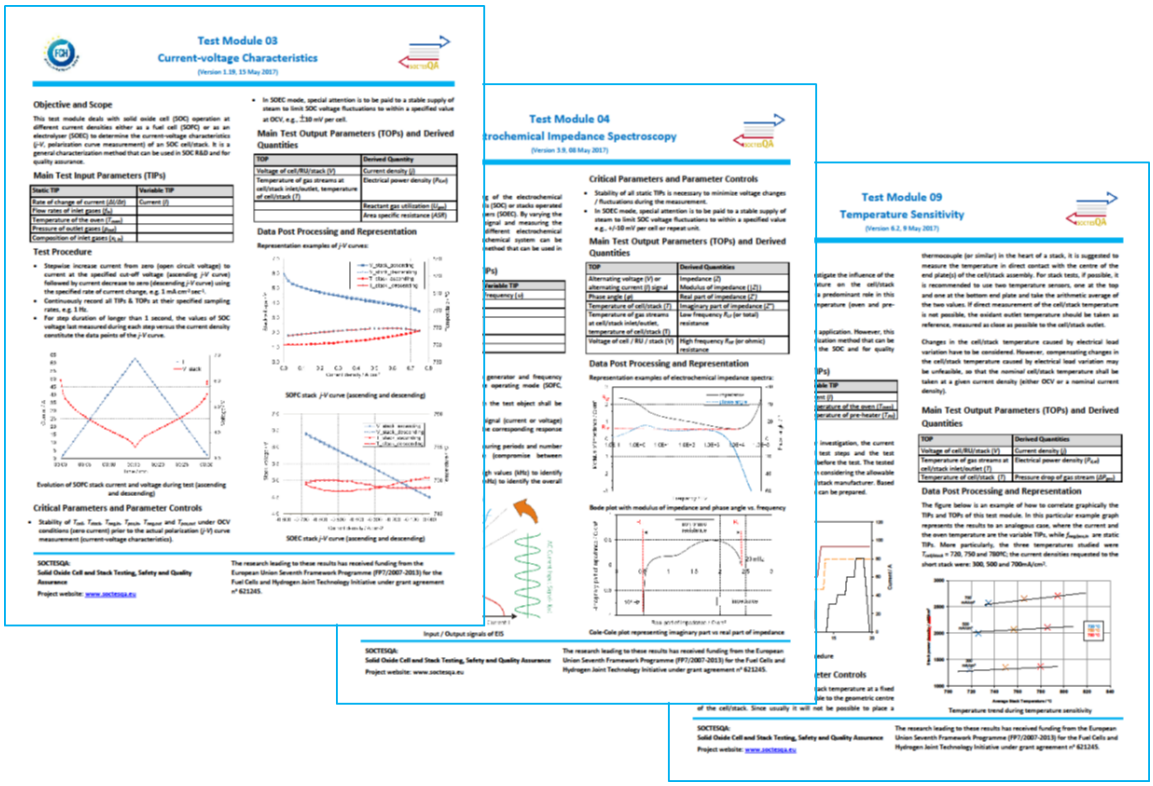

Figure 111. *Test modules short description. In particular, they are highlight Test Module 03, 04 and 09.*

After reaching this step, the last period of the PhD was focused on the uploading of the IEC 62282. Starting from the old version which concerned exclusively procedures for SOFC mode, a new version has been created. In this, all the information and results achieved during the work and related to the possibility that the device has to work also in electrolysis mode and thus as reversible system has been inserted. The document which should come out at the beginning of 2019 will provide performance requirements (effectiveness, reliability) with regards to the means (procedures, prevention, mitigation) used to achieve performance/safety targets.

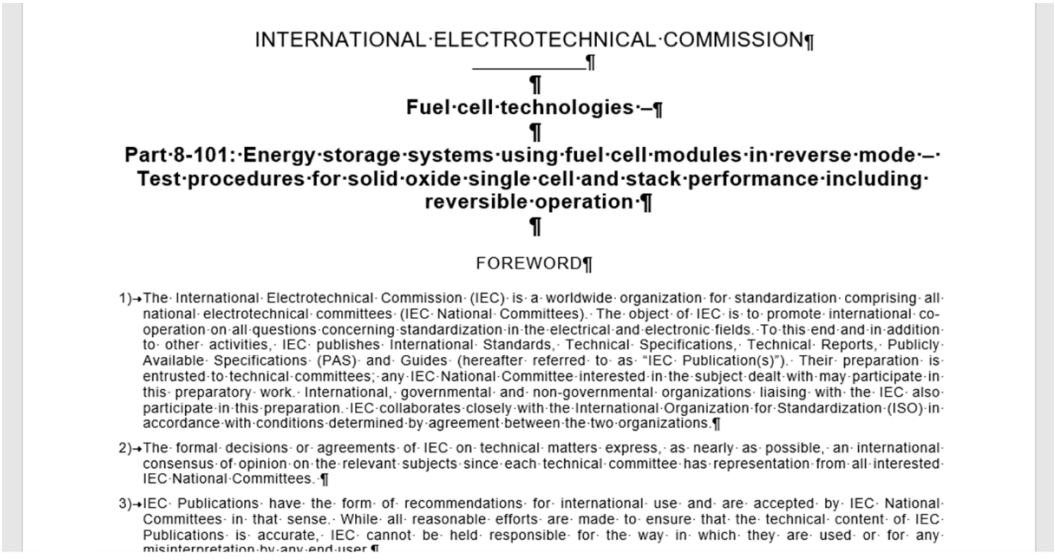

INTERNATIONAL·ELECTROTECHNICAL·COMMISSION¶

¶

Fuel·cell·technologies·–¶

¶

Part·8-101:·Energy·storage·systems·using·fuel·cell·modules·in·reverse·mode·–· Test·procedures·for·solid·oxide·single·cell·and·stack·performance·including· reversible·operation·¶

¶

FOREWORD¶

1)→The· International· Electrotechnical· Commission· (IEC)· is· a· worldwide· organization· for· standardization· comprising· all· national· electrotechnical· committees· (IEC· National· Committees).· The· object· of· IEC· is· to· promote· international· co-operation· on· all· questions· concerning· standardization· in· the· electrical· and· electronic· fields.· To· this· end· and· in· addition· to· other· activities,· IEC· publishes· International· Standards,· Technical· Specifications,· Technical· Reports,· Publicly· Available· Specifications· (PAS)· and· Guides· (hereafter· referred· to· as· "IEC· Publication(s)").· Their· preparation· is· entrusted· to· technical· committees;· any· IEC· National· Committee· interested· in· the· subject· dealt· with· may· participate· in· this· preparatory· work.· International,· governmental· and· non-governmental· organizations· liaising· with· the· IEC· also· participate· in· this· preparation.· IEC· collaborates· closely· with· the· International· Organization· for· Standardization· (ISO)· in· accordance· with· conditions· determined· by· agreement· between· the· two· organizations.¶

2)→The· formal· decisions· or· agreements· of· IEC· on· technical· matters· express,· as· nearly· as· possible,· an· international· consensus· of· opinion· on· the· relevant· subjects· since· each· technical· committee· has· representation· from· all· interested· IEC· National· Committees.¶

3)→IEC· Publications· have· the· form· of· recommendations· for· international· use· and· are· accepted· by· IEC· National· Committees· in· that· sense.· While· all· reasonable· efforts· are· made· to· ensure· that· the· technical· content· of· IEC· Publications· is· accurate,· IEC· cannot· be· held· responsible· for· the· way· in· which· they· are· used· or· for· any· misinterpretation· by· any· end-user.¶

Figure 112. *The first page of the new version of IEC 62282*

BIBLIOGRAPHY

[1] International Renewable Energy Agency (IRENA), Renewable power generation costs in 2014, Renew. Power Gener. Costs. (2014). doi:10.1007/SpringerReference_7300.

[2] N.L. Panwar, S.C. Kaushik, S. Kothari, Role of renewable energy sources in environmental protection: A review, Renew. Sustain. Energy Rev. (2011). doi:10.1016/j.rser.2010.11.037.

[3] S. Suranovic, Fossil fuel addiction and the implications for climate change policy, Glob. Environ. Chang. (2013). doi:10.1016/j.gloenvcha.2013.02.006.

[4] M. Höök, X. Tang, Depletion of fossil fuels and anthropogenic climate change-A review, Energy Policy. (2013). doi:10.1016/j.enpol.2012.10.046.

[5] S.M. Shaahid, M.A. Elhadidy, Technical and economic assessment of grid-independent hybrid photovoltaic-diesel-battery power systems for commercial loads in desert environments, Renew. Sustain. Energy Rev. (2007). doi:10.1016/j.rser.2006.03.001.

[6] G. Marbán, T. Valdés-Solís, Towards the hydrogen economy?, Int. J. Hydrogen Energy. (2007). doi:10.1016/j.ijhydene.2006.12.017.

[7] S. Rehman, I.M. El-Amin, F. Ahmad, S.M. Shaahid, A.M. Al-Shehri, J.M. Bakhashwain, A. Shash, Feasibility study of hybrid retrofits to an isolated off-grid diesel power plant, Renew. Sustain. Energy Rev. (2007). doi:10.1016/j.rser.2005.05.003.

[8] E.D. Stoutenburg, N. Jenkins, M.Z. Jacobson, Power output variations of co-located offshore wind turbines and wave energy converters in California, Renew. Energy. 35 (2010) 2781–2791. doi:10.1016/j.renene.2010.04.033.

[9] US EPA, US Environmental Protection Agency, US Environ. Prot. Agency. 1 (2012) 1–15.

[10] R. Steinberger-Wilckens, H. Nabielek, Lucerne/Switzerland: The 7th European solid oxide fuel cell forum, InterCeram Int. Ceram. Rev. 55 (2006) 359–361.

[11] B.E. Turkay, A.Y. Telli, Economic analysis of standalone and grid connected hybrid energy systems, Renew. Energy. 36 (2011) 1931–1943. doi:10.1016/j.renene.2010.12.007.

[12] M. Wang, Z. Wang, X. Gong, Z. Guo, The intensification technologies to water electrolysis for hydrogen production - A review, Renew. Sustain. Energy Rev. 29 (2014) 573–588. doi:10.1016/j.rser.2013.08.090.

[13] K. Mazloomi, C. Gomes, Hydrogen as an energy carrier: Prospects and challenges, Renew. Sustain. Energy Rev. 16 (2012) 3024–3033. doi:10.1016/j.rser.2012.02.028.

[14] O.Z. Sharaf, M.F. Orhan, An overview of fuel cell technology: Fundamentals and applications, Renew. Sustain. Energy Rev. 32 (2014) 810–853. doi:10.1016/j.rser.2014.01.012.

[15] C. Auer, M. Lang, K. Couturier, E.R. Nielsen, S.J. McPhail, G. Tsotridis, Q. Fu, S.H. Chan, Solid oxide cell and stack testing, safety and quality assurance (SOCTESQA), in: ECS Trans., 2015. doi:10.1149/06801.1897ecst.

[16] L. Jin, W.B. Guan, X. Ma, C. Xu, W.G. Wang, Achieving hydrogen production through solid oxide electrolyzer stack by high temperature electrolysis, ECS Trans. 41 (2012) 103–111. doi:10.1149/1.3702417.

[17] Q. Li, Y. Zheng, W. Guan, L. Jin, C. Xu, W.G. Wang, Achieving high-efficiency hydrogen production using planar solid-oxide electrolysis stacks, Int. J. Hydrogen Energy. 39 (2014) 10833–10842. doi:10.1016/j.ijhydene.2014.05.070.

[18] I. Bloom, L. Walker, J. Basco, T. Malkow, G. De Marco, G. Tsotridis, A Comparison of Fuel Cell Test Protocols, ECS Trans. 30 (2011) 227–235. doi:10.1149/1.3562478.

[19] A. Patyk, T.M. Bachmann, A. Brisse, Life cycle assessment of H2 generation with high temperature SOEC from the RelHy project, Int. J. Hydrogen Energy. 8 (2013) 3865–3880. doi:http://dx.doi.org/10.1016/j.ijhydene.2013.01.063.

[20] A. Choudhury, H. Chandra, A. Arora, Application of solid oxide fuel cell technology for power generation - A review, Renew. Sustain. Energy Rev. 20 (2013) 430–442. doi:10.1016/j.rser.2012.11.031.

[21] J. Guan, N. Minh, B. Ramamurthi, J. Ruud, J.-K. Hong, P. Riley, D. Weng, High Performance Flexible Reversible Solid Oxide Fuel Cell, GE Glob. Res. Cent. Rep. DE-FC36e04GO14351. (2007).

[22] I.R. Gibson, G.P. Dransfield, J.T.S. Irvine, Sinterability of commercial 8 mol% yttria-stabilized zirconia powders and the effect of sintered density on the ionic conductivity, J. Mater. Sci. 33 (1998) 4297–4305. doi:10.1023/A:1004435504482.

[23] S.P.S. Badwal, Zirconia-based solid electrolytes: microstructure, stability and ionic conductivity, Solid State Ionics. 52 (1992) 23–32. doi:10.1016/0167-2738(92)90088-7.

[24] S.P. Jiang, S.H. Chan, A review of anode materials development in solid oxide fuel cells, J. Mater. Sci. 39 (2004) 4405–4439. doi:10.1023/B:JMSC.0000034135.52164.6b.

[25] N. Laosiripojana, W. Wiyaratn, W. Kiatkittipong, A. Arpornwichanop, A. Soottitantawat, S. Assabumrungrat, Reviews on solid oxide fuel cell technology, Eng. J. (2009). doi:10.4186/ej.2009.13.1.65.

[26] S.P. Jiang, Development of lanthanum strontium manganite perovskite cathode materials of solid oxide fuel

cells: A review, J. Mater. Sci. 43 (2008) 6799–6833. doi:10.1007/s10853-008-2966-6.
[27] J.W. Stevenson, T.R. Armstrong, R.D. Carneim, L.R. Pederson, W.J. Weber, Electrochemical properties of mixed conducting perovskites La(1-x)M(x)Co(1-y)Fe(y)O(3-delta) (M=Sr,Ba,Ca), J. Electrochem. Soc. 143 (1996) 2722–2729. doi:10.1149/1.1837098.
[28] S.P. Jiang, X. Chen, Chromium deposition and poisoning of cathodes of solid oxide fuel cells - A review, Int. J. Hydrogen Energy. 39 (2014) 505–531. doi:10.1016/j.ijhydene.2013.10.042.
[29] W.Z. Zhu, S.C. Deevi, Opportunity of metallic interconnects for solid oxide fuel cells: A status on contact resistance, Mater. Res. Bull. 38 (2003) 957–972. doi:10.1016/S0025-5408(03)00076-X.
[30] V.A.C. Haanappel, V. Shemet, I.C. Vinke, S.M. Gross, T. Koppitz, N.H. Menzler, M. Zahid, W.J. Quadakkers, Evaluation of the suitability of various glass sealant - Alloy combinations under SOFC stack conditions, J. Mater. Sci. 40 (2005) 1583–1592. doi:10.1007/s10853-005-0657-0.
[31] N. Lahl, K. Singh, L. Singheiser, K. Hilpert, D. Bahadur, Crystallisation kinetics in AO- Al2O3-SiO2- B2O3 glasses (A = Ba, Ca, Mg), J. Mater. Sci. 35 (2000) 3089–3096. doi:10.1023/A/1004851418274.
[32] Y.S. Chou, J.W. Stevenson, L.A. Chick, Ultra-low leak rate of hybrid compressive mica seals for solid oxide fuel cells, J. Power Sources. 112 (2002) 130–136. doi:10.1016/S0378-7753(02)00356-7.
[33] S.C. Singhal, K. Kendall, High-temperature solid oxide fuel cells: fundamentals, design, and applicatons, 2003. doi:10.1016/B978-185617387-2/50021-0.
[34] K.J. Albrecht, R.J. Braun, Dynamic Modeling of SOFC Cogeneration Systems for Light Commercial Applications, in: ASME 2014 12th Int. Conf. Fuel Cell Sci. Eng. Technol., 2014. doi:10.1115/FuelCell2014-6403.
[35] R. Bove, S. Ubertini, Modeling solid oxide fuel cell operation: Approaches, techniques and results, J. Power Sources. (2006). doi:10.1016/j.jpowsour.2005.11.045.
[36] IPCC, IPCC Fifth Assessment Synthesis Report-Climate Change 2014 Synthesis Report, IPCC Fifth Assess. Synth. Report-Climate Chang. 2014 Synth. Rep. (2014) pages: 167.
[37] J. Hanna, W.Y. Lee, Y. Shi, A.F. Ghoniem, Fundamentals of electro- and thermochemistry in the anode of solid-oxide fuel cells with hydrocarbon and syngas fuels, Prog. Energy Combust. Sci. 40 (2014) 74–111. doi:10.1016/j.pecs.2013.10.001 Review.
[38] I. EG&G Technical Services, Fuel Cell Handbook, Fuel Cell. 7 Edition (2004) 1–352. doi:10.1002/zaac.200300050.
[39] V.M. Janardhanan, O. Deutschmann, Modeling of Solid-Oxide Fuel Cells, Zeitschrift Für Phys. Chemie. 221 (2007) 443–478. doi:10.1524/zpch.2007.221.4.443.
[40] J. Sanz-Bermejo, J. Muñoz-Antón, J. Gonzalez-Aguilar, M. Romero, Part load operation of a solid oxide electrolysis system for integration with renewable energy sources, Int. J. Hydrogen Energy. 40 (2015) 8291–8303. doi:10.1016/j.ijhydene.2015.04.059.
[41] C.H. Wendel, P. Kazempoor, R.J. Braun, Novel electrical energy storage system based on reversible solid oxide cells: System design and operating conditions, J. Power Sources. 276 (2015) 133–144. doi:10.1016/j.jpowsour.2014.10.205.
[42] C.H. Wendel, Z. Gao, S.A. Barnett, R.J. Braun, Modeling and experimental performance of an intermediate temperature reversible solid oxide cell for high-efficiency, distributed-scale electrical energy storage, J. Power Sources. 283 (2015) 329–342. doi:10.1016/j.jpowsour.2015.02.113.
[43] S. Santhanam, M.P. Heddrich, M. Riedel, K.A. Friedrich, Theoretical and experimental study of Reversible Solid Oxide Cell (r-SOC) systems for energy storage, Energy. 141 (2017) 202–214. doi:10.1016/j.energy.2017.09.081.
[44] B. Dunn, H. Kamath, J.-M. Tarascon, G.L. Soloveichik, M. Winter, R.J. Brodd, P. Simon, Y. Gogotsi, J.B. Goodenough, Y. Kim, J.M. Tarascon, M. Armand, V. Etacheri, R. Marom, R. Elazari, G. Salitra, D. Aurbach, M. Armand, J.M. Tarascon, A.S. Aricò, P. Bruce, B. Scrosati, J.M. Tarascon, W. van Schalkwijk, H. Li, Z.X. Wang, L.Q. Chen, X.J. Huang, P. Poizot, S. Laruelle, S. Grugeon, L. Dupont, J.M. Tarascon, M.N. Obrovac, L. Christensen, P. Barpanda, A. Yamada, S.C. Chung, K. Hinokuma, J.M. Tarascon, J.M. Tarascon, H. Chen, G. Girishkumar, B. McCloskey, A.C. Luntz, S. Swanson, W. Wilcke, K.T. Lee, K.M. Abraham, Z. Jiang, J.P. Zheng, R.Y. Liang, M. Hendrickson, E.J. Plichta, T. Ogasawara, A. Débart, M. Holzapfel, P. Novák, P.G. Bruce, A. Débart, A.J. Paterson, J. Bao, P.G. Bruce, Y.C. Lu, G. Girishkumar, B. McCloskey, A.C. Luntz, S. Swanson, W. Wilcke, J.F. Whitacre, A. Tevar, S. Sharma, Y.F.Y. Yao, J.T. Kummer, X.C. Lu, G.G. Xia, J.P. Lemmon, Z.G. Yang, C.H. Dustmann, G.C. Farrington, J.L. Briant, D. La Rosa, J.L. Sudworth, Z. Yang, S.F. Song, B. Dunn, M.W. Breiter, D.S. Park, C.P. de Leon, M. Bartolozzi, M. Skyllas-Kazacos, M. Rychcik, R.G. Robins, A.G. Fane, M.A. Green, M. Skyllas-Kazacos, D.H. Doughty, P.C. Butler, A.A. Akhil, N.H. Clark, J.D. Boyes, T. Nguyen, R.F. Savinell, M. Duduta, Y.H. Lu, J.B. Goodenough, Electrical energy storage for the grid: a battery of choices., Science. 334 (2011) 928–35. doi:10.1126/science.1212741.
[45] C.H. Wendel, R.J. Braun, Design and techno-economic analysis of high efficiency reversible solid oxide cell systems for distributed energy storage, Appl. Energy. 172 (2016) 118–131. doi:10.1016/j.apenergy.2016.03.054.
[46] J.B. Hansen, S.D. Ebbesen, S.H. Jensen, A. Hauch, M.B. Mogensen, M.A. Laguna-Bercero, S.D. Ebbesen, M. Mogensen, L.M. Elikan, J.P. Morris, L.M. Elikan, J.P. Wu, C.K. Wu, A.O. Isenberg, W. Dönitz, G. Dietrich, E.

Erdle, R. Streicher, W. Dönitz, E. Erdle, E. Erdle, W. Dönitz, R. Schamm, A. Koch, J.E. O'Brien, M. Ni, M.K.H. Leung, D.Y.C. Leung, X. Sun, M. Chen, S.H. Jensen, S.D. Ebbesen, C. Graves, M. Mogensen, S.H. Jensen, P.H. Larsen, M. Mogensen, A. Momma, T. Kato, Y. Kaga, S. Nagata, A. Hauch, S.D. Ebbesen, S.H. Jensen, M. Mogensen, A. Hauch, S.D. Ebbesen, S.H. Jensen, M. Mogensen, A. Hauch, S.H. Jensen, S. Ramousse, M. Mogensen, R. Knibbe, M.L. Traulsen, A. Hauch, S.D. Ebbesen, M. Mogensen, N. Osada, H. Uchida, M. Watanabe, X. Zhang, J.E. O'Brien, R.C. O'Brien, J.J. Hartvigsen, G. Tao, G.K. Housley, K. Eguchi, T. Hatagishi, H. Arai, P. Kim-Lohsoontorn, N. Laosiripojana, J. Bae, S. Elangovan, J.J. Hartvigsen, L.J. Frost, P. Moçoteguy, A. Brisse, O.A. Marina, L.R. Pederson, M.C. Williams, G.W. Coffey, K.D. Meinhardt, C.D. Nguyen, E.C. Thomsen, J.C. Ruiz-Morales, D. Marrero-López, J. Canales-Vázquez, J.T.S. Irvine, G. Tsekouras, J.T.S. Irvine, G. Tsekouras, D. Neagu, J.T.S. Irvine, X. Yang, J.T.S. Irvine, X. Yue, J.T.S. Irvine, F. Bidrawn, G. Kim, G. Corre, J.T.S. Irvine, J.M. Vohs, R.J. Gorte, B. Ge, J.T. Ma, D. Ai, C. Deng, X. Lin, J. Xu, G. Schiller, A. Ansar, M. Lang, O. Patz, W. Wang, Y. Huang, S. Jung, J.M. Vohs, R.J. Gorte, Y. Bo, Z. Wenqiang, X. Jingming, C. Jing, P. Kim-Lohsoontorn, J. Bae, P. Hjalmarsson, X. Sun, Y.L. Liu, M. Chen, M.A. Laguna-Bercero, N. Kinadjan, R. Sayers, H. El Shinawi, C. Greaves, S.J. Skinner, S.D. Ebbesen, C. Graves, A. Hauch, S.H. Jensen, M. Mogensen, A. Hauch, S.H. Jensen, J.B. Bilde-Sørensen, M. Mogensen, J.B. Hansen, E. Giglio, A. Lanzini, M. Santarelli, P. Leone, Y. Tao, S.D. Ebbesen, W. Zhang, M.B. Mogensen, W. Li, Y. Shi, Y. Luo, Y. Wang, N. Cai, V. Duboviks, R.C. Maher, M. Kishimoto, L.F. Cohen, N.P. Brandon, G.J. Offer, V. Duboviks, M. Lomberg, R.C. Maher, L.F. Cohen, N.P. Brandon, G.J. Offer, R. Knibbe, A. Hauch, J. Hjelm, S.D. Ebbesen, M. Mogensen, S.D. Ebbesen, J. Høgh, K.A. Nielsen, J.U. Nielsen, M. Mogensen, V.N. Nguyen, Q. Fang, U. Packbier, L. Blum, J. Schefold, A. Brisse, F. Tietz, F. Tietz, D. Sebold, A. Brisse, J. Schefold, J. Schefold, A. Brisse, H. Poepke, C. Graves, S.D. Ebbesen, S.H. Jensen, S.B. Simonsen, M.B. Mogensen, D.M. Bierschenk, J.R. Wilson, S.A. Barnett, C.H. Wendel, P. Kazempoor, R.J. Braun, S.H. Jensen, X. Sun, S.D. Ebbesen, R. Knibbe, M. Mogensen, L. Bernadet, G. Gousseau, A. Chatroux, J. Laurencin, F. Mauvy, M. Reytier, M. Reytier, S. Di Iorio, A. Chatroux, M. Petitjean, J. Cren, M. de Saint Jean, J. Aicart, J. Mougin, G. Lorenzi, A. Lanzini, M. Santarelli, E. Giglio, A. Lanzini, M. Santarelli, P. Leone, K.C. Tran, O. Sigurbjornsson, J.B. Hansen, N. Christiansen, J.U. Nielsen, Q. Fu, C. Mabilat, M. Zahid, A. Brisse, L. Gautier, C. Graves, S.D. Ebbesen, M. Mogensen, K.S. Lackner, W.L. Becker, R.J. Braun, M. Penev, M. Melaina, D. Connolly, B. V. Mathiesen, I. Ridjan, H. Lund, A.N. Andersen, P.A. Østergaard, B. V. Mathiesen, D. Connolly, B. V. Mathiesen, H. Lund, D. Connolly, H. Wenzel, P.A. Ostergaard, B. Möller, S. Nielsen, I. Ridjan, P. KarnOe, K. Sperling, F.K. Hvelplund, Solid oxide electrolysis – a key enabling technology for sustainable energy scenarios, Faraday Discuss. 182 (2015) 9–48. doi:10.1039/C5FD90071A.

[47] C. Graves, S.D. Ebbesen, M. Mogensen, K.S. Lackner, Sustainable hydrocarbon fuels by recycling CO 2 and H 2 O with renewable or nuclear energy, Renew. Sustain. Energy Rev. 15 (2011) 1–23. doi:10.1016/j.rser.2010.07.014.

[48] A. Buttler, R. Koltun, R. Wolf, H. Spliethoff, A detailed techno-economic analysis of heat integration in high temperature electrolysis for efficient hydrogen production, Int. J. Hydrogen Energy. 40 (2015) 38–50. doi:10.1016/j.ijhydene.2014.10.048.

[49] C.H. Wendel, P. Kazempoor, R.J. Braun, A thermodynamic approach for selecting operating conditions in the design of reversible solid oxide cell energy systems, J. Power Sources. 301 (2016) 93–104. doi:10.1016/j.jpowsour.2015.09.093.

[50] J. Larminie, A. Dicks, Fuel cell systems explained, 2003. doi:10.1002/9781118878330.

[51] A. Lasia, Electrochemical Impedance Spectroscopy and its Applications, Mod. Asp. Electrochem. 32 (1999) 143–248. doi:10.1007/0-306-46916-2{_}2.

[52] E. Barsoukov, J.R. Macdonald, Impedance Spectroscopy: Theory, Experiment, and Applications, 2005. doi:10.1002/0471716243.

[53] E. Barsoukov, J.R. Macdonald, Impedance Spectroscopy, 2005. doi:10.1002/0471716243.

[54] C. Gabrielli, Identification of electrochemical processes by frequency response analysis, Tech. Rep. No. 004/83. 4 (1998) 130. http://www.mendeley.com/research/identification-of-electrochemical-processes-by-frequency-response-analysis/.

[55] Q.A. Huang, R. Hui, B. Wang, J. Zhang, A review of AC impedance modeling and validation in SOFC diagnosis, Electrochim. Acta. 52 (2007) 8144–8164. doi:10.1016/j.electacta.2007.05.071.

[56] N. Wagner, W. Schnurnberger, B. Müller, M. Lang, Electrochemical impedance spectra of solid-oxide fuel cells and polymer membrane fuel cells, Electrochim. Acta. 43 (1998) 3785–3793. doi:10.1016/S0013-4686(98)00138-8.

[57] J. Nielsen, J. Hjelm, Impedance of SOFC electrodes: A review and a comprehensive case study on the impedance of LSM:YSZ cathodes, Electrochim. Acta. 115 (2014) 31–45. doi:10.1016/j.electacta.2013.10.053.

[58] H. Schichlein, H. Schichlein, E. Ivers-tiffe, E. Ivers-tiffe, M. Voigts, A. Kru, H. Schichlein, A.C. Mu, A. Müller, M. Voigts, Deconvolution of electrochemical impedance spectra for the identification of electrode reaction mechanisms in solid oxide fuel cells, J. Appl. …. 32 (2002) 875–882. doi:10.1023/A:1020599525160.

[59] B.A. Boukamp, A Linear Kronig-Kramers Transform Test for Immittance Data Validation, J. Electrochem. Soc. 142 (1995) 1885. doi:10.1149/1.2044210.

[60] B.A. Boukamp, Electrochemical impedance spectroscopy in solid state ionics: Recent advances, Solid State

Ionics. 169 (2004) 65–73. doi:10.1016/j.ssi.2003.07.002.
[61] J.B. Bell, A.N. Tikhonov, V.Y. Arsenin, Solutions of Ill-Posed Problems., Math. Comput. 32 (1978) 1320. doi:10.2307/2006360.
[62] M. Fuhry, L. Reichel, A new Tikhonov regularization method, Numer. Algorithms. 59 (2011) 433–445. doi:10.1007/s11075-011-9498-x.
[63] D. Calvetti, S. Morigi, L. Reichel, F. Sgallari, Tikhonov regularization and the L-curve for large discrete ill-posed problems, J. Comput. Appl. Math. 123 (2000) 423–446. doi:10.1016/S0377-0427(00)00414-3.
[64] P.C. Hansen, Analysis of Discrete Ill-Posed Problems by Means of the L-Curve, SIAM Rev. 34 (1992) 561–580. doi:10.1137/1034115.
[65] H. Iwai, N. Shikazono, T. Matsui, H. Teshima, M. Kishimoto, R. Kishida, D. Hayashi, K. Matsuzaki, D. Kanno, M. Saito, H. Muroyama, K. Eguchi, N. Kasagi, H. Yoshida, Quantification of SOFC anode microstructure based on dual beam FIB-SEM technique, J. Power Sources. (2010). doi:10.1016/j.jpowsour.2009.09.005.
[66] A. Leonide, V. Sonn, A. Weber, E. Ivers-Tiffée, Evaluation and Modeling of the Cell Resistance in Anode-Supported Solid Oxide Fuel Cells, J. Electrochem. Soc. 155 (2008) B36. doi:10.1149/1.2801372.
[67] C. Boigues-Muñoz, D. Pumiglia, S.J. McPhail, G. Santori, D. Montinaro, G. Comodi, M. Carlini, F. Polonara, More accurate macro-models of solid oxide fuel cells through electrochemical and microstructural parameter estimation - Part II: Parameter estimation, J. Power Sources. 286 (2015) 321–329. doi:10.1016/j.jpowsour.2015.03.129.
[68] A. Kromp, A. Leonide, A. Weber, E. Ivers-Tiffée, Electrochemical Analysis of Reformate-Fuelled Anode Supported SOFC, J. Electrochem. Soc. 158 (2011) B980. doi:10.1149/1.3597177.
[69] C. Endler-Schuck, A. Leonide, A. Weber, S. Uhlenbruck, F. Tietz, E. Ivers-Tiffée, Performance analysis of mixed ionic-electronic conducting cathodes in anode supported cells, in: J. Power Sources, 2011: pp. 7257–7262. doi:10.1016/j.jpowsour.2010.11.079.
[70] C. Boigues Muñoz, D. Pumiglia, F. Santoni, S.J. McPhail, G. Comodi, M. Carlini, Performance Degradation Prediction of a Low-Temperature SOFC via Impedance Spectroscopy and CFD Modelling, ECS Trans. . 68 (2015) 2227–2235. doi:10.1149/06801.2227ecst.
[71] A. Leonide, Y. Apel, E. Ivers-Tiffee, SOFC Modeling and Parameter Identification by Means of Impedance Spectroscopy, in: ECS Trans., 2009: pp. 81–109. doi:10.1149/1.3247567.
[72] V. Sonn, A. Leonide, E. Ivers-Tiffée, Combined Deconvolution and CNLS Fitting Approach Applied on the Impedance Response of Technical Ni/8YSZ Cermet Electrodes, J. Electrochem. Soc. (2008). doi:10.1149/1.2908860.
[73] H. Schichlein, A.C. Müller, M. Voigts, A. Krügel, E. Ivers-Tiffée, Deconvolution of electrochemical impedance spectra for the identification of electrode reaction mechanisms in solid oxide fuel cells, J. Appl. Electrochem. 32 (2002) 875–882. doi:10.1023/A:1020599525160.
[74] H. Zhu, A. Kromp, A. Leonide, E. Ivers-Tiffee, O. Deutschmann, R.J. Kee, A Model-Based Interpretation of the Influence of Anode Surface Chemistry on Solid Oxide Fuel Cell Electrochemical Impedance Spectra, J. Electrochem. Soc. (2012). doi:10.1149/2.046207jes.
[75] A. Leonide, Y. Apel, E. Ivers-Tiffee, SOFC Modeling and Parameter Identification by Means of Impedance Spectroscopy, in: ECS Trans., 2009. doi:10.1149/1.3247567.
[76] A. Leonide, S. Hansmann, E. Ivers-Tiffée, A 0-dimensional stationary model for anode-supported solid oxide fuel cells, ECS Trans. (2010). doi:10.1149/1.3495858.
[77] Z.B. Stoynov, D.E. Vladikova, B.G. Burdin, J. Laurencin, D. Montinaro, A. Nakajo, P. Piccardo, A. Thorel, M. Hubert, R. Spotorno, A. Chesnaud, Differential Resistance Analysis - A New Tool for Evaluation of Solid Oxide Fuel Cells Degradation, in: MRS Adv., 2017. doi:10.1557/adv.2017.592.
[78] D. Montinaro, A.R. Contino, A. Dellai, M. Rolland, Determination of the impedance contributions in anode supported solid oxide fuel cells with (La,Sr)(Co,Fe)O3-δcathode, Int. J. Hydrogen Energy. 39 (2014) 21638–21646. doi:10.1016/j.ijhydene.2014.09.081.
[79] T.L. Skafte, J. Hjelm, P. Blennow, C. Graves, Quantitative review of degradation and lifetime of solid oxide cells and stacks, EFCF 2016 Proc. (2016) B0501.
[80] A.Y. Ramenskiy, S.A. Grigoriev, E.A. Ramenskaya, A.S. Grigoriev, Technical regulation issues concerning fuel cell technologies in the Russian Federation, countries of the Eurasian Economic Union and CIS countries, Int. J. Hydrogen Energy. 42 (2017) 21250–21262. doi:10.1016/j.ijhydene.2017.04.301.
[81] J.E. O'Brien, C.M. Stoots, J.S. Herring, J. Hartvigsen, Hydrogen Production Performance of a 10-Cell Planar Solid-Oxide Electrolysis Stack, J. Fuel Cell Sci. Technol. 3 (2006) 213. doi:10.1115/1.2179435.
[82] L.M. Klyatis, Accelerated Reliability and Durability Testing Technology, 2011. doi:10.1002/9780470541609.
[83] J. Udagawa, P. Aguiar, N.P. Brandon, Hydrogen production through steam electrolysis: Model-based steady state performance of a cathode-supported intermediate temperature solid oxide electrolysis cell, J. Power Sources. (2007). doi:10.1016/j.jpowsour.2006.12.081.
[84] J.E. O'Brien, C.M. Stoots, J.S. Herring, J. Hartvigsen, Hydrogen Production Performance of a 10-Cell Planar Solid-Oxide Electrolysis Stack, J. Fuel Cell Sci. Technol. (2006). doi:10.1115/1.2179435.
[85] S.A. Alabbadi, Hydrogen oxygen steam generator integrating with renewable energy resource for electricity generation, in: Energy Procedia, 2012: pp. 12–20. doi:10.1016/j.egypro.2012.09.003.

[86] J.S. Herring, J.E. O'Brien, C.M. Stoots, G.L. Hawkes, J.J. Hartvigsen, M. Shahnam, Progress in high-temperature electrolysis for hydrogen production using planar SOFC technology, Int. J. Hydrogen Energy. (2007). doi:10.1016/j.ijhydene.2006.06.061.
[87] R. Bove, T. Malkow, A. Saturnio, G. Tsotridis, PEM fuel cell stack testing in the framework of an EU-harmonized fuel cell testing protocol: Results for an 11 kW stack, J. Power Sources. (2008). doi:10.1016/j.jpowsour.2008.02.032.
[88] L. Petruzzi, S. Cocchi, F. Fineschi, A global thermo-electrochemical model for SOFC systems design and engineering, in: J. Power Sources, 2003. doi:10.1016/S0378-7753(03)00067-3.
[89] U. Bossel, Rapid startup SOFC modules, in: Energy Procedia, 2012. doi:10.1016/j.egypro.2012.08.039.
[90] U. Bossel, Universal SOFC Module for Rapid Start-Ups, ECS Trans. . (2011). doi:10.1149/1.3569992.
[91] C. Boigues Muñoz, D. Pumiglia, S.J. McPhail, D. Montinaro, G. Comodi, G. Santori, M. Carlini, F. Polonara, More accurate macro-models of solid oxide fuel cells through electrochemical and microstructural parameter estimation - Part I: Experimentation, J. Power Sources. (2015). doi:10.1016/j.jpowsour.2015.06.118.
[92] J. Tallgren, C. Boigues Muñoz, J. Mikkola, O. Himanen, J. Kiviaho, Determination of Temperature and Fuel Utilization Distributions in SOFC Stacks with EIS, ECS Trans. (2017). doi:10.1149/07801.2141ecst.
[93] D. Borello, A. Di Carlo, C. Boigues-Munoz, S.J. McPhail, G. Cinti, D. Penchini, The influence of bio-syngas composition on the derating of solid oxide fuel cells, in: Energy Procedia, 2014. doi:10.1016/j.egypro.2014.11.1031.
[94] C. Boigues-Muñoz, G. Santori, S. McPhail, F. Polonara, Thermochemical model and experimental validation of a tubular SOFC cell comprised in a 1 kWelstack designed for μcHP applications, Int. J. Hydrogen Energy. (2014). doi:10.1016/j.ijhydene.2014.09.021.